Instituto Tecnológico GeoMinero de España

INFORME ITGE

G 5 - 004.98

TÍTULO: INFORME SOBRE EL ENSAYO DEL EQUIPO NUMIS (RMN) REALIZADO EN ARCOS DE LA FRONTERA EN MAYO DE 1998

(ANEXOS III, IV y V)

Revisión: 1ª

Autores: Juan Luis Plata Torres
Félix Manuel Rubio Sánchez-Aguililla

Fecha: Madrid, Julio 1998

40472

Secretaría de Estado de Aguas y Costas
Ministerio de Medio Ambiente

INDICE

ANEXOS

Nota: Los Anexos III, IV, V sólo acompañan a los ejemplares depositados en el Centro de Documentación del ITGE y Biblioteca de Informes de Geofísica; el Anexo VI sólo se archiva en Geofísica.

ANEXO III

IRIS Instruments

SOME RECENT PUBLICATIONS ON THE PROTON MAGNETIC RESONANCE METHOD APPLIED TO GROUNDWATER INVESTIGATIONS

January, 1998

SOME RECENT PUBLICATIONS
ON THE PROTON MAGNETIC RESONANCE METHOD
APPLIED TO GROUNDWATER INVESTIGATIONS

TITLE	AUTHORS	Conference/Editor	Year
The Proton Magnetic Resonance method for Groundwater investigations	Bernard	IRIS Document	
Natural variations in the Magnetic Resonance Signal used in PMR groundwater prospecting from the surface	Legchenko, Beauce, Guillen, Valla, Bernard	European Journal of EEGS	1998
Inversion of Surface NMR data	Legchenko, Sushakov	Geophysics	1998
Inverse problem of Magnetic Resonance Measurements applied to Water Resource Characterization	Guillen Legchenko	SEG, Dallas	1997
Application of Proton Resonance for the detection of fractured chalk aquifers from the surface	Legchenko, Baltassat Beauce, Chigot	EEGS, Aarhus	1997
Development of a Proton Magnetic Resonance equipment for Groundwater investigations	Legchenko , Beauce, Valla, Bernard, Pierrat	High Resolution Geophysics, Tucson	1997
Capability of the NMR applied to aquifers investigation from the surface	Legchenko, Beauce, Guillen, Valla, Bernard	EEGS, Nantes	1996
Some aspects of the performance of the surface NMR method	Legchenko	SEG, Denver	1996
A practical accuracy of the surface NMR measurements	Legchenko	EAGE Amsterdam	1996

TITLE	AUTHORS	Conference/Editor	Year
Detection of the water level in fractured phreatic aquifers using NMR geophysical measurements	Gev, Goldman, B Rabinovich, M Rabinovich, Issar	Journal of Applied Geophysics	1996
Groundwater NMR in conductive water	Shushakov	Geophysics	1996
Surface NMR Applied to an electroconductive medium	Trushkin, Shushakov, Legchenko	Geophysical Prospecting	1995
Surface NMR experiments to detect subsurface water at Haddam Meadows, Connecticut	Lieblich, Legchenko, Haeni, Portselan	SAGEEP, Boston	1994
Applications of the integrated NMR-TDEM method in ground water exploration in Israel	Goldman, B. Rabinovich, M; Rabinovich, Gev, Gilad, Schirov	Journal of Applied Geophysics	1994
The potential of a noise-reducing antenna for surface NMR groundwater surveys in the earth's magnetic field.	Trushkin, Shushakov, Legchenko	Geophysical Prospecting	1994
A New Direct Non-Invasive Groundwater Detection Technology for Australia	Schirov, Legchenko	Exploration Geophysics	1991
Processing of surface proton magnetic resonance signals using non-linear fitting	Legchenko, Valla	Journal of Applied Geophysics	1998
El Sistema de búsqueda, reconocimiento y valoración de aguas subterráneas. HIDROSCOPE. Análisis Físico	Técnicos de investigación hidrogeológica S.A.		

THE PROTON MAGNETIC RESONANCE METHOD FOR GROUNDWATER INVESTIGATIONS

PRINCIPLE OF THE PROTON MAGNETIC RESONANCE METHOD

The PROTON MAGNETIC RESONANCE (PMR), also known as the Nuclear Magnetic Resonance (NMR), is a property of hydrogen protons which produce a magnetic field when they are excited by an alternative field in the presence of a static magnetic field. Most hydrogen atoms located in the ground are coming from water molecules. The direct detection of water can thus be envisioned with such a method, while conventional geophysical methods only provide structural information.

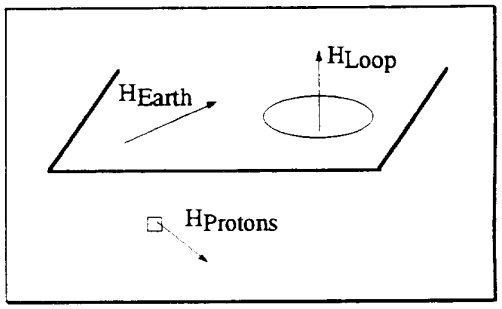

In the PMR method, three magnetic fields have to be considered:

1. the Earth's field, the amplitude of which determines the precession frequency of the protons.
2. The excitation field, produced by a current into a loop laid on the surface of the ground, at a frequency equal to the precession frequency (called the Larmor frequency).
3. The relaxation field produced by the protons excited by the previous field. The amplitude of the relaxation field measured at the surface, after the excitation current is turned off, is directly linked to the number of protons which have been excited and thus to the water content.

Source of the field	Nature of the field	The field .....
Earth	Static	... determines the precession frequency (0.5G => 2kHz)
Loop	Alternative	... excites the protons and causes their precession
Protons	Alternative	... is proportional to the water content

PMR AND PROTON MAGNETOMETRY

The PMR property is already commonly used by geophysicists in proton magnetometers, for measuring the amplitude of the Earth's magnetic field: in that case, the protons excited are those located in the sensor unit, the measured quantity is the resonance frequency of the protons and the physical quantity determined is the amplitude of the Earth's magnetic field, the variations of which are related to the magnetic underground structures. In the application of PMR to groundwater detection , the protons excited are those located in the ground, the measured quantity is the amplitude of the proton relaxation field and the physical parameter determined is the water content of the underground versus depth.

	Proton magnetometry	PMR for groundwater
Excited protons	Sensor protons	Underground protons
Measured quantity	Signal frequency	Signal amplitude
Physical parameter	The amplitude of the Earth's field	The water content of layers

IRIS INSTRUMENTS - 1, Avenue Buffon - BP 6007 - 45060 Orléans cedex 2 - France - Phone: 33 2 38 63 81 00 - Fax: 33 2 38 63 81 82 - E-mail: irisins @ibm.net

PMR BASIC EQUATIONS

The precession frequency f_0 of the protons subjected to the Earth's magnetic field H_0 is determined by the relation:

$$f_0 = H_0 \ \gamma / 2\pi$$

where γ the gyromagnetic ratio of the protons [$\gamma = 0.268$ Hz/nT]

The decay of the relaxation field produced by the protons after the excitation current has been turned off is given by the relation:

$$E = E_0 \exp(-t / T_2^*) \sin(2\pi f_0 t + \varphi_0)$$

where T_2^* is the time constant of the decay and φ_0 is the phase shift between the excitation current and the relaxation voltage measured in the loop.

T_2^* is of the order of a few tens milliseconds for clay bound water and of the order of a few hundreds milliseconds in pore free water.

The expression of the relaxation voltage measured at the surface just after the excitation current has been turned off is:

$$E_0 = \int_v 2\pi f_0 H_\perp(r) M_0 f(r) \sin\left(\frac{\gamma}{2} H_\perp(r) q\right) dv$$

where:

- M_0 is the magnetic moment of the water molecules
- $f(r)$ is the water content
- q is the pulse moment (intensity x duration)
- $H_\perp(r)$ is the component of the excitation field perpendicular to the Earth's field for a unitary current (I = 1A)

In the latter equation, it can be seen that the excitation field appears not only as a multiplicative term in the integrand which is usual in Physics, by also as an argument in a sine function, which is less usual and corresponds in fact to the proper response of the protons to the excitation.

The wavelength of this sine function depends, on the one hand, on the excitation field which is depth dependant, and on the other hand, on the pulse moment: it is therefore understandable **that the depth of investigation of the system** is closely related to the pulse moment. In practice, for a given value of the pulse moment, the main part of the signal comes from the deepest arch of the Sine function, whose position in depth is proportional to the pulse moment: lower moments thus lead to shallow investigations, while higher moments lead to deeper investigations.

The amplitude of the Earth's magnetic field has to be measured at the location of the measurements for determining the precession frequency of the protons which is proportional to this amplitude. Besides, the magnetic moment of water molecules is also proportional to this amplitude, and the relaxation voltage is thus proportional to the square of the Earth's magnetic field amplitude. **The dip of the Earth's field** in the area of the survey has to be estimated from regional magnetic maps for an adequate quantitative modelization, as in the previous equation the component of the excitation field which has to be taken into account $H_\perp(r)$ is that perpendicular to the Earth's field.

When the ground is infinitely resistive, the excitation field H(r) is the primary field of the loop in free space. **When the ground is conductive**, the excitation field is the total field (primary and secondary). A conductive ground will lead to a lower excitation field than a highly resistive one, and the depth of investigation will decrease when conductivity increases, for a given value of the pulse moment. The phase shift between the PMR signal and the excitation current in the loops permits to determine the ground conductivity and to improve the quantitative interpretation of PMR soundings.

INVESTIGATION DEPTH OF PMR

In surface PMR measurements, the depth of investigation depends on two main factors:

- **The surface of antenna** which determines the maximum volume investigated: roughly speaking, this volume is limited by the cylinder passing through the antenna and limited to a depth equal to the diameter of the antenna.

- **The moment of the excitation pulse** (product of the intensity of current by the duration of the pulse) which permits to investigate the various layers located between the surface and the maximum depth determined by the surface of the antenna.

Two other factors which depend on the local field conditions also influence the depth of investigation :

- **The rock resistivity**: a conductive ground leads to a lower depth than a resistive one, for a given antenna surface and pulse moment

- **The Earth's magnetic field**: the larger the Earth's field amplitude, the higher the signal amplitude, and the easier the detection of deep aquifers; besides, the dip of the Earth's field also influences the depth of investigation which is slightly greater for a vertical field (pole condition) than for a horizontal field (equator position).

PMR AND ELECTRICAL SOUNDING

As shown in the previous section, it is possible from surface measurements to determine the water content at various depths of investigation, that is to say to carry out an "PMR sounding" somewhat similar to a "Vertical electrical sounding" (VES) well known from geophysicists and hydrogeologists: in an electrical sounding, the parameter which sounds the ground is AB/2 (half length of the transmitting line), the measured quantity is the electric field and the physical parameter which aims at being determined is the true resistivity of the various layers at depth; in a PMR sounding, the parameter which sounds the ground, beside the loop size, is the moment of the excitation pulse (product of the intensity of current at the resonance frequency by the duration of the pulse), the measured quantity is the magnetic field produced by the excited protons and the physical parameter which aims at being determined is the water content of the various layers at depth.

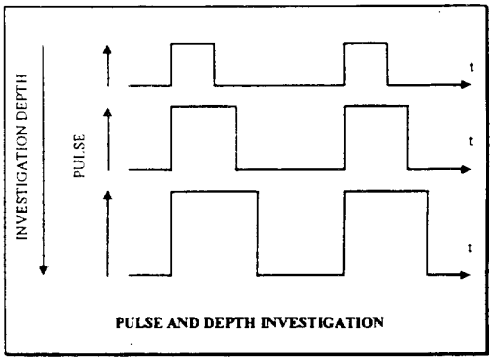

PULSE AND DEPTH INVESTIGATION

	VES SOUNDING	PMR SOUNDING
Parameter which sounds the ground	Length of Tx line AB/2	Pulse moment q = It
Measured quantity	Electric field	Proton magnetic field
Physical parameter estimated	True resistivity of each layer	Water content of each layer

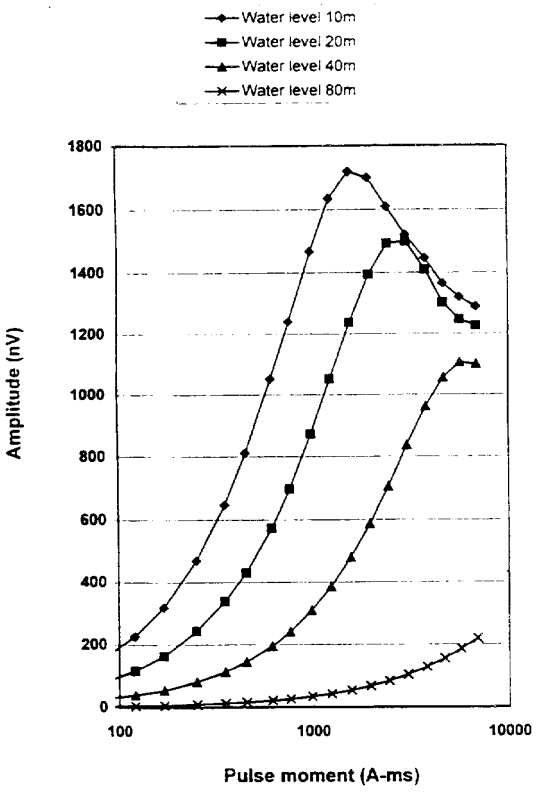

Fig 1: PMR response of a very thick layer with 20% water content, as a function of pulse moment, for various layer depths (water level). Loop diameter is 100m

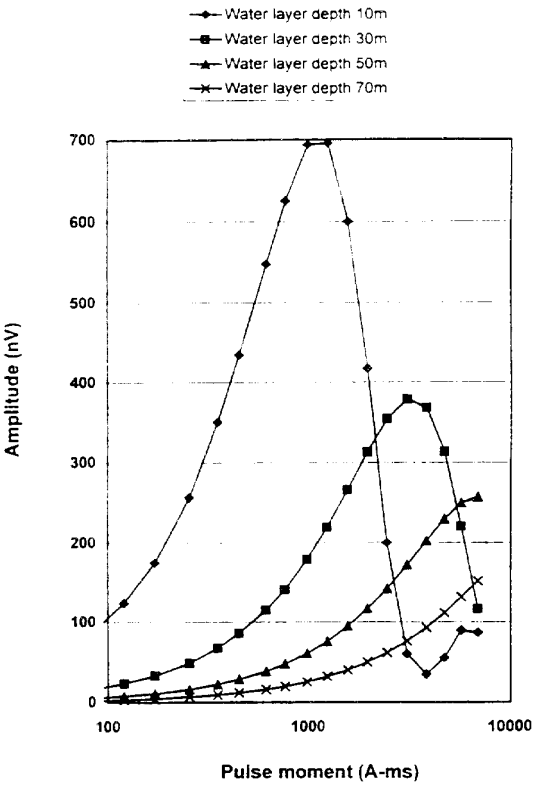

Fig 2: PMR response of a 10m thick layer with 20% water content, as a function of pulse moment, for various layer depths. Loop diameter is 100m.

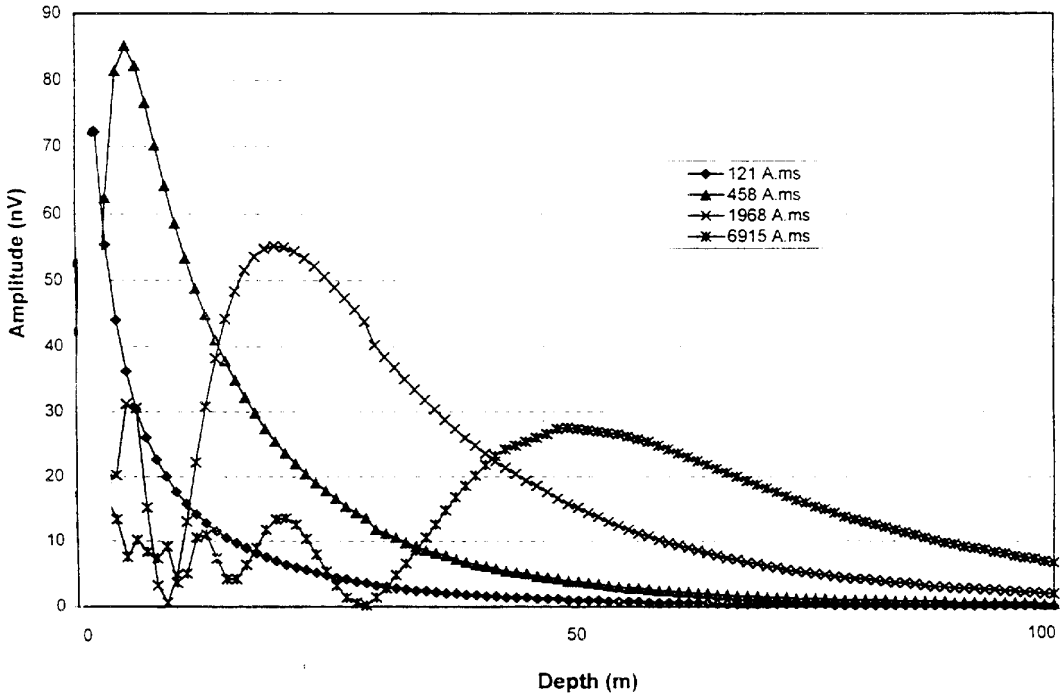

Fig 3 : Contribution, as a function of depth, of each elementary layer to the PMR response of an homogeneous ground with 20% water content, for various pulse moments. Loop diameter is 100 m.

INTERPRETATION OF PMR DATA

Interpreting PMR data consists in determining the water content of each layer, in the hypothesis where the underground is stratified at the scale of the loop dimensions. The inversion consists in processing the raw data for the whole set of pulse moments corresponding to the various depths of investigation. As for electrical sounding interpretation, indetermination and equivalence properties exist in PMR in the theoretical solutions given by inversion algorithms. However, some parameters are well defined such as the product of the thickness of a thin layer by its water content. Once again, a major advantage of the PMR method compared to more traditional methods is that PMR involves a parameter directly linked to the presence of water.

The interpretation also permits to determine the decay time constant of each layer by inverting the decay time constant of the measured signals for the whole set of pulse moments: thus, each aquifer layer can be characterized by the mean size of its pores, which is a good indicator of its permeability.

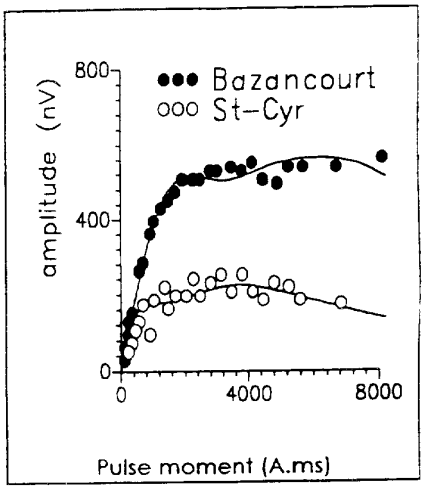

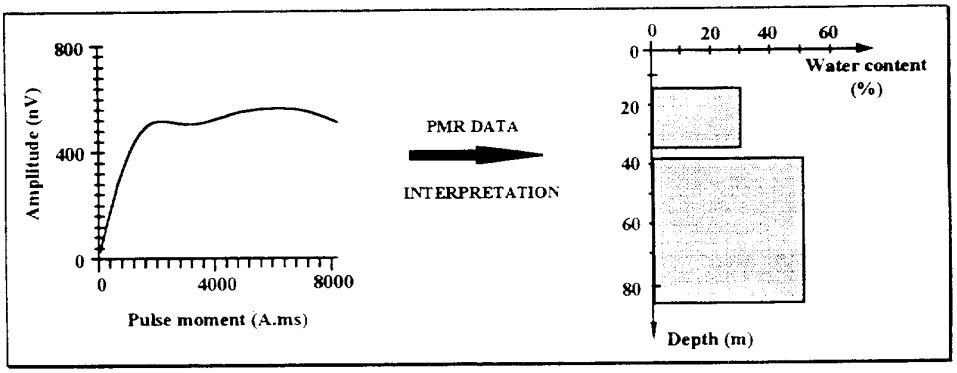

SYNTHETIC PMR SOUNDING

To have a clear understanding of the sounding capability of the PMR method, it is useful to compute the PMR response of theoretical 1D models.

Influence of the water level (fig. 1)

A two layer model has been used with 0% water for the upper one and 20% water for the lower one. The depth of the water level (top of the lower layer) has been set up at 10, 20 40 and 80 m respectively. The amplitudes of the received voltage versus the pulse moment clearly point out the influence of the pulse moment on the depth of investigation.

Effect of a water layer of finite thickness (fig. 2)

A three layer model has been used to represent an aquifer (20% water) included between two dry layers (0% water). The thickness of the water bearing layer has been fixed to 10 m in all cases ; its depth increases from 10 to 30, 50 and 70 m. The position of the maximum of the response is indeed shifted to the right side (high values of pulse moment) when the depth of the water layer increases.

Contribution of each depth in an homogeneous ground (fig. 3)

An homogeneous ground has been sliced in many layers each one having the same water content (20%) and the same thickness (1m). The response of each layer has been plotted versus depth for given values of the pulse moment: approximately 0.1, 0.5, 2 and 8 A.s. Once again, the sounding capability of the pulse moment can be checked, the response of lower moments mostly coming from shallow layers while that of higher moments mostly coming from deeper layers.

PHYSICAL PARAMETERS DETERMINED WITH PMR

In a PMR survey, the various parameters which are measured once an excitation pulse has been transmitted into the loop are the following ones:

- The amplitude E_0 of the relaxation field produced by the protons, just after the excitation current has been turned off; E_0 is directly linked to the water content.
- The decay time constant T_2^* of the relaxation field which is related to the pore size, and which permits to distinguish between pore free water and clay bound water.
- The phase shift φ_0 of the relaxation field with respect to the excitation current in the loop, which is linked to the resistivity of the ground.

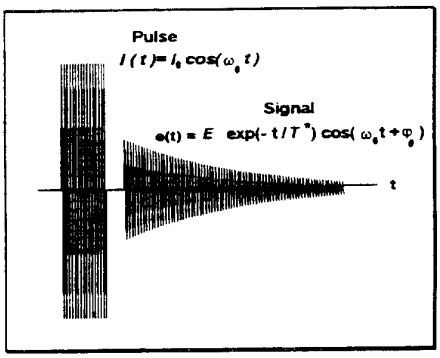

Measured quantity (versus pulse moment)	Physical parameter (versus depth)
Amplitude of the PMR signal	Water content
Decay time constant of the signal	Mean Pore size
Phase shift between signal and current	Rock layer resistivity

SOME REFERENCES TO KNOW MORE ABOUT PMR

Goldman, M., Rabinovich, B., Rabinovich, M., Gilad, D., Gev, I., and Schirov, M., 1994, Application of integrated NMR-TDEM method in ground water exploration in Israel: J.Appl.Geophys., **31**, 27-52.

Legchenko, A.V., Shushakov, O.A., Perrin, J., and Portselan, A.A., 1995, Noninvasive NMR study of subsurface aquifers in France. Abstracts of The International Exposition and SEG 65th Annual Meeting, October 9-12, 1995, Houston, USA, p.365-367.

Legchenko, A.V., A Practical Accuracy of the Surface NMR Measurements, 1996, EAGE 58th Conference and Technical Exhibition, Amsterdam.

Legchenko, A.V., Some aspects of the Surface NMR Method Performance, 1996, submitted to SEG 66th Annual Meeting, Denver.

Lieblich, D.A., Legchenko, A., Haeni, F.P., and Portselan, A., 1994, Surface nuclear NMR experiments to detect subsurface water at Haddam Meadows, Connecticut: Proceedings of the Symposium on the Application of Geophysics to Engineering and Environmental Problems, March 27-31, 1994, Boston, Massachusetts, **2**, 717-736.

Shirov, M., Legchenko, A., and Creer, G., 1991, New direct non-invasive ground water detection technology for Australia: Expl.Geophys., **22**, 333-338.

Trushkin, D.V., Shushakov, O.A., and Legchenko, A.V., 1993, Modulation effects in non-drilling NMR in the earth's field: Appl.NMR, **5**, 399-406.

Trushkin, D.V., Shushakov, O.A., and Legchenko, A.V., 1994, The potential of a noise-reducing antenna for surface NMR ground water surveys in the earth's magnetic field: Geophys.Prosp., **42**, 855-862.

Trushkin, D.V., Shushakov, O.A., and Legchenko, A.V., 1995, Surface NMR applied to an electroconductive medium: Geophys.Prosp., **43**, 623-633.

Semenov, A.G., 1987. NMR Hydroscope for water prospecting. Proceedings of the seminar on Geotomography: Indian Geophysical Union, Hyderabad, 66-67.

Semenov,A.G., Schirov,M.D. and Legchenko,A.V., 1987. On the technology of subterranean water exploration founded on application of nuclear NMR tomograph "Hydroscope". IXth Ampere summer school, Abstracts, Novosibirsk, September 20-26, 1987, p. 214.

Trushkin,D.V., Shushakov, O.A. and Legchenko,A.V., 1993. Modulation effects in non-drilling NMR in the Earth's field. Applied NMR, V5, 399-406.

Trushkin, D.V., Shushakov, O.A. and Legchenko, A.V., 1994. The potential of a noise-reducing antenna for surface NMR groundwater surveys in the earth's magnetic field. Geophysical Prospecting, v42.

PROTON MAGNETIC RESONANCE SOUNDING IN SOUTHERN CALIFORNIA

A PMR sounding field test has been carried out in the Southern California desert, to assess the efficiency of the NUMIS equipment in deep aquifer detection.
The raw data show an increase in the PMR signal at higher pulse moments corresponding to deeper layers.The interpretation confirms that water is present at a depth of the order of 100 m.The water content of the aquifer, a factured sandstone, is estimated to 20%, while the low values of the decay time (40 ms) indicate a small to medium size grain. These results are in good agreement with other known geological data.

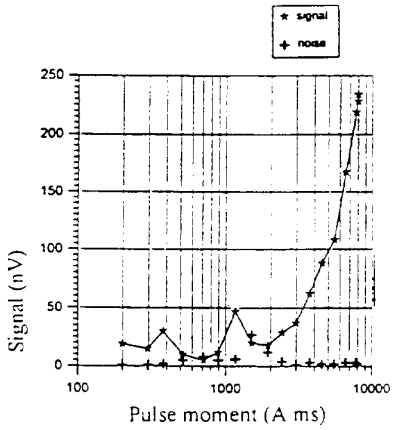

RAW DATA

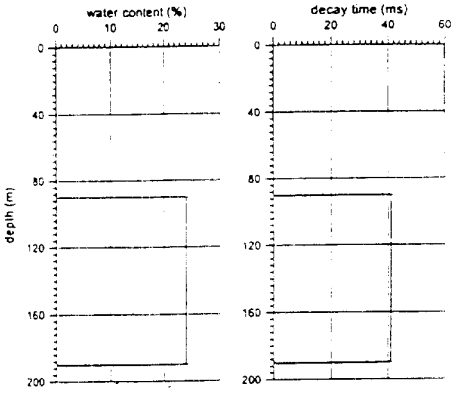

DATA INTERPRETATION

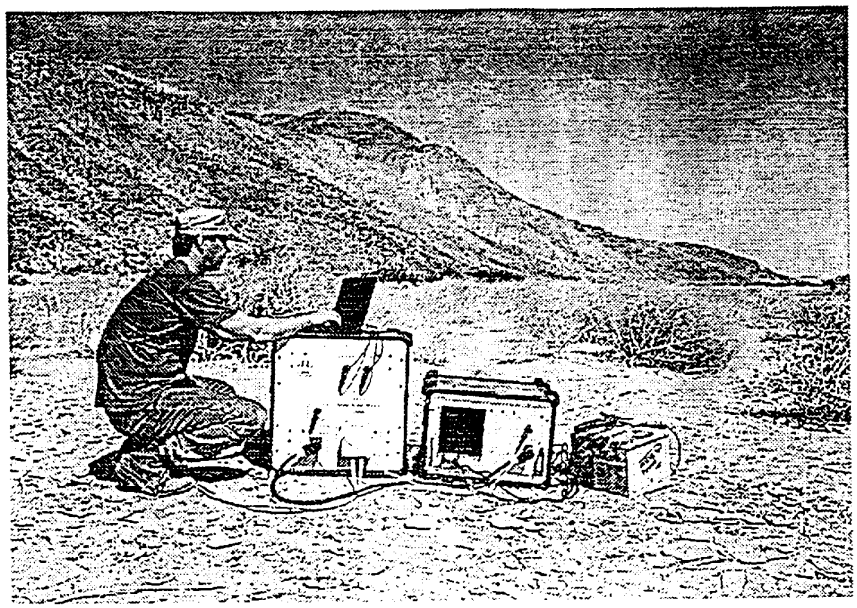

SET UP OF NUMIS EQUIPMENT IN THE FIELD

IRIS Instruments

FIELD TEST OF NUMIS SYSTEM IN ISRAEL

In the framework of a Research Contract supported by the European Community (European Project INCO-DC N°CT960122), twenty Proton Magnetic Resonance (PMR) soundings have been carried out in Israel (1997) by BRGM with NUMIS system, for improving the « rational management and exploration of groundwater resources »

In the Nitzanim area located 30 km South West of Tel Aviv, five PMR soundings have been measured along a 1 km long profile perpendicular to the sea coast

The area is characterized by an alternance of sand and discontinuous clayey layers. Despite a quite high level of industrial noise due to the presence of electric power lines in the vicinity, data have been obtained with a good measurement quality. Soundings 1, 4, 20 have been made with an 80 m side square loop, while soundings 5 and 3 have been made with an 8-shape 40 m side square loop which reduces the depth of investigation but increases the signal-to-noise ratio.

The interpretation of these soundings shows a water content of the order of 20 %, with a time constant ranging from 100 to 200 ms typical for the sandy aquifer formations. Boreholes 12/O, 12/B and 12/A found water levels at respectively 8.4, 10.6 and 20.1 m, while PMR soundings 1, 4 and 3 located near these drill holes have been interpreted with water levels at respectively 8, 10 and 17 m in good agreement with borehole data.

Along the same profile, a few TDEM soundings have been carried out by the Geophysical Institute of Israel. Both methods PMR and TDEM are complementary, since PMR is sensitive to any kind of water (fresh or saline) while TDEM is mostly sensitive to saline water. The interpretation of the PMR soundings has been made by taking into account the low resistivity of the layers shown by the TDEM measurements which slightly decreases the depth of investigation of the PMR method. A precise data interpretation in correlation with hydrogeological data coming from drillholes will be performed in the second step of this project.

IRIS INSTRUMENTS - 1, avenue Buffon, B.P. 6007 - 45060 Orléans cedex 2, France
Phone : 33 2 38 63 81 00 - Fax : 33 2 38 63 81 82 - Email : irisins @ ibm.net
BRGM & OYO Joint Venture

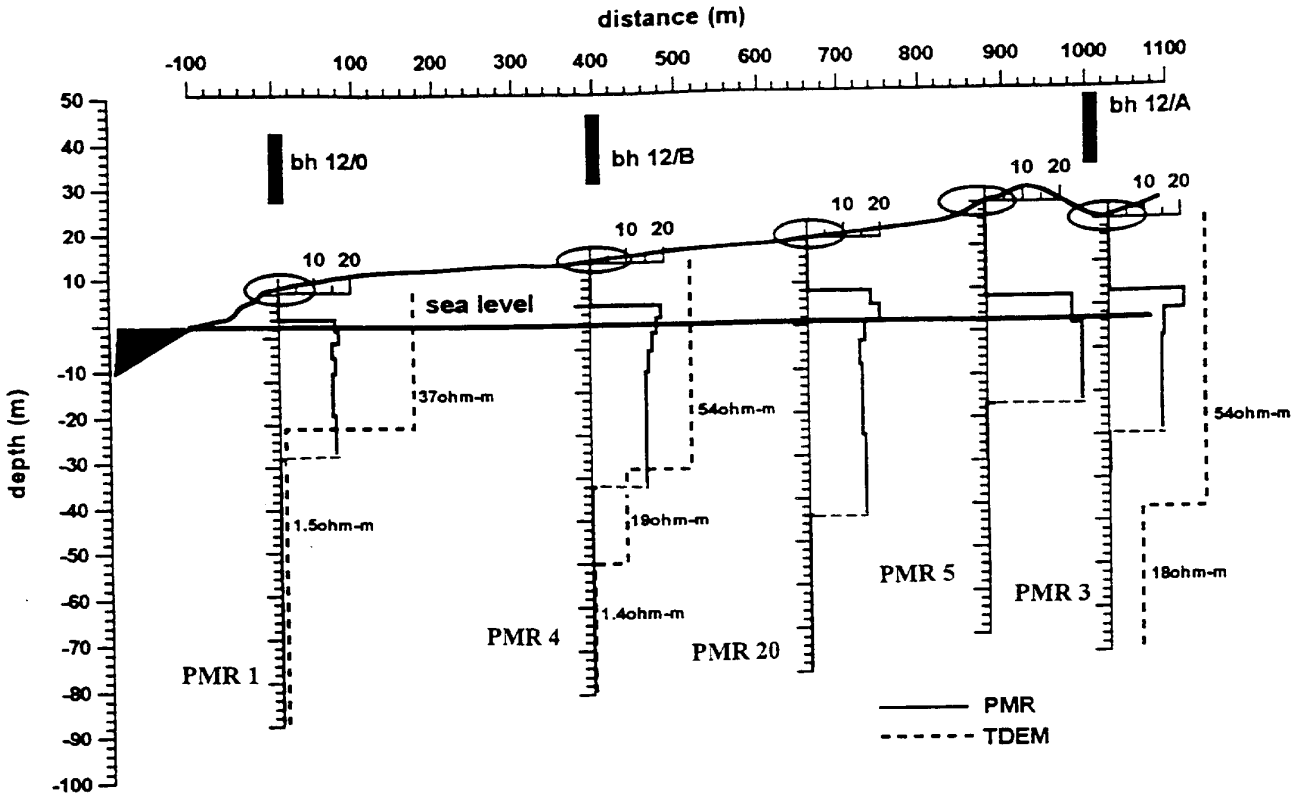

PMR and TDEM results on the Nitzanim profile

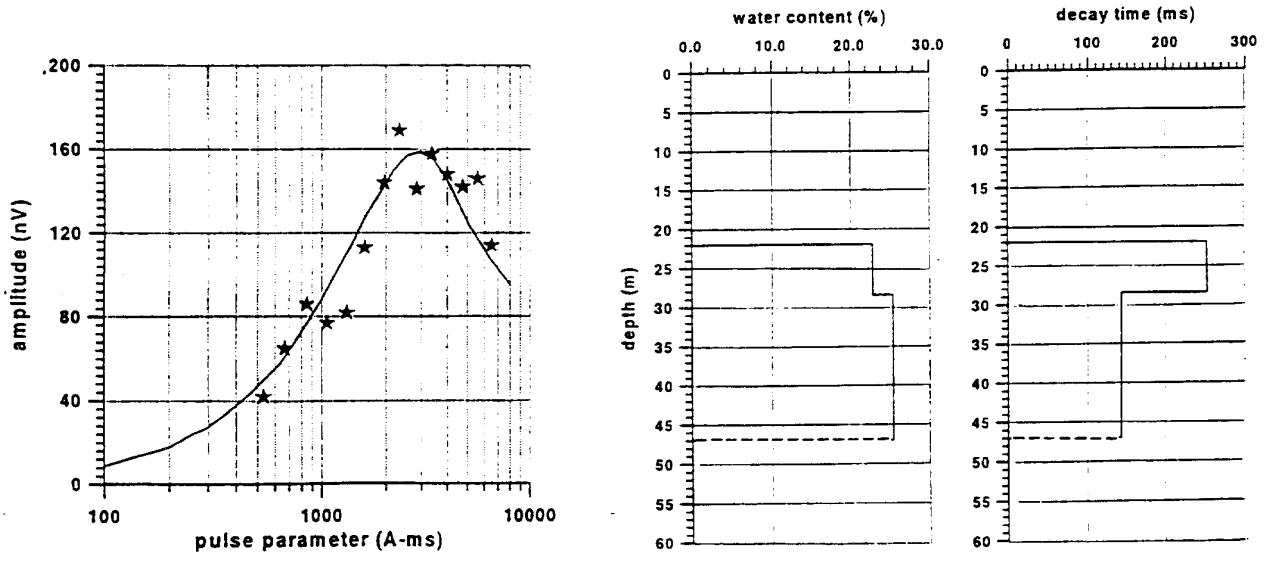

NUMIS sounding PMR 5 : experimental curve and interpretation

NATURAL VARIATIONS IN THE MAGNETIC RESONANCE SIGNAL USED IN PMR GROUNDWATER PROSPECTING FROM THE SURFACE

ANATOLY LEGCHENKO[1], ALAIN BEAUCE[1], ANTONIO GUILLEN[1], PIERRE VALLA[2] and JEAN BERNARD[2]

1 BRGM, B.P. 6009, F-45060 Orléans Cedex 2, France.
[2] IRIS Instruments, B.P. 6007,. F-45060 Orléans Cedex 2, France.

(Received November 11, 1996; revised version accepted October 24, 1997)

ABSTRACT

Legchenko, A., Beauce, A., Guillen, A., Valla, P. and Bernard, J., 1997. Natural variations in the magnetic resonance signal used in PMR groundwater prospecting from the surface. *European Journal of Environmental and Engineering Geophysics*, 2: 173-190.

Applications of the nuclear magnetic resonance phenomenon (NMR) in geophysics (proton magnetometer, NMR logging), chemistry (chemical analysis, study of the kinetics of chemical reactions), and medicine (diagnostics) are well known. The surface proton magnetic resonance (PMR) method for groundwater investigation is another, rather new, application of NMR. It was developed in the early eighties in Russia and is now is becoming a routine tool for use in geophysics.

The method has some special features which may affect the PMR signal amplitude and which therefore must be investigated. First of all, to act as a static magnetic field, which is an important parameter in the NMR theory, the geomagnetic field is used. Secondly, while a wire loop of diameter around 100 m is employed as a transmitting/receiving antenna, subsurface water-saturated layers act as investigated samples of a large volume. Both numerical modelling and experimental data were used for the analysis of the influence of the following factors on the PMR signal: the magnitude and the inclination of the geomagnetic field, the decay time of the signal (which depends on the mean size of pores of the water-saturated rocks), the electrical conductivity of the subsurface, and the antenna diameter (which should be selected in accordance with the geometry of a target (aquifers)). The most favourable conditions for the application of the method were set down as follows: the test site should be situated close to the North (or South) pole, rocks should be nonconductive, the decay time of the signal should be long (for example, the water-saturated rocks should to be composed of gravel or coarse sands). The most unfavourable conditions were taken as: a test site situated close to the equator, an aquifer situated in a 10 Ohm-m half-space, and a short signal (for example, water-saturated rocks composed of clays and very fine sands).

1359-8155/97/$5.00

Assuming that an antenna is 100 m in diameter, these cases were compared in between the worst and best conditions. It was found that even in the most unfavourable conditions the signal is large enough to be reliably detected, but possible variations in the investigated natural factors may result in a fivefold to ten-fold change in the signal amplitude depending on aquifer depth. Practically, this means that the PMR method can be used worldwide, but its performance may vary. For example, currently available PMR equipment with an antenna 100 m in diameter is able to detect a one-meter-thick layer of water down to a depth of 150 m in the most favourable conditions and only down to 40 m in the most unfavourable case.

KEY WORDS: NMR, PMR, magnetic resonance, groundwater, near-surface, aquifer, non-invasive.

INTRODUCTION

The initial idea of transforming the well-known proton magnetometer into a tool for water prospecting from the surface is ascribed to R.H. Varian (Varian, 1962). This idea was further developed and put into practice much later by a team of Russian scientists under the guidance of A.G. Semenov (Semenov et al., 1987). The first version of the instrument for measurements of magnetic resonance signals from subsurface water (*HYDROSCOPE*) was fabricated by the Institute of Chemical Kinetics and Combustion of the Russian Academy of Sciences (ICKC). The basic principal of operation of the surface proton magnetic resonance method for groundwater investigation (PMR) is similar to that of the proton magnetometer. They both assume records of the magnetic resonance signal from a proton-containing liquid (for example, water or hydrocarbons). However, while in the proton magnetometer a special sample of the liquid is placed into the receiving coil (which guarantees the existence of the signal) and only the signal frequency is a matter of interest, in the PMR a wire loop 100 m in diameter is used as a transmitting/receiving antenna and the water in the subsurface acts as a sample. Thus, in the PMR the fact of the existence or absence of the signal is directly linked with the existence or absence of the subsurface water and the direct detection of groundwater from the surface is the main distinction of the PMR. However, the reliability of the water detection largely depends on the signal amplitude. The amplitude may be affected by many factors: the magnitude and the inclination of the geomagnetic field (which varies according to the geographical co-ordinates of a test site); the electrical conductivity of the subsurface (screening effect); size and shape of the antenna; the decay time of the signal (which depends on the type of water containing rocks). It is a matter of practical importance to investigate possible variations in the magnetic resonance signal caused by these natural factors.

In this paper, experimental data and results of numerical modelling are presented. For field measurements two types of PMR equipment were used: the Russian *HYDROSCOPE* and *NUMIS*, which is a further development of the *HYDROSCOPE*. This development was made by IRIS Instruments (France) in co-operation with the Bureau de Recherches Géologiques et Minières (BRGM, France) and ICKC (Russia).

METHOD

For measurements of the magnetic resonance signal from subsurface water-saturated layers, the free induction decay (FID) method is used (Slichter, 1996). A pulse of oscillating current is passing through the transmitting coil. The frequency of the current is equal to the Larmor frequency. The pulse causes magnetic moments of investigated samples to shift away from the equilibrium position along the static magnetic field. Processing around the static magnetic field with the Larmor frequency, the magnetic moments induce an alternating magnetic field into the receiving coil which can be measured after the pulse is terminated.

In the surface-PMR method the geomagnetic field acts as the static magnetic field. It is supposed to be homogeneous all over the investigated volume. It means that the subsurface must be non-magnetic. For practical realization of the FID measurements, a wire loop is laid out on the surface. The loop is used as both transmitting and receiving antenna. It is energized by a pulse of oscillating current:

$$i(t) = I_0\cos(\omega_0 t) \quad , \quad 0 \le t \le \tau \quad . \tag{1}$$

The duration of the pulse τ may be varied, but currently in both instruments *HYDROSCOPE* and *NUMIS* it is set to be constant (τ = 40 ms). The carrier frequency of the current is equal to the Larmor frequency of protons in the geomagnetic field $\mathbf{B}_0$

$$\omega_0 = 2\pi f_0 = \gamma B_0 \quad , \tag{2}$$

where γ is the gyromagnetic ratio for the protons.

Following the classical description of the motion of a spin in the geomagnetic field (Slichter, 1996), a frame, rotating with the Larmor frequency, could be used. In order to simplify the model, the pulse is supposed to be much shorter than the decay time of the signal

$$\tau \ll T_2^* \quad . \tag{3}$$

Fig. 1 shows nuclear magnetization of protons $\mathbf{M}_0$ in this rotating frame. While the surface is assumed to be horizontal, the geomagnetic field $\mathbf{B}_0$ is inclined at the angle α. The pulse of alternating current passing through the wire creates an oscillating magnetic field $\mathbf{B}_1$. The component of the transmitted field $\mathbf{B}_{1\perp}$, which is perpendicular to the geomagnetic field, causes the nuclear magnetization of protons to shift away at the angle θ from the equilibrium position along the geomagnetic field. After the pulse is terminated, the nuclear magnetization returns to its equilibrium position and creates a decaying

alternating magnetic field. This alternating magnetic field can be measured by switching the antenna from transmitter to receiver. As $\mathbf{B}_{1\perp}$ depends on both the transmitting field $\mathbf{B}_1$ and the inclination α, the signal also should depend on the antenna configuration and on the geomagnetic field.

To find out the Larmor frequency in a field, a standard proton magnetometer may be used. The Larmor frequency of protons can be calculated using equation (2), and it could be taken as a first guess to set up the pulse frequency. For reliable detection of the signal, the pulse frequency should not differ by more than $\pm$ 10 Hz from the Larmor frequency of protons inside of water-saturated layers. Usually, outside of areas with significant magnetic anomalies, it is not difficult to get the needed accuracy. Afterwards, the PMR signal (with sufficient signal to noise ratio) should be recorded. If no signal is detected, it leads to a conclusion about the absence of subsurface water (within the sensitivity of the instrument, of course). If the signal is large enough, its frequency is measured by the instrument. This frequency is equal to the Larmor frequency of protons inside the investigated water-saturated layer. Right away, the pulse frequency should be modified according to this new value of the Larmor frequency and measurements can be started. Even over non-magnetic rocks a small vertical gradient of the geomagnetic field might be found. Variations in the geomagnetic field explain a possible difference between the Larmor frequency of protons on the surface (measured by the proton magnetometer) and within the aquifer (derived from test records). For this reason the procedure of the adjustment of the pulse frequency using the PMR signal is always recommended.

Electrically conductive rocks may also affect the alternating magnetic field $\mathbf{B}_1$ transmitted from the surface. $\mathbf{B}_1$ is not only attenuated, but it also becomes complex, which causes changes in $\mathbf{B}_{1\perp}$. Obviously, generated by protons, an oscillating magnetic field is also affected by the conductive layers. In order to study this effect in more detail, special field experiments were carried out and the reported results demonstrate changes in the magnetic resonance signal caused by the electrically conductive medium (Shushakov and Legchenko, 1994a,b; Trushkin et al., 1995; Shushakov, 1996). The problem of discrimination by PMR between electrically conductive water and electrically conductive rocks has not yet been solved and a solution of this very important problem could (if possible) be a matter of interest for further research.

The magnetic resonance signal oscillates at the Larmor frequency and has an exponential envelope:

$$e(t,q) = E_0(q) \sin(\omega t+\varphi_0) \exp(-t/T_2^*) \quad , \tag{4}$$

where E_0 is the initial amplitude, T_2^* is the decay time, φ_0 is the phase, and $q = I_0\tau$ is the pulse parameter.

As γ is the physical constant characterizing nuclei possessing with a magnetic moment, these nuclei have specific values of the Larmor frequency which is given by equation (2). Thus, by varying the frequency of the pulse in accordance with the Larmor frequency in the geomagnetic field, the chemical element for investigation may be selected. In the PMR only protons of subsurface water are a target.

E_0, T_2^* and φ_0 are to be measured by varying the pulse parameter q (in practice, only the amplitude of the pulse I_0 is varied). Methods for measurement of other characteristic time constants T_1 and T_2, which are extensively used in classical NMR, need the generation of more than just one pulse and they have not yet been adapted for the PMR. In earlier works, the following correspondence was discovered between measured parameters of the PMR signal and hydrogeological parameters of aquifers (Legchenko et al., 1990; Schirov et al., 1991; Legchenko and Shushakov, 1997): a non-zero PMR signal is linked directly with subsurface water; from $E_0(q)$ measurements, the water content, location and thickness of aquifers may be derived; the decay time T_2^* correlates with the mean size of pores of the water-saturated rocks; the phase φ_0 is sensitive to the electrical conductivity of the subsurface.

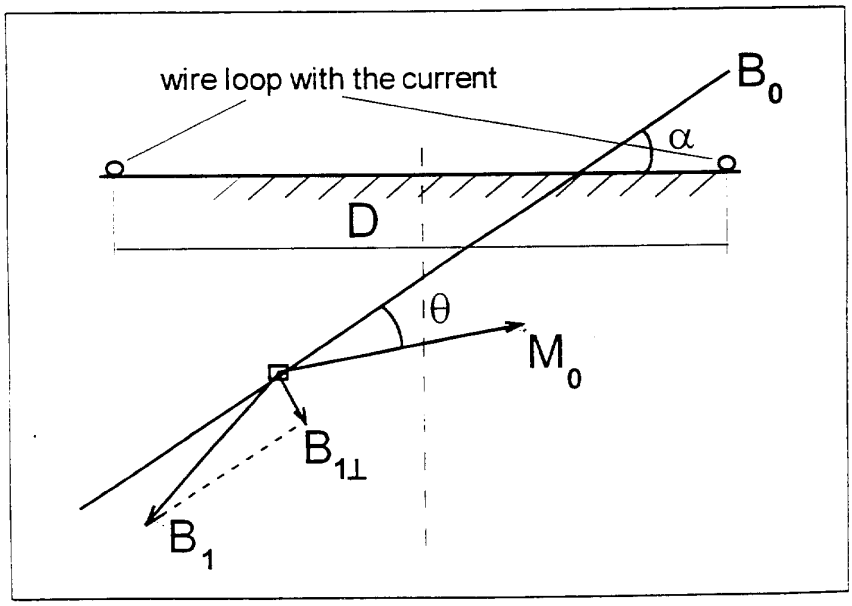

Fig. 1. Nuclear magnetization in a rotating frame.

Assuming homogeneity of the geomagnetic field and horizontal stratification, the signal can be calculated as:

$$E_0(q) = \int_0^\infty K(q,z)n(z)dz \quad , \tag{5}$$

where $K(q,z) = \omega_0 M_0 \int_{x,y} \beta_{1\perp} \sin(\theta) dxdy \quad , \quad \theta = (1/2)\gamma\beta_{1\perp} q \quad ,$

$\beta_{1\perp} = \beta_{1\perp}[\mathbf{r},\rho(\mathbf{r}),\alpha] = \beta_{1\perp}/I_0$, $\rho(\mathbf{r})$ is the rock resistivity, $0 \leq n(z) \leq 1$ is the water content, and $\mathbf{r} = r(x,y,z)$ (Shushakov and Legchenko, 1994a,b; Shushakov, 1996). Protons removed from the antenna at a distance of more than 2D (D is the antenna diameter) produce a negligible small part of the total signal, and for calculations the range of integration in equation (5) may be restricted by $x,y,z \leq 2D$.

Taking into account the fact that the nuclear spin for protons is 1/2, the following equation can be written for nuclear magnetization:

$$M_0 = (\gamma^2\hbar^2/4kT)NB_0 \quad , \tag{6}$$

where $\hbar$ and k are Planck's and Boltzman's constants, respectively, N is the number of protons per unit volume, and T is the temperature. At depths down to about 100-200 m, the number of protons in a bulk water and the temperature usually do not vary much within studied aquifers. However, the geomagnetic field can vary worldwide which significantly changes the value of M_0. From equations (2), (5) and (6) it can be shown that

$$E_0 \sim B_0^2 \quad . \tag{7}$$

The magnetic resonance signal is therefore a quadratic function of the magnitude of the geomagnetic field and it is proportional to a whole number of protons within the volume $x,y,z \leq 2D$.

The time diagram of the pulse transmission and the signal recording is depicted in Fig. 2 (Semenov et al., 1988). With *HYDROSCOPE* the pulse duration is equal to 40 ms and the pause between transmitting and receiving ("dead time") is 40 ms. With *NUMIS* the pulse is programmable and may be varied between 5 and 100 ms, and the "dead time" is 30 ms. The recording time is fixed at 200 ms with *HYDROSCOPE* and may be programmed between 100 and 1000 ms with *NUMIS*. Although with *NUMIS* the pulse duration is programmable, it seems that a 40 ms pulse is rather optimal for an antenna 100 m in diameter.

In aquifers composed by non-magnetic rocks (an important assumption for the PMR application) the decay.time of the magnetic resonance signal depends on the mean size of pores. It may vary between less than 30 ms in a very fine material aquifer (clays with fine sands) and about 1000 ms in a lake (bulk water). An effect of the mean size of pores on the measured signal was studied, taking into account this correlation between the pore size and the decay time. For signals with a decay time less than 200-300 ms, the condition given by inequality (3) is not valid and a more complicated model should be used. However, in this paper we are not going that far and we accept the simplified model also for short signals, assuming that the initial amplitude of the signal $E_0(q)$ is calculated for the instant immediately after the pulse. As the signal can be recorded with the "dead time" delay, it can be written

$$E = E_0 \exp(-t_d/T_2^*) \quad , \tag{8}$$

where E is the recorder amplitude, and t_d is the "dead time". Thus, even the simplified model demonstrates that the decay time T_2^* may affect the water-detection ability of the PMR.

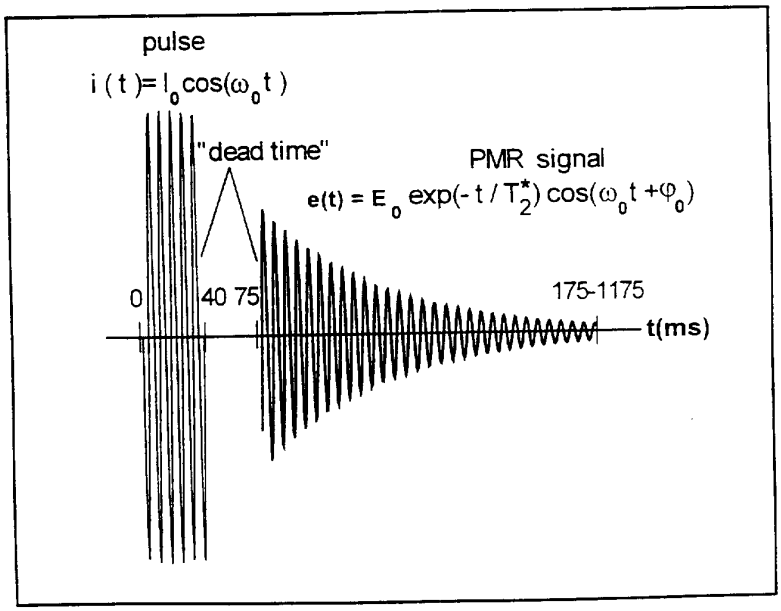

Fig. 2. The time diagram of transmission/receiving sequence.

We are now in a position to write down the most important factors which may have an effect on the measured amplitude of the magnetic resonance signal:

* the magnitude and the inclination of the geomagnetic field;
* the mean size of pores of water-saturated rocks;
* the size of the antenna;
* the electrical conductivity of the subsurface.

The influence of these factors was studied numerically using equation (5). For calculations of the transmitted magnetic field $\beta_{1\perp}$ an enhanced version of the algorithm developed by Newman et al. (1986) is used. Excluding the case when the antenna diameter is varying, a circular antenna 100 m in diameter is used for the modelling. The subsurface is assumed to be a homogeneous non-magnetic half-space of a varying electrical conductivity with a one-meter-thick infinite horizontal layer of a bulk water (the water content n = 1) in it. The electrical conductivity of the water layer is taken to be equal to the electrical conductivity of the half-space.

RESULTS

Experimental evaluation of the model

In order to evaluate the model given by equation (5), measurements from the surface of the frozen Ob reservoir near Novosibirsk city (Russia) were carried out using the *HYDROSCOPE* equipment. In fact, since the late 'seventies these measurements are a routine procedure in ICKC and data presented in this paper aim just to demonstrate with what accuracy the synthetic signal corresponds to the real one. Reliable information about the layer of water below the ice can be easily obtained by direct measurements: the water content is equal to one (n=1); the electrical conductivity of the water in the reservoir is 51 Ohm-m; the ice thickness is about one meter, and the bottom of the reservoir varies around 11 m deep. The decay time of the signal varies between 300 and 800 ms which satisfies the condition given by inequality (3). Measured amplitudes of the PMR signal versus the pulse parameter E(q) [equation (8)] are presented in Fig. 3. To fit the experimental data, the model of two water-saturated layers situated in the 51 Ohm-m half-space was used. The first layer is a water body with n = 1, and it is located at depths between 1 and 11m, which corresponds to the water profile in the reservoir. The depth, thickness, and the water content of the second layer were chosen such that the total signal calculated from the two layers together fits the field data well. This layer is located between 50 and 100 m, and the water content is equal to 0.05. The subsurface below 11 m was not investigated by drilling or other methods, and hence, neither parameters of the second layer nor the electrical conductivity of the subsurface can be justified. While the whole calculated signal from both

model layers fits the experimental data (solid line) well, the signals calculated from each layer separately are also shown in Fig. 3 (dashed lines). It is important to note that the initial part of the experimental curve ($q < 2000$ A-ms), which represents essentially a response from the water of the reservoir (which is reliably checked), is well fitted by the signal calculated from the first model layer alone (which is the model of the water in the reservoir). This fact confirms that our model corresponds sufficiently well to real measurements. Some more details about field experiments over the frozen Ob reservoir are also discussed by Schirov et al. (1991).

Although the simplified model given by equation (5) fits well with the real data measured over the Ob reservoir where signals are long, it surely must give larger errors when signals are short. To solve this problem, a more adequate (and complex) model should be developed. However, for calibration of instruments and models, only measurements over a water body were used so far.

Thus, it may be stated that currently PMR measurements provide quantitative results when signals are long (aquifers are composed of a bulk water, gravel, coarse sand), and qualitative results when they are short (fine-material aquifers). However, because errors induced by the simplified model are regular when aquifers are composed of rocks of a similar nature, variations in the signal throughout the investigated area are caused essentially by variations in the water content, and hence, even qualitative data can be used very efficiently in water prospecting for mapping of subsurface water-saturated zones.

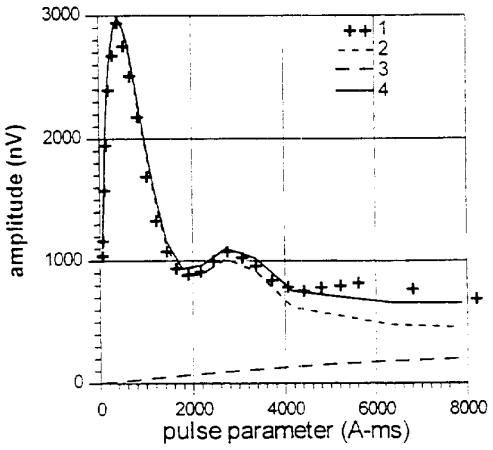

Fig. 3. Field data observed over the frozen Ob reservoir (1) and theoretical signals calculated from: (2) - a water body in the reservoir (located between 1 and 11 m deep, n = 1); (3) - subsurface water-saturated sediments (located between 50 to 100 m deep, n = 0.05); (4) - from both the water and the sediments together.

The type of water-containing rocks

The time records of both the noise and the signal made by *NUMIS* are presented in Fig. 4. No major sources of electromagnetic noises were detected during the field work and data obtained are of a good quality. The first test site, is located in Colorado, U.S.A. The aquifer is essentially composed of a fractured sandstone. The top of the aquifer is at a depth of approximately 75 m. The measured amplitude of the signal is 159 nV and the decay time is 25 ms. The second site is located in France. A water-saturated karst limestone layer between 20 and 50 m deep was found during a BRGM geological study. The measured amplitude of the signal is 230 nV and the decay time is 340 ms. The noise was measured before the pulse and is also depicted in Fig. 4. In both cases, the noise magnitude is less than 20 nV.

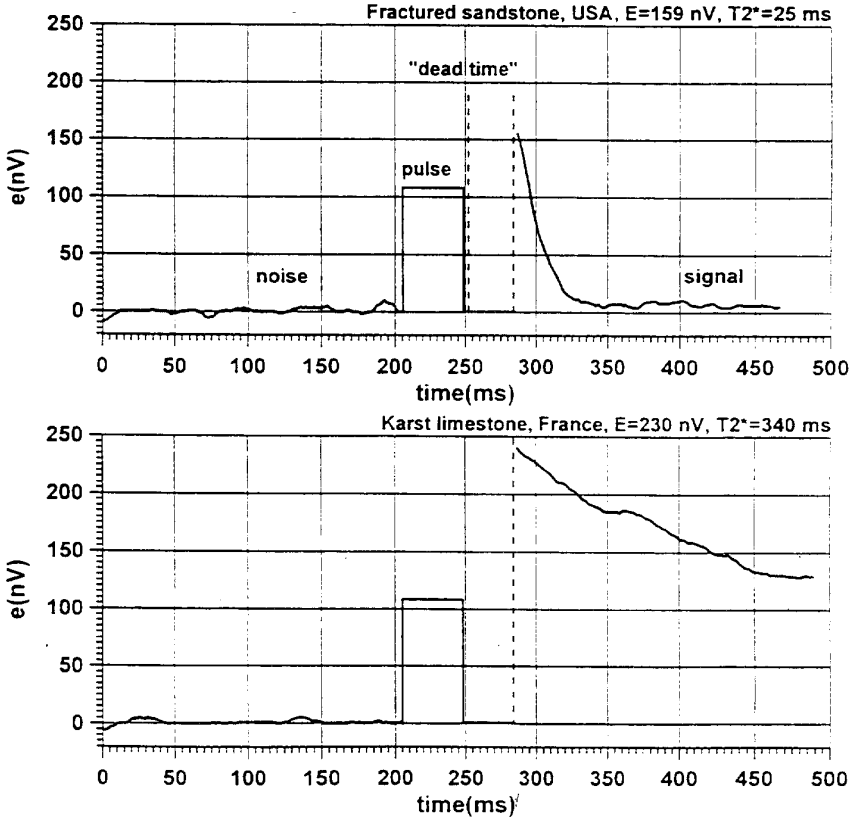

Fig. 4. Examples of noise and signal time records observed over aquifers of different types: fractured sandstone and karst limestone.

Another example of real measurements is shown in Fig. 5. Both the amplitude E(q) and the decay time T_2^* were measured. While the signal from the water-saturated karst limestone aquifer (St. Cyr-en-Val, France) has an average value of the decay time around 250 ms, the signal from the fractured chalk aquifer filled with mud (Saint Brisson sur Loire, France) has a decay time around 40 ms. Yields of the boreholes are about 100 m^3/h in St. Cyr-en-Val and less than 2 m^3/h in St. Brisson, respectively. Taking into account a relatively small difference in the amplitude of the signals measured from these aquifers, it can be concluded that the large difference in the yields is caused by the large difference in the decay times. These examples demonstrate possible variations in the decay time of the magnetic resonance signal caused by a difference in the aquifer material.

Thus, using equation (8) and taking into account that the "dead time" of the equipment is equal to 35 ms, it can be estimated that while the signal decaying with the time constant $T_2^* = 30$ ms will decrease by a factor 3.2, the signal decaying with $T_2^* = 300$ ms will suffer only by a factor 1.12. It gives an about three-fold difference in measured amplitude of the long and short signals while the initial amplitude E_0 is the same.

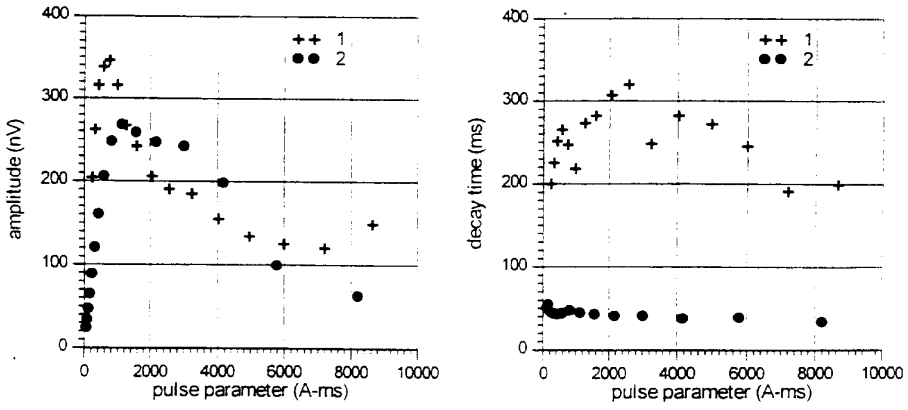

Fig. 5. Examples of field data measured from different aquifers: karst limestone (1) and fractured chalk filled with mud (2).

The geographical co-ordinates of the investigated area

The geographical co-ordinates of the investigated area may affect the PMR measurements through the magnitude and the inclination of the geomagnetic field.

As it was shown, the signal amplitude is a quadratic function of the magnitude of the geomagnetic field [equation (7)]. Since the geomagnetic field varies between 30,000 and 60,000 nT around the world, it causes four-fold changes in the PMR signal. Generally, the geomagnetic field is larger close to the poles (North or South) and smaller close to the equator. Thus, in the same hydrogeological environment the performance of the same PMR instrument depends on the geographical co-ordinates of the test site.

The inclination of the geomagnetic field also changes from the poles ($\alpha = 90°$) to the equator ($\alpha = 0°$) which has an effect on the perpendicular component of the transmitting magnetic field $\beta_{1\perp}$. This effect was studied numerically. The model consists of the one-meter-thick layer of a bulk water (n = 1) in a 500 Ohm-m half-space. The magnitude of the geomagnetic field $\mathbf{B}_0$ is fixed ($B_0 = 60{,}000$ nT) and the inclination may vary ($0° \leq \alpha \leq 90°$). As the initial amplitude of the signal $E_0(q)$ depends on the pulse parameter q and has a distinct maximum, the capability of the PMR to detect water depends on the value which the signal has at its maximum (Legchenko and Shushakov, 1997). The maximum initial amplitude of the PMR signal

$$E_{\theta max} = \max_{q}[E_0(q)] \quad , \quad q_{min} \leq q \leq q_{max} \quad , \tag{9}$$

was calculated versus depth of the model layer for various values of the inclination α [equation (5)]. Results of the numerical simulation are presented in Fig. 6. Thus, the maximum amplitude $E_{\theta max}$ [equation (9)] is sensitive to the inclination of the geomagnetic field α only when the water-saturated layer is located at a depth less than 20-25 m.

It can be numerically estimated what changes in the maximum initial amplitude $E_{\theta max}$ can be caused by difference in the geographical co-ordinates of test sites. The same model of the one-meter-thick layer of bulk water as in the previous case is used. Two extreme cases are compared. One is when the magnitude of the geomagnetic field $B_0 = 60{,}000$ nT and the inclination $\alpha = 90°$, which may correspond to a site located close to the pole (North or South). At a site close to the equator $B_0 = 30{,}000$ nT and $\alpha = 0°$ are assumed. Results of calculations are depicted in Fig. 7. Thus, caused by a difference in the geographical co-ordinates of a test site, the signal amplitude from the same water-saturated layer varies by a factor of 2 to 4 depending on the depth of the layer.

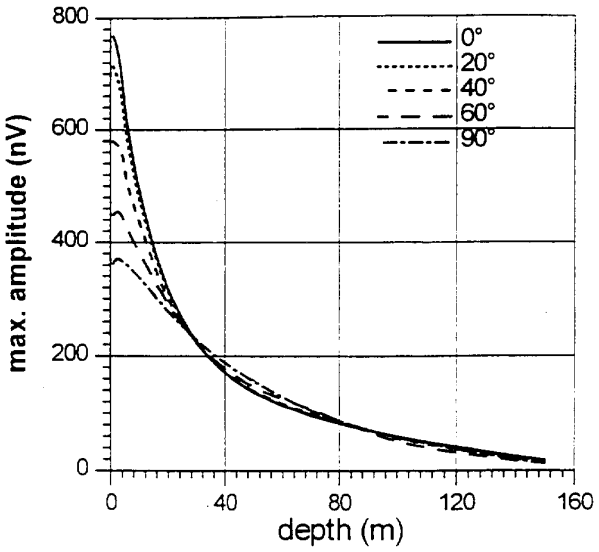

Fig. 6. The maximum signal amplitude calculated for various inclinations of the geomagnetic field.

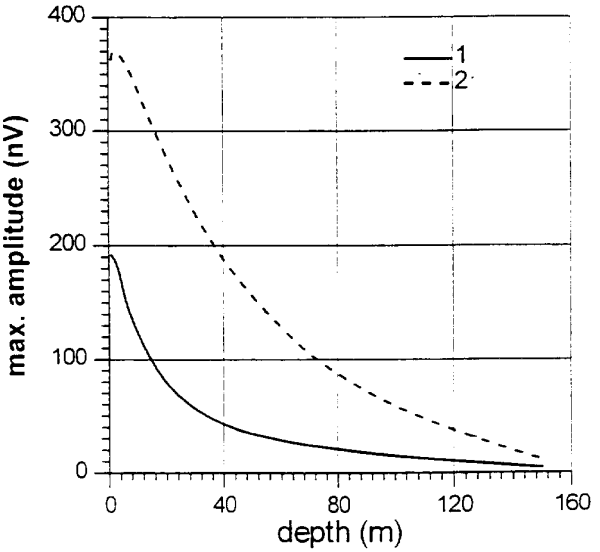

Fig. 7. Extreme variations in the signal caused by variations in the geomagnetic field depending on the geographical co-ordinates of a test site: close to the equator (1) and close to the North (or South) pole (2).

Size of the antenna

The amplitude of the PMR signal is proportional to the total volume of water in the studied aquifer (equations (5 and 6)). In the case of infinite water-saturated layers, water located away from x,y,z ≤ 2D volume contributes a negligible small part of the total signal. However, increasing the diameter of an antenna, the volume of water can be increased and hence, the signal will also increase. For demonstration, the same model of the one-meter-thick infinite layer of water was used. The signal from this layer was calculated varying the antenna diameter. The maximum initial amplitude $E_{\theta max}$ versus layer depth is shown in Fig. 8. Although the signal from infinite layers can be increased by increasing the antenna diameter, when a target is of a limited size relatively to the antenna (water lens), application of a bigger antenna does not increase the volume of water responding to the pulse and hence, may not be followed by increase in the signal.

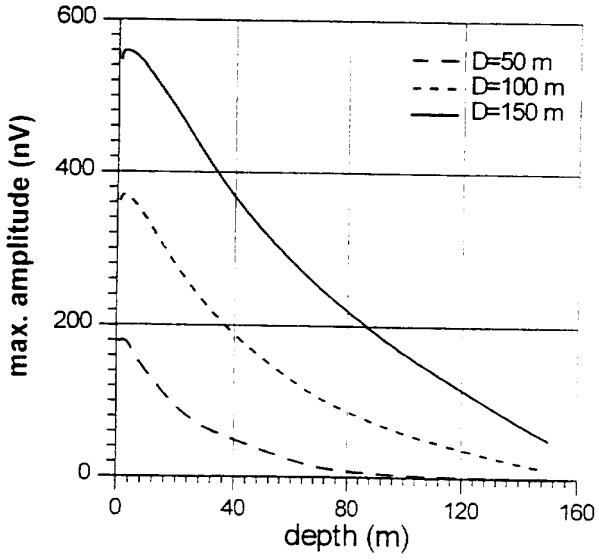

Fig. 8. The maximum signal from the one-meter-thick layer of water calculated versus layer depth for different antennas.

Electrical conductivity of rocks

As the geomagnetic field varies between 30,000 and 60,000 nT around the world, the Larmor frequency f_0 given by equation (2) also varies, between 1300 and 2600 Hz. An electrically conductive subsurface affects alternating magnetic fields and hence, affects also the PMR signal. This effect was studied using the model of the one-meter-thick layer of water in the electrically conductive half-space, with the inclination of the geomagnetic field $\alpha = 90°$ and the Larmor frequency $f_0 = 2{,}500$ Hz. The maximum initial amplitude $E_{\theta max}$ versus layer depth was calculated. Results are presented in Fig. 9. Taking into account that a signal just above a threshold value of 10-20 nV can be reliably detected using either *HYDROSCOPE* or *NUMIS*, the maximum depth of water detection depending on the subsurface can be easily estimated using the plots in Fig. 9.

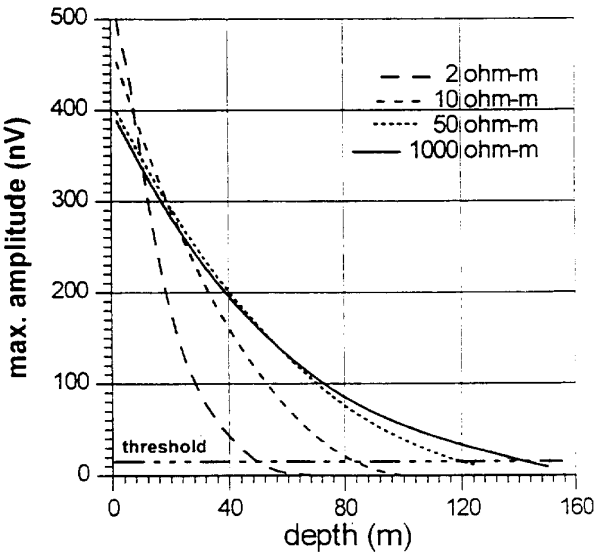

Fig. 9. Variations in the signal from the one-meter-thick layer of water in an electrically conductive half-space calculated for different values of the half-space resistivity. Only signals only above the hardware threshold can be measured.

Extreme variations in the signal

The extreme variations in the amplitude of the PMR signal caused by all the natural factors listed above together can be estimated. In order to take into account the "dead time" for calculations, instead of the maximum initial amplitude E_{0max} the maximum recorded amplitude E_{max} is used

$$E_{max} = E_{0max}\exp(-t_d/T_2^*) \quad . \tag{10}$$

The maximum signal E_{max} versus layer depth is shown in Fig. 10. The signal should range between two extremes: the most favourable case is when measurements are made close to the North (or South) pole (B_0 = 60,000 nT and α = 90°), rocks are non-conductive (500 Ohm-m), and the decay time is long (T_2^* = 800 ms). The most unfavourable case is when a test site is located close to the equator (B_0 = 30,000 nT and α = 0°), the water layer is situated in the conductive half-space (10 Ohm-m) and the decay time is short (T_2^* = 30 ms).

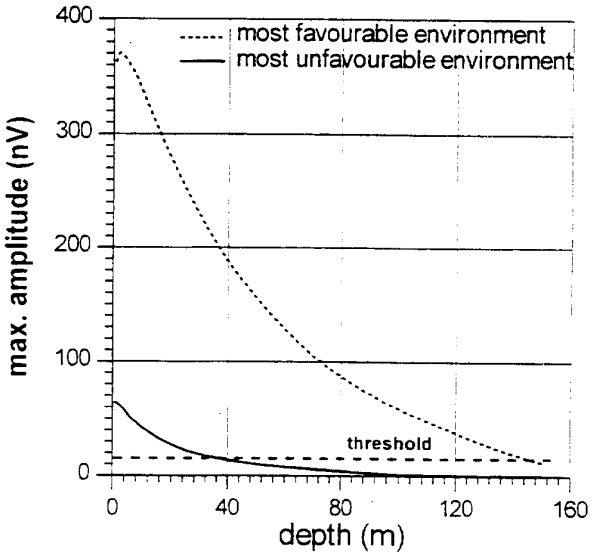

Fig. 10. Extreme variations in the signal from the one-meter-thick layer of water calculated for the most favourable and the most unfavourable environment and the hardware threshold.

A large difference in the amplitude was observed. Thus, the performance of the PMR method may vary and depends on the geophysical environment. However, even in the less favourable case, the recorded signal is large enough to be measured down to 40 meters (the detection threshold for the instrument is around 10-20 nV), which demonstrates that the method can be used successfully even in the most unfavourable environment.

The surface PMR method, used in Russia for water prospecting since 1981, was also tested in other countries (Schirov et al., 1991, Goldman et al., 1994, Lieblich et al., 1994, Legchenko et al., 1995). Measurements were made in northern parts of Russia, where the geomagnetic field is similar to that of the North pole. Water was also detected in India very close to the equator (Semenov, 1987). These results may be considered as an experimental confirmation of the capability of the method to detect water worldwide in a variety of geophysical and hydrogeological environments.

CONCLUSIONS

The influence of natural factors on the PMR signal amplitude was studied. For the numerical simulation, the model consisting of a one-meter-thick layer of a bulk water was used. It was found that:

* the worldwide variations in the geomagnetic field cause variations of the signal amplitude by a factor of 2 to 4 depending on layer depth;
* the signal amplitude measured from aquifers composed of fine rocks (clays, fine sands) may be attenuated by a factor of 3 which is caused by the "dead time" of the equipment;
* the electrically conductive subsurface may decrease the maximum depth of the water detection from 150 m (1000 Ohm-m half-space) to 50 m (2 Ohm-m half-space);
* when aquifers are horizontally stratified the signal amplitude can be increased by increasing the antenna diameter.

The most favourable and most unfavourable conditions for measurements (combinations of the studied natural factors) were compared in-between. It was found that the extreme variations in the studied natural factors may cause the PMR signal from the same layer of water to vary by a factor of 5 to 10 depending on layer depth. This means that the performance of the PMR method largely depends on the conditions of measurements. For example, currently available PMR equipment (*HYDROSCOPE* and *NUMIS*) with an antenna 100 m in diameter is able to detect the one-meter-thick layer of a bulk water down to a depth of 150 m in the most favourable conditions and only down to 40 m in the most unfavourable case.

Even in the most unfavourable conditions, the signal from subsurface water is large enough to be measured and hence the PMR method can be successfully used for aquifer investigations worldwide. However, the real performance of the method should be corrected according to the geophysical environment.

REFERENCES

Goldman, M., Rabinovich, B., Rabinovich, M., Gilad, D., Gev, I. and Schirov, M., 1994. Application of integrated NMR-TDEM method in ground water exploration in Israel. J. Appl. Geophys., 31: 27-52.

Legchenko, A.V., Semenov, A.G. and Schirov, M.D., 1990. A device for measurement of subsurface water saturated layer parameters. USSR Patent 1540515 (in Russian).

Legchenko, A.V., Shushakov, O.A., Perrin, J. and Portselan, A.A., 1995. Noninvasive NMR study of subsurface aquifers in France. Expanded Abstr., 65th Ann. Internat. SEG Mtg., Houston: 365-367.

Legchenko, A.V. and Shushakov, O.A., 1997. Inversion of surface NMR data. Geophysics, in press.

Lieblich, D.A., Legchenko, A., Haeni, F.P. and Portselan, A., 1994. Surface nuclear magnetic resonance experiments to detect subsurface water at Haddam Meadows, Connecticut. Proc. Symp. Applic. of Geophysics to Engin. and Environm. Probl., Boston, 2: 717-736.

Newman, G,A., Hohmann, G.W., Anderson, W.L., 1986. Transient electromagnetic response of a three-dimensional body in a layered earth. Geophysics, 51: 1608-1627.

Schirov, M., Legchenko, A. and Creer, G., 1991. New direct non-invasive groundwater detection technology for Australia. Expl. Geophys., 22: 333-338.

Semenov, A.G., Schirov, M.D. and Legchenko, A.V., 1987. On the technology of subterranean water exploration founded on application of nuclear magnetic resonance tomograph "Hydroscope". Abstracts, IXth Ampere Summer School, Novosibirsk, p. 214.

Semenov, A.G., 1987. NMR Hydroscope for water prospecting. Proc. Seminar on Geotomography, Indian Geophys. Union, pp. 66-67.

Semenov, A.G., Burshtein, A.I., Pusep, A.Yu. and Schirov, M.D., 1988. A device for measurement of underground mineral parameters. USSR Patent 1079063 (in Russian).

Shushakov, O.A. and Legchenko, A.V., 1994a. Calculation of proton magnetic resonance signal of underground water considering medium electrical conductivity. Geol. and Geophysics, 35: 130-136 (in Russian).

Shushakov, O.A. and Legchenko, A.V. 1994b. Ground water proton magnetic resonance in the horizontally stratified media of different electrical conductivity: Geol. and Geophysics, 35: 161-166 (in Russian).

Shushakov, O.A., 1996. Groundwater NMR in conductive water. Geophysics, 61: 998-1006.

Slichter, C.P., 1996, Principles of Magnetic Resonance, 3rd Ed. Springer Verlag, Berlin.

Trushkin, D.V., Shushakov, O.A. and Legchenko, A.V., 1995. Surface NMR applied to an electroconductive medium. Geophys. Prosp., 43: 623-633.

Varian, R.H., 1962. Ground liquid prospecting method and apparatus: US Patent 3019383.

GEOPHYSICS, VOL. 63, NO. 1 (JANUARY-FEBRUARY 1998); P. 75–84, 16 FIGS.

Inversion of surface NMR data

Anatoly V. Legchenko* and Oleg A. Shushakov‡

ABSTRACT

The main advantage of the surface nuclear magnetic resonance (NMR) method compared to other geophysical methods in the field of groundwater investigation is the ability to measure an NMR signal directly from the water molecules. An NMR signal, stimulated by an alternating current pulse through an antenna at the surface, confirms the existence of water in the subsurface with a high degree of reliability. The NMR signal amplitude depends on the pulse parameter (the product of the pulse amplitude and its duration), bulk water volume, and water depth. Measurements are performed while varying the pulse parameter, and subsequent data processing reveals the number of water-saturated layers, and data concerning their depth, thickness, and water content.

One of the major problems in the practical application of the NMR method is the very weak signal (<3000 nV); hence the problem of signal to noise ratio (S/N). S/N can be improved by stacking the signal, but measurement time is increased. We have developed an algorithm that minimizes the number of measurements (number of different values of the pulse parameter) without a loss of inversion accuracy for a given S/N ratio, making it possible to determine a set of optimal pulses for the measurements.

NMR measurements are also sensitive to the electrical conductivity of the subsurface; an electrically conductive subsurface causes variations in the depth of investigation and in the vertical resolution of the method. Experience gained from application of the method has proven that both the inversion algorithm and the analysis of the problem are efficient.

INTRODUCTION

The main advantage of the surface NMR method, compared with other geophysical methods for water prospecting is that the surface measurement of the nuclear magnetic resonance (NMR) signal from water molecules in the subsurface ensures that it only responds to the subsurface water. Used routinely in Russia and tested in other countries (Schirov et al., 1991; Goldman et al., 1994; Lieblich et al., 1994) the method has demonstrated its potential.

Because the parameters of currently available surface NMR equipment, such as Hydroscope (ICKC, Russia) and NUMIS (IRIS Instruments, France), do not permit measurements of the very short signals (less then 30 ms) corresponding to "bounded" water in the subsurface, the vertical distribution of the water content deduced from the NMR data corresponds to the location and amount of "free" water in the aquifers. Free water distribution in the subsurface is a solution of integral equation and, like many other ill-posed problems, the inversion is sensitive to field measurement errors caused by external electromagnetic interferences such as electrical discharges in the atmosphere, magnetic storms, and all kinds of electrical currents through the subsurface. Interferences may also be caused by cultural noise produced by power lines, electrical generators and engines. In addition, the electrical conductivity of the subsurface (the operational frequency is between 1.5 and 2.8 kHz) not only attenuates the signal, but also has an effect on the kernel of the integral equation. Knowledge of this effect is important for the practical application of the method and for data interpretation.

Total time of field work, which is a matter of practical importance, depends largely on the number of measurements required for the extraction of the information from the noise-contaminated data. However, as the relaxation time of the NMR signal in water-saturated nonmagnetic rocks depends on the mean size of the pores and varies from tens to hundreds of milliseconds (Schirov et al., 1991), measurements cannot be repeated more frequently than every few seconds.

To minimize the field work time, we have developed an algorithm for optimizing the number of measurements based on an evaluation of the signal to noise ratio (S/N) using the Tikhonov regularization method for data inversion. We used computer simulation to estimate the performance of the NMR

Manuscript received by the Editor October 10, 1995; revised manuscript received April 25, 1997.
*BRGM-DR/GIG, 3, Avenue C. Guillemin-BP 6009, 45060 Orleans cedex 2, France. E-mail: a.legchenko@brgm.fr.
‡Russian Academy of Sciences, Institute of Chemical Kinetics and Combustion, 3, Institutskaya Street, Novosibirsk, 630090, Russia and Novosibirsk State University, Novosibirsk, Russia.

method over electrically conductive subsurface rocks. With a conductive half-space model, all calculations were performed using a circular 100 m diameter antenna, a vertical geomagnetic field with the magnitude of 58685.45 nT, and the corresponding Larmor frequency of protons in water $\omega_0/2\pi = 2500$ Hz. Natural noises (interference) were simulated by computer-generated random numbers.

THEORY

Quantitative determination of subsurface water

If V is the total volume of the subsurface, V_W is the part of the subsurface filled with water, and V_R is the part of the subsurface occupied by rocks, and we can write $V = V_W + V_R$. Assuming that the water (V_W) and rocks (V_R) are homogeneously distributed in the total volume V, we can use the volume per unit (for example, $V = 1$ m^3) instead of using the total volume of the subsurface. The water (V_W) in a porous medium can be divided into two parts: free water V_F (water which is unattached to grain walls and can be extracted from the rock) and bounded water V_B (water which is captured by grains and cannot be extracted). Thus, we also assume that $V_W = V_F + V_B$. These two parts of subsurface water are distinguished by a fundamental difference in the decay time between the NMR responses from free water and those from bounded water: the signal decay time generated by bounded water is much shorter. Although further research is required to establish a precise relationship between the decay times of the NMR signal and the hydrogeological parameters of water in a porous medium, our experience in NMR application allows us to assume, with sufficient accuracy, that the decay time for bounded water is less than 20–30 ms and for free water it is between 30 and 1000 ms. Parameters of surface NMR equipment currently available, such as Hydroscope (ICKC, Russia) and NUMIS (IRIS Instruments, France), do not permit measurements of the very short signals (less than 30 ms); hence we may say that only signals from the free water (V_F) are measured. Thus, we can tell that the water content is the part of the total volume of the subsurface occupied by the free water: $n = V_F/V$. For example, in a dry rock $n = 0$ and in a bulk water of a lake $n = 1$.

Surface NMR method

A wire antenna is laid out on the ground, normally in a circle with a diameter of between 10 and 200 m, depending on the depth of aquifers; it may also be laid out in a "figure of eight" to improve S/N ratio (Trushkin et al., 1994). The antenna is then energized by a pulse of alternating current

$$i(t) = I_0 \cos(\omega_0 t), \qquad 0 < t \le \tau. \tag{1}$$

where I_0 and τ are respectively the pulse amplitude and duration. The frequency of the current ω_0 is equal to the Larmor frequency of the protons in the geomagnetic field $\omega_0 = \gamma H_0$, with H_0 being the magnitude of the geomagnetic field and γ the gyromagnetic ratio for the protons (the physical constant).

The pulse causes precession of the protons around the geomagnetic field, which creates an alternating magnetic field that can be detected using the same antenna after the pulse is terminated (the free induction decay method). In practice, the NMR response recording is possible after an instrumental delay ("dead time"). The time diagram of the signal measurement process is depicted in Figure 1. Oscillating with the Larmor frequency, the NMR signal $e(t, q)$ has an exponential envelope and depends on the pulse parameter $q = I_0\tau$

$$e(t, q) = e_0(q) \exp(-t/T_2^*) \cos(\omega_0 t + \varphi_0), \tag{2}$$

where T_2^* is the spin-spin relaxation time, and φ_0 is the phase of the NMR signal.

The initial amplitude $e_0(q)$ can be calculated as (Trushkin et al., 1995):

$$e_0(q) = \omega_0 M_0 \int_V h_{1\perp} \sin\left(\frac{1}{2}\gamma h_{1\perp} q\right) n(\mathbf{r})\, dV(\mathbf{r}), \tag{3}$$

where M_0 is the nuclear magnetization for the protons, $h_{1\perp} = H_{1\perp}/I_0 = f(\mathbf{r}, \rho(\mathbf{r}), \alpha)$, with $H_{1\perp}$ being the transmitting magnetic field component perpendicular to the geomagnetic field, α the geomagnetic field inclination, $\rho(\mathbf{r})$ the subsurface resistivity, $0 \le n(\mathbf{r}) \le 1$ the water content, and $\mathbf{r} = r(x, y, z)$ the coordinate vector.

Assuming that stratification is horizontal and the vertical distribution of resistivity is known ($\rho(\mathbf{r}) = \rho(z)$), equation (3) of the signal amplitude e_0 can be simplified to a Fredholm linear integral equation of the first kind written as

$$e_0(q) = \int_0^L K(q, z) n(z)\, dz, \tag{4}$$

where

$$K(q, z) = \omega_0 M_0 \int_{x,y} h_{1\perp} \sin\left(\frac{1}{2}\gamma h_{1\perp} q\right) dx\, dy. \tag{5}$$

Numerical results show that the distant protons produce a negligibly small signal; hence we can limit integration by $x^2 + y^2 \le (2D)^2$ and $L = 2D$, where D is the antenna diameter.

An example of the NMR signal ($e_0(q)$), calculated for a 5-m-thick layer of bulk water ($n = 1$) situated at various depths in the nonconductive half-space, demonstrates the method's capability of determining a subsurface water location caused by the distinct differences in the shape of the signal (Figure 2). Results of NMR signal modeling over a conductive subsurface are also given in Shushakov (1996).

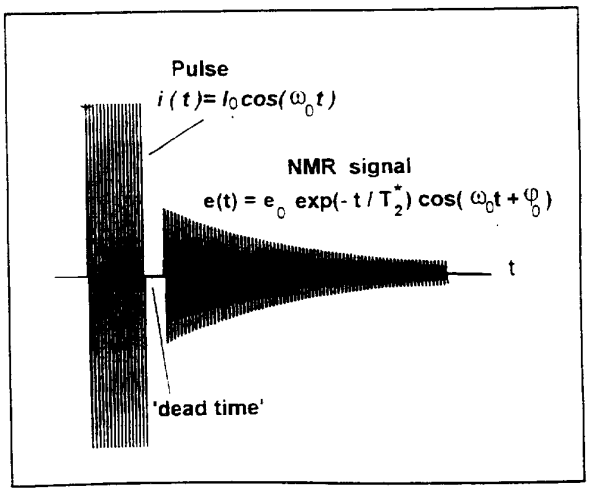

FIG. 1. Time diagram of the NMR signal measurements.

Variation of the geomagnetic field also causes the NMR signal to vary (Trushkin et al., 1993). Here, however, we assume the geomagnetic field to be homogeneous over the whole volume and unchanged during the measurements.

Inversion algorithm

The vertical distribution of water content $n(z)$ is resolved by equation (4). This linear equation may be solved by projecting it onto finite-dimensional subspace, and approximated by the projected equation

$$\sum_j \phi_j(q_i) n_j = e_{0i}, \tag{6}$$

where $i = 1, 2, \ldots, I$, $j = 1, 2, \ldots, J$, and $\phi_j(q)$ is a set of kernel vectors obtained by projecting the kernel $K(q, z)$ on a set of basis functions $b_j(z)$, so that

$$n(z) = \sum_j n_j b_j(z), \tag{7}$$

and

$$\phi_j(q) = \int_0^L K(q, z) b_j(z)\, dz. \tag{8}$$

From a physical point of view, the problem allows the basis functions to be assumed as box-car functions. Hence, the kernel vectors are the elementary responses from the layers of water ($n_j = 1$), characterized by their depth z and thickness Δz. When the depth intervals are

$$0 \le z \le L, \qquad \Delta z_j = z_{j+1} - z_j, \qquad L = \sum_{j=1}^{J} \Delta z_j, \tag{9}$$

the basis functions are

$$b_j(z_j \le z < z_{j-1}) = 1, \qquad b_j(z < z_j, \quad z \ge z_{j+1}) = 0. \tag{10}$$

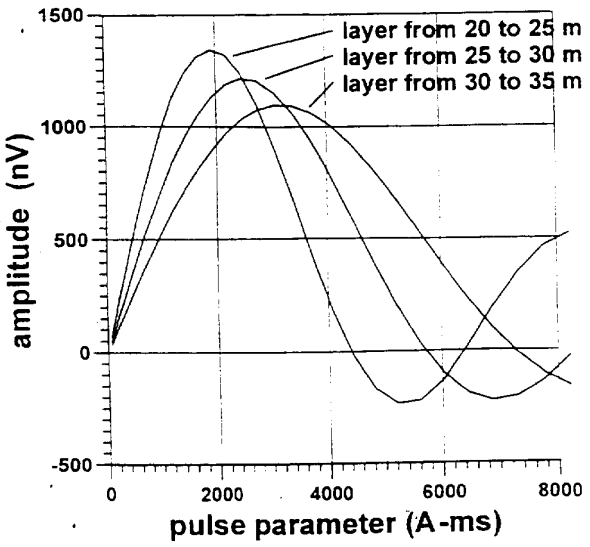

FIG. 2. Initial amplitude of the NMR signal versus pulse parameter, calculated for a 5-m-thick layer of bulk water situated at the depths of 20, 25, and 30 m.

and the kernel vectors are

$$\phi_j(q) = \int_{z_j}^{z_{j-1}} K(q, z)\, dz. \tag{11}$$

The vertical resolution of the method depends on the magnetic field created by the antenna: the larger the gradient of the field, the better the resolution. The magnetic field of the circular antenna with a current passing through is well known; the gradient of the field is large closer to the surface and decreases with increasing depth. Consequently, the resolution of the NMR is also better closer to the surface. The vertical resolution corresponds to thicknesses of the basis functions, and hence,

$$\Delta z_1 \le \Delta z_2 \le \cdots \le \Delta z_j \le \cdots \le \Delta z_J. \tag{12}$$

In a matrix notation, projected equation (6) can be written as

$$\underline{\mathbf{A}}\mathbf{n} = \mathbf{e}_0, \tag{13}$$

where $\underline{\mathbf{A}} = [a_{i,j}]$ is a rectangular matrix of $I \times J$ with the elements $a_{i,j} = \phi_j(q_i)$; $\mathbf{e}_0 = (e_{01}, e_{02}, \ldots, e_{0i}, e_{0I})^T$, $e_{0i} = e_0(q_i)$ being the set of experimental data; and $\mathbf{n} = (n_1, n_2, \ldots, n_j, \ldots, n_J)^T$, $n_j = n(\Delta z_j)$ being the vertical distribution of water content, and the symbol T denoting transposition.

Numerical solution of matrix equation (13) is highly dependent on the choice of basis functions. For a unique and stable solution, the kernel vectors must be linearly independent. In this case, the number of the basis functions is small and, in spite of the uniqueness, such a solution has no practical importance because of a large discretization error. Increasing the number of basis functions reduces the error resulting from discretization, but the stability of the solution suffers because of the ill-conditioning of the problem. To establish a rule for determining the number of basis functions, we use the linear algebra definition: the matrix $\underline{\mathbf{A}}$ is singular if the homogeneous system

$$\underline{\mathbf{A}}\mathbf{v} = 0, \tag{14}$$

has a nontrivial solution. This means that some of the columns (or lines) of matrix $\underline{\mathbf{A}}$ are linearly dependent.

If system (14) does not have a nontrivial solution, we can write

$$\underline{\mathbf{A}}\mathbf{v} = \mathbf{g}, \tag{15}$$

where $\mathbf{v} = (v_1, v_2, \ldots, v_j, \ldots, v_J)^T$ is still an undefined vector, and $\mathbf{g} = (g_1, g_2, \ldots, g_i, \ldots, g_I)^T$ is the linear combination vector. From a practical point of view, it is important to not only know whether the vector $\mathbf{g} = 0$, but also how close it may be to zero. For this purpose, we may estimate the square norm of the vector $\mathbf{g}$ given by the quadratic expression

$$\mathbf{v}^T \underline{\mathbf{C}}\, \mathbf{v} = |\mathbf{g}|^2, \tag{16}$$

where

$$\underline{\mathbf{C}} = \underline{\mathbf{A}}^T \underline{\mathbf{A}}. \tag{17}$$

If there are kernel vectors that are not mutually independent, there are also the vectors $\mathbf{v}$, which make the square norm of the linear combination small, $|\mathbf{g}|^2 \to 0$. The extrema of the quadratic expression (16) are known from matrix theory, and are given if the previously introduced vectors $\mathbf{v}$ are the eigenvectors of the matrix $\underline{\mathbf{C}}$. The values of the expression at the

extrema are the eigenvalues of $\underline{\mathbf{C}}$, corresponding to selected eigenvectors. This can be written as

$$\underline{\mathbf{V}}^T \underline{\mathbf{C}}\, \underline{\mathbf{V}} = \Lambda, \tag{18}$$

where $\underline{\mathbf{V}} = [v_{i,j}]$ is the matrix of eigenvectors, and Λ is the diagonal matrix of eigenvalues of the matrix $\underline{\mathbf{C}}$ with the elements λ_j.

Stability of the matrix $\underline{\mathbf{C}}$ can be estimated using the concept of condition number

$$cond(\underline{\mathbf{C}}) = (\lambda_{max}/\lambda_{min}) \geq 1, \tag{19}$$

where λ_{max}, λ_{min} are the maximum and minimum eigenvalues of the matrix $\underline{\mathbf{C}}$. In general, a linear system with a small condition-number value is more stable than a system with a large one.

For a finite, positive-definite matrix $\underline{\mathbf{C}}$, the largest eigenvalue is

$$\lambda_{max} < \sum_j \lambda_j = \sum_j c_{jj} = Tr(\underline{\mathbf{C}}), \tag{20}$$

where c_{jj} are the diagonal elements of the matrix $\underline{\mathbf{C}}$. These diagonal elements (c_{jj}) are finite-real numbers and they depend mainly on the scaling of the problem. Consequently, λ_{max} depends also on the scaling, and the linear dependence of the kernel vectors does not have much of an effect on λ_{max}. However, $\lambda_{min} = |\mathbf{g}|^2_{min}$ is the square norm of the linear combination vector and may be negligibly small with the same scaling if some of the kernel vectors are linearly dependent. Hence, if some of the kernel vectors are not linearly independent, then $\lambda_{min} \to 0$, $\lambda_{max} \approx const$, and $cond(\underline{\mathbf{C}}) \to \infty$, and the solution becomes unstable. Thus, by varying the linear dependence between the kernel vectors we can influence the stability of the solution.

The linear dependence between any two vectors can be estimated using the correlation coefficient between them

$$r_{j,k} = \frac{\int \phi_j(q)\phi_k(q)\,dq}{\sqrt{\int \phi_j^2(q)\,dq \int \phi_k^2(q)\,dq}}. \tag{21}$$

When the vectors are linearly dependent, $abs(r_{j,k}) \to 1$. The kernel vectors $\phi_j(q_i)$ also are the columns of the matrix $\underline{\mathbf{A}}(a_{i,j} = \phi_j(q_i))$, and the correlation coefficient between two of them is

$$r_{j,k} = \frac{\sum_{i=1}^{I} a_{i,j} a_{i,k}}{\sqrt{\sum_{i=1}^{I} a_{i,j}^2 \sum_{i=1}^{I} a_{i,k}^2}}, \tag{22}$$

where $a_{i,j}$, $a_{i,k}$ are elements of the j and k columns of the matrix $\underline{\mathbf{A}}$.

Now we can express the matrix of the correlation coefficients as

$$\underline{\mathbf{R}} = \underline{\mathbf{D}}\,\underline{\mathbf{C}}\,\underline{\mathbf{D}}, \tag{23}$$

where $\underline{\mathbf{R}} = [r_{j,k}]$ is a matrix of $J \times K$, $J = K$, the elements $r_{j,k} = r_{k,j}$ are the correlation coefficients between the j and k columns of the matrix $\underline{\mathbf{A}}$, and $\underline{\mathbf{D}}$ is the diagonal matrix with the elements

$$d_{j,j} = 1 \Big/ \sqrt{\sum_i a_{i,j}^2}. \tag{24}$$

Thus, when the kernel vectors are not linearly independent $abs(r_{j,k}) \to 1$ and $cond(\underline{\mathbf{C}}) \to \infty$. So, the correlation coefficient between the two most linearly dependent kernel vectors can be used for the matrix stability evaluation. For L_2 norm, $cond(\underline{\mathbf{A}}) = \sqrt{cond(\underline{\mathbf{C}})}$; hence, the linear dependence between the kernel vectors affects not only the stability of the matrix $\underline{\mathbf{C}}$ but also the stability of the matrix $\underline{\mathbf{A}}$.

The kernel vectors $\phi_j(q)$ can be calculated for various depths z_j and thicknesses Δz_j of the basis functions. These vectors depend on the vertical gradient of the magnetic field of the antenna. The greater the difference between z_j and z_k, the more $\phi_j(q)$ and $\phi_k(q)$ are linearly independent because of a greater difference in the antenna magnetic field at these two depths. If the columns of the matrix $\underline{\mathbf{A}}$ correspond to the kernel vectors arranged by increasing depth. Then, taking into account thickness condition (12), we can write

$$r_{j,j} = 1, \qquad r_{j,j-2} < r_{j,j-1} < r_{j,j}, \qquad r_{j,j+2} < r_{j,j+1} < r_{j,j}. \tag{25}$$

This relationship between the correlation coefficients, based on knowledge of the physical property of the problem, can be illustrated by two numerical examples:

1) The depth interval between 0 and 100 m is divided into layers of equal thickness $\Delta z_j = 1$ m. The correlation coefficient, equation (22), was calculated between the layer situated at different fixed depths and all the other layers (Figure 3). The depth of a layer was taken as the depth to the top of that layer. As was expected for layers of equal thickness, the farther apart the layers, the more they are linearly independent.
2) Calculations were performed for a layer with $\Delta z_j = 1$ m, situated at different fixed depths and another layer at the same depth, but with variable thickness (Figure 4). The larger the differences in thickness between the layers, the more they are linearly independent.

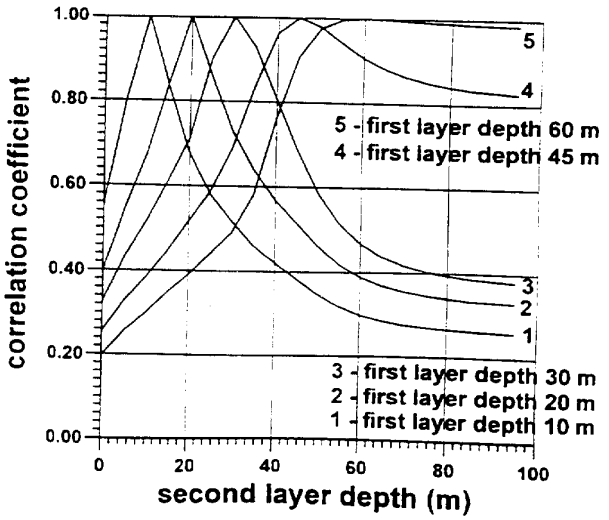

FIG. 3. The correlation coefficient between two signals from 1-m-thick water layers. One layer is held at fixed depths (top of the layer) of 10, 20, 30, 45, and 60 m, respectively, while the depth of the top of the other layer varies.

So, by varying both z_j and Δz_j it is possible to acquire sets of kernel vectors with an expected linear dependence.

We can define the parameter for the discretization of the integral equation as the correlation coefficient between two successive kernel vectors $\phi_j(q)$ and $\phi_{j+1}(q)$, which have a physical sense of the NMR signals from the water layers, situated at neighboring depths. For the matrix $\underline{\mathbf{A}}$, it is the correlation coefficient between the j and $j+1$ columns: $r_{1,2} = r_{2,3} = \cdots = r_{j,j+1} = \cdots = r_{J-1,J} = R$. Discretization with parameter R allows us to determine the maximum number of basis functions with homogeneously distributed linear dependence. When R is fixed, the number of the basis functions J with the depth z_j and the thickness Δz_j for each one is also fixed. We are also sure that the correlation coefficient between any two columns (the kernel vectors) is not more than R. By varying R, it is possible to manage the condition number of the matrix $\underline{\mathbf{A}}$. The matrix $\underline{\mathbf{R}}$ for this special case is symmetric and diagonally dominant

$$\underline{\mathbf{R}} = \begin{bmatrix} 1 & R & r_{1,3} & \cdot & r_{1,k} & \cdot & \cdot & r_{1,K} \\ R & 1 & R & \cdot & r_{2,k} & \cdot & \cdot & r_{2,K} \\ r_{3,1} & R & 1 & \cdot & \cdot & \cdot & \cdot & \cdot \\ \cdot & \cdot & R & \cdot & R & \cdot & \cdot & \cdot \\ r_{j,1} & r_{j,2} & \cdot & \cdot & 1 & \cdot & \cdot & r_{j,K} \\ \cdot & \cdot & \cdot & \cdot & R & \cdot & R & \cdot \\ \cdot & \cdot & \cdot & \cdot & \cdot & \cdot & 1 & R \\ r_{J,1} & r_{J,2} & \cdot & \cdot & r_{J,k} & \cdot & R & 1 \end{bmatrix}. \quad (26)$$

From the matrix $\underline{\mathbf{R}}$ we can conclude that either of the two neighboring elements of the solution n_j, n_{j+1} are equally vulnerable to noise, and can be accurately found only when the parameter of discretization R is accorded with experimental errors so that R becomes smaller as the errors become larger ($0 \le abs(R) \le 1$). When the errors and R stay unchanged, well-separated elements can be resolved with higher accuracy then neighboring ones. Practically, this means that boundaries of water-saturated subsurface layers are always determined with a lower accuracy than those of two layers that are well separated by depth. More information regarding the application of the matrix of the correlation coefficients for linear problem analysis can be found in Tarantola (1987).

Numerical calculations of the condition number of the matrix $\underline{\mathbf{A}}$ versus the correlation coefficient R (Figure 5) confirm the existence of the relationship between the two parameters. The eigenvalues were calculated by the standard Jacobi method (Stoer and Bulirsch, 1980) for $\underline{\mathbf{C}} = \underline{\mathbf{A}}^T\underline{\mathbf{A}}$ matrix and afterwards, as $cond(\mathbf{A}) = \sqrt{cond(\underline{\mathbf{A}}^T\underline{\mathbf{A}})}$, for $\underline{\mathbf{A}}$ itself. To calculate the elements of the matrix $\underline{\mathbf{A}}$, we assume equal thicknesses $\Delta z = \Delta z_1 = \Delta z_2$ for the kernel vectors and their depths $(z_j + \Delta z_j/2)$. By varying Δz, we calculate $\phi_1(q)$, $\phi_2(q)$ so that $r_{1,2} = R$. Subsequently, all layers that follow and their related kernel vectors $\phi_j(q)$ can be deduced easily by varying Δz_j [taking into account thickness condition (12)] to get $r_{j-1,j} = R$.

The condition number of the matrix $\underline{\mathbf{A}}$ can be used for estimating the relative error amplification

$$\sqrt{(|\delta n(z)|^2/|n(z)|^2)} \le cond(\underline{\mathbf{A}})\sqrt{(|\varepsilon(q)|^2/|e_0(q)|^2)}. \quad (27)$$

where $|\varepsilon(q)|^2$ is the experimental data error, $|e_0(q)|^2$ is the signal, $|\delta n(z)|^2$ is the error of the solution, and $|n(z)|^2$ is the solution itself. The condition number is the less optimistic evaluation of the error amplification. Meanwhile, for determining the reasonable number of basis functions, it is also possible to employ the average relative error amplification, as proposed by Twomey (1974)

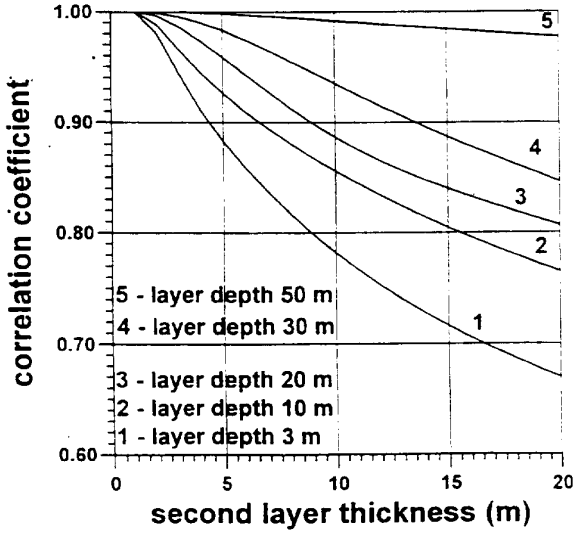

FIG. 4. Correlation coefficient between two NMR signals. One signal is from a 1-m-thick water layer, located at depths (top of the layer) of 3, 10, 20, 30, and 50 m respectively, and the other signal is from a water layer located at the same depth (top of the layer), but with varying thickness.

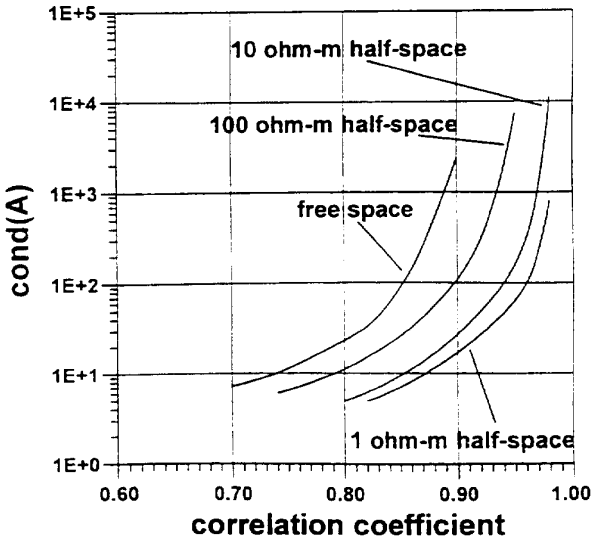

FIG. 5. Relationship between the condition number of the matrix $\underline{\mathbf{A}}$ and the correlation coefficient R as a function of half-space resistivity.

$$k_\varepsilon = \sqrt{(|\delta n(z)|^2/|n(z)|^2)}/\sqrt{(|\varepsilon(q)|^2/|e_0(q)|^2)}$$

$$= \frac{1}{J}\sqrt{\sum_{j=1}^{J}(1/\lambda_j)\sum_{j=1}^{J}\lambda_j}, \qquad (28)$$

where λ_j is the eigenvalues of the matrix $\underline{C}$. The general nature of the result will be unchanged if the criteria are varied, but based on numerical results and practical experience, we use criteria given by equation (28).

The average relative error amplification can be calculated for various values of the correlation coefficient R (Figure 6). There is a relationship between the two parameters, that is quite similar to the one in Figure 5.

We prescribe the relative error of the solution to be $\sqrt{(|\delta n(z)|^2/|n(z)|^2)} = 1$, and assume that this represents a limit where the solution is still reliable. The relative error of the data $\sqrt{(|\varepsilon(q)|^2/|e_0(q)|^2)}$ can be evaluated before the measuring is started. It does not take much time, because the number of measurements for this evaluation can be much smaller than the number of measurements required for inversion. We also assume that the average noise magnitude remains fairly constant during the measuring time, and that it is independent of the pulse parameter. Thus it can be expressed

$$k_\varepsilon = \sqrt{|e_0(q)|^2/|\varepsilon(q)|^2} = S/N. \qquad (29)$$

Knowing S/N, we can find k_ε and subsequently R using the graph depicted in Figure 6. When the basis functions (and hence the kernel vectors) have been determined, the number of measurements may be taken as the same ($I = J$). The values of q can be selected so that the signal is measured by the pulse parameter values corresponding to maximums of the kernel vectors (Figure 7). Some of the kernel vectors are shown in Figure 2, and their maximums are clearly distinguished. Figure 7 shows the relationship between the mean depth of the basis function $(z_j + \Delta z_j/2)$ and the pulse parameter value q_{em}, by which the kernel vector is maximum ($\phi_{j\max} = \phi_j(q_{emj})$). This relationship leads to the determination of the values of the pulse parameter $q_i = q_{emj}$.

Discretization carried out with the correlation coefficient R as a parameter, taking into account S/N evaluation, allows determination of the reasonable minimum number of measurements. It also enables estimation of the vertical resolution for a given S/N because of the existing relationship between the correlation coefficient and the thickness of the basis function. The example of this relationship in Figure 8, calculated for the free-space model, numerically demonstrates the general idea that vertical resolution drops at greater

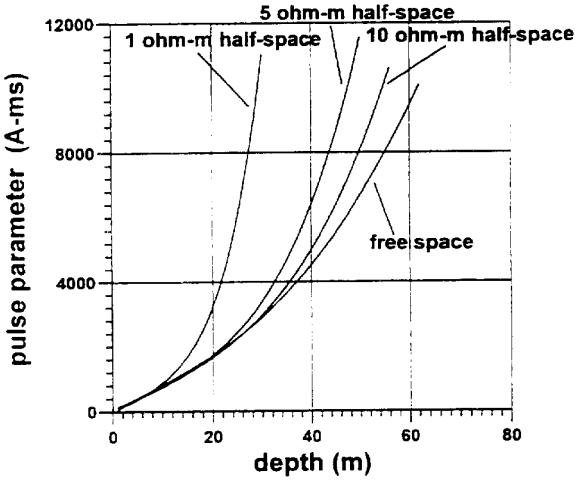

FIG. 7. Relationship between the mean depth of the water-saturated layer $(z_j + \Delta z_j/2)$ and the pulse parameter at the NMR response maximum (i.e., $\phi_{j\max} = \phi_j(q_{emj})$).

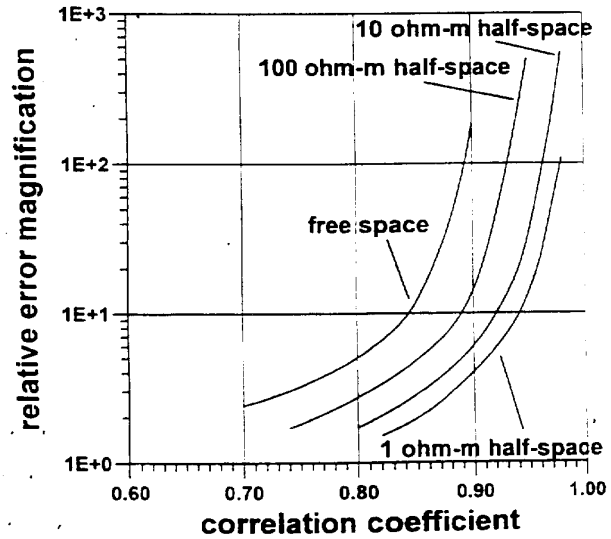

FIG. 6. Average relative error amplification versus correlation coefficient R, calculated for models with various half-space resistivity.

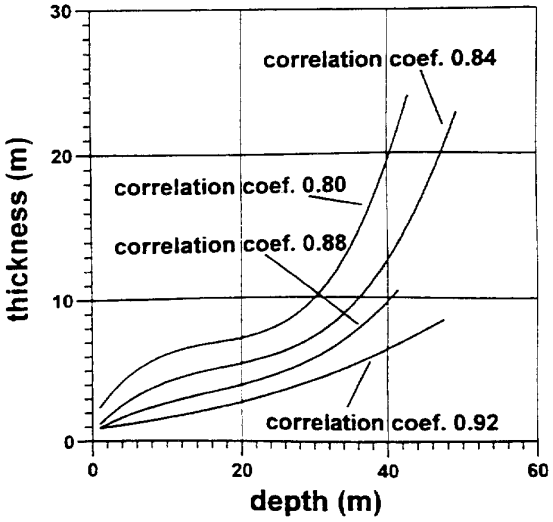

FIG. 8. The thickness of the j model layer (Δz_j) versus its mean depth $(z_j + \Delta z_j/2)$ for various R calculated using the free-space model.

depths. Resolution also depends on S/N, because smaller R values correspond to smaller S/N values.

We can also compare the vertical resolution for half-space models of various electrical resistivity (Figure 9). Calculations were performed with $k_\varepsilon \approx 100$ for each one to eliminate S/N influence and demonstrate only the effect of electrical conductivity. For electroconductive models, the results reveal better resolution close to the surface. This can be explained by a more abrupt change of the antenna magnetic field in a conductive medium. The screening effect, which induces a decrease in the depth of the investigation limit, is demonstrated in Figure 10, where the depth of the top of a 1-m-thick water layer ($n = 1$)

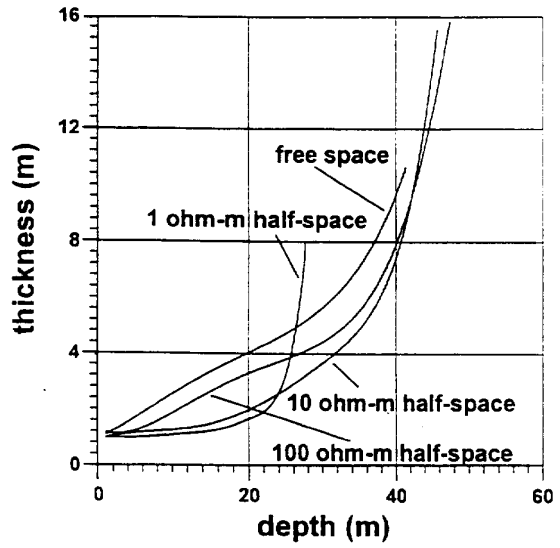

FIG. 9. The thickness of the j model layer (Δz_j) versus its mean depth ($z_j + \Delta z_j/2$), calculated using various half-space resistivity models with average relative error amplification $k_\varepsilon = 100$.

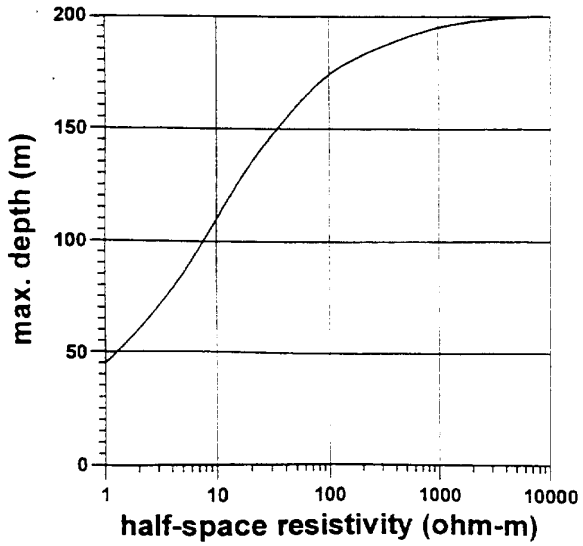

FIG. 10. The maximum depth detection for a 1-m-thick bulk water layer versus the resistivity of the half-space.

is depicted versus the half-space resistivity. The depth was calculated to obtain the maximum initial amplitude of the NMR signal ($q = q_{cm} \leq 12\,000$ A-ms), here equal to 25 nV, which is assumed to be the limit of instrumental sensitivity. We may conclude from Figures 9 and 10 that the influence of electrical conductivity is highly important when the half-space resistivity is less than 10 ohm-m, but that it is considerably less for values greater than 100 ohm-m.

The inversion was carried out according to the well-known Tikhonov regularization method (Tikhonov and Arsenin, 1977). To find an approximate solution of the matrix equation (13), this method supposes minimization of the Tikhonov functional

$$M_\eta(n) = \|\underline{\mathbf{A}}\,\underline{\mathbf{N}}_\eta - \mathbf{e}_{0\varepsilon}\|_{L_2} + \eta\|\underline{\mathbf{N}}_\eta\|_{L_2} = \min. \qquad (30)$$

where the matrix $\underline{\mathbf{A}}$ is a product of the initial linear integral equation (4) discretization, $\mathbf{e}_{0\varepsilon}$ is the vector of the experimental data contaminated by the noise $\varepsilon = \|\varepsilon\|_{L_2}$, $\underline{\mathbf{N}}_\eta$ is the solution vector that minimizes the Tikhonov functional (30), and $\eta > 0$ is the parameter of regularization.

To solve this minimization problem, we followed the discrepancy principle introduced in Morozov (1966), which is based on the fact that for erroneous data, it does not make much sense to have the residual $\|\underline{\mathbf{A}}\underline{\mathbf{N}}_\eta - \mathbf{e}_{0\varepsilon}\|_{L_2}$ smaller than the experimental error. Hence, for a given $\varepsilon > 0$, we need to find a solution with a residual $\|\underline{\mathbf{A}}\underline{\mathbf{N}}_\eta - \mathbf{e}_{0\varepsilon}\|_{L_2} \leq \varepsilon$ and stabilize it by making $\|\underline{\mathbf{N}}_\eta\|_{L_2}$ small. $\underline{\mathbf{N}}_\eta$ is an approximation of the solution of matrix equation (13). When $\varepsilon \to 0$, $\eta(\varepsilon) \to 0$ and $\underline{\mathbf{N}}_\eta \to \underline{\mathbf{N}}$. For the optimization itself, we used the conjugate gradient method (Stoer and Bulirsch, 1980).

We are now in a position to summarise the points discussed above in an algorithm for the measurement and inversion of surface NMR data. The steps for the proposed algorithm are enumerated below:

1) Measure the noise and evaluate $N = \|\varepsilon\|_{L_2}$.
2) Using a few values of the pulse parameter q, estimate the average level of the NMR signal $S = \|e_0\|_{L_2}$.
3) Compute the average relative error amplification $k_\varepsilon = S/N$.
4) Use the relationship between the correlation coefficient and the error amplification $k_\varepsilon = k_\varepsilon(R)$, calculated in advance, to find the correlation coefficient R between the kernel vectors for the given k_ε.
5) Calculate the kernel vectors with the given R.
6) Assuming that the number of measurements is equal to the number of the basis functions, select pulse parameter values so that $q_i = q_{cm_i}$.
7) Using the noise evaluation ε, minimize the Tikhonov functional (30). The vector $\underline{\mathbf{N}}_\eta$ is an approximation of the solution of the initial integral equation (4).

RESULTS AND DISCUSSION

Synthetic data inversion

To numerically demonstrate the performance of the proposed inversion algorithm, we used a two-layer model consisting of two 10-m-thick horizontal, homogeneous, infinite

water-saturated layers situated in free space at depths of 10 and 30 m, respectively. The water content of each layer was taken to be equal to 0.2 ($n = 0.2$), corresponding to 20% of free water, and the Larmor frequency was assumed to be equal to $\omega_0/2\pi = 2500$ Hz. A 100-m-diameter circular antenna was used to calculate the NMR signal. Experimental errors were simulated by adding zero mean random noise to the model data.

The inversion results are presented in Figure 11. Using knowledge of the S/N, an optimal number of the basis functions (J) and hence a minimal number of the measurements ($I = J$) were determined using the correlation coefficient R. This solution (thin solid line) fits the model quite well (dashed line) when S/N = 100. However, when S/N = 2, the fit to the model is very poor. Increasing the number of measurements does not improve the solution for a given S/N significantly, and to demonstrate this, inversion was also performed using a larger number both of the basis functions ($R = 0.94$, $J = 24$) and of measurements ($I = 32$). The solution is shown by the thick solid line. For practical purposes, the two solutions for each value of S/N are similar. However, the number of measurements, and hence the measurement time, are different. An example of the synthetic data (asterisks) used for the inversion (S/N = 10), and reconstructed theoretical signals are presented in Figure 12. All the measurements were employed for inversion with $R = 0.94$ and only those marked by circles for inversion with $R = 0.86$. A good fit is obtained for both the theoretical curves and the model data contaminated by noise, but the solution using $R = 0.86$ is preferable because of the smaller number of measurements.

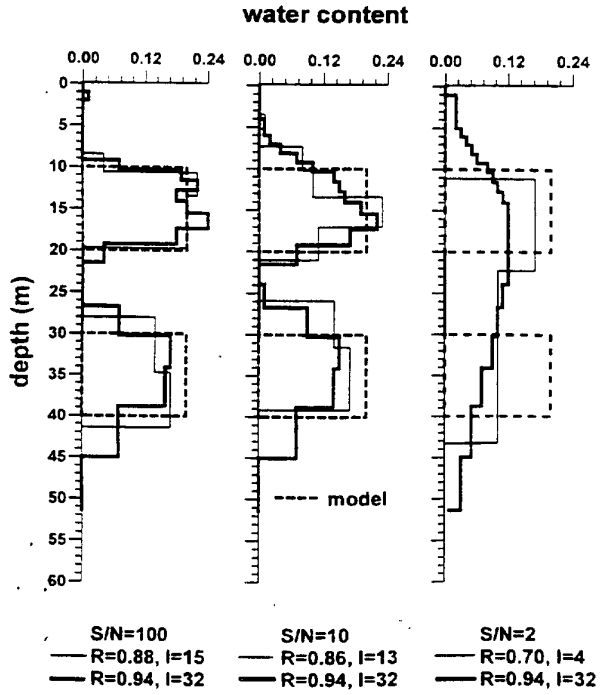

FIG. 11. Results of the inversion of synthetic data with random noise added.

Field data inversion

Field experiments were carried out both in Russia and in France over well-known aquifers.

At the test site near Novosibirsk, Russia, an aquifer consisting of medium- to coarse-grained sand is located approximately between 20 and 40 m. The water is fresh, and the resistivity of the first 50 m is around 50 ohm-m. The resistivity was measured by the dc resistivity method. A more conductive layer of clay below 50 m did not significantly influence the measured normal moveout (NMR) signal. The measurements were performed near borehole N 37. The lithological log of the borehole and the inversion results are presented in Figure 13. The inclination of the geomagnetic field at the test area is approximately 72° and S/N = 48. According to our experience, this level of S/N is high and the inversion results should therefore be reliable. The optimal number of basis functions was found to be 14 ($J = 14$), and hence 14 measurements were chosen ($I = 14$). Inversion with $J = 14$, $I = 14$ is shown by the dashed line in Figure 13. Inversion with $J = 27$, $I = 28$ was also performed (solid line) to demonstrate that there is no fundamental difference between the two solutions. A water-saturated zone detected by NMR between 20 and 50 m coincides quite well with the lithological log. As the practical accuracy of field measurements does not allow accurate detection of layer boundaries at depths below 40 m, it is hard to determine the exact location of the base of the aquifer. Experimental data and reconstructed theoretical signals are presented in Figure 14. They coincide well and demonstrate the accuracy of the inversion. The measurements employed in the optimal inversion ($J = 14$, $I = 14$) are marked with circles.

At the test area of St-Cyr-en-Val, France, three aquifers were determined during a BRGM geological study. The upper aquifer consists of a stratum of mixed gravel, sand, and clay, approximately 20–25-m thick. The two others consist of water-saturated karst limestone separated by a sandstone layer

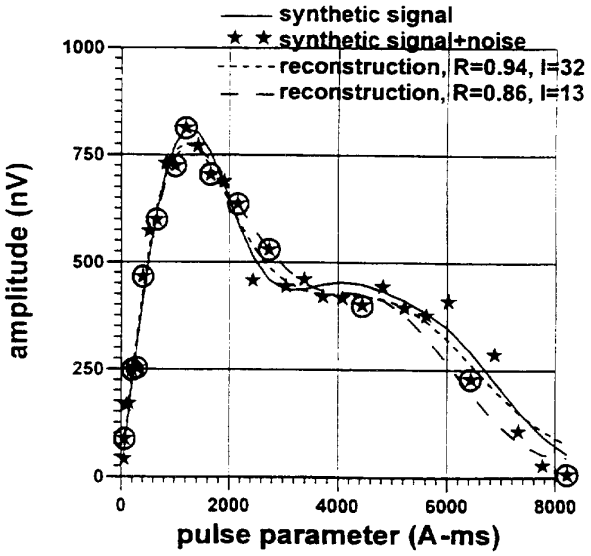

FIG. 12. Synthetic data with random noise added (S/N = 10), and the NMR signal amplitudes reconstructed from inversion results for the model shown in Figure 11.

at a depth of 50–60 m. The total thickness of the karst limestone aquifers is about 40–50 m and the average porosity is approximately 10%. Water transmissivity of the karst limestone is around 0.28 sq.m/s. The lithological log of borehole N 268, situated approximately 600 m from the NMR test site, the surface dc resistivity method and the NMR data interpretation results are presented in Figure 15. The dc resistivity measurements performed did not indicate any significant difference between the borehole site and the NMR test site itself. The noise estimation was S/N = 7.8. For the inversion, we used an optimal ($J = 10$, $I = 10$, dashed line) and a nonoptimal ($J = 27$, $I = 27$, solid line) set of measurements. The matrix $\underline{\mathbf{A}}$ was calculated using the subsurface resistivity vertical distribution data, measured by the dc resistivity method. The geomagnetic field inclination is equal to 62°. Once again, both solutions were found to be similar. The observed difference between the depth of the detected shallow aquifer and the water table may be explained by noise influence on the interpretation results. Because of the lack of a borehole at the test site itself, it is not possible to verify the exact depth and thickness of this shallow, fairly irregular aquifer. The limestone aquifer between 28 and 52 m is quite extensive throughout the area, and is well-detected by NMR. No water was found below 60 m. This negative result may be explained easily by the existence of an electrically conductive shallow layer (approximately 25 m thick, with a resistivity of 9 ohm-m), whose screening effect decreases the depth of investigation. Reconstructed theoretical signals from detected aquifers (Figure 16) correspond well with the true measurements, considering the fairly large dispersion of the noise-contaminated data. The measurements used for the inversion with $J = 10$, $I = 10$ are marked by circles.

CONCLUSIONS

The algorithm of measurement optimization for the surface NMR method, with the correlation coefficient between the kernel vectors as a parameter of the discretization, makes it possible to determine the reasonable minimum number of measurements, and therefore, minimize duration of field measurement without a loss of information for a given S/N. Inversion based on the Tikhonov regularization method is stable within a wide range of signal to noise ratios.

Depth of investigation and vertical resolution depend on the electrical conductivity of the subsurface. Where conductive layers are present, the screening effect, which attenuates the NMR signal, results in a decrease in the depth of investigation. For example, with a 100-m-diameter circular antenna, a vertical geomagnetic field of $\alpha = 90°$, and a Larmor frequency of $\omega_0/2\pi = 2500$ Hz, the maximum depth of investigation varies from 200 m for free space to 48 m for a 1 ohm-m half-space.

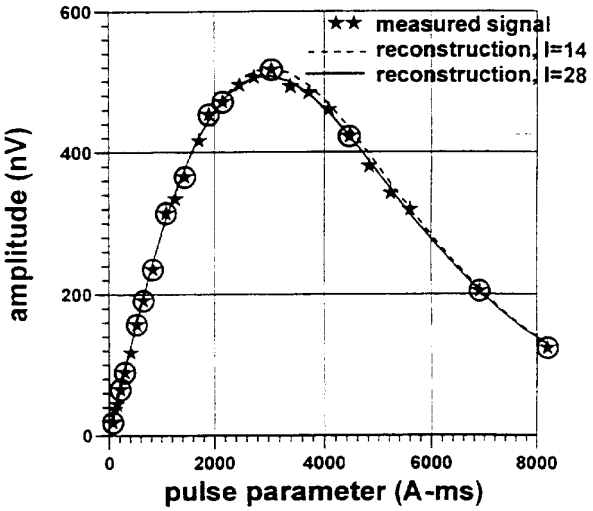

FIG. 14. The NMR field data (asterisks) from the test site at Novosibirsk plotted with the theoretical reconstruction based on inversion results.

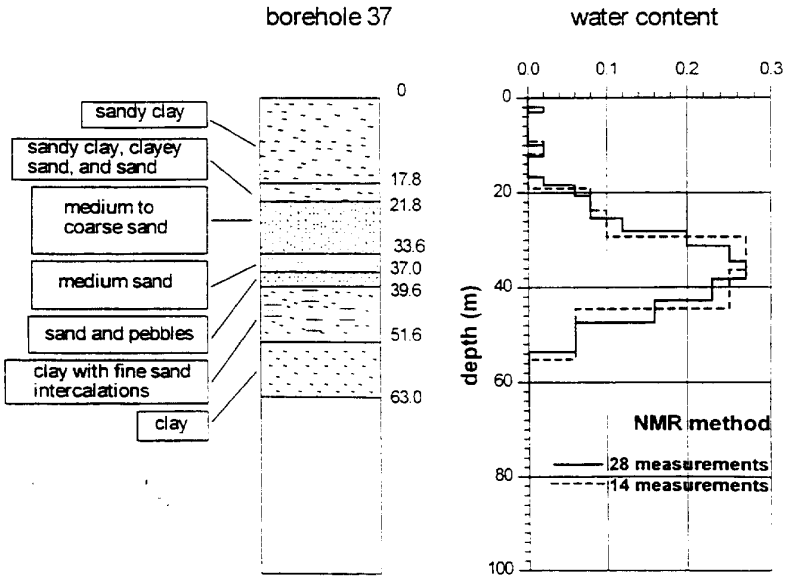

FIG. 13. Lithological log of borehole N 37 near Novosibirsk together with the results from inversion of the NMR field data set.

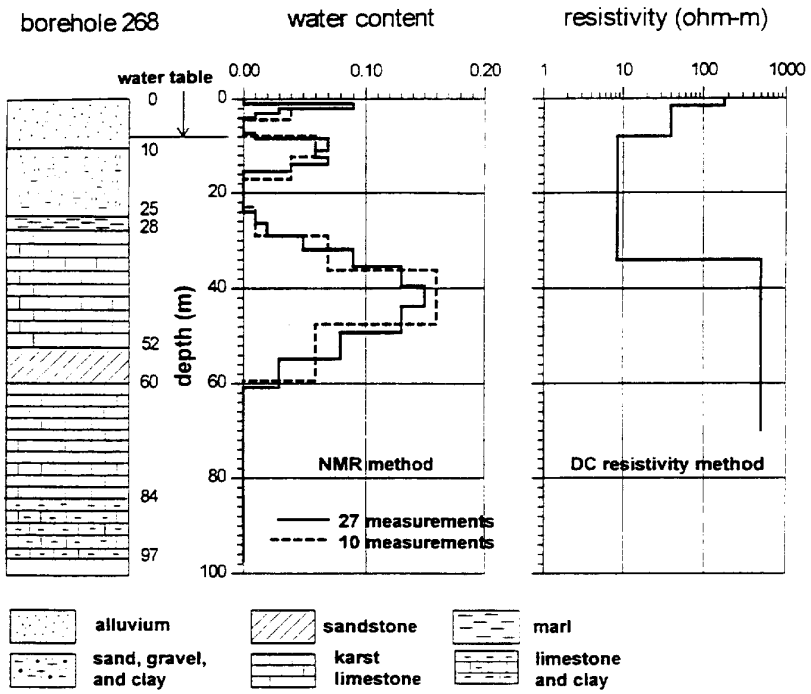

FIG. 15. Inversion results from NMR and dc resistivity soundings and a lithological log from a nearby borehole (N 268) at St-Cyr-en-Val.

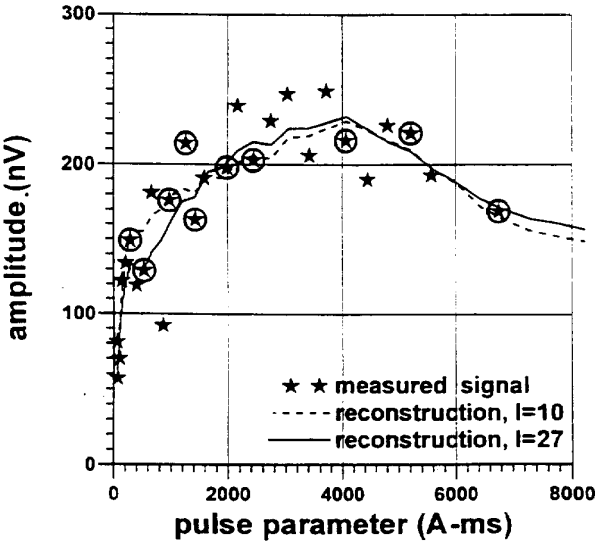

FIG. 16. The NMR field data (asterisks) from the test site at St-Cyr-en-Val plotted with the theoretical reconstruction based on inversion results.

Within the resistivity interval 10 to 100 ohm-m, the maximum depth of investigation varies from 110 to 170 m, respectively.

ACKNOWLEDGMENTS

The authors would like to acknowledge the assistance of BRGM, France, for the results of the NMR field tests and the geological data, and thank A. Straub, A. Beauce and P. Valla for fruitful discussions which helped to improve the paper.

REFERENCES

Goldman, M., Rabinovich, B., Rabinovich, M., Gilad, D., Gev, I., and Schirov, M., 1994, Application of integrated NMR-TDEM method in groundwater exploration in Israel: J. Appl. Geophys., **31**, 27–52.

Lieblich, D. A., Legchenko, A., Haeni, F. P., and Portselan, A., 1994, Surface nuclear magnetic resonance experiments to detect subsurface water at Haddam Meadows, Connecticut: Proc. of Symp. on Application of Geophysics to Engineering and Environmental Problems: Environ. and Eng. Geophys. Soc. **2**, 717–736.

Morozov, V. A., 1966, On the solution of functional equations by the method of regularization: Soviet Math. Doklady, **7**, 414–417 (English translation).

Schirov, M., Legchenko, A., and Creer, G., 1991, New direct noninvasive groundwater detection technology for Australia: Expl. Geophys., **22**, 333–338.

Shushakov, O. A., 1996, Groundwater NMR in conductive water: Geophysics, **61**, No. 4, 998–1006.

Stoer, J., and Bulirsch, R., 1980, Introduction to numerical analysis: Springer-Verlag, Berlin.

Tarantola, A., 1987, Inverse problem theory: Methods for data fitting and model parameter estimation: Elsevier Science Publ. Co., Inc.

Tikhonov, A., and Arsenin, V., 1977, Solution of ill-posed problems: John Wiley & Sons, Inc.

Trushkin, D. V., Shushakov, O. A., and Legchenko, A. V., 1993, Modulation effects in non-drilling NMR in the earth's field: Appl. Magnetic Resonance, **5**, 399–406.

——— 1994, The potential of a noise-reducing antenna for surface NMR ground water surveys in the earth's magnetic field: Geophys. Prosp., **42**, 855–862.

——— 1995, Surface NMR applied to an electroconductive medium: Geophys. Prosp., **43**, 623–633.

Twomey, S., 1974, Information content in remote sensing: Appl. Opt., **13**, No. 4, 942–945.

Paper presented at the EEGS Aarhus'97 Meeting

APPLICATION OF PROTON MAGNETIC RESONANCE FOR DETECTION OF FRACTURED CHALK AQUIFERS FROM THE SURFACE

A.V. Legchenko, J.M. Baltassat, A. Beauce, BRGM, France and **D. Chigot,** Antea, France

ABSTRACT

Direct measurement of Proton Magnetic Resonance (PMR) signal from water molecules guarantees a high reliability of the water detection. It is the main distinction of the PMR compared to other geophysical tools. Interpretation of experimental data reveals location of aquifers, theirs depth and water content. A mean size of pores of the water-saturated rocks can also be estimated.

Currently the method is mostly developed for investigation of sedimentary aquifers. Meanwhile the physical principles of the method allow to use it also for detection of water in fractured rocks and for discrimination among aquifers composed by different types of rock. This field study was performed in order to calibrate the PMR signal generated by water in fractured chalk aquifers.

It was found that the decay time of the PMR signal is the most suitable parameter which can be used for characterization of aquifers. However, the water content is also an important parameter for localization of aquifers and for comparison of bulk volume of water in aquifers composed by similar rocks.

INTRODUCTION

The Surface PMR method for water prospecting was recently developed in Russia and this method is now a subject for further development in BRGM. The main preference of the PMR in comparison with other geophysical methods is a direct correlation of the PMR signal with existence or absence of water.

In order to detect fractured waterfull zones, which can be used for water supply of Saint Brisson sur Loire (France), a field study was performed by BRGM in November-December of 1996. Totally 17 sites around St. Brisson were investigated by PMR. Results of this PMR survey were compared with boreholes data.

METHOD

A wire loop is laid down on the ground. It is energized by a pulse of alternating current

$$i(t) = I_0 \cos(\omega_0 t). \qquad (1)$$

Frequency of the current is equal to the Larmor frequency in the geomagnetic field H_0

$$\omega_0 = \gamma H_0, \qquad (2)$$

where λ is the gyromagnetic ratio for protons. The method is selective and no other response at this frequency can appear. The PMR signal is

$$e(t) = E_0(q)\ \sin(\omega_0 t + \varphi_0)\ \exp(-t / T_2^*), \qquad (3)$$

where T_2^* is the spin-spin relaxation time and φ_0 is the phase. The amplitude $E_0(q)$ and the decay time $T_2^*(q)$ are measured varying the pulse parameter $q = I_0 \tau$, where I_0, τ are the amplitude and duration of the pulse respectively. Joint inversion of the $E_0(q)$ and $T_2^*(q)$ data allows determination of the vertical distributions of water content and decay time.

Using the water content, the bulk volume of water, the depth and the thickness of aquifers can be found. For example, the water content in waterless rocks is equal to zero, and in a bulk water of a lake it is equal to 100%. The decay time correlates with a mean size of pores of water-containing rocks. Empirical relationship between the decay time and the type of rocks is shown in the table (Shirov et al.,1991):

Decay time (ms)	Water containing strata
< 30	sandy clays
30 - 60	clayey sands, very fine sands
60 - 120	fine sands
120 - 180	medium sands
180 - 300	coarse and gravelly sands
300 - 600	gravel deposits
600 - 1000	surface water bodies

RESULTS

Field measurements were performed by the NUMIS PMR instrument. During this survey an antenna in a shape of figure eight was used. The maximum depth of investigation with this antenna is approximately 40-50 meters.

Geology of St. Brisson area is presented by chalk overlaid by rather irregular 5-20 meter thick layers of clay and sand. If the upper part of the chalk is fractured, it might contain water. These fractured zones are used for water supply. Sand and clay aquifers also can be saturated by water, but yield of these aquifers is relatively small and unstable (Chigot, 1996).

In order to demonstrate capability of the PMR to discriminate aquifers composed by different rocks we present here results obtained over three sites. The PMR data were compared with borehole data. Site 1 presents a fractured chalk aquifer fulfilled by mud. Yield of the borehole on this site was found to be less than $1 m^3/h$. This type of aquifer can not be used for water

supply. The borehole drilled on site 2 produces $18m^3/h$. On this site the aquifer is composed essentially by fractured chalk. This type of rock can be used for water supply and it is a target for water investigation. Sand and clay aquifer on site 3 is rather irregular and is not a matter of our interest. Results of field measurements (the amplitude and the decay time) are depicted in Figure 1. The signal (and hence the water) was detected in all three sites. The largest amplitude was found on site 1 which corresponds to the largest volume of water. But the smallest decay time indicates that most of the water in this aquifer is bounded and we should expect rather low yield for a borehole (and this was proved later after drilling). Sand and clay aquifer on site 3 produces the longest signal (the largest decay time) and from the PMR data we may expect better yield than on site 1. But sand lenses are hydraulically separated in this area and after a short period of time the borehole produces almost nothing. The decay time on site 2 was found to be about 80 ms. Measurements over fractured chalk aquifers at few other sites also indicated a decay time of about 80-100 ms. With some degree of reliability this decay time value can be used as a specific characteristic of the waterfull fractured chalk.

Inversion results are shown in Figure 2. They generally correspond well to aquifers detected by boreholes. Reconstructed theoretical signals shown in Figure 1 by solid lines fit well experimental data.

CONCLUSIONS

Field measurements in St-Brisson area demonstrated that in complicated hydrogeological environment (different types of water-saturated rocks), reliable detection of presence or absence of subsurface water is not sufficient for resolving water supply problems.

In order to calibrate the PMR response different aquifers in St-Brisson area were investigated. It was experimentally found that a decay time of 80-100 ms may characterize fractured chalk aquifers useful for water supply purposes. Aquifers which generate signals with decay times lower than 60 ms can also be composed by fractured chalk, but they do not produce much water. Decay times greater than 150 ms correspond to water-saturated sand aquifers. The water content is a less reliable characteristic of the aquifers. It can be explained by the fact that bounded water also gives a PMR response but this water can be hardly extracted from the aquifer.

In general, a decay time of 80-100 ms can be also found over sedimentary aquifers. Hence it cannot be used as the unique parameter for discrimination of fractured zones everywhere without signal calibration.

REFERENCES

Chigot, D., 1996, Compte rendu da la campagne de sondage de reconnaisance réalisée sur la commune de Saint Brisson sur Loire (45), rapport ANTEA, Novembre 1996. (in French)

Shirov, M., Legchenko, A., and Creer, G., 1991, New direct non-invasive ground water detection technology for Australia: Expl. Geophys., **22**, 333-338.

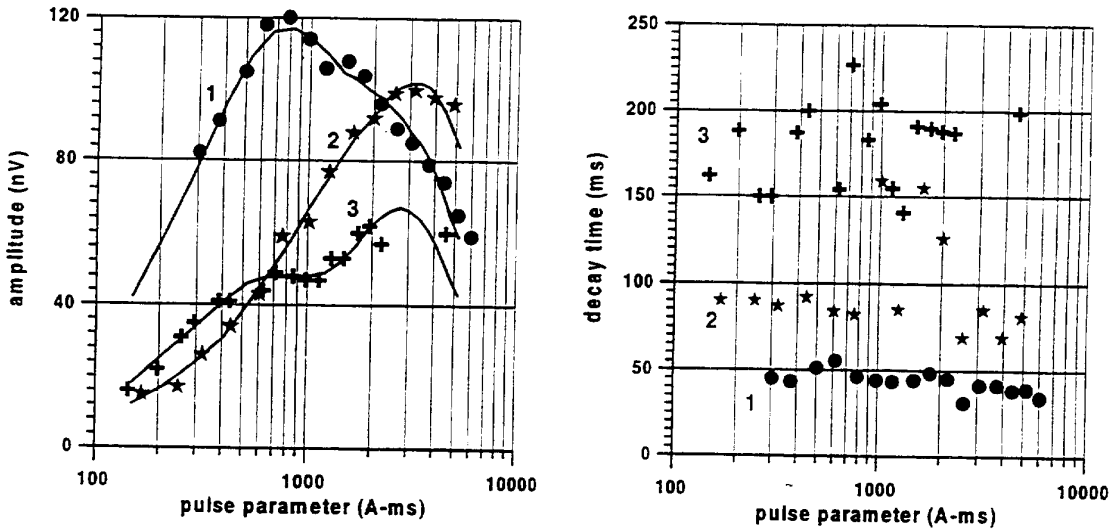

FIG.1. Measured parameters of the PMR signal. 1 - fractured chalk fulfilled with mud; 2 - fractured chalk; 3 - sand and clay. Solid line - theoretical signal calculated using results of inversion.

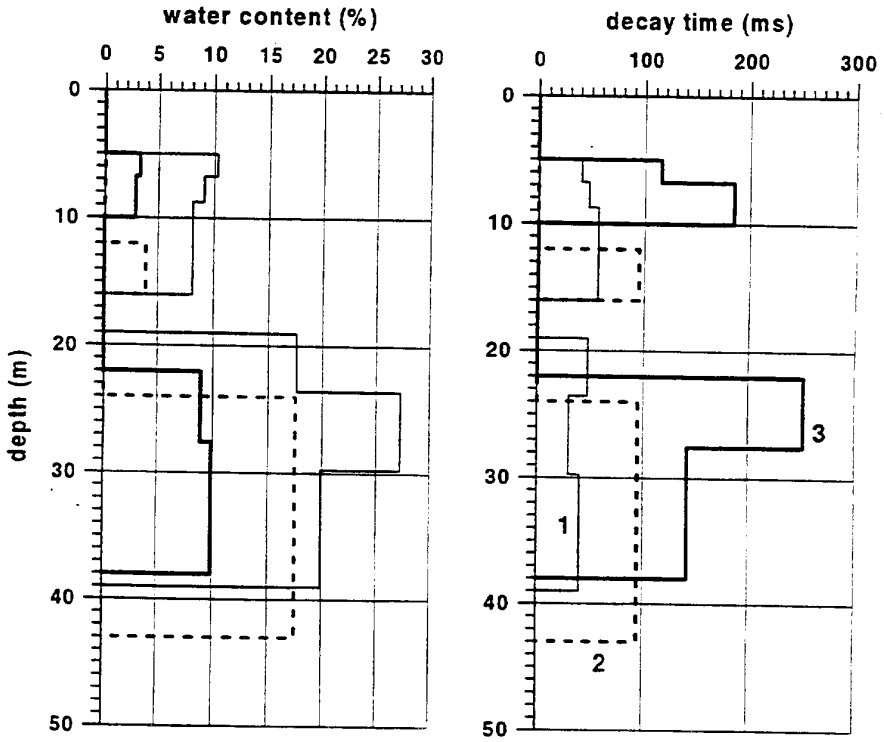

FIG.2. Inversion results. 1 - fractured chalk fulfilled with mud; 2 - fractured chalk; 3 - sand and clay.

Paper presented at the SEG Dallas'97 annual meeting

Inverse problem of Magnetic Resonance Measurements applied to Water Resource Characterization

Antonio Guillen and Anatoly Legchenko, BRGM*

Summary

Proton Magnetic Resonance (PMR) is probably the only known surface geophysical method that allows direct detection of groundwater. It also determines important informations such as the number of aquifers, theirs depths, thickneses and water content. These informations are given by the solutions of the inverse problem. The problem is ill-posed which means nonuniqueness of the solution. Analysis of possible variations of the solution caused by external noises, provides an important information for measurements interpretation.

In order to find possible variations of the parameters of detected aquifers within a given accuracy of measurements, the linear programming was applied. Using ideas proposed by Parker in 1975 for gravity data interpretation, similar criteria were developed for the PMR problem.

A few examples of both synthetic and real data inversion demonstrate application of the developed criteria to interprete PMR data. Results were compared with those obtained by commonly used Tikhonov regularization method.

Introduction

The Proton Magnetic Resonance (PMR) is a particular case of the Nuclear Magnetic Resonance (NMR) phenomenon. In this special case no other nuclei than protons are employed. The main distinction of the PMR is a direct detection of groundwater from the surface. Interpretation of PMR measurements is based on resolving of the inverse problem; this, in turn, involves various relevant hydrogeological parameters such as the water content, the depth, and the thickness of detected aquifers.

With some assumptions, the problem is a linear one. Currently the Tikhonov regularization method for inversion of the PMR data is used. It gives solution based on an estimation of the accuracy of measurements. However, we can also obtain other solutions restricting geometry of water-saturated layers. Solutions obtained with these restrictions may reveal extremities of the solutions space (possible variations of the solution) within a given accuracy of measurements.

For the demonstrations we used synthetic data and then applied the method to real data measured in the vicinity of a borehole (St. Godon community in France). For both synthetic and real cases we used an antenna in a shape of an eight figure, but application of other antenna does not change the general nature of the results.

Method

A 314-m-long wire is laid down on the ground in a shape of the figure eight and is used as both transmitting and receiving antenna. It is energized by a pulse of alternating current of specific frequency $\omega_0 = \lambda H_0$ (Larmor frequency). Precession of the nuclear magnetization of protons M_0 around the geomagnetic field, caused by the pulse, creates an alternating magnetic field of the Larmor frequency, which is measured after the pulse is terminated (Legchenko, et al., 1995). The amplitude of the signal is (Trushkin et al., 1995)

$$E_0(q) = \omega_0 M_0 \int_V h_{1\perp} \sin(\frac{1}{2}\lambda h_{1\perp} q) n(\mathbf{r}) d\mathbf{r}, \qquad (1)$$

where $q = I_0 \tau$ is the pulse parameter, $h_{1\perp}(\mathbf{r}, \rho(\mathbf{r}), \alpha)$ is a component of the antenna's magnetic field perpendicular to the geomagnetic field and created by $I_0 = 1A$, $\rho(\mathbf{r})$ is the rock resistivity, α is the inclination of the geomagnetic field, $n(\mathbf{r})$ is the water content and $\mathbf{r} = r(x, y, z)$.

Inverse Problem of Magnetic Resonance Measurements

If we have M measurements of the signal and assume a horizontal stratification, then equation (1) can be discretized and written as : $E_{0j} = \sum_i G_{i,j} n_i, \qquad i = 1,2,..,N, \qquad (2)$

where N is the number of the model layers, $G_{i,j}$ is the Green's function for a pulse q_j

$$G_{i,j} = \omega_0 M_0 \int_{x=-\infty,y=-\infty,z=z_i}^{x=+\infty,y=+\infty,z=z_{i+1}} h_{1\perp} \sin(\frac{1}{2}\lambda h_{1\perp} q_j) d\mathbf{r}, \qquad (3)$$

where z_i and z_{i+1} are the depth of the top and of the bottom of a layer i respectively , and $0 \le n_i \le 1$ is the water content in the layer i . Equation (2) can be written in a matrix form as

$$\mathbf{GN} = \mathbf{e}, \qquad (4)$$

where $\mathbf{G} = \left[G_{i,j} \right]$, $\mathbf{N} = (n_1, n_2, .., n_N)$ is a vector of the solution, $\mathbf{e} = (e_1, e_2, .., e_M)$ is a vector of measured data.
The subsurface may be divided into two groups: aquifers ($n_i > 0$) and dry rocks ($n_i = 0$). So, the problem of aquifers localization is related with quantitative determination of the water content which is the solution of matrix equation (4).

Consider now that measurements were performed with a noise ε. In this case the Tikhonov regularization method can be used. It gives an unique and in some term optimal solution with erroneous data using accuracy of measurements. This method assumes a minimization of the Tikhonov functional (Tikhonov and Arsenin, 1977).

However, many other solutions than those given by regularization solutions can be found within given accuracy of measurements. Choice of one of them largely depends on taken assumptions about solution. For inversion of measured data with added restrictions of the solution the linear programming technique can be used (Cuer and Bayer, 1980). It supposes resolution of the linear system

$$\begin{cases} E_{0j} - \varepsilon \le G_{i,j} n_i \le E_{0j} + \varepsilon \\ 0 \le n_i \le 1 \end{cases} \qquad (5)$$

In addition to system (5) other constrains may be established by looking for parameters which characterize the groundwater distribution i.e depth, thickness and water content in each aquifer. In our work, we used ideas proposed by (Parker, 1975), (Cuer and Bayer, 1980), and by (Guillen and Minichetti, 1984) for gravity data inversion.

The following restrictions of the solution were used for solving system (5):

1. The top of the aquifer (z_{top}) is the top of the water-saturated layer k ; such that $n_i = 0$ when $i < k$, and $n_i > 0$ when $i = k$. This evaluation will give us the maximum depth that should be drilled in order to reach a water-saturated interval: this is an important economic consideration in exploration.

2. The bottom of the aquifer (z_{bot}), is the bottom of the water-saturated layer l ; such that $n_i > 0$ when $i \le l$, and $n_i = 0$ when $i > l$. This evaluation will give us the minimum depth that needs to be drilled to intersect the aquifer.

3. Δz_{max} is the maximum possible thickness of a uniform water-saturated layer associated with the data. Thus, for $k \le l$, $n_i = 0$ when $i < k$; $n_i > 0$ when $k \le i \le l$; $n_i = 0$ when $i > l$; $n_k = n_{k+1} = .. = n_l$, and $l - k = \max$. This solution allows us to determine the maximum thickness of the aquifer and consequently the minimum value of the water content (n_{min}).

4. Δz_{min} is the thickness of the most compact distribution of water. Thus, for $k \le l$, $n_i = 0$ when $i < k$; $n_i > 0$ when $k \le i \le l$; $n_i = 0$ when $i > l$; $n_k = n_{k+1} = .. = n_l$, and $l - k$ = min. This solution also gives us the maximum value of the water content (n_{max}).

Examples

An example of synthetic data interpretation is shown in Figure 1. The model consists of one water-saturated layer at the depth between 10 and 20 m. The water content is 0.2. Inversion was performed for three different values of the computer generated random noise using both the regularization and the linear programming method. As it was expected, solutions obtained by both methods are close to the model with smaller magnitude of the noise and are less accurate with increasing noise levels.

The real data interpretation is presented in Figure 2. In the test site (St. Godon, Loiret, France) one aquifer was intersected by the borehole. The aquifer is composed essentially by fractured chalk. The water table is 13.4 m, the bottom of the aquifer is 50 m. The most productive part of the aquifer is located between 35 and 50 m, and the yield of the borehole is 18 m^3/h. Average magnitude of the noise was about 20 nV, while the signal was varying between 20 and 80 nV. By both methods the bottom of the aquifer was not detected. It can be explained by a lack of resolution at 50 m (the max. depth of investigation with the antenna we used is about 50 m). According to the borehole data the water saturation increases from 17 to 35 m depth and remains stable down to 50 m, what corresponds well to increase in the water content for regularization method. The linear programming results show that the top of the aquifer should be located deeper than 8 m (z_{top}) and the bottom deeper than 31 m (z_{bot}). The water content can vary between 0.09 and 0.35 (n_{min} and n_{max}) and the thickness between 8 and 30 m (Δz_{min} and Δz_{max}). The minimum thickness solution indicates that the depth of middle of the water-saturated interval should be at 28 m.

Conclusions

Application of the linear programming together with the regularization method for interpretation of magnetic resonance measurements allows better localization of observed aquifers. While the Tikhonov regularization method provides the unique solution based on the estimation of noise, the linear programming allows analysis of possible variations of depth, thickness and water content of detected aquifers within a given accuracy of measurements.

These algorithms can be used with a PC which means that interpretations can be made in real time in the field. Generalization to the non-tabular 2D case and even to the 3D case can be considered without any theoretical or practical specific difficulty.

Acknowledgements

We would like to thank A. Beauce and J.M.Baltassat of BRGM for their participation in preparation of this presentation.

References

Cuer, M. and Bayer, R., 1980, Fortran routines for linear inverse problems: Geophysics, **45**, 1706-1719.
Guillen, A. and Menichetti, V., 1984, Gravity and magnetic inversion with minimization of a specific functional: Geophysics, **49**, 1354-1360.
Legchenko, A.V., Shushakov, O.A., Perrin, J. and Portselan, A.A., 1995, Noninvasive NMR study of subsurface aquifers in France: Abstracts of The International Exposition and SEG 65th Annual Meeting, October 9-12, 1995, p.365-367.
Parker, R.L., 1975, The theory of ideal bodies for gravity intrpretation: Geophys.J.Roy.Astr.Soc., **42**, 315-334.
Tikhonov, A. and Arsenin, V., 1977, Solution of ill-posed problems: John Wiley & Sons, Inc.
Trushkin, D.V., Shushakov, O.A. and Legchenko, A.V., 1995, Surface NMR applied to an electroconductive medium: Geophys.Prosp., **43**, 623-633.

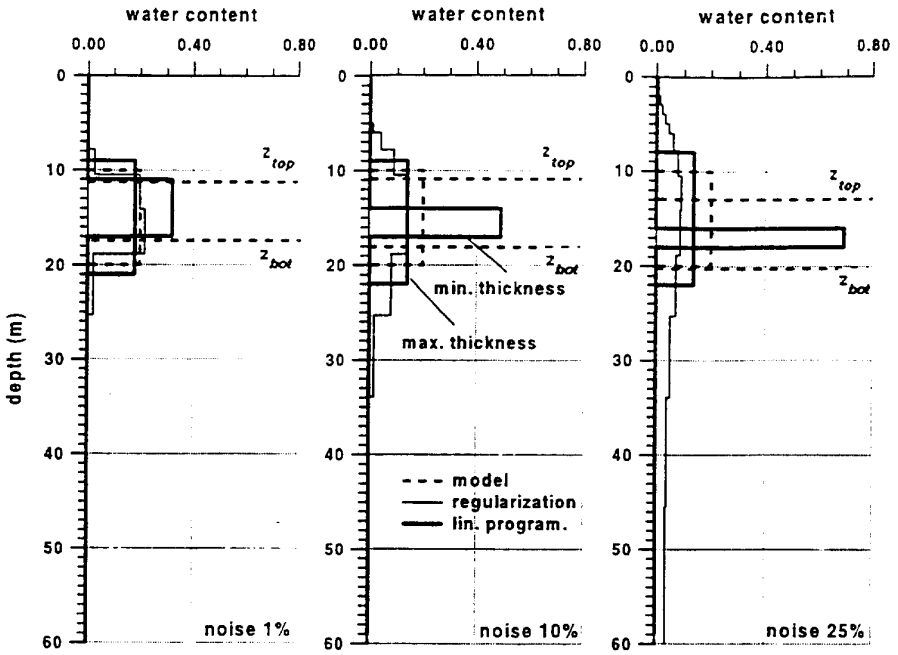

Fig.1. Example of synthetic data interpretation.

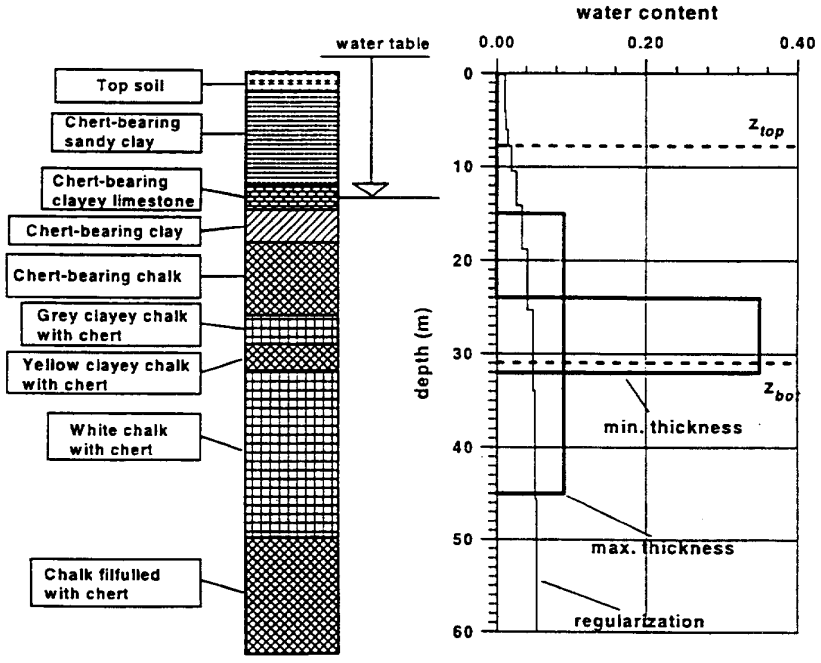

Fig.2. Example of real data interpretation.

DEVELOPMENT OF A PROTON MAGNETIC RESONANCE EQUIPMENT FOR GROUNDWATER INVESTIGATIONS

A. LEGCHENKO, A. BEAUCE, P. VALLA *BRGM **
J. BERNARD, G. PIERRAT *IRIS INSTRUMENTS ***

The Proton Magnetic Resonance method (PMR), also known as the Nuclear Magnetic Resonance method (NMR), is a property of Hydrogen protons which produce a magnetic field when they are excited by an alternative field in the presence of a static magnetic field. Most Hydrogen atoms located in the ground coming from water molecules, the direct detection of water can be envisioned from surface measurements with such a method, while conventional geophysical methods only provide structural information.

PRINCIPLE OF THE PMR METHOD

In the PMR method, <u>three magnetic fields have to be considered</u>:

- The Earth's field, the amplitude of which determines the precession frequency of the protons.
- The excitation field, produced by a current into a loop laid on the surface of the ground, at a frequency equal to the precession frequency (called the Larmor frequency).
- The relaxation field produced by the protons excited by the previous field. The amplitude of the relaxation field measured at the surface after the excitation current is turned off, is directly linked to the number of protons which have been excited and thus to the water content.

<u>The precession frequency f_0 of the protons</u> subjected to the Earth's magnetic field H_0 is determined by the relation:

$$f_0 = H_0 \gamma / 2\pi$$

where g the gyromagnetic ratio of the protons [$\gamma = 0.268$ Hz/nT]

<u>The decay of the relaxation field</u> produced by the protons after the excitation current has been turned off is given by the relation:

$$E = E_0 \exp(-t / T_2^*) \sin(2\pi f_0 t + \varphi_0)$$

where T_2^* is the time constant of the decay and φ_0 is the phase shift between the excitation current and the relaxation voltage measured in the loop. T_2^* is of the order of a few tens milliseconds for clay bound water and of the order of a few hundreds milliseconds for pore free water.

* BRGM: Av. de Concyr - BP 6009 - 45060 ORLEANS 02, FRANCE
Phone: (+33) 2.38.64.34.34 Fax: (+33) 2.38.64.35.18
** IRIS INSTRUMENTS: 1, avenue Buffon - BP 6007 - 45060 ORLEANS02, FRANCE
Phone: (+33) 2.38.63.81.00 Fax: (+33) 2.38.63.81.82

The measuring process includes the following steps:

The transmitting antenna consisting of a 100m diameter loop is laid on the ground, allowing a depth of investigation of the order of 100m.

The value of the excitation frequency is determined in relation with the amplitude of the local Earth's magnetic field. This frequency varies between 1.5 and 3.0 kHz.

The excitation current is transmitted into the loop with intensities up to 200-300A during pulses of a few tens milliseconds, at the excitation frequency.

The relaxation field of the protons is measured in the same loop, after the excitation current is turned off ; **The voltage measured** in the loop is of the order of a few tens to a few thousands nanovolts. Stacking is used to enhance the signal.

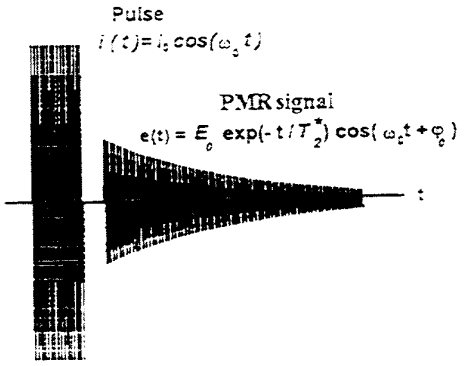

PULSE AND PMR SIGNAL

PMR MODELIZATION AND DATA INTERPRETATION

The pulse moment (product of the intensity of current at the resonance frequency by the duration of the pulse) controls the depth of investigation of the measurement. A PMR sounding corresponds to the signal values obtained for a whole set of pulse moments.

The sounding effect of PMR measurements can be shown with a synthetic model: a three layer model has been used to represent an aquifer (20% water) included between two dry layers (0% water). The thickness of the water bearing layer has been fixed to 10 m in all cases ; its depth increases from 10 to 30, 50 and 70 m. The position of the maximum of the response is indeed shifted to the right side (high values of pulse moment) when the depth of the water layer increases.

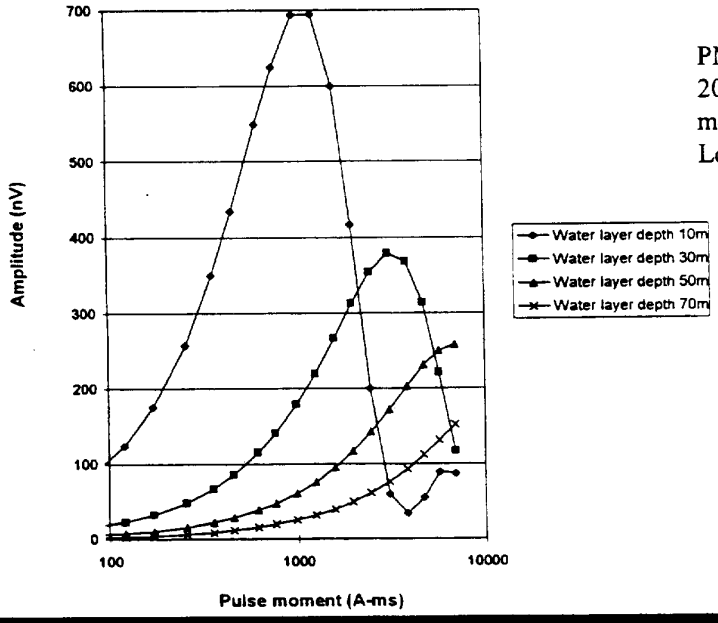

PMR response of a 10m thick layer with 20% water content, as a function of pulse moment, for various layer depths.
Loop diameter is 100m.

The amplitude E_0 of the voltage measured just after the excitation current has been turned off (t=0) is:

$$E_0 = \int_v 2\pi f_0 H_\perp(r) M_0 f(r) \sin\left(\frac{\gamma}{2} H_\perp(r) q\right) dv$$

where:

M0	is the magnetic moment of the water molecules
f(r)	is the water content
q	is the pulse moment (intensity x duration)
$H_\perp(r)$	is the component of the excitation field perpendicular to the Earth's field for a unitary current (I = 1A)

In the latter equation, it can be seen that the excitation field appears not only as a multiplicative term in the integrand which is usual in Physics, by also as an argument in a sine function, which is less usual and corresponds in fact to the proper response of the proton to the excitation.

The wavelength of this sine function depends, on the one hand, on the excitation field $H_\perp(r)$ which is depth dependant, and on the other hand, on the pulse moment (q): it is therefore understandable **that the depth of investigation of the system** is closely related to the pulse moment. In practice, for a given value of the pulse moment, the main part of the signal comes from the deepest arch of the Sine function, whose position in depth is proportional to the pulse moment: lower moments thus lead to shallow investigations, while higher moments lead to deeper investigations.

DESCRIPTION OF THE PMR EQUIPEMENT

A new technology equipment, NUMIS, based on this PMR method has been recently developed in the framework of a cooperation between ICKC (Russia), BRGM and IRIS INSTRUMENTS (France).

The NUMIS equipment consists of:

- a converter unit powered by two 12V batteries,
- a transmitter-receiver unit for pulse generation and signal measurement,
- a wire loop used both as a transmitting and a receiving antenna,
- a PC computer for the control of the whole system and for data processing and interpretation.

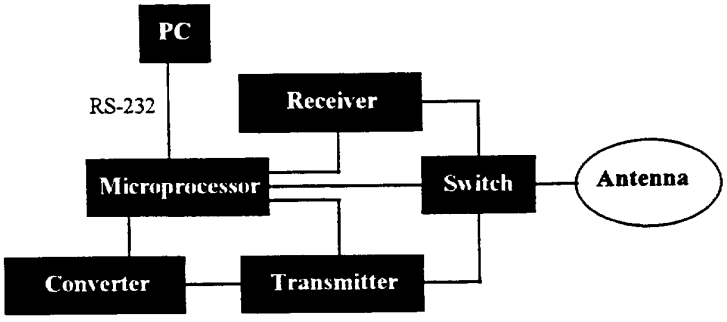

NUMIS SCHEMATIC DIAGRAM

For interpreting a PMR sounding, it is assumed that the underground is stratified at the scale of the loop dimentions. The inversion gives estimates of the water content, the mean pore size (deduced from the decay time constant of the relaxation field), and the depth of each layer.

The NUMIS equipment has been tested in France at Bazancourt site (fractured chalk) and at St Cyr en Val (karztified limestone) with shallow water levels in both cases. The interpretation of PMR measurements shows a good agreement with known geological data.

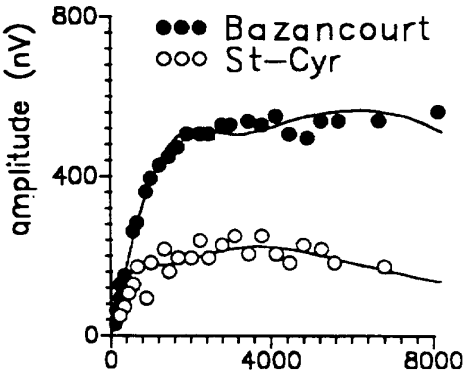

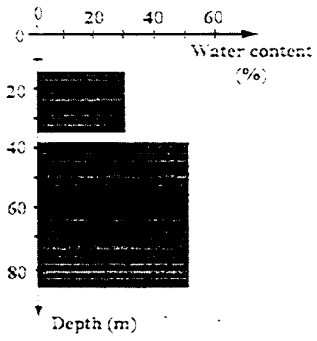

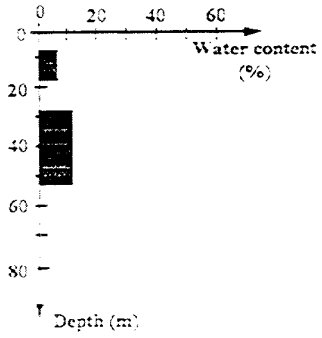

Bazancourt data interpretation *Saint-Cyr data interpretation*

Other field tests carried out in Nevada and Southern California pointed out aquifer layers at depth down to 80-100 m.

CONCLUSION

The PMR method is very promising for assessing the hydrogeological interest of aquifer layers. The NUMIS equipement has confirmed its capability of reaching depths of investigation down to one hundred meters. More tests will be carried out to check the response of the PMR method in various hydrogeological backgrounds.

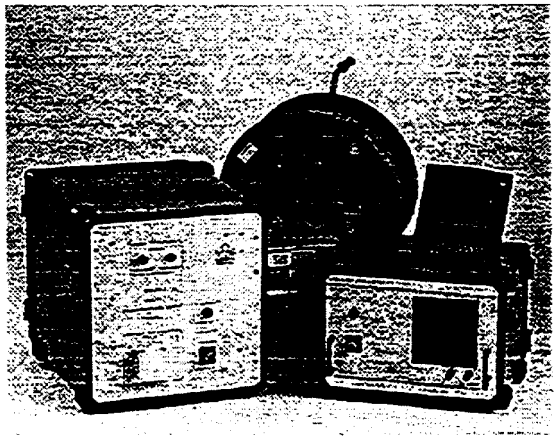

Nantes - France

2, 3, 4, 5 septembre 1996

Environmental and Engineering Geophysical Society European section

CAPABILITY OF THE NMR APPLIED TO AQUIFERS INVESTIGATION FROM THE SURFACE

Anatoly Legchenko, Alain Beauce, Antonio Guillen, Pierre Valla, BRGM, Orléans, France
and **Jean Bernard,** IRIS Instruments, Orléans, France

Introduction

Initial idea to transform the well known proton magnetometer into a tool for water prospecting from the surface belongs to R.H. Varian (Varian, 1962). This idea was realised much later by a team of Russian scientists under the guidance of A.G. Semenov (Semenov et al., 1987, Semenov, 1988). The Surface NMR Method is used in Russia for water prospecting since 1981. It also was tested in other countries (Shirov et al., 1991, Goldman et al., 1994, Lieblich et al., 1994, Legchenko et al., 1995). The method allows not only to detect the presence or absence of subsurface water-saturated layers but also to locate aquifers and study the water content and mean size of pores of each one.

In this paper we present a numerical evaluation of depth of investigation and vertical resolution of the method depending on the latitude of a test site. Practical examples demonstrate the NMR signal records over aquifers of different types.

Method

A 100-m-diameter wire loop is energized by a pulse of oscillating current. The carrier frequency of the current is equal to the Larmor frequency $\omega_0 = \lambda H_0$ in the geomagnetic field $\mathbf{H}_0$. The transmitted oscillating magnetic field causes nuclear magnetization of the protons to shift away from its equilibrium position along the geomagnetic field. After the pulse is terminated the NMR signal

$$e(t) = E_0(q)\ \sin(\omega_0 t + \varphi_0)\ \exp(-t/T_2^*) \qquad (1)$$

can be recorded using the same antenna. As λ is the gyromagnetic ratio for the protons, no other response will appear. The initial amplitude E_0, the decay time T_2^* and the phase φ_0 must be measured.

Assuming homogeneity of the geomagnetic field and horizontal stratification, it can be written:

$$E_0(q) = \int_0^L K(q,z)n(z)dz, \qquad (2)$$

where $K(q,z) = \omega_0 M_0 \int_{x,y} h_{1\perp}\ \sin(\frac{1}{2}\lambda h_{1\perp} q)dxdy$, $q = I\tau$ is the pulse parameter and I, τ are respectively the pulse amplitude and duration, $h_{1\perp}(\mathbf{r}, \rho(\mathbf{r}), \alpha)$ is a component of the antenna's

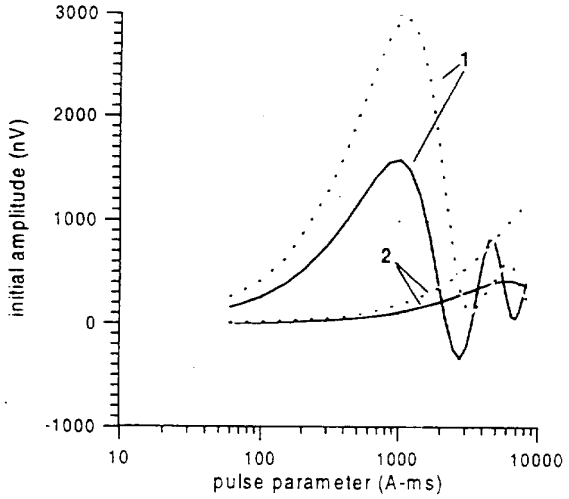

Fig.1 Calculated NMR signal.

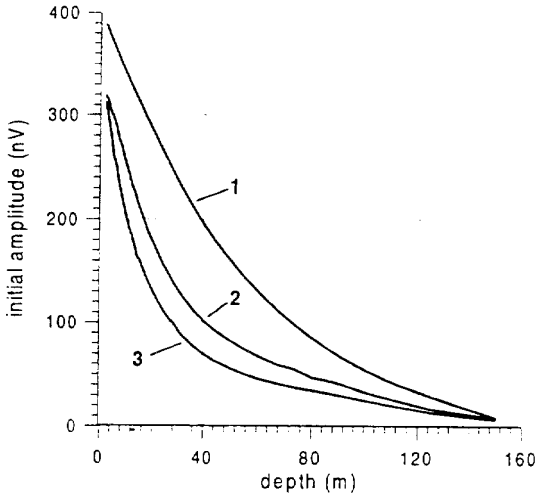

Fig.2 Max. amplitude of the NMR signal.

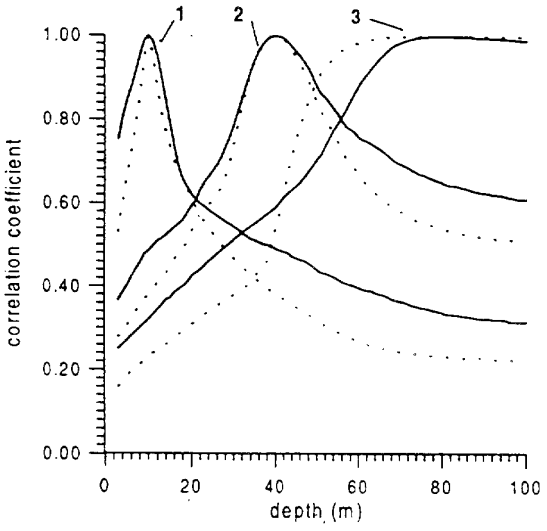

Fig.3 Correlation between calculated signals.

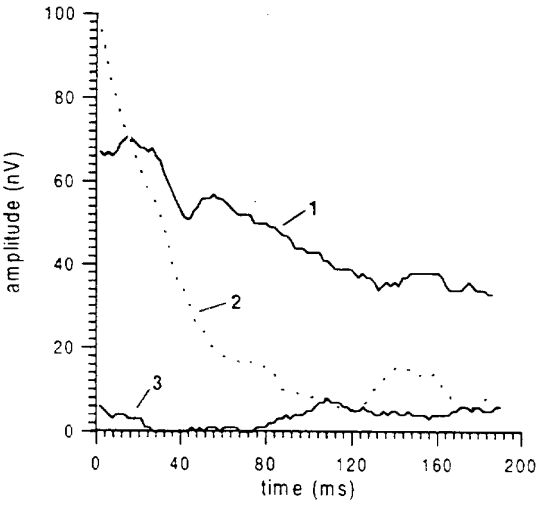

Fig.4 Examples of the recorded signals.

magnetic field perpendicular to the geomagnetic field and created by $I = 1A$, $\rho(\mathbf{r})$ is the rock resistivity, α is the geomagnetic field inclination, $L \approx 2D$ where D is the antenna's diameter, $n(z)$ is the water content ($0 \le n(z) \le 1$), and $\mathbf{r} = r(x, y, z)$.

From the solution of integral equation (2) the location and water content of aquifers can be derived. The decay time of the NMR signal correlates with the mean size of pores of water containing rock and the phase depends on rocks electrical conductivity.

Results

Transmitting component of the antenna magnetic field $h_{1\perp}(\mathbf{r}, \rho(\mathbf{r}), \alpha)$ and magnitude of the geomagnetic field $\mathbf{H}_0$ both depend on the latitude of the test site. The NMR signal initial amplitude versus the pulse parameter is depicted in Figure 1. It was calculated at the geomagnetic pole ($\alpha = 90°$, dashed line) and at the equator ($\alpha = 0°$, solid line) assuming the water content $n = 1$. The first layer (1) is situated between 10 and 20 m and another one (2) between 60 and 70 m. Both amplitude and shape of the signals vary.

Ability of the method to detect water depends on the signal amplitude. Numerical results presented in Figure 2 show the maximum amplitude of the signal from one-meter-thick water layer ($n = 1$) versus the layer depth. The pulse parameter varies from 60 and 12000 A-ms. Line 1 corresponds to $\alpha = 90°$, line 2 to $\alpha = 45°$ and line 3 to $\alpha = 0°$. Taking into account that for existing equipment (Hydroscope, NUMIS) the limit of sensitivity is about 15-20 nV (Beauce et al., 1996), we can conclude that the one-meter-thick layer of water can be detected at a maximum depth of about 120 m when the geomagnetic field is vertical, and 100 m when it is horizontal.

The shape of the signal depends on the depth of an aquifer. It allows to discriminate aquifers situated at different depths. But even if the signals are large enough to be measured, it is not possible to discriminate aquifers if the signals from these aquifers are linearly dependent. The linear dependence between two signals can be evaluated using the correlation coefficient. In order to study capability of the method to locate aquifers, the correlation coefficient was calculated between two one-meter-thick layers of water. Results are depicted in Figure 3. Depth of the first layer is fixed at 10 m (line 1), 40 m (line 2) and 80 m (line 3). The correlation coefficient is calculated versus depth of the other layer. The solid line corresponds to a horizontal geomagnetic field and the dashed line to a vertical one. We can conclude that in the horizontal geomagnetic field correlation between the signals is a bit smaller, but it does not change the general tendency: the correlation increases with increasing depths. The maximum depth where the signals are not completely linearly dependent is about 60 m in case of the vertical field and 70 m in case of the horizontal one.

Examples of the NMR signals versus time (free induction decay) measured by NUMIS NMR instrument are presented in Figure 4. The signals 1 and 2 are recorded in the same test site with different values of the pulse parameter ($q = 877$ A-ms and $q = 9004$ A-ms respectively). Two aquifers are known at this site. The first aquifer is composed by sand and gravel and is located at a depth between 5 and 15 m. Depth of the other aquifer is about 80-90 m. The water containing rock is a fractured sandstone. The rocks resistivity is about 50 ohm-m. The geomagnetic field inclination is 60°. The record with $q = 877$ A-ms corresponds mainly to the shallow aquifer, and with $q = 9004$ A-ms to the deeper one. The difference in decay time

indicates a difference in the type of water containing rocks. Rather large signal from the 80-m-deep aquifer confirms numerical result indicating a depth limit of the method of about 100-120 m. Signal 3 is recorded in a waterless area with the pulse parameter $q = 8853$ A-ms. This example demonstrates a noise record and can be used for evaluation of the equipment.

Conclusions

The NMR signal depends on the latitude of the test site. The amplitude measured in vertical and horizontal fields differs in 2-3 folds.

Numerical modelling reveals that for a 100 m circular antenna, a one-meter-thick layer of water (water content 100%) can be detected down to 120 m when the geomagnetic field is vertical and only to 100 m when it is horizontal. The layers can be discriminated down to a maximum depth of about 70 m in case of the horizontal field, and 60 m in case of the vertical one.

In noiseless environment the noise level of NUMIS NMR equipment used for the experiments was found to be about 15 nV. Amplitude of the NMR signal was recorded from an aquifer 80-90 m deep. The signal is about 100 nV in a 60° geomagnetic field. It allows to anticipate that this aquifer also would be detected at 110-130 m deep.

Field records of the signal demonstrate the sensitivity of the NMR to aquifer parameters.

References

Beauce A., Bernard J., Legchenko A., and Valla P., 1996 - Une nouvelle méthode géophysique pour les études hydrogéologiques: l'application de la résonance magnétique nucléaire. Hydrogéologie, **1**, pp. 71-77.

Goldman M., Rabinovich B., Rabinovich M., Gilad D., Gev I., and Schirov M., 1994 - Application of integrated NMR-TDEM method in ground water exploration in Israel: Journal Appl. Geophys., **31**, pp. 27-52.

Legchenko A.V., Shushakov O.A., Perrin J., and Portselan A.A., 1995 - Noninvasive NMR study of subsurface aquifers in France. Abstracts of The International Exposition and SEG 65th Annual Meeting, October 9-12, 1995, Houston, USA, pp. 365-367.

Lieblich D.A., Legchenko A., Haeni F.P., and Portselan A., 1994 - Surface nuclear magnetic resonance experiments to detect subsurface water at Haddam Meadows, Connecticut: Proceedings of the Symposium on the Application of Geophysics to Engineering and Environmental Problems, March 27-31, 1994, Boston, Massachusetts, **2**, pp. 717-736.

Shirov M., Legchenko A., and Creer G., 1991 - New direct non-invasive ground water detection technology for Australia. Expl.Geophys., **22**, pp. 333-338.

Semenov A.G., Burshtein A.I., Pusep A.Yu., and Schirov M.D., 1988, (in Russian). - A device for measurement of underground mineral parameters. USSR Patent 1079063.

Semenov A.G., Schirov M.D. and Legchenko A.V., 1987. - On the technology of subterranean water exploration founded on application of nuclear magnetic resonance tomograph "Hydroscope". IXth Ampere summer school, Abstracts, Novosibirsk, September 20-26, 1987, p. 214.

Varian R.H., 1962 - Ground liquid prospecting method and apparatus, US Patent 3019383.

IRIS Instruments

SEG International Exposition
and Sixty-Sixth Annual Meeting

November 10–15, 1996
Denver

Some aspects of the performance of the Surface NMR Method

A.V.Legchenko, BRGM*

Summary

Although Nuclear Magnetic Resonance (NMR) measures the signal directly from subsurface water molecules and is hence a direct method for water prospecting from the surface, the small amplitude of the NMR signal and the relatively complicated nature of this phenomenon do not encourage geophysicists to use this technique for everyday field work. The basic principles of operation, the general design of the instrument and the inversion technique presented in this paper provide a better understanding of the Surface NMR Method.

A field study was performed in France in order to demonstrate the consistency of NMR results. The noise level was around 10-30 nV in the natural electromagnetic environment. The signal over the studied aquifers depends on the pulse parameter and varied from 40 to 260 nV. The mean square error of the NMR signal recording was less than 8 nV. Inversion was stable and enabled the identification of several aquifers, their depth and their water content. The results are in fairly good agreement with the borehole lithological log and DC resistivity data.

Introduction

Nuclear Magnetic Resonance (NMR) is a phenomenon based on the properties of atomic nuclei. In the geomagnetic field the NMR signal can be recorded from any proton-containing liquid such as hydrocarbons or water (Varian, 1962). For the Surface NMR Method, the maximum depth of investigation is currently limited to 100-150 m, and hence only water is a target. The presence or absence of the NMR signal is directly related to the presence or absence of subsurface water. The interpretation of experimental data can reveal the presence of aquifers, their location and their water content.

The NMR signal is sensitive to aquifer parameters (Shirov *et al.*, 1991), but other factors, such as electromagnetic interference or inhomogeneities in the geomagnetic field, may also have an influence on the relatively weak signal (no more than 4000-5000 nV). Signal instability in the same geological environment can cause errors in data interpretation, reducing the advantages of the method.

In order to assess the consistency of NMR results, repetitive measurements were performed in France during November and December 1995. These measurements were subject to inevitable variations in the antenna position, the amount of cars passing-by, the weather conditions and the natural electromagnetic noise. Measurements were carried out using the 'NUMIS' NMR, manufactured by IRIS Instruments as part of the Cooperation Agreement between BRGM and ICKC. This new equipment is a development of the Russian NMR instrument 'Hydroscope', created by ICKC and tested in France in 1992 (Legchenko *et al.*, 1995).

This paper presents a summary of the basic principles of the method, a short description of the measuring instrument, the data-inversion technique and the results.

Method

In order to record the NMR signal, a 100-m-diameter wire loop is laid out on the ground that serves as both the transmitting and receiving antenna. It is energized by a pulse of oscillating current with a rectangular envelope. The carrier frequency of the current is equal to the Larmor frequency $\omega_0 = \lambda H_0$ in the geomagnetic field $\mathbf{H}_0$. As λ is a gyromagnetic ratio for the protons, no other response will appear. The transmitted oscillating magnetic field causes nuclear magnetization of the protons to shift away from its equilibrium position along the geomagnetic field. Assuming homogeneity of the geomagnetic field and horizontal stratification, the initial amplitude of the NMR signal E_0 is:

$$E_0(q) = \int_0^L K(q,z)n(z)dz, \qquad (1)$$

Performance of the Surface NMR Method

where $K(q,z) = \omega_0 M_0 \int_{x,y} h_{1\perp} \sin(\frac{1}{2}\lambda h_{1\perp} q)dxdy$, $q = I\tau$ is the pulse parameter and I, τ are respectively the pulse amplitude and duration, $h_{1\perp}(\mathbf{r}, \rho(\mathbf{r}), \alpha)$ is a component of the antenna's magnetic field perpendicular to the geomagnetic field and created by $I = 1A$, $\rho(\mathbf{r})$ is rock resistivity, α is the geomagnetic field inclination, $L \approx 2D$, where D is the antenna's diameter, and $0 \le n(z) \le 1$ is the water content, $\mathbf{r} = r(x,y,z)$.

Numerical modelling of equation (1) reveals that method sensitivity decreases with increasing depth of the aquifer, as is demonstrated in Figure 1. The contribution to the total signal from a 1-m-thick water layer was calculated versus the layer's depth for a 100-m-diameter antenna and $q_{max} = 7000$A-ms.

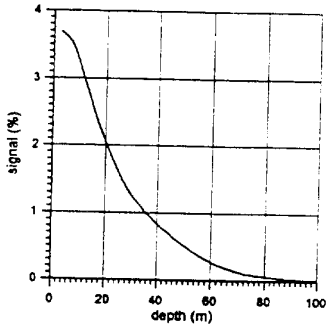

Fig. 1. Part of the total signal, contributed by a 1-m-thick water layer versus the layer's depth.

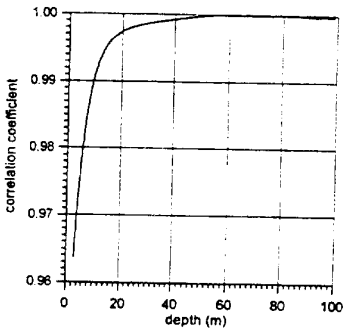

Fig. 2. Correlation between signals from two consequtive 1-m-thick water layers versus their depth.

The case of 100% is assumed to be a 100-m-thick water layer at the surface, i.e. 0-100 m depth. The ability of the method to constrain the depth of the aquifer can be demonstrated using a correlation coefficient R between signals from two, 1-m-thick water layers, one directly above the other with no interval inbetween. The correlation coefficient is depicted in Figure 2 versus the layer's depth. When $R \to 1$, the signals from the layers are linearly dependent. Consequently, it is uncertain from which layer the signal is recorded, and thus the depth of the layers cannot be precisely calculated. The modelling results show that the presence of a 1-m-thick water layer can be detected down to a depth of 60-80 m, but that its depth can be detected only down to 15-20 m. In practice, the method's performance also largely depends on the signal to noise ratio (S/N).

Equipment

The NMR instrument consists of an oscillating-current generator, a receiver, an NMR signal detector,, an antenna and a microprocessor (Figure 3). The antenna is used for both transmission of the oscillating magnetic field and reception of the NMR signal. The microprocessor switches the antenna from generator to receiver mode by an electronic switch. It also controls the generation of the reference frequency equal to the Larmor frequency. An envelope of the signal from the phase-sensitive detector is recorded by the microprocessor in digital form. A portable PC is used for data processing. The PC is connected to the microprocessor by a standard RS-232 serial link. The antenna is made of a piece of copper wire 314 m long, and 25 mm^2 in cross-section. Two car batteries of 60 A-h are used for the power supply, which enable the instrument to operate all day without charging. The equipment weighs about 200 kg. A 4-wheel drive Jeep is used for transportation and field work.

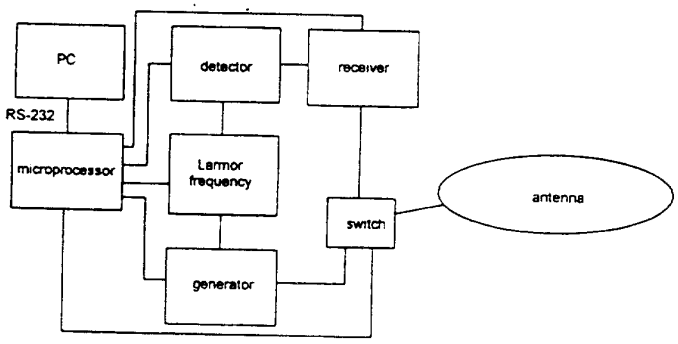

Fig. 3. Schema of the NMR instrument.

Inversion

The vertical distribution of water content $n(z)$ is a solution of the integral equation (1). Layers with $n(z) > 0$ correspond to aquifers. This linear equation may be solved by projecting it onto finite dimensional subspace, and approximated by a projected equation. In a matrix notation the projected equation can be written as

$$\mathbf{A}\ \mathbf{n} = \mathbf{e}_0, \qquad (2)$$

where $\mathbf{e}_0 = (e_{01}, e_{02}, .., e_{0i}, .., e_{0I})^T$, $e_{0i} = e_0(q_i)$ is the set of experimental data, $\mathbf{n} = (n_1, n_2, .., n_j, .., n_J)^T$, $n_j = n(z_{j+1} - z_j)$, is the water content, $\mathbf{A} = \left[a_{i,j} \right]$ is a rectangular matrix of $I \times J$ with the elements $a_{i,j} = \int_{z_j}^{z_{j+1}} K(q_i, z)\, dz$. Symbol T denotes transposition.

Inversion was carried out using the Tikhonov regularization method (Tikhonov and Arsenin, 1977). In order to find an approximation of the solution of the matrix equation (2), this method implies minimization of the Tikhonov functional

$$M_\eta(n) = \left\| \mathbf{A}\ \mathbf{N}_\eta - \mathbf{e}_{0\varepsilon} \right\|_{L_2} + \eta \left\| \mathbf{N}_\eta \right\|_{L_2} = \min, \qquad (3)$$

where $\mathbf{e}_{0\varepsilon}$ is the vector of the experimental data, contaminated by the noise $\varepsilon = \left\| \varepsilon \right\|_{L_2}$, $\mathbf{N}_\eta$ is the vector, minimizing the Tikhonov functional (3), and $\eta > 0$ is the parameter of regularization.

To solve this minimization problem, we applied the discrepancy principle (Morozov, 1966). It assumes that if data are erroneous, the residual will be minimized to the level of the experimental error. Hence, for a given $\varepsilon > 0$, we need to find a solution with residual $\left\| \mathbf{A}\ \mathbf{N}_\eta - \mathbf{e}_{0\varepsilon} \right\|_{L_2} \le \varepsilon$ and stabilize it by making $\left\| \mathbf{N}_\eta \right\|_{L_2}$ small. $\mathbf{N}_\eta$ is an approximation of the solution of the matrix equation (2). When $\varepsilon \to 0$, $\eta(\varepsilon) \to 0$ and $\mathbf{N}_\eta \to \mathbf{N}$.

Discretization of the integral equation (1) was carried out in order to provide a constant value for the coefficient of correlation between the neighbouring layers (Legchenko and Shushakov, 1995). The resulting matrix $\mathbf{A}$ is 18×15. The problem is solved by the conjugate gradient method (Stoer and Bulirsch, 1980), taking into account that $n(z) \ge 0$.

Results and discussion

A test site for the field experiments was selected that had no major sources of external electromagnetic interference in the vicinity. Noise evaluation gave an average value of 250-350 nV, with small variations during the tests. Noise was measured using a band-pass filter with a bandwidth of $((\omega_0 / 2\pi) \pm 200 Hz)$.

There are two aquifers at the test site of St-Cyr-en-Val, P4. The upper aquifer is irregular and consists of a stratum of mixed gravel, sand and clay, approximately 20-25 m thick. The other aquifer is fairly extensive through the area and consists of water-saturated karst limestone separated by a sandstone layer at a depth of 50-60 m. The total thickness is about 70-80 m. Water transmissivity is around 0.28 m^2/s. Rock resistivity, measured using the surface DC resistivity method, was 180 ohm-m from 0 to 1.5 m, 60 ohm-m from 1.5 to 5 m, and 33 ohm-m from 5 to 100 m. The depth of the water table was 4 m in a shallow borehole close to the test site.

Seven sets of measurements were performed (seven curves $E_0(q)$). The stacking number was set at 10. With 10 stackings, each measurement takes about 30 minutes. Increasing the stacking number can improve S/N, but measurement time also increases. Figure 4 gives the NMR signal amplitude versus pulse parameter; all recordings (asterisks) are shown to give an indication of data dispersion. The noise was recorded before the pulse, stacked and filtered. The mean square variation of the noise is also depicted in order to evaluate the electromagnetic environment during measuring. S/N depends on the pulse

parameter and can be further improved by increasing the stacking number. The maximum mean square error of the signal recorded is 8 nV, whereas the signal itself varies between 40 and 260 nV.

Figure 5 shows the lithological log of borehole 268, located approximately 2 km from the test site, and the inversion results. Each set of data ($E_0(q)$) was inverted separately and an average solution ($n(z)$) with a mean square variation was deduced. Two aquifers were determined by the NMR method. The top of the shallower aquifer coincides well with the water table. No data are available to specify the bottom of this irregular aquifer, but the waterless interval between the aquifers is well detected. A water-saturated karst limestone aquifer is found below 30 m. Its position is in good agreement with the borehole data. No water was detected below 60 m, which can be explained by the screening effect of electrically conductive rocks that decreases the depth of investigation. There is some uncertainty in determining the water content, but the NMR results are consistent for the location of the two aquifers.

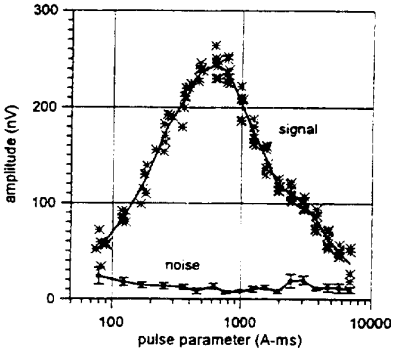

Fig. 4. Experimental data.

Conclusions

The observed variations for both the measured data and the inversion results at the same test site are acceptable, and thus demonstrate the Surface NMR Method reliability. The results obtained are in good agreement with the geological data.

Where noise level after stacking and filtering is between 10 and 30 nV, the signal amplitude depends on the pulse parameter and varies between 40 and 260 nV. Repetitive measurements reveal that the mean square error of signal recording is less than 8 nV.

The Tikhonov regularization method used for the NMR data inversion allows the reliable determination of aquifer position and water content. Inversion results are more reliable for aquifers at depths of less than 40-50 m, and only the presence or absence of water can be detected deeper than 50 m. Electrical conductivity of the rock can influence the depth of investigation.

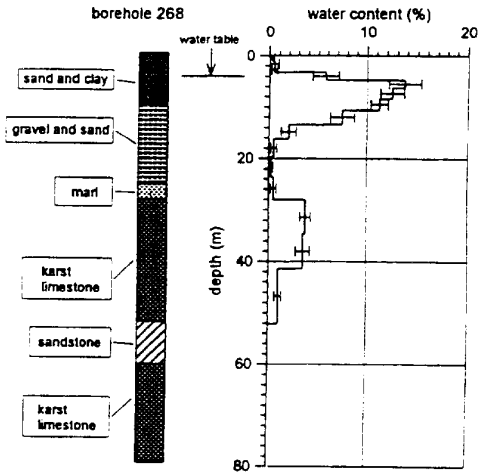

Fig. 5. Borehole 268 lithological log and inversion results.

Acknowledgements

The author would like to thank J. Pierrat of IRIS-Instruments and J. Perrin of BRGM for their assistance in the field experiments, and also A. Beauce and P. Valla of BRGM for fruitful discussions that helped improve the presentation of results.

References

Legchenko, A.V., Shushakov, O.A., Perrin, J., and Portselan, A.A., 1995. Noninvasive NMR study of subsurface aquifers in France. Abstracts of The International Exposition and SEG 65th Annual Meeting, October 9-12, 1995, Houston, USA, p.365-367.

Legchenko, A.V. and Shushakov, O.A., 1995. Surface NMR data inversion, submitted to Geophysics.

Morozov, V.A., 1966. On the solution of functional equations by the method of regularization, Soviet Math. Doklady 7, 414-417 (English translation).

Shirov, M., Legchenko, A. and Creer, G., 1991. New direct non-invasive ground water detection technology for Australia, . Exploration Geophysics, 22, 333-338.

Stoer, J. and Bulirsch, R., 1980. Introduction to numerical analysis: Springer-Verlag Berlin.

Tikhonov, A. and Arsenin, V., 1977. Solution of ill-posed problems, Wiley and Sons, Washington D.C.

Varian, R.H., 1962. Ground liquid prospecting method and apparatus, US Patent 3019383.

58th EAGE Conference and Technical Exhibition,
Amsterdam, The Netherlands,
3 - 7 June 1996

A PRACTICAL ACCURACY OF THE SURFACE NMR MEASUREMENTS

A.V. LEGCHENKO
BRGM - DR/GIG, PO Box 6009, 45060 Orléans, France

A measurement of a Nuclear Magnetic Resonance (NMR) signal directly from subsurface water molecules is the most important distinction of the NMR in comparison with other methods of geophysics. The existence or absence of the NMR signal with a high degree of reliability also proves the existence or absence of subsurface water. The surface NMR system "Hydroscope" was developed by ICKC in the early eighties. It was tested in many countries in a variety of geological environments. The results affirm that parameters of the NMR signal depend on parameters of the aquifer. However the weakness of the signal, whose amplitude is not more than just a few micro volts, rises a question about the accuracy of the field measurements.

In order to study variations of the NMR signal from one measurement to another, field tests were performed in France in November 1995 in St Cyr-en-Val and Bazancourt. The "Hydroscope" was tested earlier at the same sites in June 1992 (Legchenko *et al.*, 1994). A new equipment developed in framework of co-operation agreement between BRGM and ICKC was used for the field tests in 1995. In this new instrument many parts have been modified using the experience of the "Hydroscope" practical application. A good correlation between the two time separated sets of measurements can also prove stability of the NMR signal itself.

A circular wire loop with a diameter of 100 m is laid down on the ground and is used as an antenna for both transmitting and receiving. It is energized by an alternative current pulse of specific frequency, which is equal to the Larmor frequency for protons in the geomagnetic field $\omega_0 = \lambda H_0$, where H_0 is the geomagnetic field and λ is the gyromagnetic ratio. After the pulse is terminated, the antenna is switched from transmitter to receiver and the NMR signal can be recorded. The recorded signals in two different sites are presented in Figure 1. To be sure that it is nothing else but the NMR signal, the noise records before the pulse are also depicted. The amplitude (e), the decay time (T_2^*) and the phase (ph)

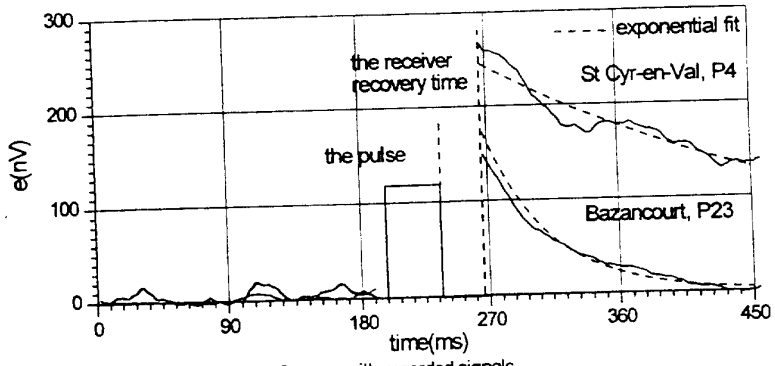

Fig.1 Measuring time diagram with recorded signals.

of the signal must be measured. For the inversion these measurements should be repeated with different values of the pulse parameter $q = I\tau$, where I, τ are the pulse amplitude and the duration. The mean square error between the parameters of the signal measured in every record and its average value through a number of records is used for an estimation of accuracy of the measurements. The correlation coefficient between $e(q)$, $T_2^*(q)$, $ph(q)$ curves of every measurement and the average ones is used as an evaluation of the stability.

Figure 2 presents the average signal amplitude $e(q)$ in St Cyr-en-Val with the error bars through 18 measurements and the results of the 1992 field tests. The noise before the pulse was stacked and filtered the same way as the signal. The errors depend on the signal to noise ratio (S/N) and the noise origin. For example with S/N=4 the mean square errors are: $\varepsilon_e \approx 5\%$, $\varepsilon_T \approx 20\%$, $\varepsilon_{ph} \approx 2\%$ (St Cyr-en-Val) and $\varepsilon_e \approx 5\%$, $\varepsilon_T \approx 6\%$, $\varepsilon_{ph} \approx 2\%$ (Bazancourt). The 20% error on the decay time measurement in St Cyr-en-Val may be easily explained by a high similarity between one of the power line harmonics (2000 Hz) and a very long signal (350 ms) of about the same frequency (the Larmor frequency is 2005.2 Hz). Eight successive measurements of $e(q)$, $T_2^*(q)$, $ph(q)$ at the same site in Bazancourt reveal a high correlation between the measurements as it is shown in Figure 3. The correlation coefficients between the average curves of 1995 and the 1992 data are: $R_e = 0.9978$, $R_T = 0.9984$ and $R_{ph} = 0.9925$.

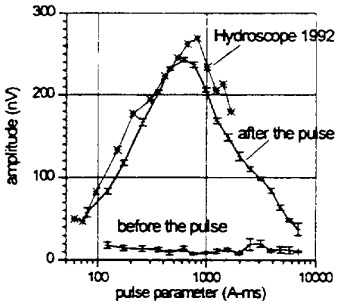

Fig.2 St Cyr-en-Val, P4, recorded amplitude and mean square error bars.

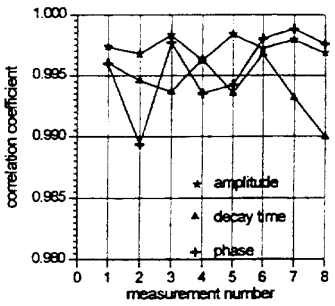

Fig.3 Bazancourt, P23, correlation between the measurements and the average value.

So, the noninvasive measurements of the NMR signal from subsurface water-saturated layers are repetitive and rather accurate. The calculations through 26 field measurements (after 10 stacking and filtering) reveal that the mean square errors are less than 5% for amplitude and phase. For decay time in Bazancourt the error is less then 6% and in St Cyr-en-Val less than 20%. Correlation coefficient between the measurements at the same site is over 0.98 for all the parameters except the decay time in St Cyr-en-Val (>0.92). The time separation and the change of season between the 1992 and 1995 field tests did not show any significant difference between the measured at the same sites parameters of the NMR signal.

References

Legchenko, A.V., Shushakov, Perrin, J., and Portselan, A.A.. 1995, Noninvasive NMR study of subsurface aquifers in France. Abstracts of "The International Exposition and SEG 65th Annual Meeting, October 9-12, 1995, Houston, USA", p.365-367.

ELSEVIER

Journal of Applied Geophysics 34 (1996) 277–282

APPLIED GEOPHYSICS

Detection of the water level in fractured phreatic aquifers using nuclear magnetic resonance (NMR) geophysical measurements

Israel Gev [a], Mark Goldman [b], Boris Rabinovich [b], Michael Rabinovich [b], Arie Issar [a]

[a] *Institute for Desert Research, Ben-Gurion University of the Negev, Sde Boker, Israel*
[b] *Institute for Petroleum Research and Geophysics, P.O.B. 2286, Holon 58122, Israel*

Received 24 November 1994; accepted 3 January 1996

Abstract

Correlation of geophysical data collected using the NMR method in the Negev Desert, Israel, with hydrogeological data from nearby observation wells is presented. The experiment was conducted near Kibbutz Revivim in the Besor drainage system (Fig. 1). The objective of the survey was to detect groundwater layers in the Quaternary cover filling and Eocene fractured aquifers down to a depth of 100 m. The experiment was performed using a combination of two different geophysical techniques, namely the NMR and time domain electromagnetic (TDEM) methods. The geophysical results were verified by measuring the water level in three observation wells, two of which were drilled several months after the geophysical survey was carried out.

The water level measured in these follow-up observation wells shortly after drilling did not coincide with the geophysical data. However, it settled over a period of time and finally stabilized at a depth very similar to that obtained from the NMR measurements. This phenomenon is caused by the fractured nature of the phreatic aquifer. Since the flow of water in such aquifers is confined by the fractures, the appearance of water in the well during or shortly after drilling is determined solely by the intersection of the well and the fracture. Our experiments showed that geophysical measurements in fractured phreatic aquifers may have a distinct advantage over direct borehole measurements, since the former average the depth to the water table over large areas (several thousand square meters) while the latter are limited by the area of the borehole cross-section (several tens of square centimeters).

1. Introduction

Application of the NMR method to groundwater exploration is still in the experimental stage. However, even the very first, and meanwhile statistically not well substantiated results, show exceptional features of the method in direct detection of groundwater at relatively shallow depths (Schirov et al., 1991; Goldman et al., 1994). During an extensive feasibility study survey carried out in Israel in 1992, using the integrated NMR/TDEM method, fairly good agreement between the geophysical and borehole data was reported (Goldman et al., 1994). Of a total of 36 NMR stations, four measurements were carried out near Kibbutz Revivim in the Besor drainage system in the Negev Desert, Israel (Fig. 1).

The object of this experiment was to detect groundwater layers in the Quaternary cover filling and Eocene fractured layers to a depth of about 100 m. The geophysical results were verified by measuring the water level in the observation well closest to the geophysical measurement site. Since water salinity plays no role in the present investigation, only NMR results as compared with borehole data will be

PII S0926-9851(96)00004-3

discussed in this paper. The appropriate TDEM results have been presented in part in a previous publication (Goldman et al., 1994). Two of the NMR stations were established near existing observation wells and the correlation of geophysical and well data carried out during the survey showed a reason-

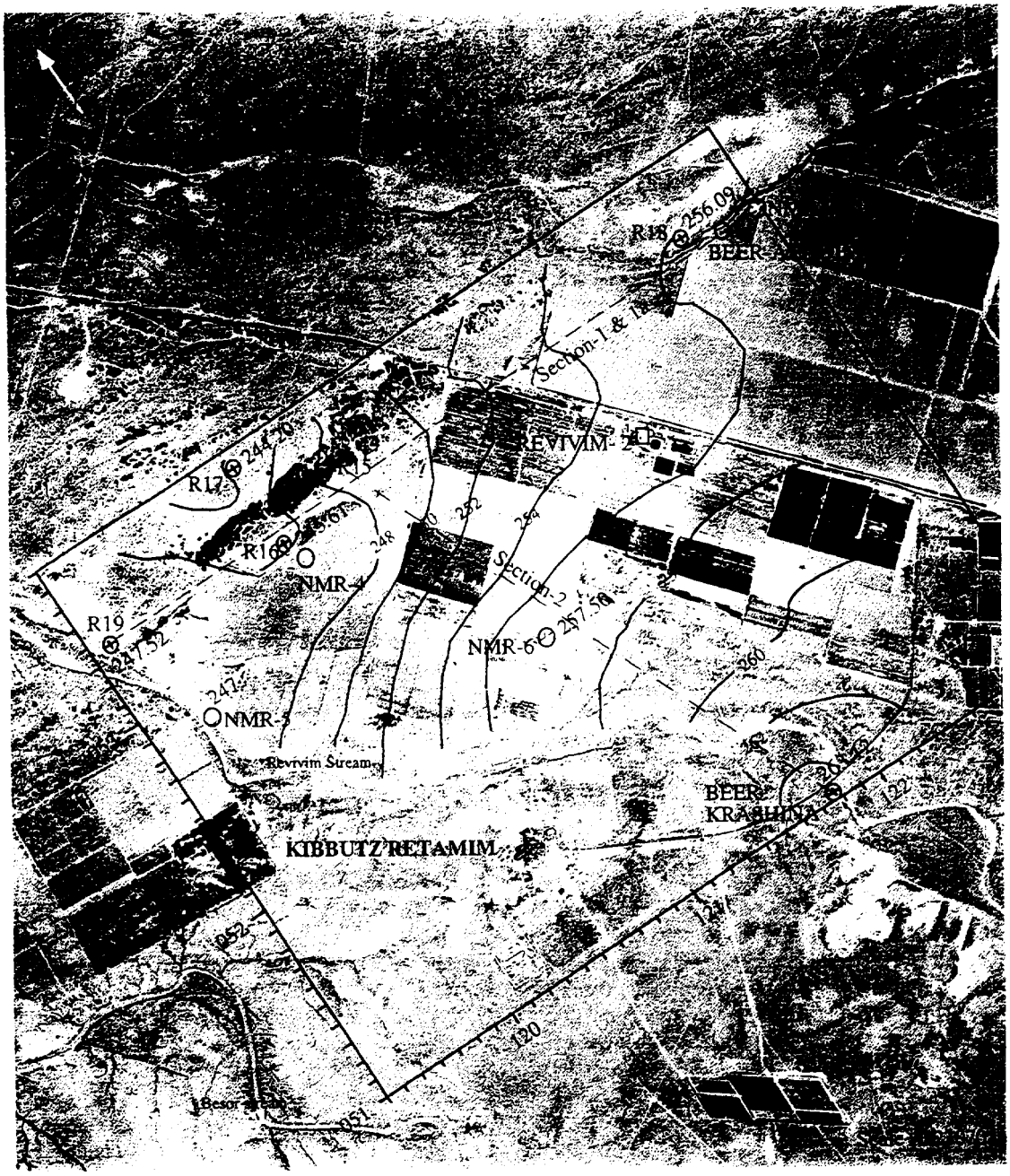

Fig. 1. Location map of the integrated NMR/TDEM survey and water level potential map of the Revivim area, the Negev desert, Israel.

able coincidence between the two with regard to the depth to the water table (Goldman et al., 1994).

A completely different phenomenon was observed in two other NMR measurements when they were compared with the results of follow-up drilling. The water level obtained from the well data in both observation wells during drilling was significantly deeper than that shown by the NMR measurements. Moreover, the water level derived from the NMR data was much better suited to the interpolated depth from the existing wells in the area than that derived from the new wells. Repeat measurements were, therefore, carried out a few days later and yielded a fairly good match with the NMR results. This paper discusses a possible explanation for this curious phenomenon.

2. Geological setting

The geological section of the research site within the upper 100 m is composed of three main units:

1. Sand dunes of Holocene age and bedded silt layers of Pleistocene age with a maximum thickness of about 15 m.

2. Conglomerate layers of Pliocene age varying between zero to 5 m in thickness.

3. Chalky bedrock of Eocene age.

The chalk layer is filled with multilayered tectonic joints several meters in length and also with short, single layer joints. These joints can be observed in the outcrops along stream channels as well as in the numerous caves appearing in the same formation, 7 km to the north of the research site (Nisim, 1991).

3. Comparison of NMR and borehole data

Since both acquisition and interpretation of the NMR data collected at the research site in question, as well as the basic principles of the method, have already been described in detail (Goldman et al., 1994), we may proceed directly to the comparison. Fig. 1 is the site location map; R18 and R19 (Fig. 1) are the follow-up boreholes drilled after the above NMR/TDEM survey was carried out. A hydrogeological cross-section between the two wells is shown in Fig. 2. The water level observed during drilling of boreholes R18 and R19 was 18 m and 16 m, respectively; over the few days following, however, the water level rose and stabilized at corresponding depths of 10 m and 12 m. The latter depths coincide fairly well with those obtained in the nearby NMR stations (NMR-5 and NMR-7, respectively).

Examination of the records of existing wells R15 and R16 showed that the water levels measured in R15 both during and after drilling, did not show any significant discrepancies in depth, which was constantly approximately 15.5 m. At the same time the water level measured in well R-16 during drilling was 17 m and this stabilized at a depth of 11 m after some 24 h. This latter depth coincides fairly well with that obtained at the nearby NMR-4 station (Fig. 2). Thus, there was a noticeable delay in water level stabilization in all the wells in which groundwater was found in the fractured chalk rocks. The possible mechanism of this phenomenon is illustrated by a schematic drawing (Fig. 3). Levels observed in boreholes A and B should show a marked difference during drilling; indeed, borehole A which does not penetrate multilayer joints in the vicinity of the regional water level, will show a somewhat greater depth down to the water table during drilling. Nevertheless, the water level in the borehole will rise after a time to the regional level to attain hydrostatic equilibrium and, vice versa, the water level observed in borehole B will be fairly similar during drilling and after, since it penetrates multilayer joints in the vicinity of the regional water level (Fig. 3).

In contrast to the fractured part of the aquifer, water levels observed in the porous part of the aquifer (e.g. conglomerates) should be essentially the same both during and after drilling. This feature was in fact observed in borehole R15, while the water level measured during the drilling the rest of boreholes was found within the fractured chalk layer.

For convenience, the comparison of borehole and NMR results is presented in Table 1 in which, unlike Fig. 2, only the depths to the water table are presented. It should also be noted that, owing to resolution limitations, the NMR results are shown in ranges of 1 or 2 m. The Table clearly shows that the NMR results are fairly similar to those obtained in the boreholes after the water level has stabilized. The most likely explanation for this phenomenon is the

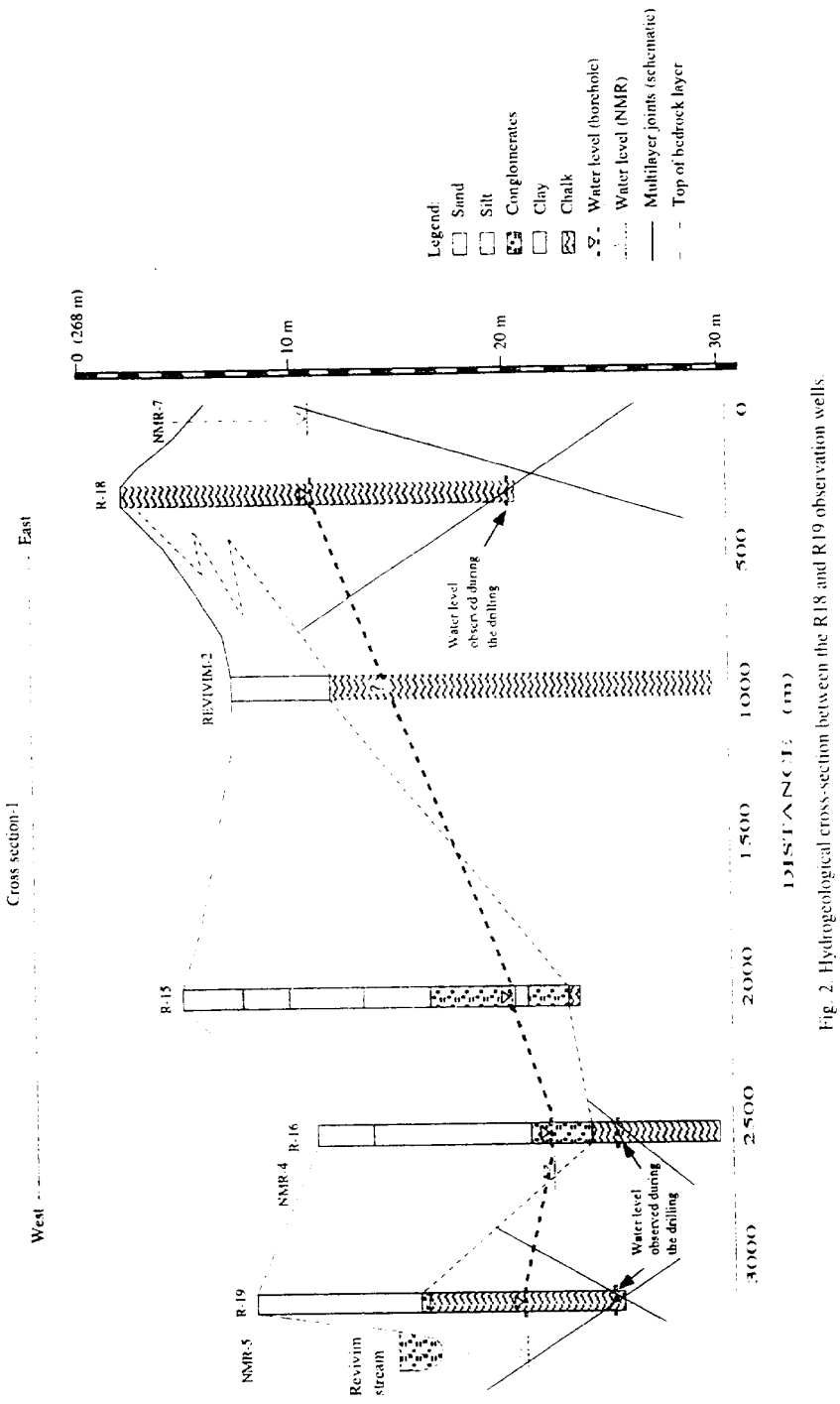

Fig. 2. Hydrogeological cross-section between the R18 and R19 observation wells.

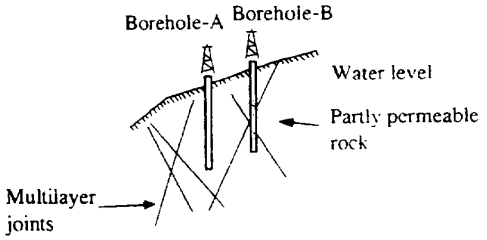

Fig. 3. Schematic diagram of the boreholes penetrating the fractured aquifer.

difference in the investigation scale between the borehole and NMR measurements. Indeed, the investigation area of the well is limited by the cross-section of the hole which never exceed a few hundred cm^2 and, thus, the probability of crossing a multilayer joint in the appropriate depth of the regional groundwater level is rather small.

The investigation area of the NMR measurements is roughly determined by the transmitter loop area and can, therefore, reach tens of thousands m^2. In general, this feature of the NMR method (and some other geophysical techniques) represents one of its major drawbacks (low lateral resolution). However, in the case of fractured aquifers, averaging the results over large areas facilitates accurate detection of the depth down to the water table in real time. In this respect NMR measurements may be considered as more accurate than direct borehole measurements.

All observation wells within the considered profile (excluding Revivim-2) have been drilled to the depth of up to 18 m only (Fig. 2). At the same time the NMR measurements have detected also much deeper water saturated layers (Fig. 4). Therefore the comparison of NMR and well data was made for the upper NMR layer only (layer no. 1 in Fig. 4). The deeper NMR layers can be most likely identified with different fractured zones of the chalk aquifer.

A summary of the NMR data with regard to

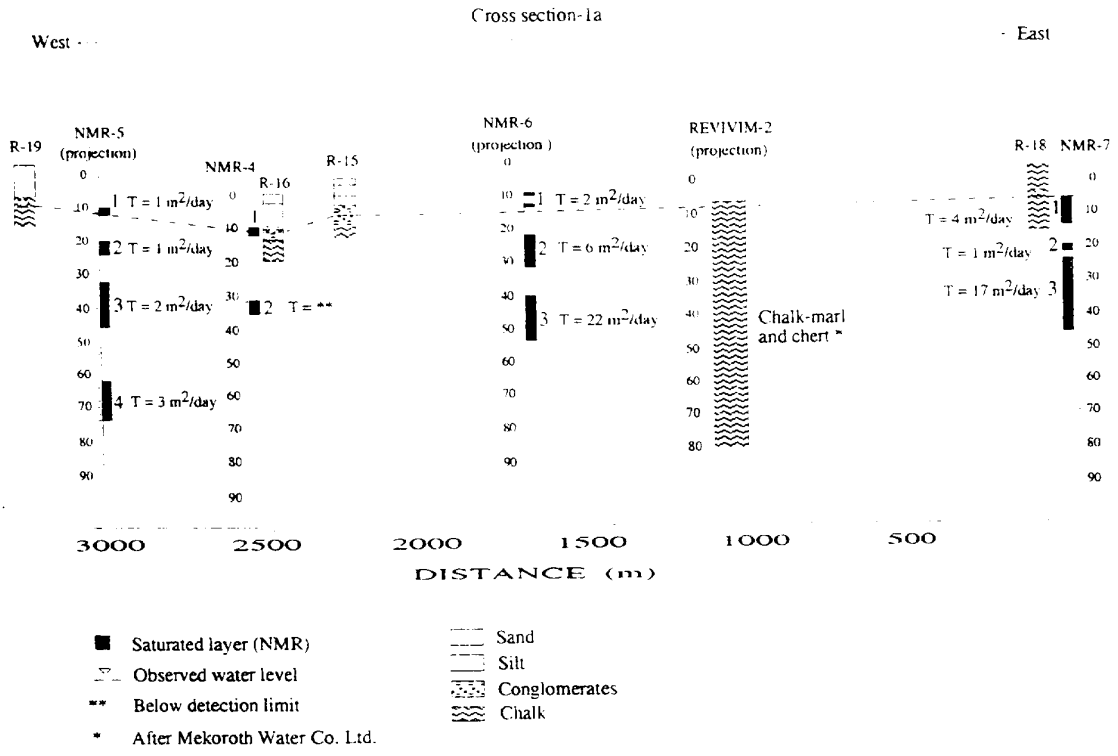

Fig. 4. Complete NMR results and hydrogeological data from adjacent wells along the profile as shown in Fig. 2

Table 1
Depth to water table (m) as observed during the drilling and after reaching a steady state compared with NMR measurements

Well-R16		NMR-4	Well-R18		NMR-7	Well-R19		NMR-5
During	After		During	After		During	After	
17	11	10–12	18	10	10–11 (after projecting to well R18)	16	12	10–12

Table 2
Water content in m^3 per m^2 in each NMR layer

NMR layer no.	NMR-4		NMR-5		NMR-6		NMR-7	
	Depth	Volume	Depth	Volume	Depth	Volume	Depth	Volume
1	10–12	0.02	10–12	0.02	9–13	0.02	6–14	0.08
2	32–36	0.04	20–24	0.04	22–32	0.18	20–22	0.02
3			32–46	0.14	40–54	0.42	24–46	0.38
4			62–74	0.12				

depths, thicknesses and volume of water is presented in Table 2. These data show that the amount of water increases with depth and this phenomenon can most likely be explained by the increasing density of joints at the appropriate depth.

The NMR measurements for the upper phreatic aquifer are summarized in Fig. 1 in the form of a water level potential map. This map shows that the general direction of flow in the aquifer is northwest and the general gradients from the Atadim and Revivim streams run toward the central part of the basin.

4. Conclusions

Within the framework of its applicability (reasonably high signal-to-noise ratio, relatively shallow depth to target), the NMR method provides a fairly accurate evaluation of the water level and the amount of groundwater in the subsurface. If, in addition, the water is located in a fractured phreatic aquifer, the regional water level can be more accurately determined using the NMR method than by direct borehole measurements taken either during drilling or shortly after. This curious phenomenon is explained by the much larger area of investigation used by the NMR method ($\sim 10^{-4}$ m^2) than that limited by the borehole cross-section (~ 0.015 m^2). The probability of encountering multilayer joints at a depth corresponding to the regional water level is, thus, significantly higher for the NMR method.

References

Goldman, M., Rabinovich, B., Rabinovich, M., Gilad, D., Gev, I. and Schirov, M., 1994. Application of the integrated NMR-TDEM method in groundwater exploration in Israel. J. Appl. Geophys., 31: 27–52.

Nissim, I., 1991. Characterization of hydrogeological system in arid zones. Eocene chalk of the Avdat group, central and northern Negev, Israel. M.Sc. Thesis, Hebrew University, Jerusalem.

Schirov, M., Legchenko, A. and Creer, G., 1991. A new direct non-invasive groundwater detection technology for Australia. Explor. Geophys., 22: 333–338.

GEOPHYSICS, VOL. 61, NO. 4 (JULY-AUGUST 1996); P. 998–1006. 7 FIGS.

Groundwater NMR in conductive water

Oleg A. Shushakov*

ABSTRACT

A surface method of groundwater prospecting using nuclear magnetic resonance (NMR) in the Earth's magnetic field is under study. The technique is employed for hydrogeological surveys down to a depth of about 100 m. The advantage of this method is that an NMR signal can be observed only in the presence of groundwater. A circular wire loop with a diameter of 100 m is laid out on the ground to excite and receive the NMR signal. An oscillating current with a rectangular pulse-shape is passed through the loop, with the carrier-frequency being equal to the proton-resonance frequency in the Earth's field. The excitation pulse is followed by a nuclear induction emf caused by the free Larmor precession in the Earth's field.

Of practical importance is the effect of the electrical conductivity of the ground on a groundwater NMR survey. Finite-ground conductivity can result in induced currents that can screen the NMR signal. The calculations of NMR signals are based on the transformation of Maxwell's equations in terms of magnetic Hertz potentials through use of the reciprocity principle. Groundwater NMR is measured with an instrument designed at the Institute of Chemical Kinetics and Combustion, Russian Academy of Science, Novosibirsk. Experiments were conducted in the Altay region of Russia. Both NMR-signal amplitude and phase, were measured and compared with the calculated results for horizontally stratified media. Borehole logs and vertical-resistivity profiles were also used for evaluation of results.

The conductivity is shown to affect both phase and amplitude of the NMR signal at resistivities of a few to a few tens of ohm-m depending on the depth of the water-saturated layers. There is good agreement between calculated and experimental data. It is also established that the measurements of only NMR amplitude and phase are not sufficient for determining groundwater salinity.

INTRODUCTION

The original idea of surface groundwater prospecting using nuclear magnetic resonance (NMR) was introduced by Anderson (Varian, 1962). The first device, mathematical description, and an inversion method were developed by Semenov et al. (1982). The technology of groundwater surveys involving NMR was developed further by Semenov et al. (1982, 1988, 1989). The method is used to explore for groundwater up to a depth of about 100 m (Semenov, 1987a). This novel geophysical technique has been referred to as the "Hydroscope" (Semenov et al., 1982; Semenov, 1987b).

The technique can be used to register the magnetic-resonance signal of water protons in the Earth's magnetic field, $\mathbf{H}_0$, which is of the order of $5 \cdot 10^{-5}$ T. The resonance signal has a frequency of about 2 kHz in field $\mathbf{H}_0$, and is excited by a transmission field $\mathbf{H}_1(\mathbf{r}) \cdot e^{-i\omega t}$ at the resonance frequency. Unlike conventional geophysical prospecting tools, the NMR method's selective characteristics permit new equipment to respond only to the water target. The effect of other minerals and structures on the NMR signal is only indirect, such as screening and relaxation of the NMR signal (Semenov, 1987a; Semenov et al., 1989).

It is important to consider the influence of the geoelectric structure of the earth on the surface NMR signal. High conductivity (low resistivity) is inherent in both saline water-saturated layers and, for example, clay-rich rocks. The resistivity of clay-rich soil and rock can be as low as 1–10 ohm-m, which is similar to saline-water–saturated rocks. In this case the model of the earth as a conductive half-space is a good description.

The aim of the present contribution is to compare the experimental and calculated surface NMR of groundwater response in conductive media.. It is not always possible to describe earth formations as a simple, homogeneous half-space. Therefore, the more general model of a horizontally-

Manuscript received by the Editor June 1, 1993; revised manuscript received August 6, 1995.
*Russian Academy of Sciences, Institute of Chemical Kinetics & Combustion, 3, Institutskaya Street, Novosibirsk, 630090, Russia and Novosibirsk State University, Novosibirsk, Russia.

stratified medium is also considered to compare calculations with experimental data.

BASIC PRINCIPLES OF SURFACE NMR IN THE EARTH'S FIELD

The method is based on the principle of observation of the proton magnetic resonance in the Earth's field of hydrogen ^1H atoms contained in groundwater molecules H_2O.

The geomagnetic field $\mathbf{H}_0$ sets up a net nuclear spin population in thermal equilibrium, which provides a macroscopic magnetic moment $\mathbf{M}_0$ (r) oriented parallel to $\mathbf{H}_0$ (Abragam, 1961)

$$\mathbf{M}_0(\mathbf{r}) = n(\mathbf{r})\,\frac{\gamma^2\hbar^2}{3kT}\,S(S+1)\cdot\mathbf{H}_0, \qquad (1)$$

where $n(\mathbf{r})$ is the number of magnetic nuclei per unit volume, $S = 1/2$ is the nuclear spin, $\hbar$ and k are Planck and Boltzman's constants, and T is the temperature.

A circular wire loop with a diameter of 100 m is laid out on the ground. This serves as both source antenna and NMR signal receiver. A sinusoidal current pulse with a rectangular envelope is passed through the loop to excite the NMR signal. The carrier frequency of the oscillating current in this pulse is equal to the Larmor frequency ω_L of protons in the Earth's magnetic field $\mathbf{H}_0$ (Semenov et al., 1982, 1988, 1989)

$$\omega_L = \gamma_H \cdot H_0, \qquad (2)$$

where γ_H is the gyromagnetic ratio of protons.

After the pulse, which generates the oscillating field $\mathbf{H}_1(\mathbf{r})\cdot e^{-i\omega t}$, the vector $\mathbf{M}_0(\mathbf{r})$ is tilted away from the vector $\mathbf{H}_0$ by the angle

$$\theta(\mathbf{r}) = 0.5\cdot\gamma_H\cdot H_{1\perp}(\mathbf{r})\cdot\tau_p, \qquad (3)$$

where $\mathbf{H}_{1\perp}(\mathbf{r})$ is the alternating field component that is normal to $\mathbf{H}_0$, and τ_p is the pulse duration. The coefficient 0.5 is caused by the linear rather than circular polarization of $\mathbf{H}_{1\perp}$ (r). The component of macroscopic nuclear magnetization that is normal to $\mathbf{H}_0$ is

$$M_\perp(\mathbf{r}) = M_0(\mathbf{r})\cdot\sin\theta(\mathbf{r}). \qquad (4)$$

Following the pulse, when $\mathbf{H}_1(\mathbf{r})\cdot e^{-i\omega t}$ is removed, the vector $\mathbf{M}_\perp(\mathbf{r})$ freely precesses about the geomagnetic field at the Larmor frequency ω_L.

The emf induced into the loop by the magnetic field of groundwater nuclear magnetization is determined by integrating over the volume (Semenov et al., 1988)

$$E_0(Q) = (\omega/I)\int_V M_\perp(\mathbf{r})H_{1\perp}(\mathbf{r})\,dV(\mathbf{r}), \qquad (5)$$

where I is the amplitude of the excitation current $I\cdot e^{-i\omega t}$, $Q = I\cdot\tau_p$ is the excitation pulse intensity, and $E_0(Q)$ is the NMR signal that is measured.

The depth of water-saturated layers can be determined from the NMR signal amplitude dependence on the excitation-current pulse intensity Q. Figure 1 shows the dependence of the surface NMR amplitude on the current pulse intensity Q, calculated for a 10-m thick model horizontal water layer located at different depths (10–20 m, 30–40 m, and 50–60 m). A strong correlation of a maximum NMR signal with the location depth of water is clear from this example.

I have earlier discussed the effects of variations in the Earth's field $\mathbf{H}_0$ on the surface NMR signal in Trushkin et al. (1993). Some aspects of correlation between the NMR relaxation time and water-bearing soil grain size are discussed in Semenov (1987a and b) and Schirov et al. (1991). Different antenna types, such as a noise-reducing figure-of-eight-shaped antenna, are investigated in Trushkin et al. (1994).

CALCULATION OF THE SURFACE NMR SIGNAL CONSIDERING FORMATION CONDUCTIVITY

In electrically conductive media, the magnetic fields of the loop and groundwater magnetic nuclei are changed in amplitude and phase because of the screening effect of induced currents in the intervening conductive media.

The time-harmonic electric and magnetic fields $\mathbf{E}\cdot e^{-i\omega t}$ and $\mathbf{H}\cdot e^{-i\omega t}$ in source-free media of magnetic permeability μ, dielectric permittivity ε, and conductivity σ satisfy Maxwell's equations

$$\begin{cases} curl\ \mathbf{H} = (\sigma - i\omega\varepsilon)\cdot\mathbf{E} \\ curl\ \mathbf{E} = i\omega\mu\mathbf{H} \\ div\ \mathbf{H} = div\ \mathbf{E} = 0. \end{cases} \qquad (6)$$

To calculate the excitation magnetic field of the loop and the surface NMR signal, a good first approximation is a model of two homogeneous half-spaces, i.e., nonconductive (air) and electrically conductive (earth). In this case, electric and magnetic fields are called normal. Sommerfeld (1926) was the first to calculate the normal field of a magnetic dipole, and the normal electromagnetic field around a loop-shaped current source was studied by Ryu et al. (1970). For a more detailed presentation see Wait (1982).

Assume that the wire loop is to be placed at the origin of a cylindrical coordinate system (r, φ, z), so that the wire is laid along the circle $r = R_0$ in the plane $z = 0$. A homogeneous and uniform formation with conductivity $\sigma_1 = \sigma$ fills the

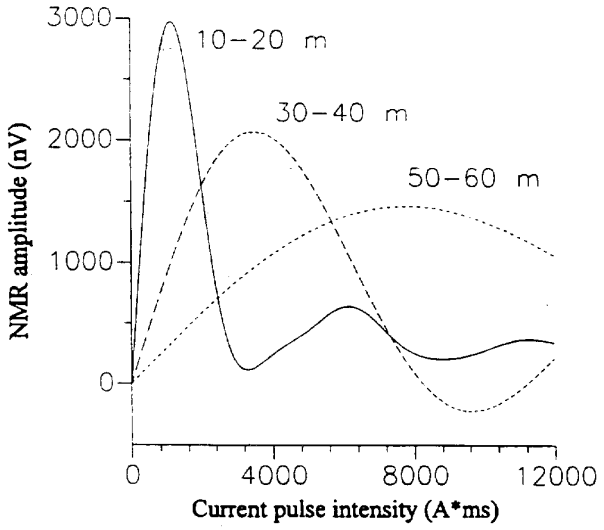

FIG. 1. An example of the dependence of surface NMR amplitude on current pulse intensity calculated for a 10-m–thick model horizontal water layer located at depths from 10–20 m, 30–40 m, and 50–60 m.

half-space $z > 0$, the air conductivity being $\sigma_0 = 0$ (Figure 2). Because of axial symmetry, the magnetic Hertz potential (Nisbet, 1955) only has a vertical component.

In the half-space $z > 0$, the solution of equation (6) for the magnetic field of the loop has the form (Shushakov and Legchenko, 1992, 1994a)

$$H_{1z}(\mathbf{r}) = IR_0 \int_0^\infty \frac{m^2}{m+u} e^{-uz} J_1(R_0 m) \cdot J_0(rm)\, dm \qquad (7)$$

$$H_{1r}(\mathbf{r}) = IR_0 \int_0^\infty \frac{mu}{m+u} e^{-uz} J_1(R_0 m) \cdot J_1(rm)\, dm, \qquad (8)$$

where $u = (m^2 - \varepsilon\mu\omega^2 - i\sigma\mu\omega)^{1/2}$ and J are Bessel functions.

The magnetic dipole fields over a horizontally stratified formation were studied by Wait (1951, 1952) and several other authors (compiled in Wait, 1982). The equations in Shushakov and Legchenko (1994b) for the magnetic field of the circular loop over the horizontally stratified earth, as well as equations (7) and (8) for the conductive half-space, are used for the calculations in the present paper.

The alternating magnetic field is doubly screened as a result of the finite electrical conductivity of the medium. First, the field $\mathbf{H}_1(\mathbf{r}) \cdot e^{-i\omega t}$ of the loop is screened during the exciting pulse. Then, the field created by macroscopic transverse nuclear magnetization freely precessing in the Earth's magnetic field is screened upon the NMR signal observation. A reciprocity principle (Frank and Mises, 1935), which allows the change of source and a receiver in electromagnetic field calculations, is widely used in geophysics. To calculate the field created by the precessing nuclear magnetization with regard to conductivity, it is reasonable to use the reciprocity principle, because of the absence of cylindrical symmetry in the magnetic field of nuclei with the arbitrary geomagnetic field inclination (Shushakov and Legchenko, 1992, 1994a).

The excitation field $\mathbf{H}_1(\mathbf{r}) \cdot e^{-i\omega t}$ can be regarded as a complex value in expression (5) in the presence of formation conductivity. Equations (3) and (4) can be rewritten as

$$\theta(\mathbf{r}) = 0.5 \cdot \gamma_H \cdot |H_{1\perp}(\mathbf{r})| \cdot \tau_p, \qquad (9)$$

$$\mathbf{M}_\perp(\mathbf{r}) = [\mathbf{M}_0(\mathbf{r}) \times \mathbf{H}_1(\mathbf{r})/|H_1(\mathbf{r})|] \cdot \sin\theta(\mathbf{r}). \qquad (10)$$

The NMR signal is also a complex value possessing amplitude and phase. The vector model of NMR signal formation (Abragam, 1961) gives the expression

$$E_0(Q) = (\omega/I) \int_V \{M_\perp(\mathbf{r}) H_{1\perp}^2(\mathbf{r})/|H_{1\perp}(\mathbf{r})|\}\, dV(\mathbf{r}). \qquad (11)$$

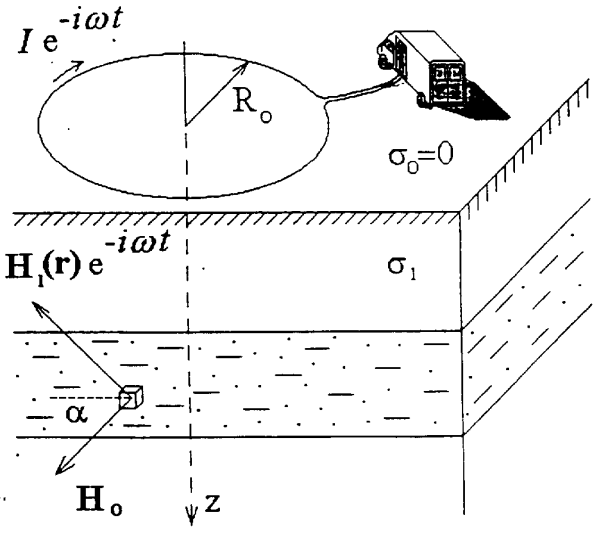

FIG. 2. Schematic representation of the R_0 radius excitation loop, model half-spaces of $\sigma_0 = 0$ conductivity (air) and $\sigma_1 = \sigma$ (earth), and the coordinate system. Also shown schematically are the magnetic fields acting on the elementary aquifer volume: the Earth's magnetic field is $\mathbf{H}_0$ and the current loop oscillating field is $\mathbf{H}_1(\mathbf{r}) \cdot e^{-i\omega t}$.

EXPERIMENT

The measurements of groundwater NMR were carried out with the equipment developed by A.G. Semenov and his co-workers at the Institute of Chemical Kinetics and Combustion, Russian Academy of Sciences, Novosibirsk (Semenov et al., 1982). Unlike conventional techniques, (Semenov et al., 1987, 1988) the amplitude as well as the phase of the NMR signal was measured. The dependence of the NMR signal phase on conductivity was verified first by Semenov et al. (1989).

The field experiments were performed in the Altay region of Russia near Malinovoe Lake. The measured data were compared with the calculations made for a horizontally stratified medium (Shushakov and Legchenko, 1994b). The stratified-medium model was developed from borehole logs, vertical resistivity profiles, and salinity data, obtained from the Zapsibgeologiya report (1988).

Figure 3 shows the vertical geological cross-section and resistivity profile of a test site. The apparent resistivity varies along the profile. At borehole site 153, the measured resistivities are 50 ohm-m with AB/2 separation equal to 25 m and more than 100 ohm-m for AB/2 equal to 60 m. At borehole site 16, however, the resistivities are 4 and 6 ohm-m, respectively. For hole 17, the resistivities are 1.5 and 2 ohm-m.

For borehole 17 the stratigraphic logs show a thick water-containing strata (aquifer) from 13 to 31.3 m depth and aquifer from 49 to 55.8 m. (The absolute elevation is shown in Figure 3 instead of the depths for each borehole). The total dissolved solids (salinity) of underground water in the aquifers is 12 g/l and 0.4 g/l, respectively. For borehole 16 there is an aquifer from 19 to 34.2 m with salinity of 3 g/l, and an aquifer from 39 to 45 m with 0.47 g/l salinity. At borehole site 153, the salinity was much less than 0.5 g/l. The salinity at borehole 153 was estimated from the data of the nearby borehole that penetrates the aquifer, denoted by a dashed line in Figure 3.

The geological profile, shown in Figure 3 was obtained using data from nearby boreholes, as well as those shown in the cross-section, and it is assumed that the profile represented is reliable. Furthermore, the calculations testify to a smaller NMR signal magnitude from deeper high-conductivity layers. Therefore, the assumption made does not allow for significant errors for the layer at the depth of 54–61 m in borehole site 16.

RESULTS AND DISCUSSION

Figure 4 shows the calculated NMR signal amplitude and phase as a function of excitation-current pulse intensity for a 10-m-thick model horizontal water layer located at different depths (10–20 m, 30–40 m, 50–60 m) and as a function of half-space conductivity. The conductivity of the water-saturated layer is the same as that of the half-space. The geomagnetic field inclination was assumed to be 90°.

According to the calculations, the electrical conductivity has a great effect on the phase and amplitude of the NMR signal. For greater depth of a water-saturated layer, the characteristic resistivity at which the changes occur is even larger. This dependence correlates with that of a skin effect depth on the resistivity. More subtle physical effects of an electromagnetic field like interference or diffraction are expected in layered media. Their consideration, however, is beyond the scope of this paper.

Figure 5 depicts the NMR-signal phase and amplitude versus excitation-pulse intensity, for a water-saturated layer at depth from 10 to 20 m, located in a uniform half-space with 1 ohm-m resistivity, and for three different inclinations of the Earth's magnetic field. The conductivity of the water-saturated layer is the same as that of the half-space. As indicated by the calculations shown in Figures 4 and 5, the influence of conductivity on the NMR signal is more significant than the dependence on the geomagnetic-field inclination. This is because the vertical component of the magnetic field of the loop shows different changes with increasing depth than the horizontal one.

Figure 6 shows the NMR-signal phase and amplitude for a water layer from 50 to 60 m located in a horizontally layered medium. The conductive layer with a thickness of 10 m and a resistivity of 1 ohm-m is situated in different positions with

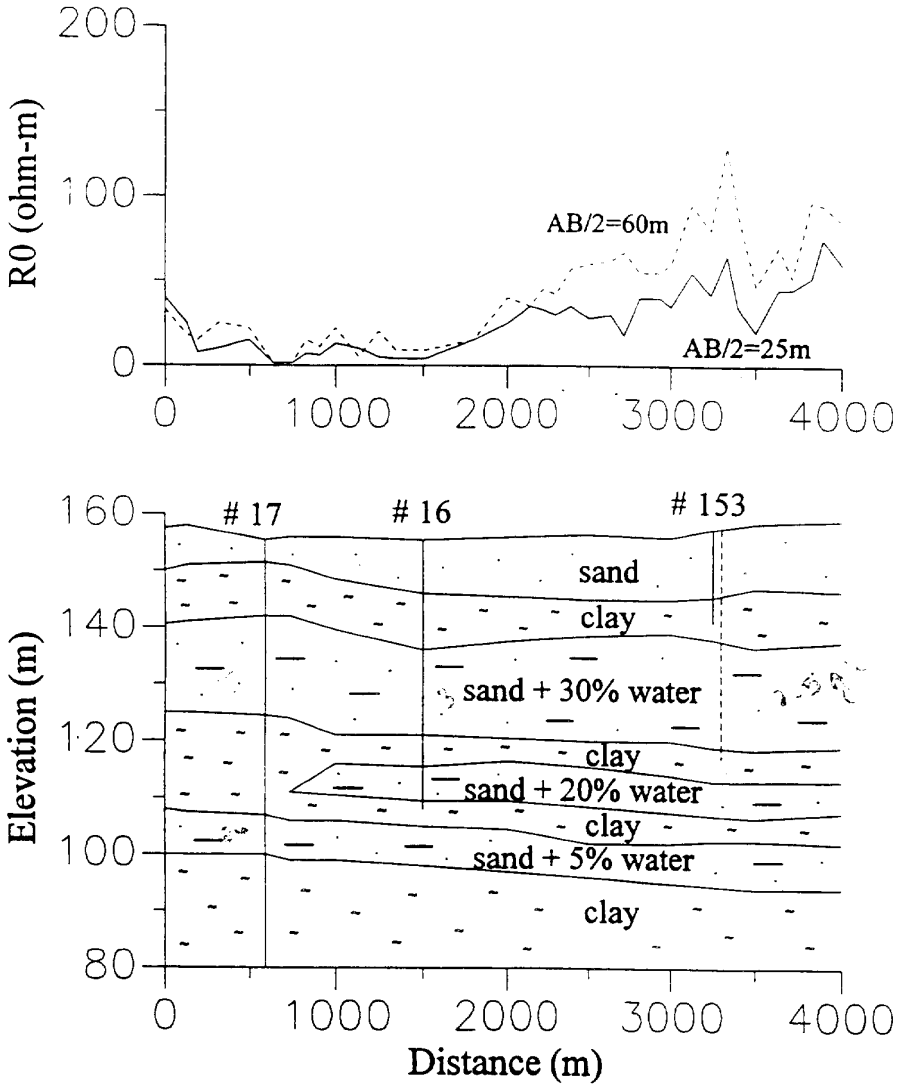

FIG. 3. Vertical geological cross-section of the test site. At the top are horizontal resistivity profiles with AB/2 separation equal to 25 m (solid line) and AB/2 equal to 60 m (dashed line).

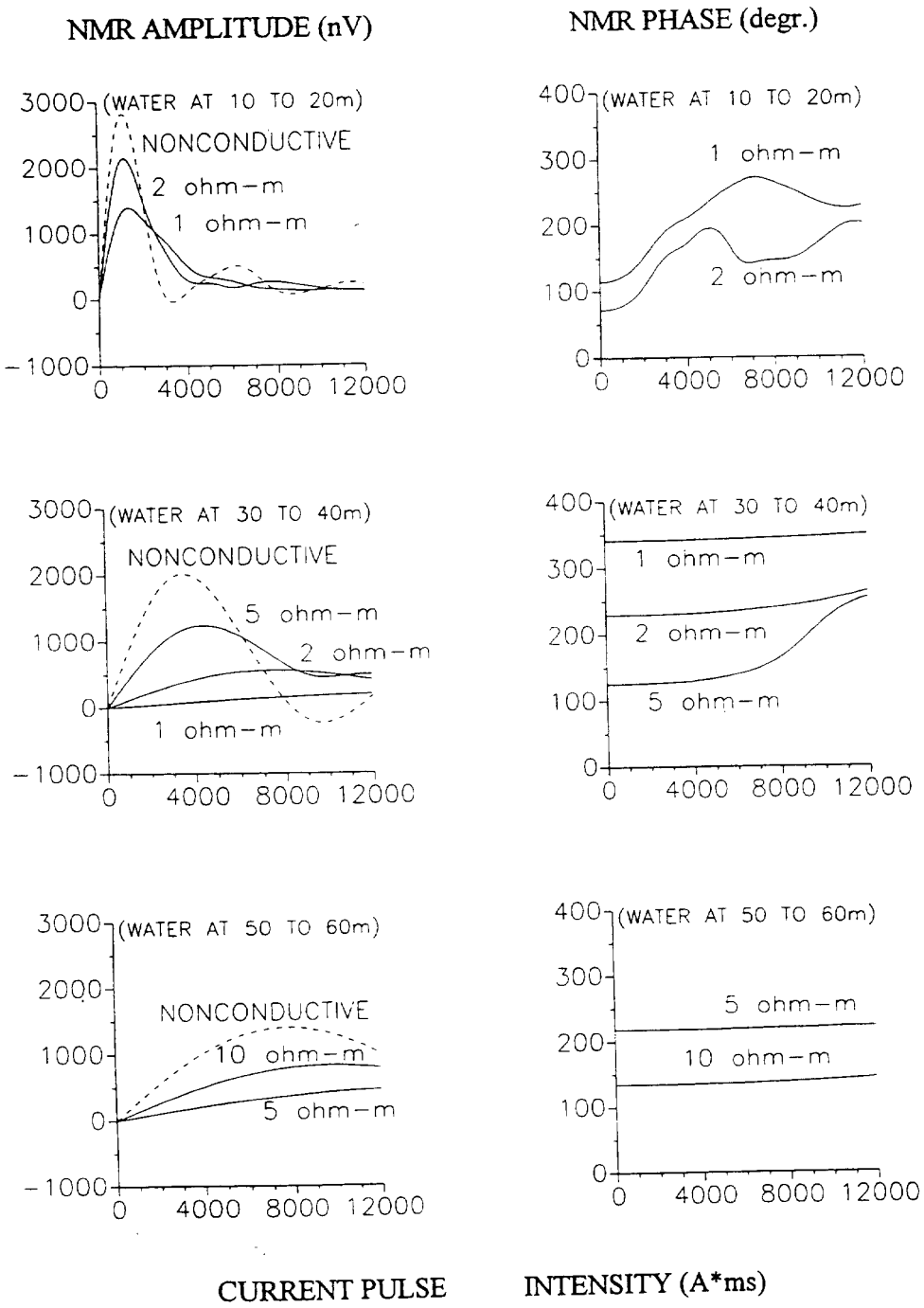

FIG. 4. NMR signal amplitude and phase versus excitation-pulse intensity, calculated for different conductive half-space resistivities as shown and at different depths for the 10-m–thick, water-saturated layer.

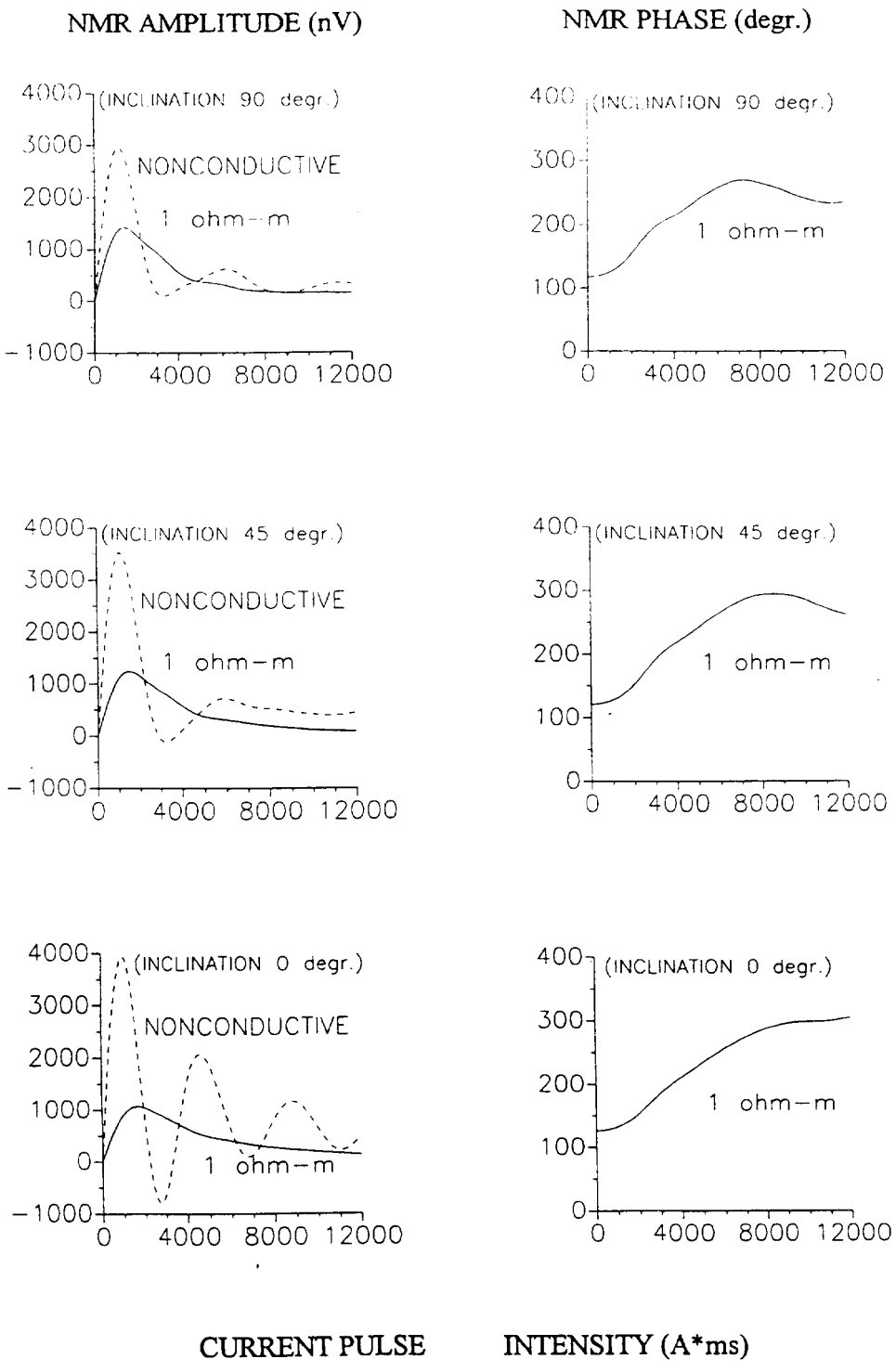

FIG. 5. NMR signal amplitude and phase against excitation pulse intensity calculated with different geomagnetic field inclinations. The half-space resistivity is 1 ohm-m. Dashed line shows the NMR signal in a nonconducting half-space.

respect to the water layer. When a conductive layer is located above the water-saturated layer, Figure 6 indicates a decrease in the NMR-signal amplitude. If the conductive layer is under the water-saturated layer, the NMR-signal amplitude increases. When the depths of the conductive and water-saturated layers coincide, the NMR-signal amplitude and phase change with the thickness of the layers. In practice, this effect corresponds to the case of a layer saturated with saline water located in a weakly conductive medium. These results contradict the measurements proposed by Semenov et al.'s (1989) for a groundwater salinity by the NMR-signal phase. Thus, it is concluded that saline and fresh water cannot be distinguished by measuring only NMR-signal amplitude and phase.

Figure 7 compares the calculated and measured NMR-signal phase and amplitude at borehole sites 153, 17, and 16. The resistivity of soil was estimated from the resistivity profile (Figure 3) using a one- or two-layer earth model (Wait, 1982). The groundwater salinity data and the loop impedance measurements (Trushkin et al., 1995), as well as location of strata boundaries (Figure 3) were also taken into account to estimate the resistivity of aquifers.

The location of aquifers in borehole 153 was determined from the geologic profile (Figure 3). The volume content of water $n(z)$ in equation (1) was calculated from the NMR data, and, in addition, the experimentally determined location of stratum boundaries coincides with the data in Figure 3. A resistivity high was observed at borehole site 153 (Figure 3). Therefore, the volume content of water $n(z)$, obtained at borehole site 153 by the NMR data-inversion algorithm that regards as well as disregards the conductivity, is reliable. The surface NMR inversion procedure is described shortly in Trushkin et al. (1995).

Since the greatest distance between boreholes is only 2.7 km, it is assumed that the principal properties of water-bearing rock, such as porosity, do not significantly change along the cross-section (Figure 3) and, therefore, the water content $n(z)$ does not appreciably vary within each water-saturated layer.

There are three aquifers at borehole site 153 (15–33 m, 43–50 m and 54–61 m) with, as determined from the NMR data, a volume water content $n(z) \cdot 100$ [equation (1)] of 30%, 20%, and 5%, respectively. The resistivity is about 50 ohm-m using a one- or two-layer model. According to the modeling results considered above, this level of medium resistivity has practically no effect on the surface NMR signal.

For borehole site 17, the calculations were performed for two aquifers at 13–31 m and 50–56 m depth, which provided 30% and 5% water content, respectively. The resistivity of the near-surface layer (from 0 to 13 m), determined from the dc apparent resistivity data and from the cross-section (Figure 3), was about 1.5 ohm-m. The resistivity of the aquifer at 13 to 31 m, estimated from the salinity data and the loop impedance measurement, was approximately the same value.

At borehole site 16, the NMR signal was calculated for three layers, 19–34 m (30% water), 39 to 45 m (20% water), and 49 to 57 m (5% water). The resistivity was determined to be 4 ohm-m from 0 to 40 m, and 7 ohm-m from 40 m to downward.

Figure 7 indicates a fair agreement between calculated and measured data. It should be noted, however, that the calculated NMR-signal amplitudes at borehole sites 16 and 17 correspond, in the absence of conductivity, to the measured-signal amplitude at borehole site 153. At the same time, when conductivity is taken into account, the NMR-signal amplitude decreases about three times for borehole 17 and two times for borehole 16.

CONCLUSIONS

The NMR signal caused by groundwater was calculated as a function of conductivity. For a uniform half-space, with a

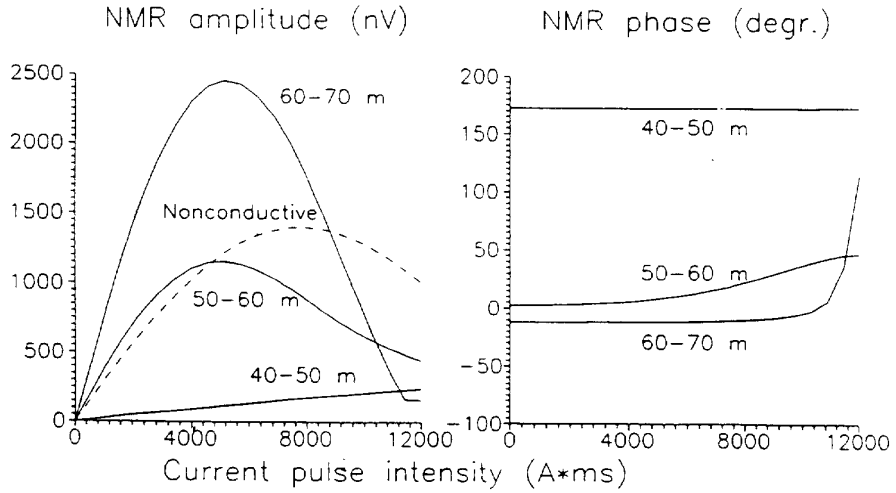

FIG. 6. NMR signal amplitude and phase as a function of excitation-pulse intensity calculated for a three-layer formation model and a different relative arrangement of the water-saturated and conductive layer. Aquifer is located at a depth of 50 to 60 m. The depth of the conductive layer is shown in the figure; this layer has a resistivity of 1 ohm-m. The dashed line shows the NMR signal amplitude in the absence of the 1 ohm-m conductive layer.

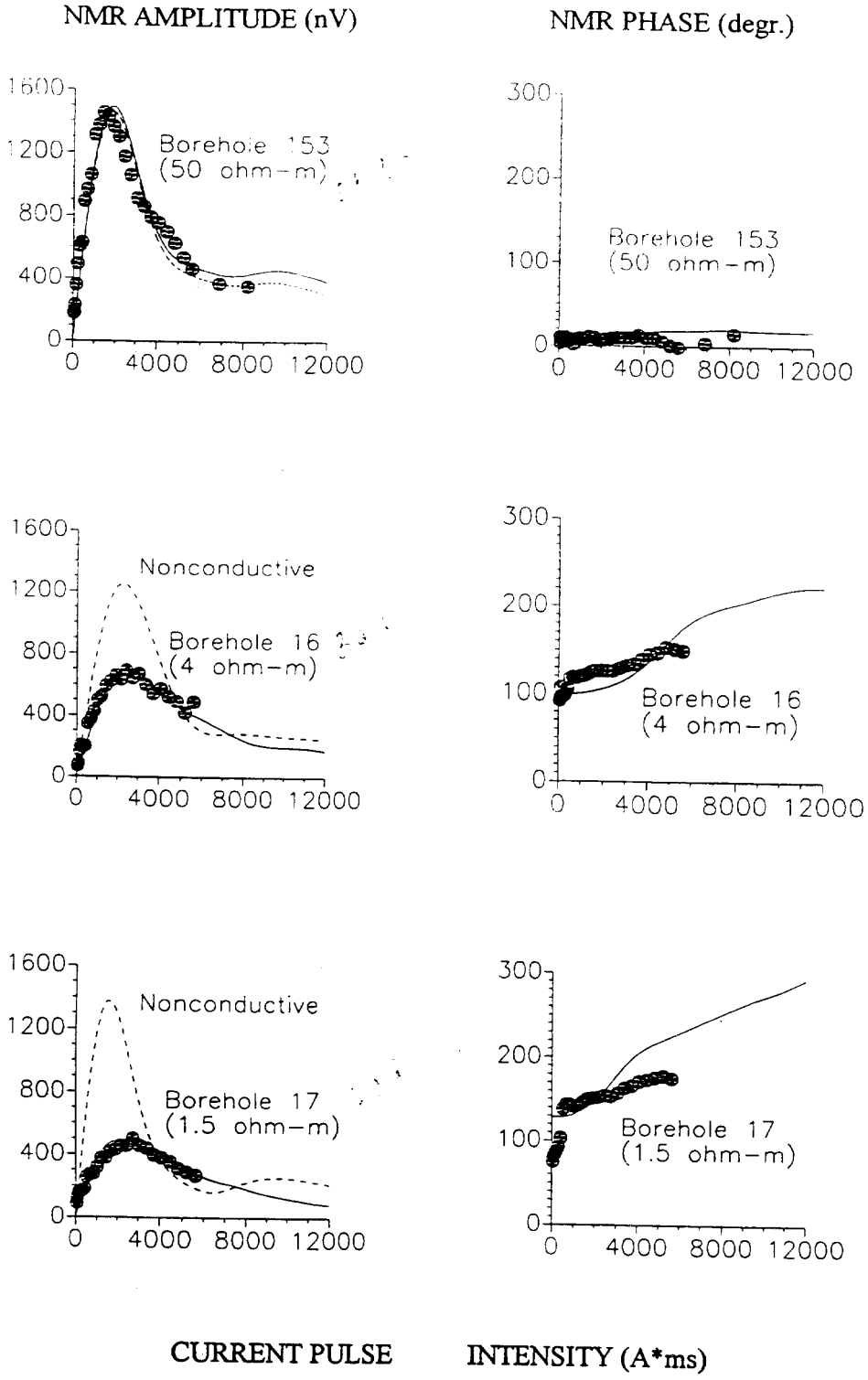

FIG. 7. Comparison of measured with calculated NMR amplitude and phase, as a function of excitation pulses at borehole sites 153, 17, and 16. Points show the experimental results, solid lines represent calculations. Dashed lines show calculated NMR signal amplitude in the absence of conductive layers.

resistivity of a few ohm-m to several tens of ohm-m (depending on the depth of water-saturated layers), the NMR-signal amplitude and phase are shown to vary substantially because of magnetic-field screening.

When the formation is conductive, the NMR-signal curve shape versus excitation-pulse intensity (e.g., maximum position) undergoes considerable modification.

The dependence of the NMR-signal phase and amplitude on geomagnetic field inclination has been studied by taking into account an oscillating magnetic-field screening that results from the conductivity of the medium. From this, the Earth's field inclination has been shown to have a minor affect on the NMR signal.

Calculated and experimental groundwater NMR signals have been compared in terms of formation conductivity. Good agreement was found between these data.

Some characteristics of groundwater NMR-signal behavior have been examined for layered formations, specifically. It is shown that the groundwater salinity cannot be determined by measuring only the NMR-signal amplitude and phase.

While working toward this publication, I also investigated the integration of an electromagnetic method and surface NMR into one device, using the same antenna (Trushkin et al., 1995). This led to a significant improvement in the NMR-signal-inversion result, with only a minor complication in the surface NMR method.

ACKNOWLEDGMENTS

The author is grateful to D. V. Fitterman, A. Sezginer, and D. K. Butler for fruitful suggestions about improvement of this paper, to M. D. Schirov for assistance in obtaining the borehole and resistivity data, and to A. V. Legchenko for valuable discussions. H. M. Kluyver edited the final version of this paper.

REFERENCES

Abragam, A., 1961, The principles of nuclear magnetism: Oxford Univ. Press.

Frank, P., Mises, R., 1935, Riemann-Weber's Differentialgleichungen der mathematischer Physik: Vieweg.

Nisbet, A., 1955, Hertzian electromagnetic potentials and associated gauge transformations: Proc. Roy. Soc., A231, 250–263.

Ryu, J., Morrison, H. F., and Ward, S. H., 1970, Electromagnetic field about a loop source of current: Geophysics, **35**, 862–896.

Schirov, M. D., Legchenko, A. V., and Creer, J. G., 1991, New direct non-invasive groundwater detection technology for Australia: Expl. Geophys., **22**, 333–338.

Semenov, A. G., 1987a, The experience of application of nuclear magnetic resonance for the exploration of subterranean waters: IXth Ampere summer school on magnetic resonance, Novosibirsk, Abstracts, 61.

——— 1987b, NMR Hydroscope for water prospecting: Proc. of a seminar on Geotomography: Indian Geophys. Union, 66–67.

Semenov, A. G., Burshtein, A. I., Pusep, A. Yu, and Schirov, M. D., 1988, A device for measurement of underground mineral parameters: USSR Patent 1079063. (in Russian).

Semenov, A. G., Pusep, A. Yu, and Schirov, M. D., 1982, Hydroscope-An installation for prospecting without drilling: USSR Acad. Sci., Novosibirsk, 1–26. (in Russian).

Semenov, A. G., Schirov, M. D., and Legchenko, A. V., 1987, On the technology of subterranean water exploration founded on application of the nuclear magnetic resonance tomograph "Hydroscope": IXth Ampere summer school on magnetic resonance, Novosibirsk, Abstracts, 214.

Semenov, A. G., Schirov, M. D., Legchenko, A. V., Burshtein, A. I., and Pusep, A. Yu, 1989, Device for measuring the parameter of underground mineral deposit: Great Britain Patent 2198540B.

Shushakov, O. A., and Legchenko, A. V., 1992, Calculation of the proton magnetic resonance signal from groundwater considering the electroconductivity of the medium: Russian Acad. of Sci., Inst. of Chem. Kinetics and Combustion, Novosibirsk, issue No. 36, 1–26. (in Russian).

——— 1994a, Calculation of a proton magnetic resonance signal of underground water considering medium electrical conductivity: Geol. and Geophys., **35**, No. 3, 130–136. (in Russian).

——— 1994b, Groundwater proton magnetic resonance in the horizontally stratified media of different electrical conductivity: Geol. and Geophysics, **35**, No. 10, 161–166. (in Russian).

Sommerfeld, A., 1926, Uber die Ausbreitung der Wellen in der drahtlosen Telegraphie: Ann. d. Phys., **81**, 1135–1153.

The Zapsibgeologiya Report of Geophysical Surveys, 1982–1988: 1988, Barnaul. (in Russian).

Trushkin, D. V., Shushakov, O. A., and Legchenko, A. V., 1993, Modulation effects in non-drilling NMR in the Earth's field: Appl. Mag. Resonance, 5, 399–406.

———. 1994, The potential of a noise-reducing antenna for surface NMR groundwater surveys in the earth's magnetic field: Geoph. Prosp., **42**, 855–862.

——— 1995, Surface NMR application to an electroconductive medium: Geoph. Prosp., **43**, 623–633.

Varian, R. H., 1962, Ground liquid prospecting method and apparatus: US. Patent 3019383.

Wait, J. R., 1951, The magnetic dipole over the horizontally stratified earth: Can. J. Phys. Sci., **29**, 577–592.

——— 1952, Mutual inductance on a two-layer earth: Can. J. Phys. Sci., **30**, 450–452.

——— 1982, Geo-electromagnetism: Academic Press, Inc.

Paper presented at the SEG Houston'95 annual meeting

Noninvasive NMR study of subsurface aquifers in France

Anatoly V. Legchenko, Oleg A. Shushakov, Russian Academy of Sciences; Jose A. Perrin, BRGM, France; and Alexander A. Portselan, Hydrogeotom Ltd., Russia

Summary

The fact that nuclear magnetic resonance (NMR) measures the signal directly from subsurface water molecules is the main advantage of this technique compared to other geophysical methods. The basic principles presented in this paper provide an understanding of the NMR method in relation to aquifer investigation.

Interpretation of experimental data may reveal a number of aquifers, their location and their water content. The method enables an estimation of the mean grain size of the water-saturated rock and provides information regarding electrical conductivity distribution in the rock.

An example of application of this method in France demonstrates its performance over different types of aquifers.

Introduction

Both the method and equipment used for non-invasive NMR groundwater investigation were developed by a team in Russia under the guidance of A.G. Semenov (Semenov *et al.*, 1988).

The method is assumed to record the magnetic resonance signal directly from the subsurface water molecule protons. Data processing enables location of the aquifer and determination of other parameters. Compared to other geophysical tools, the selective characteristics of NMR means that it only responds to the water target itself.

This new method, used successfully since the early eighties in Russia, is still unknown to the western world. The purpose of this paper is to explain to a wide audience what type of aquifer data may be obtained using this new tool.

Unlike other reported field tests (Shirov *et al.*, 1991, Goldman *et al.*, 1994), fractured rock aquifers (limestone, chalk) were investigated in France.

Theory

In order to record the NMR signal, an antenna, consisting of a piece of wire, is laid out on the ground in the shape of a circle with a diameter of approximately 100 m. An oscillating current pulse with a rectangular envelope is passed through the wire. The carrier frequency of the current is equal to the Larmor frequency $\omega_0 = \lambda H_0$ in the geomagnetic field $\mathbf{H}_0$ (Abragam, 1961). As a result, the transmitted oscillating magnetic field component $h_{1\perp}(\mathbf{r}, \rho(\mathbf{r}))$ causes nuclear magnetization of the protons $\mathbf{M}_0(\mathbf{r})$ (Figure 1) to shift away from the equilibrium position along the geomagnetic field at the angle

$$\theta = (1/2)\lambda\, h_{1\perp}(\mathbf{r}, \rho(\mathbf{r}))q, \qquad (1)$$

where $q = I\tau$ is the pulse intensity and I, τ are respectively the pulse amplitude and duration, $\rho(\mathbf{r})$ is rock resistivity, $\mathbf{r} = r(x, y, z)$. The vector $\mathbf{M}_0(\mathbf{r})$ rotates around the

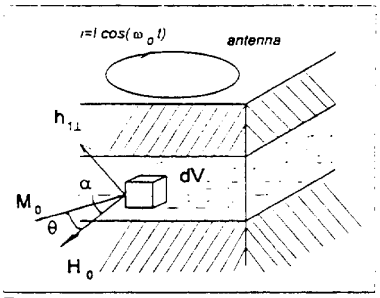

Fig.1. Nuclear magnetization movement vector diagram.

geomagnetic field with the Larmor frequency and creates an oscillating magnetic field. As λ is a gyromagnetic ratio for the protons, no other response will appear and existence of the NMR signal after the pulse termination guarantees the presence of subsurface water. For infinite horizontal homogeneous layers, the NMR signal is a function of depth (Shushakov and Legchenko, 1994a,b),

$$E_0(q) = \int_0^L K(q, \rho(z), \alpha, z) n(z) dz, \qquad (2)$$

where

$$K(q, \rho(z), \alpha, z) = \omega_0 M_0 \int_{x,y} h_{1\perp}(\mathbf{r}, \rho(z), \alpha)\ \sin(\theta) dx dy,$$

E_0 is the initial amplitude of the NMR signal, α is the geomagnetic field inclination, $L \approx 2D$, where D is antenna diameter, and $0 \le n(z) \le 1$ is the water concentration.

Assuming that the geomagnetic field is homogeneous over all the studied aquifers and that stratification is horizontal, the recorded NMR signal can be presented as

$$e(t, q) = \int_0^L A(z, q)\ \sin(\omega_0 t + \varphi_0(z, \rho(z)))dz, \qquad (3)$$

where $A(z, q) = K(q, \rho(z), \alpha, z) n(z)\ \exp(-t / T_2^*(z))$,

$\varphi_0(z, \rho(z))$, $T_2^*(z)$ is the NMR signal phase and spin-spin relaxation time constant.

The initial amplitude of the NMR signal corresponds to the location and bulk water volume of the aquifers, decay time correlates with the mean grain size of water-saturated rock and phase follows the rock electrical conductivity (Legchenko *et al.*, 1990).

Inversion of the equations (2) and (3) allows determination of water concentration ($n(z)$), mean value of the NMR signal decay time ($T_2^*(z)$) and rock resistivity ($\rho(z)$) as a function of depth.

For inversion, the well-known Tikhonov regularization method was used (Tikhonov and Arsenin, 1977). Antenna impedance data were also taken into account (Trushkin *et al.*, in press).

Data interpretation

The following information about each of the aquifers can be obtained from the NMR signal:

1) water concentration $n(z)$ enables determination of depth, thickness and bulk water volume. Absence of the NMR signal ($E_0(q) = 0$ for any q) guarantees with high reliability the absence of subsurface water.

2) decay time ($T_2^*(z)$) corresponds to the mean grain size of the water-saturated rock. There is an empirical correlation between rock type and decay time for sedimentary rocks (Shirov *et al.*, 1991). There is a general tendency for decay time to be longer for coarser-grained material (up to 700-800 ms for free water in a lake), and shorter for fine-grained material (less than 30 ms in clay).

There is a relationship between the borehole yield in the study area and both water concentration and decay time. The yield may be estimated without any additional data using the NMR method, but borehole pumping test results at one of the sites of the area must be used for a precise determination of its absolute value. Experience gained from long term application of the surface NMR method for water prospecting in Russia indicates that the number of required boreholes can be significantly reduced.

Results and discussion

Field experiments with the 'Hydroscope' instrument were carried out in France in 1992 over well-known aquifers, studied previously, using traditional methods including borehole tests, by BRGM. Where antenna diameter is D, the area investigated using NMR can be approximated to a vertical coaxial cylinder of 2D in the horizontal plane and 1D in the vertical plane.

At the first test area of St-Cyr-en-Val, three aquifers were determined during the BRGM geological study. The upper aquifer consists of a stratum of mixed gravel, sand and clay, approximately 20-25 m thick. The two other aquifers consist of water-saturated karst limestone separated by a sandstone layer at a depth of 50-60 m. The total thickness is about 70-80 m and the average porosity is approximately 10%. Water transmissivity is around 0.28 sq.m/s.

At the Bazancourt test area there is an aquifer made up essentially of cracked chalk but with other material in the top few meters, and with an average porosity of about 40%. The permeability of the chalk mainly depends on its consolidation and the development of fractures. This aquifer is fairly homogeneous and its thickness is approximately 100-120 m. Water transmissivity is about 0.036 sq.m/s.

Amplitude, decay time and phase parameters of the NMR signal were measured. Experimental data (dots), depicted in Figures 2, 3 and 4, indicate a significant difference between signals recorded at these two sites.

The lithological log of borehole N268, situated approximately 600 m from the NMR test site, and the interpretation results of the NMR data are presented in Figure 5. The observed difference between the depth of the detected shallow aquifer and the water table may be explained both by existing moisture detected by NMR, and noise influence on the interpretation results. Due to the lack of a borehole at the test site itself, it is not possible to verify the exact location of this fairly irregular aquifer. The limestone aquifer between 28 and 52 m is quite extensive throughout the area. It is well-detected by NMR. No water was found below 55 m. This negative result may be easily explained by the existence of an electrically conductive shallow layer whose screening effect decreases the depth of investigation. The determined NMR signal decay time values for both aquifers are in good agreement with the geological description of the water-saturated rocks (material is quite coarse grained). The observed resistivity distribution indicates lower values for the shallow aquifer. For the comparison, DC resistivity method data are presented.

In the Bazancourt area, borehole N22 is located 325 m from the test site. Unfortunately, no deeper borehole exists close to the test site. A lithological log and interpretation results of NMR data are presented in Figure 6. Two aquifers were detected by the NMR method. The location of the upper layers coincides well with the measured water table level. Due to the lack of geological data it is not possible to discuss the observed dry interval between 33 and 38 m. According to geological data, the chalk aquifer must be approximately 100-120 m deep, but the lack of resolution with depth does not enable detection of its base with NMR. Short decay time of the signal was observed which is normal for fine-grained material, and correlates very well with much lower values of water transmissivity at Bazancourt compared to the other test site of St-Cyr-en-Val.

The results of antenna impedance measurements and water chemical analysis, and the geological description of the area prove the absence of high conductivity in the rocks, as indicated by NMR.

Reconstructed theoretical signals of detected aquifers (solid lines on Figures 2, 3 and 4) correspond quite well with true measurements.

Electromagnetic interference observed during the tests did not affect the interpretation results.

Conclusions

A large variation of the measured NMR signals over selected aquifers (water transmissivity differs about 10 fold) demonstrates the high sensitivity of this method to aquifer parameters.

Parameters obtained during study of the aquifers are in quite good agreement with existing geological data.

The presented method, based on direct measurement of the NMR signal from subsurface water, generally enables determination of aquifer parameters (depth, thickness, water content and mean grain size) without any information regarding the subsurface structure in a variety of geological environments.

References

Abragam, A., 1961. The principles of nuclear magnetism: Oxford University press.

Goldman, M., Rabinovich, B., Rabinovich, M., Gilad, D., Gev, I. and Schirov, M. 1994. Application of integrated NMR-TDEM method in ground water exploration in Israel, Journ. of Appl. Geophysics, 31, 27-52.

Legchenko, A.V., Semenov, A.G., and Shirov, M.D., 1990, (in Russian). A device for measurement of subsurface water saturated layers parameters. USSR Patent 1540515.

Semenov, A.G., Burshtein, A.I., Pusep, A.Yu., and Schirov, M.D., 1988, (in Russian). A device for measurement of underground mineral parameters. USSR Patent 1079063.

Shirov, M., Legchenko, A. and Creer, G. 1991. New direct non-invasive ground water detection technology for Australia, Exploration Geophysics, 22, 333-338.

Shushakov, O.A. and Legchenko, A.V. 1994a. Calculation of proton magnetic resonance signal of underground water considering medium electric conductivity. Geol. and Geophysics, 1994, 35, No3, 130-136. (in Russian).

Shushakov, O.A. and Legchenko, A.V. 1994b. Ground water proton magnetic resonance in the horizontally stratified media of different electrical conductivity, Geol. and Geophysics, 35, No 10, 161-166. (in Russian).

Tikhonov, A. and Arsenin, V. 1977. Solution of ill-posed problems, Wiley and Sons, Washington D.C.

Trushkin, D.V., Shushakov, O.A. and Legchenko, A.V., Surface NMR application to an electroconductive medium, Geophysical Prospecting, in press.

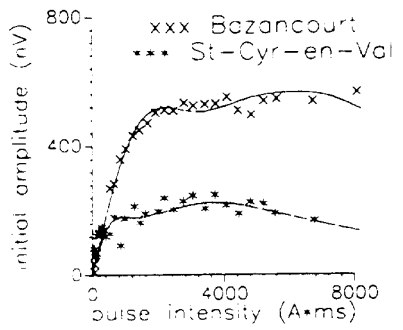

Fig.2. NMR signal amplitude.

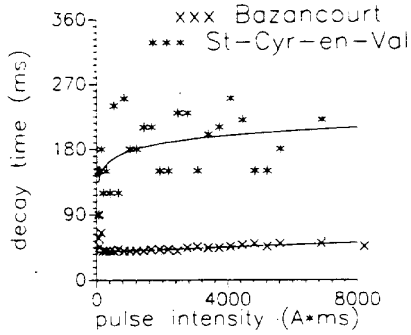

Fig.3. NMR signal decay time.

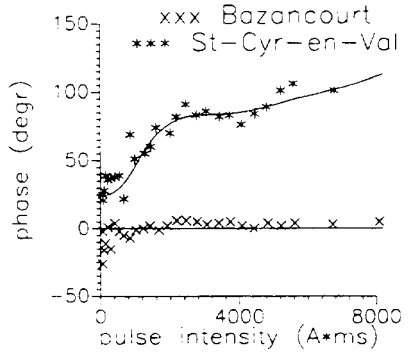

Fig.4. NMR signal phase.

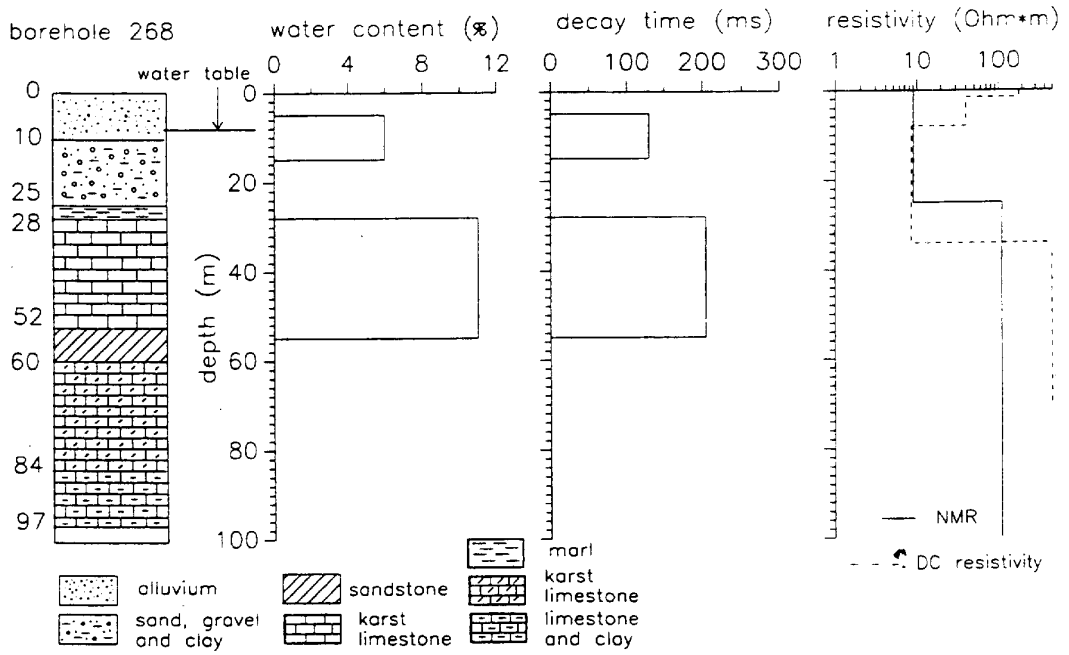

Fig.5. Interpretation results. St-Cyr-en-Val area.

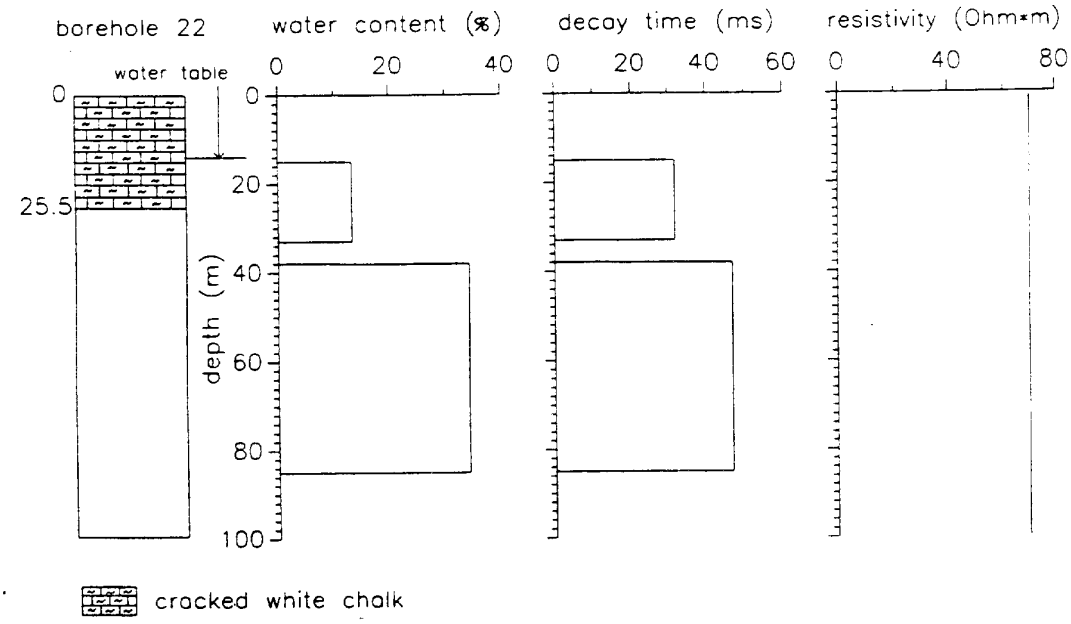

Fig.6. Interpretation results. Bazancourt area.

Geophysical Prospecting, 1995, 43, 623–633

Surface NMR applied to an electroconductive medium[1]

D.V. Trushkin,[2] O.A. Shushakov[2, 3] and A.V. Legchenko[3]

Abstract

An integrated electromagnetic and nuclear magnetic resonance (NMR) method is proposed for investigating highly conductive soil areas. Using a simple model of a homogeneous half-space and the same antenna for both methods, a significant improvement in the NMR data interpretation is obtained. A case study has shown fair agreement between the results from computer modelling, field tests, and data from a nearby observation well. The electromagnetic method and the half-space model were selected for easy integration into an existing instrument used for the NMR method. A more accurate knowledge of the conductivity distribution with depth will further improve the final result.

Introduction

Surface nuclear magnetic resonance (NMR) in the earth's magnetic field, as developed by Semenov *et al.* (1989), is the subject of several studies (Semenov 1987; Semenov *et al.* 1989). The method can be used for non-invasive recording of the NMR signal of subterranean proton-containing liquids at depths down to 100 m or more.

A circular wire loop laid on the ground is employed to excite and receive the NMR signal. In our experiments, a circular antenna of diameter 100 m is used. Rectangular pulses of alternating current are passed through the wire with a frequency equal to that of the proton resonance in the geomagnetic field. The excitation pulse is followed by an induced EMF signal due to the free Larmor precession of the groundwater nuclear magnetization in the earth's magnetic field. Both the upper and lower boundaries of the subsurface water-saturated layers can be determined from the amplitude of the NMR signal and the setting of the loop current pulse intensity which is the product of the pulse amplitude and its duration (Semenov *et al.* 1989).

Various natural factors affect the NMR signal. The effects of the frequency of the excitation current pulse and the variation in magnitude of the earth's magnetic

[1] Received October 1993, revision accepted November 1994.

[2] Novosibirsk State University, 2 Pirogova St., Novosibirsk, 630090, Russia.

[3] Russian Academy of Sciences Institute of Chemical Kinetics and Combustion, 3 Institutskaya St., Novosibirsk, 630090, Russia.

field on the NMR signal have been studied by Tushkin, Shushakov and Legchenko (1993). The surface NMR method is sensitive to any external electromagnetic field source, such as a power-line. In order to solve this problem, the use of a different antenna, less sensitive to external noise than the circular antenna, has been investigated (Tushkin, Shushakov and Legchenko 1994). The influence of the medium conductivity on the amplitude and phase of the NMR signal has also been investigated (Shushakov and Legchenko 1994a, b, c).

Integrated NMR and electromagnetic method

The NMR signal $e_0(q)$ can be calculated using the following equation (Shushakov and Legchenko 1994a, b):

$$e_0(q) = (\omega/I) \int_V M_0(\mathbf{r})[H_{1\perp}^2(\mathbf{r})/|H_{1\perp}(\mathbf{r})|] \sin\theta(\mathbf{r})\, dV(\mathbf{r}), \tag{1}$$

where $\theta(\mathbf{r}) = 0.5\gamma_H |H_{1\perp}(\mathbf{r})| \tau_p$, $\omega = \gamma_H H_0$, $q = I\tau_p$, γ_H is the gyromagnetic ratio for a proton, $\mathbf{H}_0$ is the geomagnetic field, $\mathbf{M}_0(\mathbf{r})$ is the equilibrium macroscopic nuclear magnetization, $\mathbf{H}_{1\perp}(\mathbf{r})$ is perpendicular to the $\mathbf{H}_0$ component of the loop oscillating field, τ_p is the current pulse duration and I is the loop current amplitude.

The circular loop employed in the surface NMR method to excite and receive the NMR signal can also be used to determine the effect of the medium conductivity on the signal measurement. The technique proposed is similar to the inductive method of electrical geophysical exploration (Wait 1981).

The low-frequency alternating current passing through the loop in a conductive medium under the action of an electromagnetic field (the primary field) induces electric currents. These give rise to a secondary electric field which, with the primary field, forms the total field. In this case, the measured loop impedance changes.

The complex impedance of a loop of radius r_0 and wire cross-sectional radius a, situated in free space on the surface of a non-magnetic ($\mu = 1$), conductive half-space, is expressed by the following equation:

$$Z(\omega) = Z_0(\omega) + \omega L_1(\omega), \tag{2}$$

where

$$L_1(\omega) = i\pi r_0^2 \mu_0 \int_0^\infty J_1^2(\lambda r_0) e^{-\lambda a} \alpha(\lambda)\, d\lambda, \tag{3}$$

$Z_0(\omega)$ is the loop impedance in free space for the loop current frequency ω, $L_1(\omega)$ is the mutual inductance of the loop and the electroconductive half-space, J_1 is the Bessel function, $\alpha(\lambda)$ is the reflection coefficient characterizing the electromagnetic properties and the geometry of the conducting half-space (Wait 1958). For a homogeneous half-space,

$$\alpha(\lambda) = [\lambda - m(\lambda)]/[\lambda + m(\lambda)], \tag{4}$$

where $m(\lambda) = (\lambda^2 - k^2)^{1/2}$, $k^2 = i\sigma\mu_0\omega$, and σ is the electrical conductivity of the half-space.

Figures 1 and 2 depict the calculated imaginary and real parts of the complex impedance of a loop of radius 50 m located on the surface of a homogeneous half-space, for various frequencies of the current passing through the loop. The calculations were performed for copper wire of cross-sectional radius 2.3 mm. As can be seen in Figs 1 and 2, both parameters depend on the half-space resistivity.

In order to determine the boundaries of the water-saturated layers, (1) must be solved. In the case of horizontal, infinite, water-saturated, conductive layers, the following equation can be used instead of (1):

$$\int_0^\infty K(q, z) f(z)\, dz = e_0(q), \tag{5}$$

where

$$K(q, z) = (\omega M_0/I) \int_{x, y} [H_{1\perp}^2(x, y)/|H_{1\perp}(x, y)|] \sin\theta(x, y)\, dx\, dy, \tag{6}$$

$f(z)$ is the water concentration and z is the depth.

Equation (5) was solved by discretization of the initial integral equation, followed by the solution of a set of linear equations. Because the problem is ill-posed, the Tikhonov regularization method was used (Tikhonov and Arsenin 1977). The inverse problem (5) with the kernel (6) is linear in conductive areas (Legchenko 1992).

The modelling results of the influence of the conductivity on the NMR signal

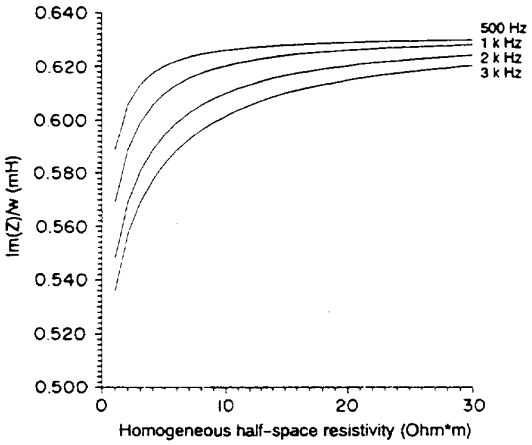

Figure 1. Graph showing the inductance of the copper wire loop of radius 50 m and cross-sectional radius 2.3 mm situated on the surface of a homogeneous conductive half-space versus the half-space resistivity, calculated for various frequencies of the loop current.

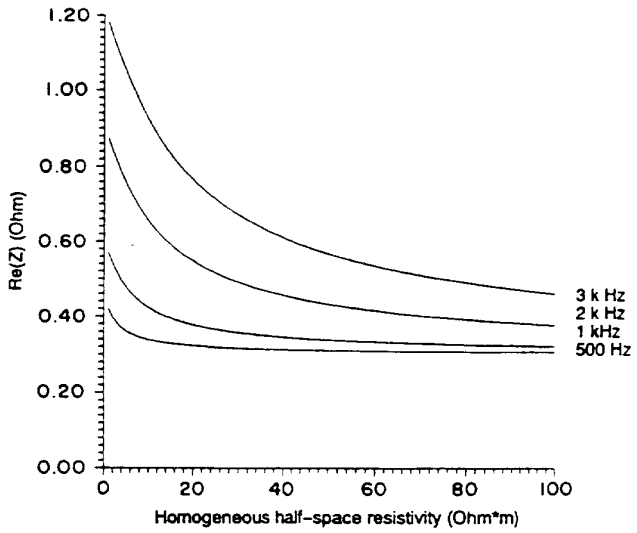

Figure 2. Graph showing the resistance of the copper wire loop of radius 50 m and cross-sectional radius 2.3 mm situated on the surface of a homogeneous conductive half-space versus the half-space resistivity, calculated for various frequencies of the loop current.

and the inverse problem solution are shown in Figs 3 and 4, respectively. For the numerical experiments, model consisting of two water-saturated layers, situated between 10 and 20 m and between 50 and 70 m, each with 10% water, was selec-

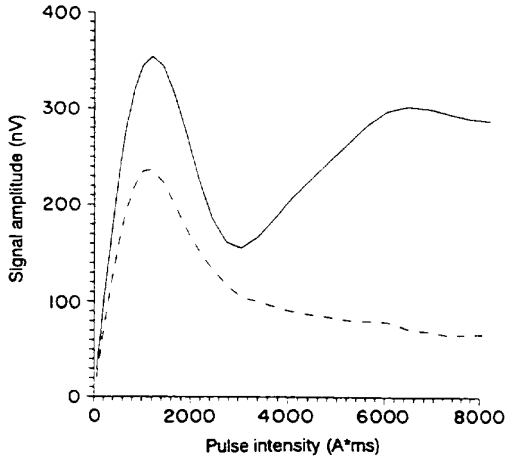

Figure 3. The NMR signal calculated for a model consisting of two water-saturated layers situated between 10 and 20 m and between 50 and 70 m with 10% water in each layer. The solid line is the signal for the case of the model in free space, the dashed line is for the model in an electrically conductive half-space of resistivity 2 Ωm.

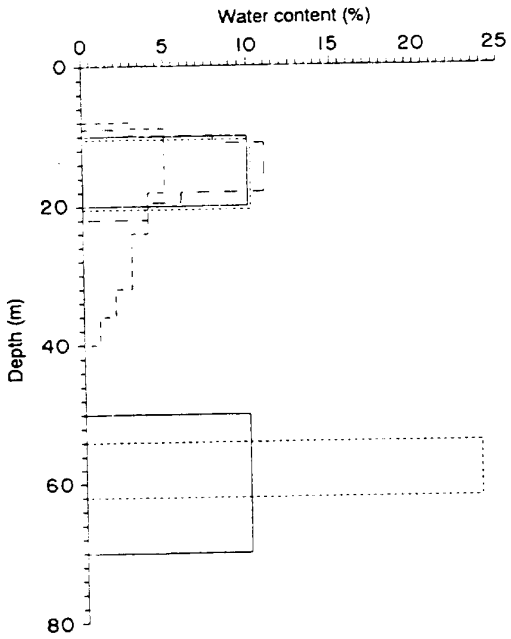

Figure 4. Inversion example for the model in Fig. 3. The solid line indicates the model, the dashed lines, in order of increasing intervals, show: (1) the model in free space; (2) the model in a conductive half-space, inversion with neglecting conductivity; (3) the model in a conductive half-space, inversion accounting for conductivity.

ted. The Larmor frequency was taken as 2500 Hz. Two cases were studied: (1) with the water layers in free space and (2) with the same layers in a conductive half-space of resistivity 2 Ωm. The effect of the conductivity on the NMR signal is not only to decrease it, but also to change the shape of the curve. The result is a distortion in the inverse problem solution. When conductivity data are available, the inversion result is considerably improved for the upper layer, but the second layer is not detected due to the screening effect and thus the absence of signal from that layer.

Goldman *et al.* (1994) observed some lack of correlation between TDEM and NMR data during field tests in areas of high rock conductivity, between observation wells. This could be explained by conductivity influence, which was not taken into account during the NMR data inversion.

Experimental results

Experiments were carried out near the village of Nizhnechumanka in the Altai region at borehole No. 64. The data obtained were compared with those previously obtained from boring and electrical logging (Fig. 5). Borehole No. 64 was selected

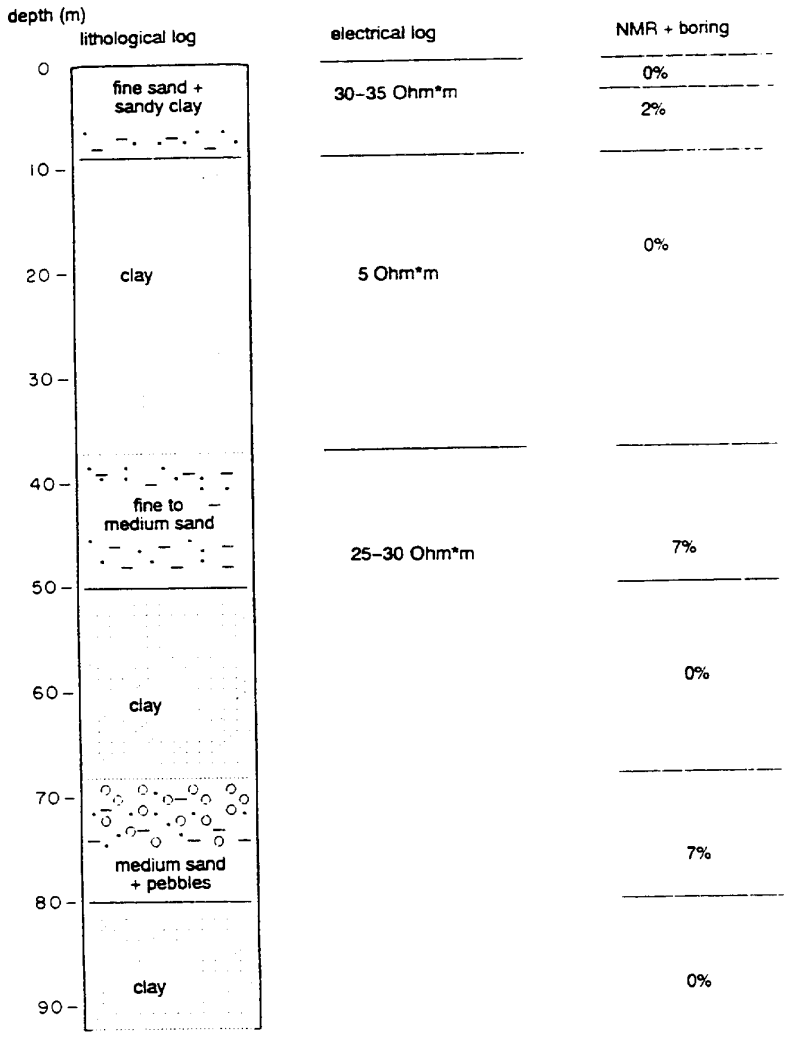

Figure 5. Borehole No. 64. The lithological log, the electrical log and the surface NMR interpretation data, obtained from borehole data.

due to the contrasting change in resistivity with depth: 30–35 Ωm from 0–9 m, 5 Ωm from 9–37 m, and 25–30 Ωm for depths of more than 37 m. According to the borehole data, there are three aquifers present, at depths of 2.5–9 m, 37–50 m and 68–80 m. The borehole and electrical logging data were obtained in the Geologo-Geophysical Expedition in the 15th region.

The surface NMR method was performed using a "Hydroscope" instrument, manufactured at the Institute of Chemical Kinetics and Combustion (Semenov 1987). The Larmor frequency was equal to 2475 Hz. A circular loop of radius 50 m, consisting of copper wire of cross-sectional area 17 sq. mm, was used both to record the NMR signal and to measure the electrical conductivity of the medium. The loop impedance was measured using a digital inductance and resistance meter E7-8 at a frequency of 1 kHz.

In order to calibrate the complex impedance $Z(\omega)$ of the loop, special experiments were performed on the surface of the frozen Ob water reservoir near the town of Berdsk. The water resistivity measurements were carried out using a measured cell with two metal plates calibrated by measuring the resistivity of various concentrations of sodium chloride solution in water. According to the measurement data, the resistivity of the water between 1 and 14 m below the surface was 47 Ωm.

The calibration measurements gave the following values for the loop impedance: Im $(Z)/\omega = 0.631$ mH $\pm$ 1%, Re $(Z) = 0.330$ Ω $\pm$ 10%. The same values for the inductance and the resistance were obtained when calculated by standard methods (Kalantarov and Tseitlin 1986). The experimental values for the inductance and the resistance measured at borehole No. 64 were Im $(Z)/\omega = 0.616$ mH $\pm$ 1%, Re $(Z) = 0.477$ Ω + 10%. According to Figs 1 and 2, the resistivity of the half-space at the test site must be 7.5 Ωm.

Because of the problem of direct comparison of the NMR data with data from other geophysical methods the following method (Shushakov and Legchenko 1994c), based on both computer modelling and field experiments, was used. Borehole cross-sections and electrical logging data were used to determine all the aquifer boundaries and the distribution of electrical conductivity with depth. Measurements of the NMR signal enabled us, using (5) and (6), to determine the percentage of water in every water statum. Additional information on aquifer boundaries and the conductivity distribution from borehole lithological and electrical logs made the interpretation of the NMR data more reliable than in the routine case using NMR data only, and the results can be used as the correct water concentration distribution with depth. All the data obtained at the test site are shown in Fig. 5.

Figure 6 shows a comparison of the experimental data (dots) with the calculated data (solid line), with respect to medium conductivity, in the homogeneous half-space model of resistivity 7.5 Ωm. It can be seen that the NMR signal calculated using a conductive homogeneous half-space model is in fair agreement with the NMR signal obtained experimentally. For comparison, the NMR signal calculated neglecting the medium conductivity (dashed line) is shown. In this case the large divergence from the experimental data is obvious. Thus the model of a conductive medium in the form of a homogeneous half-space can be used with the surface NMR method to solve both direct and inverse problems.

Figures 7, 8 and 9 demonstrate inversion of the experimental NMR data from borehole No. 64. In Fig. 7, the dashed line represents the NMR inverse problem

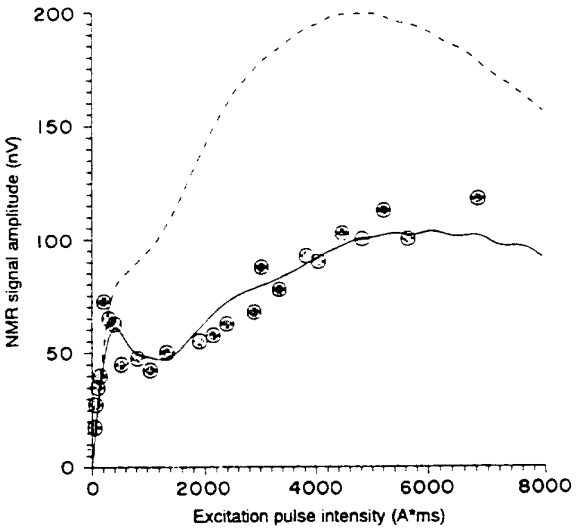

Figure 6. Comparison of the calculated NMR signal amplitude versus the current pulse intensity, with respect to the medium conductivity using the model with a homogeneous half-space of resistivity of 7.5 Ωm and the experimental data obtained at borehole No. 64. The dashed line denotes the calculated groundwater NMR signal amplitude neglecting the electrical conductivity of the soil.

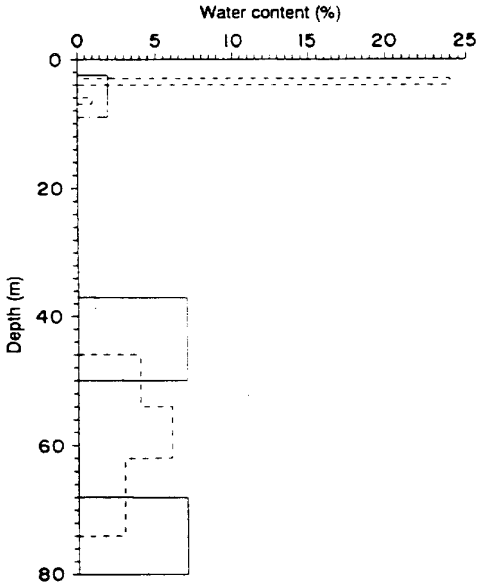

Figure 7. Comparison of the data from borehole No. 64 (solid line) with the solution of the inverse problem using the free-space model (dashed line).

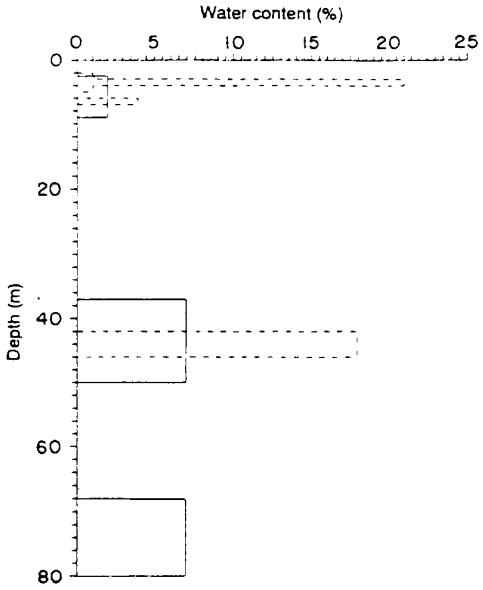

Figure 8. Comparison of the data from borehole No. 64 (solid line) with the solution of the inverse problem using the model of a homogeneous half-space with resistivity 7.5 Ωm determined by measuring the loop impedance (dashed line).

solution using the free-space model. This solution differs from the data obtained from the borehole (solid line). In Fig. 8 the borehole data are compared with the solution of the inverse problem using the homogeneous half-space model of resistivity of 7.5 Ωm, obtained by measuring the loop impedance. It can be seen that the main aquifer (from 37 to 50 m) is fairly well approximated. Figure 9 shows the solution using the horizontally stratified model, corresponding to the electrical log at borehole No. 64. The inversion result is further improved, but the bottom layer has not been detected.

According to the field experiments, the most significant improvement occurred for the aquifer situated at a depth between 37 and 50 m. The deep aquifer (68–80 m) was not detected. This could be explained by the screening effect, and it correlates with the modelling results (Figs 3 and 4). Two main factors affect the detection of the upper aquifer. Firstly, the shallow strata of sand and clay are less homogeneous than at greater depths; secondly, the available borehole data (shallow part of the log) are inaccurate.

Conclusions

The surface NMR method for groundwater prospecting has obvious advantages due to direct measurement of the subsurface water NMR signal. One of the limi-

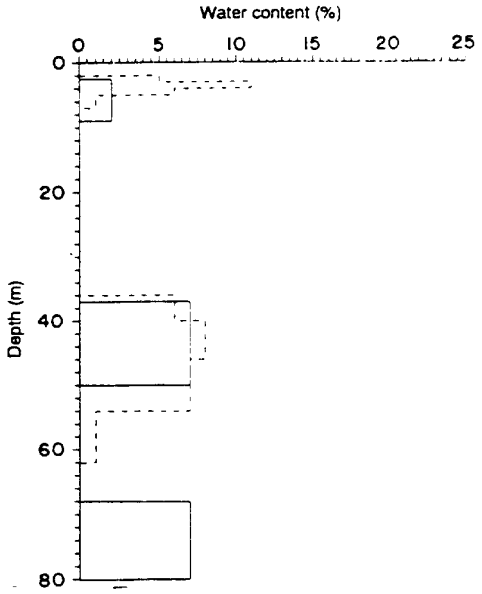

Figure 9. Comparison of the data from borehole No. 64 (solid line) with the solution of the inverse problem using the model of a horizontally stratified half-space, corresponding to the distribution of electrical conductivity with depth according to the electrical log at borehole No. 64 (dashed line).

tations of the method is the effect of rock conductivity on the NMR signal and, as a result, the distortion of the inverse problem solution.

The integration of an electromagnetic and an NMR method into one device using the same antenna and a homogeneous half-space model was investigated. This led to a significant improvement in the inversion result with only minor complications in the NMR method.

Using a horizontally layered model and the distribution of electrical conductivity with depth, it is possible to improve NMR data inversion results in highly conductive rock areas to the accuracy of the method in non-conductive rock areas.

The screening effect causes the depth of investigation to be decreased and to depend on the rock conductivity value. This decrease in the depth of investigation cannot be compensated for mathematically, but needs an increase in both the sensitivity of the NMR signal receiver and the power of the excitation pulse generator to overcome it.

References

Goldman, M., Rabniovich B., Rabinovich M., Gilad D., Gev I. and Schirov M. 1994. Application of integrated NMR-TDEM method in groundwater exploration in Israel. *Journal of Applied Geophysics* 31, 27–52.

Kalantarov P.L. and Tseitlin L.A. 1986. *Inductances Calculation* (in Russian). Leningrad, Energoatomizdat, 415.

Legchenko A.V. 1992. *Solution of the NMR geotomography inverse problem* (in Russian). Ph.D. thesis. Computing Centre, the Siberian Branch of the Russian Academy of Sciences, Novosibirsk.

Semenov A.G. 1987. NMR hydroscope for water prospecting. Proceedings of Seminar on Geotomography, Indian Geophysical Union, Hyderabad, 66–67.

Semenev A.G., Schirov M.D., Legchenko A.V., Burshtein A.I. and Pusep A. Ju. 1989. Device for measuring the parameters of underground mineral deposit. GB Patent 2198540B.

Shushakov O.A. and Legchenko A.V. 1994a. Calculation of proton magnetic resonance signal of underground water considering medium electric conductivity. *Geology and Geophysics* 35, 130–136 (in Russian).

Shushakov O.A. and Legchenko A.V. 1994b. Groundwater proton magnetic resonance in the horizontally stratified media of different electrical conductivity. *Geology and Geophysics* 35(10), 161–166 (in Russian).

Shushakov O.A. and Legchenko A.V. 1994c. Groundwater NMR in conductive media. *Geophysics*, in press.

Tikhonov A. and Arsenin V. 1977. *Solution of Ill-Posed Problems*. John Wiley & Sons, Inc.

Trushkin D.V., Shushakov O.A. and Legchenko A.V. 1994. The potential of a noise-reducing antenna for surface NMR groundwater surveys in the earth's magnetic field. *Geophysical Prospecting* 42, 855–862.

Wait J.R. 1958. Transmission and reflection of electromagnetic waves in the presence of stratified media. *Journal of Research of the National Bureau of Standards (US)* **61**, 205–232.

Wait J.R. 1981. *Geo-Electromagnetism*. Academic Press, Inc. p. 235.

Symposium on the Application of Geophysics
to Engineering and Environmental Problems

March 27-31, 1994
Boston, Massachusetts

SURFACE NUCLEAR MAGNETIC RESONANCE EXPERIMENTS TO DETECT SUBSURFACE WATER AT HADDAM MEADOWS, CONNECTICUT

By D.A. Lieblich, USGS, Hartford, Conn.; A. Legchenko, Institute of Chemical Kinetics and Combustion, Novosibirsk, Russia; F. P. Haeni, USGS, Hartford, Conn.; and A. Portselan, Firm Hydrogeotom, Moscow, Russia

ABSTRACT

Nuclear magnetic resonance (NMR) techniques have been adapted to surface geophysical prospecting by scientists at the Institute of Chemical Kinetics and Combustion, Novosibirsk, in Russia. The first tests of this method in the U.S. were conducted in the summer of 1993 through a joint collaboration between the U.S. Geological Survey; the U.S. Environmental Protection Agency; the Institute of Chemical Kinetics and Combustion, Novosibirsk, Russia; and Firm Hydrogeotom, Moscow, Russia. NMR "soundings" were conducted at 10 sites throughout the U.S. The results from Haddam Meadows State Park, Connecticut, are reported here. They are of interest, in part, because Haddam Meadows was found to be a "high noise" site for the NMR soundings but is considered to be a fairly typical site, in terms of noise, for urban and many rural areas.

A volume fraction of water histogram, divided into three possible pore-size components, as a function of depth is the result of an inversion program that runs on the hardware in the field. The presence of water is indicated in each of the nine NMR soundings. A general trend of coarsening pore-size and increasing volume fraction of water with depth, indicated in the NMR soundings, correlates directly to the coarsening of glacial deposits with depth, seen in the well and test hole data. In greater detail, a broader pore-size distribution and an increasing small pore component is indicated at depths directly above an abrupt decrease in total volume fraction of water to zero, in some NMR soundings; no water is indicated below this. The broader pore-size distribution and an increasing small pore component are interpreted to indicate poorly sorted ice contact and (or) till deposits. The abrupt decrease in the volume fraction of water may indicate the overburden-bedrock transition or, the transition to a dense till overlying the bedrock. Other details of the pore-size distribution and volume fraction of water variation, as a function of depth, appear to be related to sorting. A lack of lateral correlation between NMR soundings is the result of laterally discontinuous geologic layers, which is indicated in the core and cuttings logs. An "average" of the lateral heterogeneity, on the scale of a single NMR sounding, is sensed by the sounding.

The NMR sounding results indicate a variable depth water table, inconsistent with the well data. Two factors that may account for the variation of the depth to the water table, as interpreted from the NMR sounding results, are: (a) the predominance of fine grained sediments, primarily silt and very fine sand, and; (b) noise. The relative importance of each of these factors cannot be assessed at present. An adaptation of the NMR sounding loop geometry and signal stacking improved the signal-to-noise ration (S/N) by about 30 times, allowing measurements to be collected within 100 m of power lines. S/N levels between about 1 and 6 are lower than desirable but were considered acceptable: expected geological trends are mappable in the NMR soundings, although no quantitative results exist to verify repeatability.

INTRODUCTION

Nuclear magnetic resonance (NMR) has played an important role in a number of fields including physics, chemistry, biology, and medicine since it was first discovered in the 1940s by Felix Bloch (Bloch and others, 1946) and Edward Purcell (Purcell and others, 1946). Geophysically, NMR has been used in proton precession magnetometers for years (Telford and others, 1976) since Packard and Varian's (1958) first demonstration of NMR in the earth's magnetic field. More recently, NMR has been used for laboratory petrophysical studies (Straley and others, 1991; Hedberg and others, 1993) and in borehole tools (Kleinberg and others, 1992; Miller and others, 1990). Semenov (1987) described the surface NMR method, Semenov and others (1990) described the instrument used in this study, and Schirov and others (1991) have presented the results of the application of this method in Australia.

NMR provides a unique tool for investigating the physical properties of the subsurface because it is primarily sensitive to the number of hydrogen atoms, and therefore water, present. The presence (or absence) of water plays a pivotal role in determining many bulk properties of rocks such as elastic moduli, bulk density, resistivity, and dielectric constant. Inversion of surface NMR data provides information on the subsurface water distribution. The knowledge of subsurface water distribution can provide critical information for the interpretation of other geophysical data. Additionally, the water distribution provides hydrologic information that cannot be obtained using any other noninvasive method.

This paper presents the results of a field study conducted at Haddam Meadows State Park in Connecticut. The paper includes a summary of NMR theory, the results of the NMR soundings at Haddam State Park, a comparison of these results to well and test hole data, a discussion of the effects of certain simplifying assumptions, and some topics that are currently being researched.

THEORY

General Principles

NMR, in bulk matter, is a method whereby the macroscopic magnetism of a large number of atomic nuclei is used to obtain information on their physical and chemical environment (Abragam, 1961; Pake, 1993). The method is based upon the magnetic moment of a single atomic nucleus (nuclear paramagnetism) arising from a nonzero spin angular momentum. When placed in a static magnetic field, a macroscopic sample containing many such nuclei develops a macroscopic magnetism aligned with the static magnetic field. The macroscopic magnetization is the vector sum over all individual nuclear magnetic moments but is conveniently described by the magnetic moment per unit volume: the product of the nuclear magnetic susceptibility (a Boltzmann distribution) and the static field vector (Abragam, 1961).

Incident electromagnetic energy at the angular frequency ($\omega_L = 2\pi f_L$) can be absorbed by the nucleus. The Larmor frequency (f_L), defined as the product of the static field magnitude (about 0.5 oersted or $0.5/(4\pi$ E -3) a/m in SI units, for the earth) and the gyromagnetic ratio of the nucleus ((2.67528 ± 0.00006) E4 Hz oersted^{-1}, or (2.67528 ± 0.00006) E4 * 4π E -3 Hz/ (a/m) in SI units, for a proton in a water molecule, after correction for diamagnetic effect, see Thomas and others, 1950) divided by 2π, and is about 2 kHz in the earth's magnetic field. Upon absorption of a quantum of incident energy, the magnetic moment vector is deflected from

its equilibrium position in the static magnetic field, reflecting the higher energy state of the nucleus. If the incident field is rapidly extinguished, the nuclear precession about the static field can be measured.

Decay of the net magnetization vector, after deflection from its equilibrium position, is exponential and can be described by two characteristic times: T_1 (the spin-lattice or longitudinal relaxation time) and T_2 (the spin-spin or transverse relaxation time). T_1 is the time required for the macroscopic magnetization vector to regain thermal equilibrium with the static field. T_2 is the time required for the component of the macroscopic magnetization vector, perpendicular to the static field (fig. 1), to decay to zero. This decay is caused by the dispersal of individual magnetic moment vectors away from the expected direction of the macroscopic magnetic moment vector, in a homogeneous field. The inhomogeneity causing this dispersal can be the result of inhomogeneity of the external static magnetic field (if this is known the measured transverse relaxation time is referred to as T_2^*) and (or) inhomogeneity caused by the fields of local neighboring magnetic moments. Because of the dispersal of individual magnetic moments, the magnitude of an induced electromotive force (emf) in a coil oriented (for example) perpendicular to the static field direction will decay at a rate that is faster than the characteristic time T_1, for undispersed moments.

The sequence of events: forced rotation of the macroscopic magnetization vector ($\mathbf{M}_0$), transverse relaxation (T_2), and longitudinal relaxation (T_1) are depicted in figure 1 (a, b, and c, and d respectively) for an initial macroscopic magnetization vector parallel to the z' axis, the direction of the static magnetic field ($\mathbf{H}_0$), and a pulsed field ($\mathbf{H}_1$) along the x' axis. Note that the primes (') on the axes refer to a frame rotating relative to a fixed laboratory reference frame (x, y, z) at the Larmor frequency. This removes the precessional motion in the static field and thereby simplifies the picture and the phenomenological Bloch equations describing the precessional motion (Abragam, 1961; Farrar and Becker, 1971; Fukushima and Roeder, 1981).

NMR From the Surface of the Earth

The NMR system used in this study was designed to detect subsurface water to depths of approximately 100 m, depending upon the conductivity of the bulk rock. A number of variables that are either not present in other applications, or, are made to be of negligible influence through careful design of the instrument and control over the sample, must be considered in this application. The variables arise primarily because of the constraints imposed on the method by the earth: (1) surface NMR deals with large volumes of rock, and (2) surface NMR uses the earth's magnetic field as the static field. Electromagnetic noise is also a problem, and will be considered in the section on field results. Because of the large volumes of rock, and because the earth is layered (to a first approximation), we expect the water distribution to be a function of position below the surface of the earth. Additionally, the large volumes of rock cause the incident field to be inhomogeneous over the sample: the volume of earth over which the perturbing field is greater than zero. Previous NMR methods for investigating the earth's subsurface assumed a homogeneous half space. They were capable of discerning (a) the presence or absence of water by the presence or absence of an NMR free precession signal; and (b) a bulk porosity (Varian, 1962; Barringer and White, 1968) or a bulk porosity distribution (Barringer and White, 1968) from the decay time(s). The fundamental difference between these methods and the present method is the assumption of a 1D layered earth in which the volume

fraction of water (sometimes called "free" water) and its associated NMR decay time(s) (representing the physico-chemical environment of the water) varies as a function of depth. Decay times (T_1 and T_2) can be shown to be directly related to pore-size (Straley and others, 1991).

Use of the earth's field as the static field (2 above) means that we must either assume that it is homogeneous over the volume investigated, or, develop a method to measure and account for its inhomogeneity. Because the static magnetic field may be slightly inhomogeneous over the volume investigated, T_2^* is used to denote a measured transverse relaxation time. Methods of accounting for an inhomogeneous static field are presented in the discussion section.

Although excitation of an NMR signal can be accomplished by a continuous wave, pulsed methods offer distinct advantages (Farrar and Becker, 1971; Fukushima and Roeder, 1981). The present method uses pulse excitation: a wire loop is energized with a pulse of alternating current (I amps) at the Larmor frequency (f_L). The time variation of current in the loop can be written as

$$I(t) = I_0 \cos(2\pi f_L t), \tag{1}$$

where I_0 is the current amplitude, $2\pi f_L = \gamma H_0$, γ being the gyromagnetic ratio of the proton (defined previously), H_0 is the magnitude of the earth's magnetic field, and t is time. The voltage induced in the loop by the free precession of protons in the water, enclosed in a rock with a single pore-size, is an exponentially decaying function of time and is given by

$$E(t) = -E_0 e^{-t/T_2^*} \cos(2\pi f_L t + \phi), \tag{2}$$

where T_2^* is defined previously, and ϕ is a phase term that is zero for nonconductive rocks, as assumed here. E_0 is the initial maximum voltage induced in the loop. It can be written as a function of pulse intensity ($q = I_0 t_p$), pulse intensity being the product of input current (I_0) and pulse duration (t_p):

$$E_0(q) = \int_V 2\pi f_L H_\perp(r) M_0 \sin(0.5\gamma H_\perp(r)\, q) f(r)\, dV \tag{3}$$

The argument of the sine function in equation 3 gives the angle through which the equilibrium magnetization (M_0) in an elemental volume (dV) is rotated by $H_\perp(r)$, the component of the incident field perpendicular to the static field, at the position r, and for a 1-amp current in the loop. The 0.5 accounts for the circularly polarized component of the incident linearly polarized field, rotating at the Larmor frequency. The function $f(r)$ represents the volume fraction of water in an elemental volume located at r. Thus, $M_0 \sin(0.5\,\gamma H_\perp(r)\, q) f(r)\, dV$ gives the component of magnetization perpendicular to the equilibrium magnetization in the volume element at r. This magnetization is converted to a voltage through multiplication by $2\pi f_L H_\perp(r)$ which gives the magnitude of the time varying flux through the loop. Note that $2\pi f_L M_0$, are constants and could be removed from under the integral but are included to clarify the physical meaning of the terms involved.

For horizontal stratification, $f(r)$ becomes only a function of depth (z) and equation 3 can be simplified to

$$E_0(q) = \int_0^{Z_{max}} \int_S 2\pi f_L H_\perp(r) M_0 \sin(0.5\gamma H_\perp(r) q)\, ds f(z)\, dz = \int_0^{Z_{max}} K(q, z) f(z)\, dz \qquad (4)$$

Bounds on the surface S that have been found to account for most of the signal contribution satisfy $x^2 + y^2 \leq 3\,D^2$, where D is the diameter of the loop. This provides an indication of the area over which the assumption of a constant volume fraction of water applies. For example, it covers a radius of about 173 m for a loop with radius 50 m. Z_{max} is the maximum depth from which signal can be measured: it is about two loop diameters. Figure 2 shows $E_o(q)$ modeled for each of three 10-m thick layers at different depths. The results were obtained using a loop of 100-m diameter and assuming a horizontal static field. The "period" of the $E_o(q)$ curve can be seen to be a strong function of layer depth: the first half cycle is stretched in q as depth is increased, reflecting the decay of the input field with depth. The magnitude of the curve, for a given layer thickness and depth, would change if the volume fraction of water contained in the layer changed. Inversion of the $E_o(q)$ curve, over a layered subsurface, yields the volume fraction of water as a function of depth ($f(z)$). In addition, it is possible to recover the pore-size distribution as a function of depth by rewriting equation 2 as

$$E(t) = \sum_{i=1}^{N} \sum_{j=1}^{M} -E_0(i)_j e^{-t/T_2^*(i)_j} \cos(2\pi f_L t + \phi) \qquad (5)$$

where a discretization of the function $f(z)$ has been introduced (i varies from 1 to N layers) to account for the discrete nature of the measurements ($E_o(q)$) and a finite number of pore-sizes has been introduced (j varies from 1 through M pore-sizes) to represent the pore distribution in a given layer (i).

FIELD RESULTS

The NMR method was tested during the summer of 1993 through a collaboration of the U.S. Geological Survey (USGS); the U.S. Environmental Protection Agency (USEPA); the Institute of Chemical Kinetics and Combustion, Novosibirsk, Russia; and Firm Hydrogeotom, Moscow, Russia. Experiments were conducted at Haddam Meadows State Park, on the western bank of the Connecticut River (fig. 3). The availability of geologic, hydrologic, and geophysical data from this site was the primary reason it was selected for the NMR investigation. The USGS has used this site as a geophysical test site and, as a result of ground truth testing, also has test holes and wells (fig. 3) on the site. One well (JL1) reached bedrock at approximately 43 m.

Initial NMR soundings were attempted using a circular loop of 100 m diameter. The magnitude of the voltage induced in the loop by electromagnetic (EM) noise was found to be in the microvolt range whereas the NMR signal varied up to a few hundred nanovolts, giving a signal-to-noise ratio (S/N) of less than 0.1. This S/N is insufficient to obtain reliable results from inversion of the field data. Although signal stacking was used, it required a significant

increase in the time per NMR sounding. Approximately two hours was allowed per sounding as a compromise between S/N improvement and time per sounding. The resulting improvement of about 10 to 15 times in S/N was still insufficient to obtain reliable results.

Assuming that a power line along the road (fig. 3) was the primary source of EM noise: the circular loop was reconfigured into a figure-eight shape with its 100-m long axis oriented parallel to the power line to minimize any inductive coupling to the loop. Theoretical analysis detailing the effectiveness of this loop geometry as a means of limiting this type of electromagnetic noise are given in Truskin and others (in press). Orientation of the loop axis was done empirically by reorienting the axis of the loop until a minimum induced voltage was measured. Despite the imprecise orientation and geometry of the figure-eight loop, the magnitude of the noise was found to decrease by about 3 to 5 times. Improvements of about 30 to 75 times were achieved with stacking. The post stacking S/N was generally between 1 and 6; this allowed reliable inversion using an algorithm that accounted for the new geometry. Nine NMR soundings were collected using the figure-eight geometry.

Results from eight of the nine NMR soundings, showing volume fraction of water, divided into three possible pore-size components, as a function of depth, were projected into two section lines A-A' (fig. 4) and B-B' (fig. 6). Correlation of pore-size to grain-size is based upon empirical data relating relaxation times to grain size in water-bearing layers (table 1). It should be noted that the relation between relaxation time and the grain size of water-bearing strata, as shown in table 1, is indirect: NMR relaxation time is related to pore-size. (See theory section and "porosity" subsection of discussion section.) For sediments with a single size of spherical grain (very well sorted), relaxation time is directly related to both grain size and pore-size; for grain-size mixtures (less well sorted) the relation between decay time and grain size is more complex. Still further complexity can result from mineral mixtures, saturating fluid mixtures, and many other variations that are common in most sediments.

Water is indicated in each of the NMR soundings (figs. 4 and 6). The vertical distribution of water, indicated in the NMR soundings, is heterogeneous, and the pore-size distribution changes with depth. In addition, there appears to be little lateral continuity of what might be called a "pore or pore water facies" (figs. 4 and 6) despite the proximity of the NMR soundings to each other (generally less than 250 m). A general trend towards coarsening with depth is seen in the two figures. In addition, there is a general trend towards increasing volume fraction of water with increasing depth that terminates abruptly.

Estimates of the depth to the water can be made directly from the NMR soundings, without using the well and test hole data. The depth to the water table, interpreted as the first occurrence of a volume fraction of water, or the first consistent occurrence of a volume fraction of water, is variable over the site. However, the land surface elevation changes little over the site (2.8 0.5 m) and the river is within about 300 m of the furthest NMR sounding, indicating that little variation is expected.

Table 1. Approximate observed relaxation time (T_2^*) in water-bearing strata, derived from an empirical, field data base (from Schirov and others, 1991, table 1).

Relaxation time (milliseconds)	Water-bearing strata
less than 30	sandy clays
30 - 60	clayey sands, very fine sands
60 - 120	fine sands
120 - 180	medium sands
180 - 300	coarse and gravelly sands
300 - 600	gravel deposits
600 - 1,500	surface water bodies

COMPARISON OF NMR RESULTS TO WELL AND TEST HOLE DATA

Available well data is summarized, for each section, in figures 5 and 7. Core and "split spoon" data were collected and analyzed by Gorin (1989). Records of the cuttings logs from wells without core were used where the well is near a NMR sounding. Likewise, logs obtained from split spoon samples were used for test holes without core, when the test hole is near a NMR sounding. The well and test hole records are generalized from the originals, converted from feet to meters, and discretized to 1-m intervals. In the process, some qualitative information that may have a significant influence on the quality of correlations between the NMR results and those obtained from the wells and test holes, was lost. Vertical positioning of contacts, in each of the wells and test holes of figures 5 and 7, is estimated to be within $\pm$ 0.5 m of the originals. Core loss was generally less than 2 percent of the total core length in any given interval with the total over all intervals being less than 15 percent loss. Cores from TH-33C and TH34C were exceptions; a significant amount of the total cored interval was lost. Lost intervals were interpolated on the basis of the continuity of boundaries on either side and small samples recovered.

Lateral and vertical heterogeneity indicated by the NMR soundings is also seen in the well and test hole data (figs. 5 and 7). Lateral heterogeneity is present on a scale smaller than a single loop. This can be seen in the logs of TH-37C and TH-38C, of figure 5. Coarse material is present at shallower depths in TH-38C than in TH-37C. The loop at NMR sounding 75 covered both locations, thereby producing a vertical section that "averaged" the lateral heterogeneity within the layers beneath it. This may also explain the indication of water at 1 to 2 m in NMR sounding 75 as being the result of the coarser shallow layers to the south. Despite the proximity of NMR soundings 71, 72, and 78 (fig. 6) the lateral heterogeneity seen in the well and test hole data (fig. 7), is reproduced in NMR soundings 71 and 78. NMR sounding 72, intermediate between 71 and 78, shows a poor correlation to the nearest test hole, TH-23. This may also be explained by the NMR "averaging" the significant lithologic changes indicated, over the short distance, between JL1 and TH-33C (fig. 7).

Generally, good agreement is obtained between the grain size changes shown in individual wells and pore-size changes indicated by the nearest NMR sounding: a simple, direct, relation between the pore and grain size applies (generally) at this site. The depth intervals over which these changes occur, however, are less well correlated. A general trend of coarsening pore-size with depth, seen in the NMR soundings, correlates to the observed coarsening of glacial deposits with depth, seen in the well and test hole data. In addition, the NMR soundings indicate a trend towards increasing volume fraction of water (total porosity) with increasing depth. This is an important hydrological observation, as it is possible for the pore spectrum to coarsen with depth without an increase in total volume fraction of water. A trend, formed by the abrupt termination (in the NMR soundings) of the largest volume fractions, at the deepest depths, may indicate the boundary between stratified glacial drift and the underlying bedrock or till. Available well and test hole logs provide no information on the increasing volume fraction of water with depth and are too shallow to verify the configuration of the bedrock surface. Details of the vertical variations may be due to sorting. For example, the qualitative information left out of the generalized log indicates that the gravel interval of TH-23 is "dirty" or poorly sorted. This may explain the absence of an NMR signal from this interval; small grains in between the gravel matrix decrease the average pore-size below the threshold required for measurable signal.

Gorin's (1989) interpretation of the core data, with the aid of ground penetrating radar data, was that the progressive retreat of the glaciers, in a northwesterly direction, left: (a) bedrock overlain by till that changes upwards into poorly sorted ice marginal deposits, which are in turn overlain by deltaic deposits; (b) an erosional surface cutting into the previous deltaic deposits; and (c) recent (Holocene) river deposits overlying the remaining glacial sediments. This complex glacial and post-glacial history can explain the lack of significant lateral correlation of the "pore water facies", indicated by the individual NMR soundings. In addition, the geological expectation that the coarsest glacial deposits (usually referred to as ice-contact deposits and till) directly overlie the bedrock, at this site, may explain the trend towards increasing volume fraction of water with depth, particularly at depths above the abrupt change to no volume fraction of water. The poor sorting expected in these deposits would imply, at least, a distribution of NMR relaxation times and possibly a predominance of short times (small pores). A broader pore-size distribution and an increasing small pore component is indicated at depths directly above an abrupt decrease in total volume fraction of water to zero in some NMR soundings; no water is indicated below this depth. These indications of poorly sorted sediments at the deepest levels of the NMR soundings further support the interpretation of the abrupt change below them as an indication of the top of bedrock or dense till.

Well data indicate the water table is about 2 m below the surface, slightly less than the elevation of the surface (2.8 ± 0.5 m) above sea level (river level) at the site. The NMR sounding results indicate a variable depth water table, inconsistent with the well data.

DISCUSSION

NMR Soundings, Wells, and Test Holes

Two factors that may account for the variation of the depth to the water table, as interpreted from the NMR sounding results, are: (a) the predominance of fine grained sediments, primarily silt and very fine sand and; (b) noise. The relative importance of each of these factors cannot be assessed at present.

Volume fractions of water near 50 percent (NMR soundings 77, 76, and 71) may be in error. It is not possible to determine, at this time, the noise contribution to the larger values of volume fraction of water (near 50 percent) although it can be said that no clear correlation of noise level with large volume fractions of water is seen. Other contributions to very large values could include the depth below which signal is assumed negligible, and errors in the inversion of figure-eight loop data. These factors, in addition to lateral averaging by the NMR and differences in discretization of geology versus NMR soundings, may contribute to discrepancies between the grain-size distribution indicated in well and test hole logs and the pore-size distribution indicated in the NMR soundings. Logging and elevation errors may also play a role.

Homogeneous Static Field

The measurements described here implicitly assume a homogeneous static field if $T_2^* = T_2$. Although measurements of frequency shift are made, as a function of q, these data are not used in the present implementation. In addition, it is possible: (a) to directly obtain information on the static field homogeneity by using more sophisticated input pulse sequences, or; (b) to eliminate the dependence of the measurement on the field inhomogeneity, if present (Farrar and Becker, 1971, Fukushima and Roeder, 1981). Application of the spin echo method (Hahn, 1950) to NMR measurements in the earth's field, as described by Bloom and Mansir (1958), is one such example. Spin echoes have been investigated in relation to the present method by Legchenko and Shusakov (1991).

Effect of Conductivity

The effect of conductivity is to attenuate the EM field with depth, at a rate that is greater than in a nonconductive earth, and, to shift the phase of the induced field relative to the input field. Including conductivity in the forward and inverse problems may enable the recovery of a conductivity as a function of depth profile as well as more accurate determination of the volume fraction of water as a function of depth profile. Such information could also be used in joint inversions of NMR and other electrical and (or) EM data. Alternatively, this formulation would allow other data to be used to more accurately invert the NMR data. Although measurement of the phase shift is made as a function of q, it has not been used in the interpretation method used in this study. Shusakov and Legchenko (1992) have investigated the use of phase information in the reconstruction of the volume fraction of water as a function of depth profiles in conductive terrains in Russia.

"Porosity" Derived From NMR

Throughout this paper, one of the results from the inversion of the NMR data have been referred to as "volume fraction of water". The reason for this is that the NMR technique is (generally) sensitive to a subset of the total water present in the pores of the rock. Short decay

times, associated with small pores (due to the increased influence of the chemically and electrically bound volume fractions of water in these pores), are not sensed because instrument characteristics require a delay in time between initiation of the NMR signal and its measurement. Additionally, the possibility that the pore space is not 100 percent filled with water (as for example if air or other fluids containing a negligible number of protons are present in the pore space) increases the possible total porosity to still greater values, and may also shorten the decay time(s). Thus, the volume fraction of water indicated by the NMR is a lower bound on the total porosity. It is, however, the most hydrologically important volume fraction in that it is that portion which is most likely to be removable from the rock (Straley and others, 1991). Knight and Endres (1990) have given an indication of the magnitude of the water bound to a pore surface (as opposed to that bound within minerals), and thereby provided an indication of the nature of the lower bound on total porosity: bound water may constitute as much as 15 percent of the total pore volume for surface area to volume ratio of the order 1 E6 cm^{-1}.

Gross subdivision of the NMR signal into three porosity regimes is an approximation. Laboratory studies (Gallegos and others, 1987; Straley and others, 1991;and D'Orazio and others, 1989) have indicated that porous materials are more accurately modeled by a broad pore spectrum. More sophisticated mathematical methods for obtaining estimates of this spectrum are available (D'Orazio and others, 1989; Whittall and MacKay, 1989), however, further research is necessary to evaluate the stability of such estimates in the presence of noise.

ACKNOWLEDGMENTS

This paper benefited from a review by Dr. A. Sezginer of Schlumberger Doll Research, Dr. Tom Grover of the USGS, and Mr. Sean Lawlor of the USGS.

NOTICE

CONCLUSIONS

1. Water is indicated in each of the nine NMR soundings.
2. A general trend of coarsening pore-size and increasing volume fraction of water with depth, indicated by the NMR soundings, correlates directly to the coarsening of glacial deposits with depth, seen in the well and test hole data.
3. In greater detail, a broader pore-size distribution and an increasing small pore component is indicated at depths directly above an abrupt decrease in total volume fraction of water to zero, in some NMR soundings; no water is indicated below this. The broader pore-size distribution and an increasing small pore component are interpreted to indicate poorly sorted ice contact and (or) till deposits. The abrupt decrease in the volume fraction of water may indicate the overburden-bedrock transition or the transition to a dense till overlying the

bedrock. Other details of the pore-size distribution and volume fraction of water variation, as a function of depth, appear to be related to sorting.

4. Apart from the general depth trends mentioned above, there is a lack of lateral correlation between NMR soundings. This is the result of laterally discontinuous geologic layers, indicated in the core and cuttings logs. The wells and test holes show that lateral heterogeneity is present on a scale smaller than a loop: individual NMR sounding results are therefore "averaged" representations over the heterogeneous layers beneath them and are thus difficult to directly correlate, interval for interval, to cores and cuttings logs, at this site.
5. The NMR sounding results indicate a variable depth water table, inconsistent with the well data. Two factors that may account for the variation of the depth to the water table, as interpreted from the NMR sounding results, are: (a) the predominance of fine grained sediments, primarily silt and very fine sand, and; (b) noise. The relative importance of each of these factors cannot be assessed at present.
6. The figure-eight loop and signal stacking improved the S/N by about 30 times, allowing measurements to be collected within 100 m of power lines. S/N levels between about 1 and 6 are lower than desirable but were considered acceptable: expected geological trends are mappable in the NMR soundings, although no quantitative results exist to verify repeatability.
7. Discrepancies between the NMR results and the well data may be attributable to a number of factors (in addition to the averaging mentioned above) including: pore-size to grain size correlation, noise, discretization in the inversion, depth below which the signal is assumed zero, errors in the inversion of figure-eight loop data, logging errors, and elevation errors. Further research and site investigations would be necessary to indicate the role played by each of these factors.

REFERENCES

Abragam, A., 1961, The principles of nuclear magnetism: Oxford, Oxford University Press, 599 p.

Barringer, A.R. and White, J.F., 1968, assignors, Groundwater survey method and apparatus: U.S. Patent #3,398,355.

Bloom, A., and Mansir, D., 1958, Measurement of nuclear induction relaxation times in weak magnetic fields: Phys. Rev., v. 93, p. 941.

Bloch, F., Hansen, W.W., and Packard, M.E., 1946, The nuclear induction experiment: Phys. Rev., v. 70, p. 474-485.

D'Orazio, F., Tarczon, J.C., Halperin, W.P., Eguchi, K., and Mizusaki, T., 1989, Application of nuclear magnetic resonance pore structure analysis to porous silica glass: J. Appl. Phys., v. 65, p. 742-750.

Farrar, T.C. and Becker, E.D., 1971, Pulse and Fourier Transform NMR: New York, Academic Press, 115p.

Fukushima, E., and Roeder, S.B.W., 1981, Experimental pulse NMR: New York, Addison-Wesley, 539 p.

Gallegos, D.P., Munn, K., Smith, D.M., and Stermer, D.L., 1987, A NMR technique for the analysis of pore structure: application to materials with well defined pore structure: J. Colloid Interface Sci., v. 119, p. 127-140.

Gorin, S.R., 1989, Exploration of subsurface interfaces using high-frequency seismic reflection and ground-penetrating radar methods, Middletown, Connecticut, Wesleyan University, unpublished Masters thesis, 136 p.

Hahn, E.L., 1950, Spin echoes: Phys. Rev., v. 80, p. 580-594.

Hedberg S.A., Knight, R.J., MacKay, A.L., and Whittall, K.P., 1993, The use of nuclear magnetic resonance for studying and detecting hydrocarbon contaminants in porous rocks: Water Resources Research, v. 29, p. 1163-1170.

Kleinberg R.L., Sezginer, A., and Griffin, D.D., 1992, Novel NMR apparatus for investigating an external sample: Jour. Mag. Res., v. 97, p. 466-485.

Knight, R., and Endres, A., 1990, A new concept in modeling the dielectric response of sandstones: defining a wetted rock and bulk water system: Geophysics, v. 55, p. 586-594.

Legchenko, A.V. and Shusakov, O.A., 1991, Optimization of measurements in geophysical NMR-tomography and comparison of various measurement techniques: Russian Academy of Sciences, Institute of Chemical Combustion, Siberian Branch, Novosibirsk, issue no. 35, p. 1-37, in Russian.

Miller, M.N., Paltiel, Z., Gillen, M.E., Granot, J., and Bouton, J.C., 1990, Spin echo magnetic resonance logging: porosity and free fluid index determination: 65th Ann. Tech. Mtg., Soc. Pet. Eng., New Orleans, September 23-26, p. 321-334.

Packard, M. and Varian, R., 1958, Free nuclear induction in the Earth's magnetic field: Phys. Rev., v. 93, p. 941.

Pake, G.E., 1993, Nuclear magnetic resonance in bulk matter: Physics Today, v. 46, p. 46-51.

Purcell, E.M., Torrey, H.C., and Pound, R.V., 1946, Resonance absorption by nuclear magnetic moment in a solid: Phys. Rev., v. 69, p. 37-38.

Schirov, M., Legchenko, A., and Creer, G., 1991, A new direct noninvasive groundwater detection technology for Australia: Exploration Geophysics, v. 22, p. 333-338.

Semenov, A.G., 1987, "NMR Hydroscope" for water prospecting, *in* Proceedings of the seminar on Geotomography: Indian Geophysical Union, Hyderabad, December 30-31, p. 66-67.

Semenov, A.G., Schirov, M.D., Legchenko, A.V., Burshtein, A.I., and Pusep, A.J., 1990, Device for measuring the parameter of an underground mineral deposit: Great Britain Patent #2198540B.

Shusakov, O.A., and Legchenko, A.V., 1992, Calculation of the proton nuclear magnetic resonance signal from ground water considering the electroconductivity of the medium: Russian Academy of Sciences, Institute of Chemical Combustion, Siberian Branch, Novosibirsk, issue no. 36, p. 1-26, in Russian.

Straley C., Morriss, C.E., Kenyon, W.E., and Howard, J.J., 1991, NMR in partially saturated rocks: laboratory insights on free fluid index and comparison with borehole logs: 32nd Annual Logging Symposium, SPWLA, June 16-19, p. 1-25, also in The Log Analyst.

Telford, W.M., Geldart, L.P., Sheriff, R.E., and Keys, D.A., 1976, Applied Geophysics: New York, Cambridge University Press, 860 p.

Thomas, H.A., Driscoll, R.L., and Hipple, J.A., 1950: Phys. Rev., v. 78, p. 787-790.

Truskin, D.V., Shushakov, O.A., and Legchenko, A.V., in press, Potentialities of jamproof antenna to non-drilling NMR in the earth field: Geophysical Prospecting.

Whittall, K.P., and MacKay, A.L., 1989, Quantitative interpretation of NMR relaxation data: J. Mag. Res., v. 84, p. 134-152.

Varian, R.H., 1962, assignor, Ground liquid prospecting method and apparatus: U.S. patent #3,019,383.

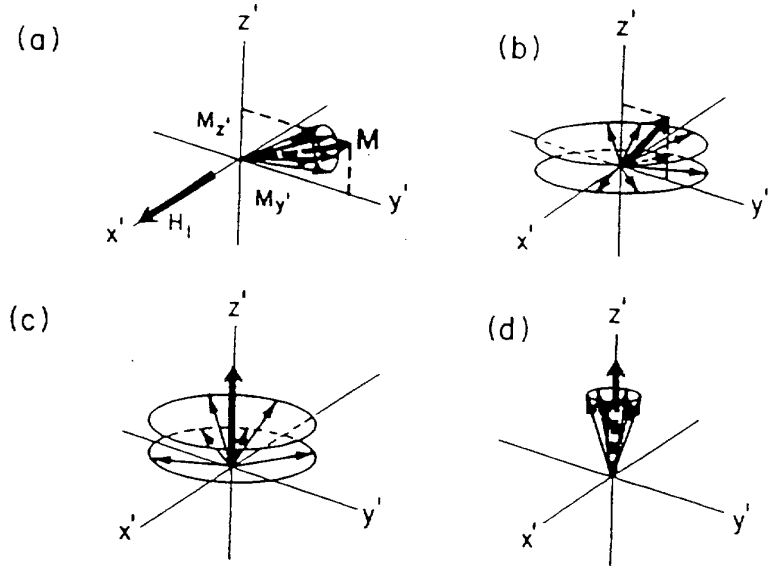

Figure 1. The sequence of events in a typical NMR experiment: (a) forced rotation of the macroscopic magnetization vector (M_0) for an initial macroscopic magnetization vector parallel to the z' axis, also the direction of the static magnetic field ($\mathbf{H}_0$), and the pulsed field ($\mathbf{H}_1$) along the x' axis; (b and c) dephasing of the nuclear moments that produced the magnetic moment $\mathbf{M}_{y'}$, in (a), over the transverse relaxation time (T_2), thereby reducing $\mathbf{M}_{y'}$ to zero; and (d) reestablishment of $\mathbf{M}_{z'}$ at its equilibrium value (M_0) after the longitudinal relaxation time (T_1). Note that the primes (') on the axes refer to a frame rotating relative to a fixed laboratory reference frame (x, y, z) at the Larmor precession frequency in order to remove the precessional motion in the static field (adapted from Farrar and Becker, 1971, fig. 1.4).

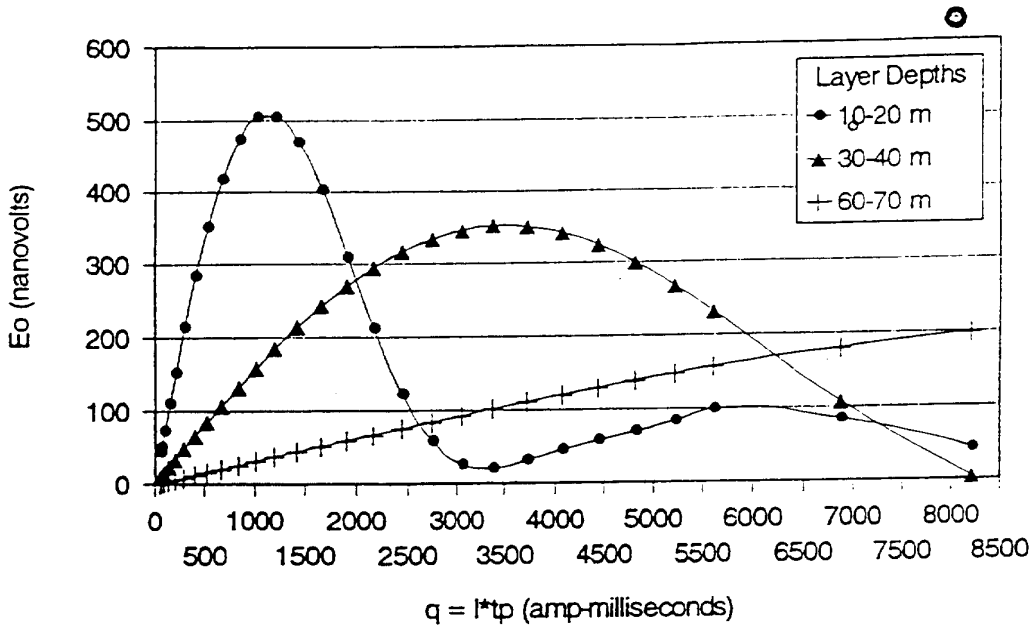

Figure 2. $E_o(q)$ modeled for each of three 10-m thick layers at different depths, using a loop of 100 m diameter and assuming a horizontal static field. Each layer contains a 20 percent volume fraction of water. See text for details.

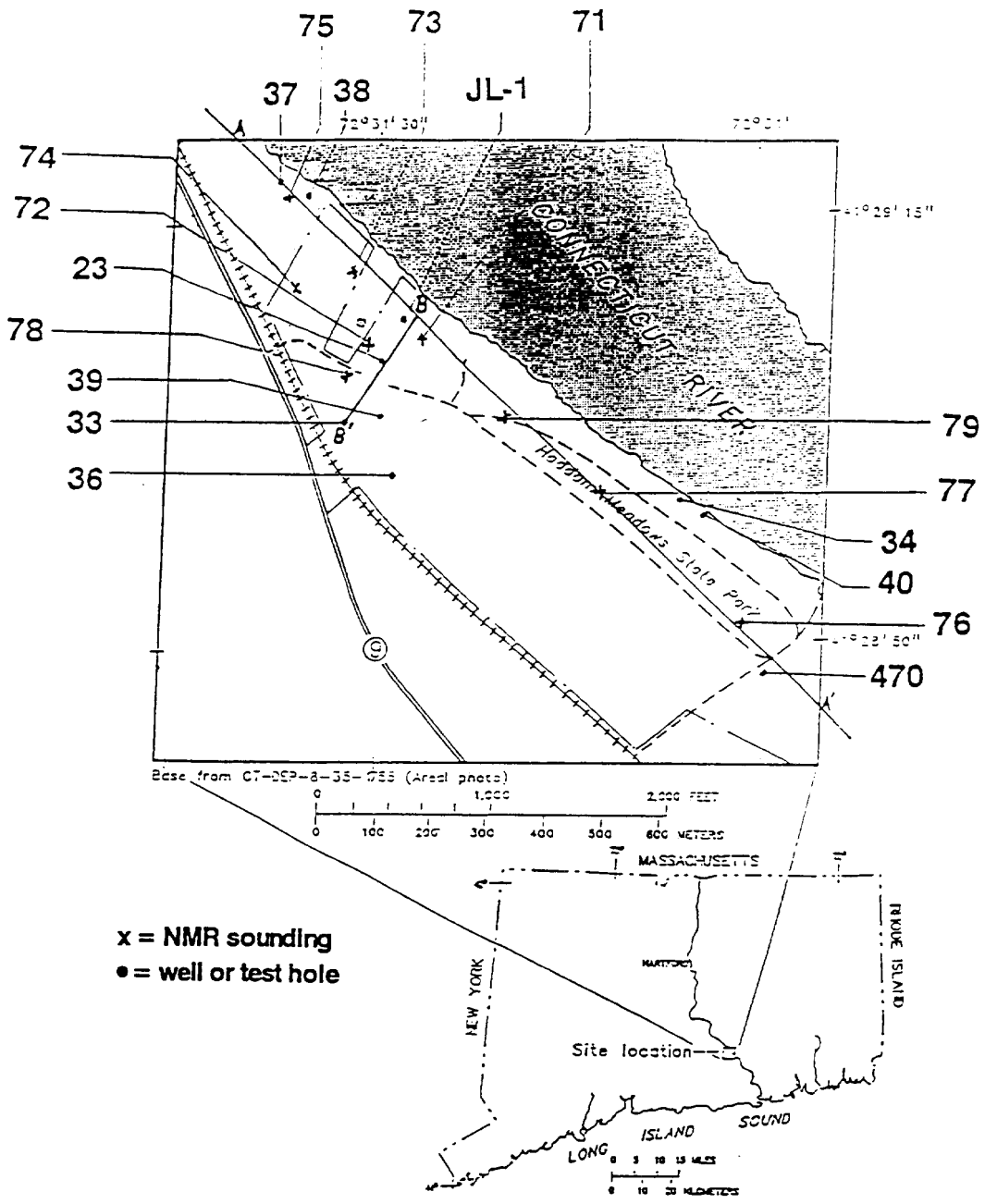

Figure 3. Site map showing the locations of NMR soundings, wells, and test holes. The two section lines used in subsequent figures, A-A' and B-B', are also shown.

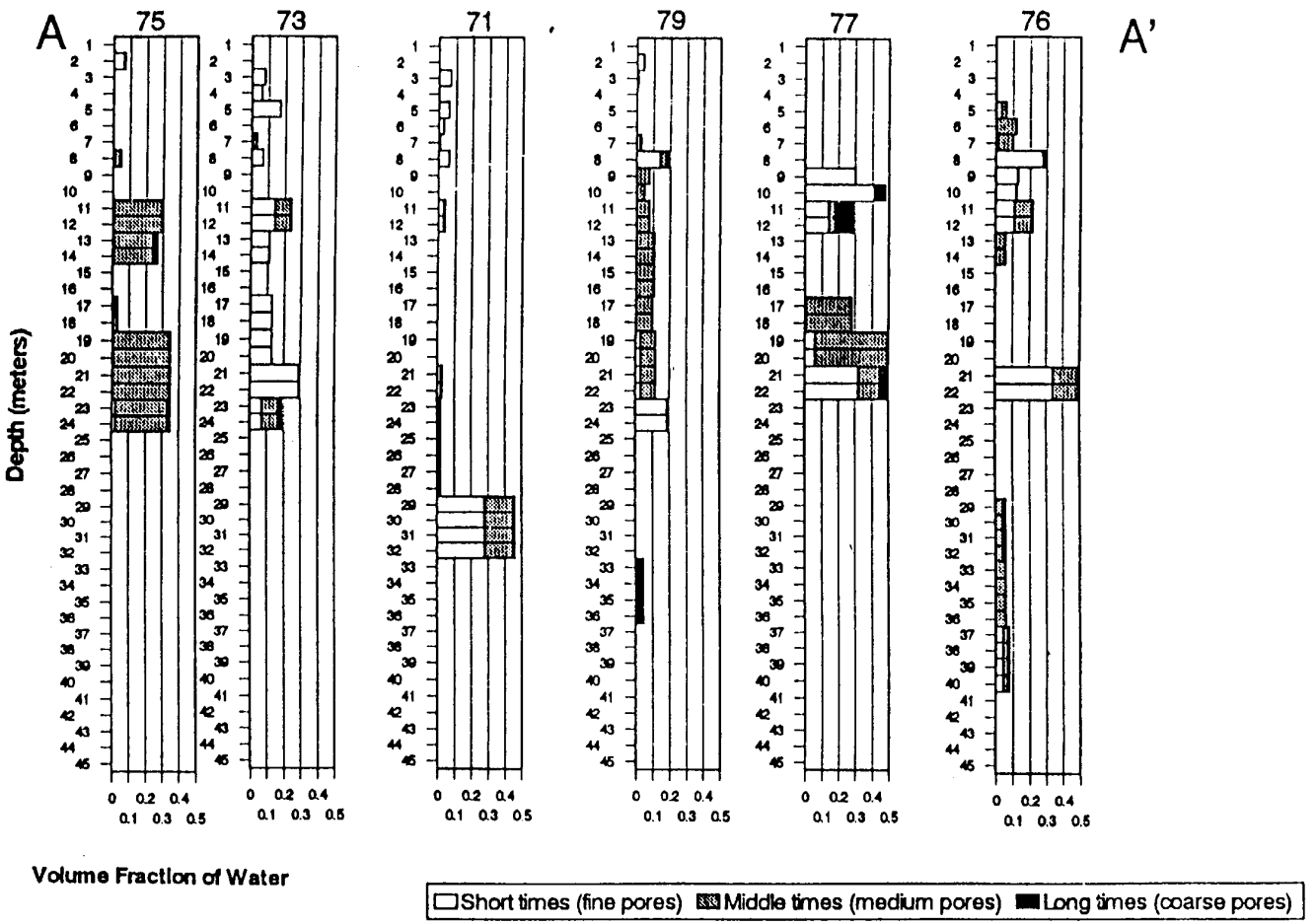

Figure 4. NMR soundings along section A-A' giving the volume fraction of water as a function of depth. Note that the depth interval referred to by the boundaries of a rectangular division is offset 0.5 m upwards (towards the surface of the earth) in figures 4 through 7. For example, the interval from 1.5 to 2.5 m in NMR sounding 75 refers to the interval from 1 to 2 m.

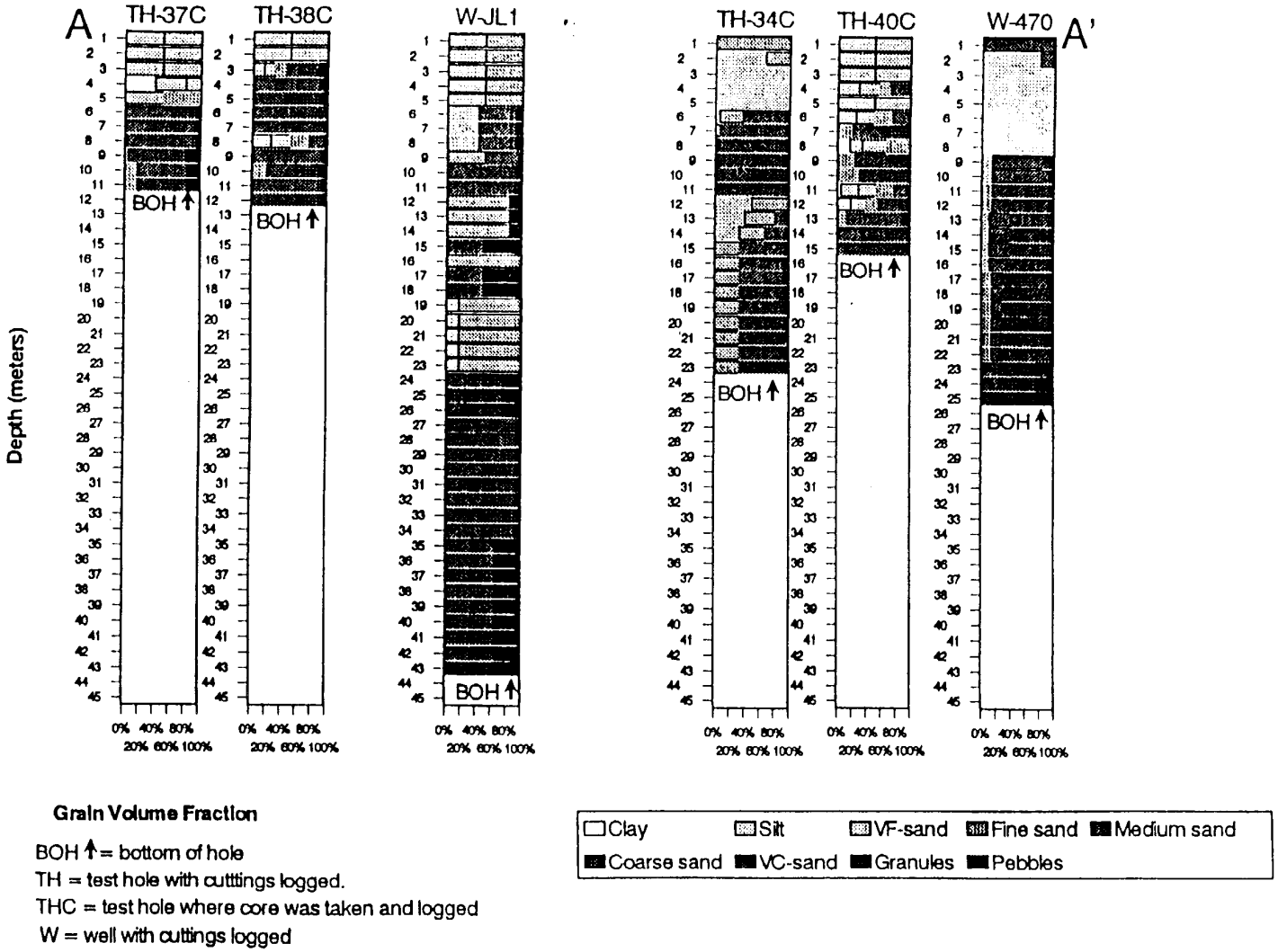

Figure 5. Wells and test holes along section A-A' giving the grain-size distribution as a function of depth.

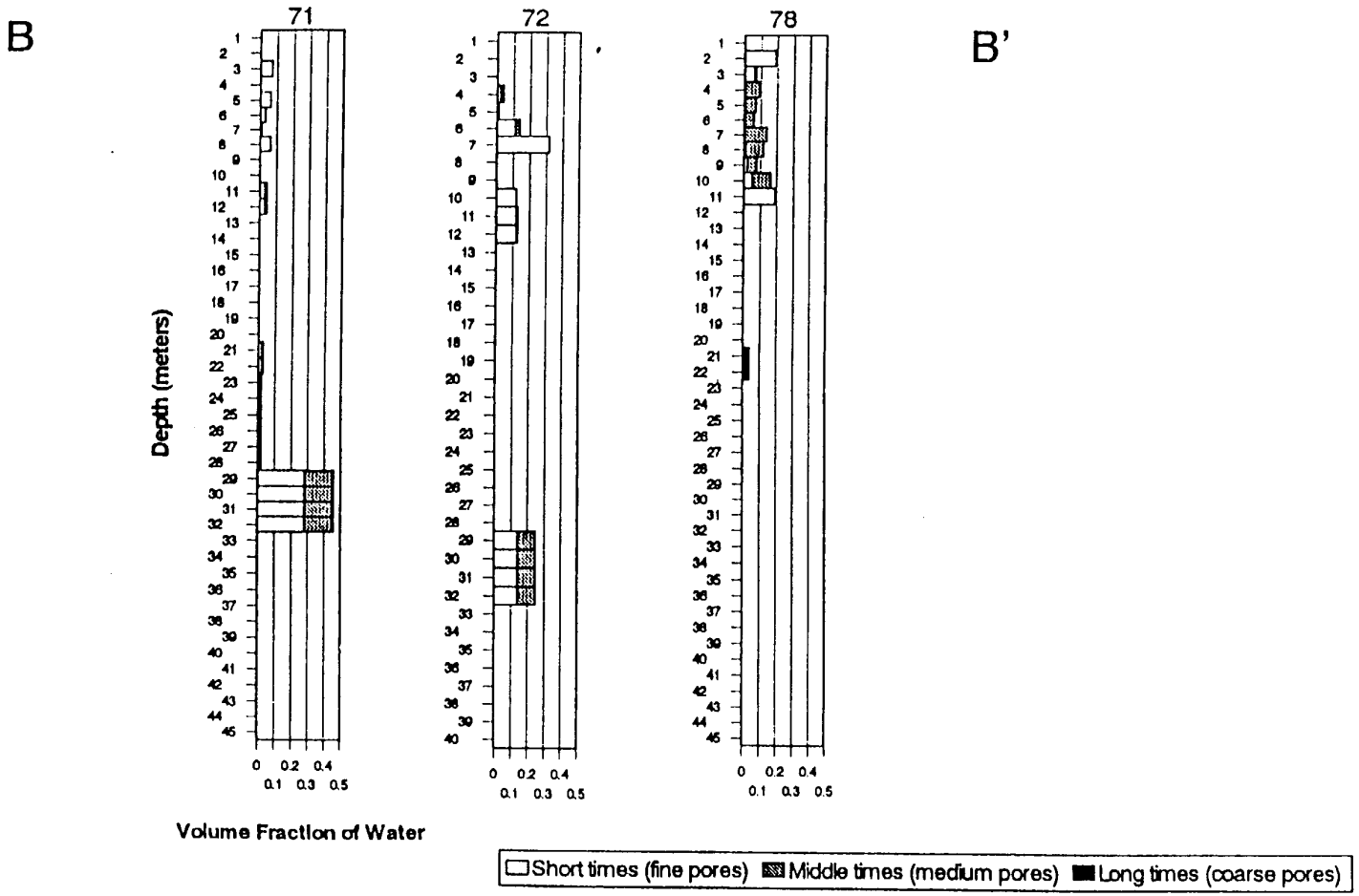

Figure 6. NMR soundings along section B-B' giving the volume fraction of water as a function of depth.

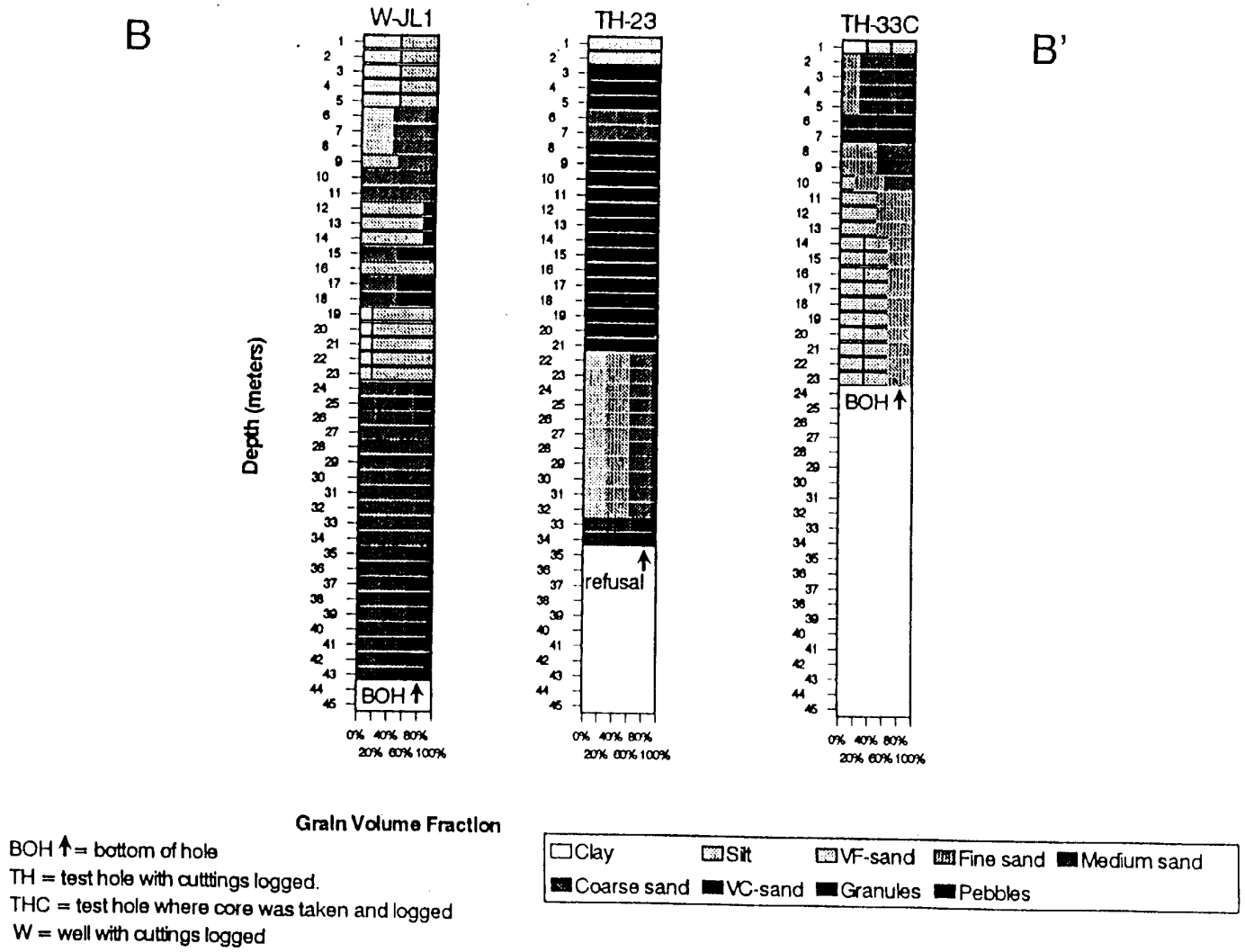

Figure 7. Wells and test holes along section B-B' giving the grain-size distribution as a function of depth.

Journal of Applied Geophysics, 31 (1994) 27–52
Elsevier Science B.V., Amsterdam

Application of the integrated NMR–TDEM method in groundwater exploration in Israel

M. Goldman[a,1], B. Rabinovich[a], M. Rabinovich[a], D. Gilad[b], I. Gev[c] and M. Schirov[d]
[a]*The Institute for Petroleum Research and Geophysics, Holon, Israel*
[b]*The Hydrological Service of Israel, Jerusalem, Israel*
[c]*Institute of Desert Research, Sde Boker, Israel*
[d]*The Institute of Chemical Kinetics and Combustion, Novosibirsk, Russian Federation*

(Received March 22, 1993; accepted after revision April 16, 1993)

ABSTRACT

The Nuclear Magnetic Resonance (NMR) method is the only physical tool currently available which is able to detect directly the presence of fresh water in the subsurface. The Time Domain Electromagnetic (TDEM) method, in turn, has been proven highly efficient in detecting saline groundwater. The combined application of these two methods is the most promising way to delineate accurately groundwater-bearing aquifers and to evaluate the quality of the water. This idea was tested during the feasibility study carried out under different hydrogeological conditions throughout Israel during August–September 1992. The Russian Hydroscope and Geonics *PROTEM*-IV instruments were used for the NMR and TDEM measurements, respectively.

A total of 36 NMR and 12 TDEM stations was established, mostly in close proximity to existing observation wells. Among these only 19 NMR measurements showed reasonable signal-to-noise characteristics, while the rest were obviously distorted by ambient noise. The number of distorted measurements could have been even greater had they been carried out at all points planned. However, a significant number of the NMR stations were cancelled due to their proximity (less than 1–1.5 km) to electric power lines. As a result almost the entire Mediterranean coast of Israel, which was originally chosen as the main test site for this survey, turned out to be unsuitable owing to the low ambient noise protection of the Hydroscope. Another serious limitation of NMR measurements is the maximum penetration depth. The deepest information obtained during the feasibility study was from a depth of 74 m.

Nevertheless, within the framework of its applicability, the NMR measurements proved to be sufficiently accurate and to have a high resolving capability. A comparison with the borehole data shows that, in most cases, NMR is able not only to detect the presence of water, but also to delineate different subaquifers. At the same time, however, the transmissivity and aquifer texture are much less reliably detected. The combined application of the NMR and TDEM methods may essentially improve the reliability of the interpretation. In all cases where the NMR anomaly fits the drop in TDEM resistivity, water of a different salinity is found at approximately the same depth. A reasonable correlation between the interpreted resistivities and water salinities is obtained for these horizons. However, if only one method indicates the presence of water, this, in many cases, was not confirmed by the borehole data. The TDEM anomalies were obviously caused by low-resistivity lithologies, while some of the false NMR signals could be explained by a low signal-to-noise ratio.

As regards the freshwater/seawater interface, this was, in all cases, accurately detected by the TDEM measurements alone. It is interesting to note that at the same depth, NMR measurements indicated a drastically increasing anomaly followed by the absence of water at greater depths. The latter can most likely be explained by the very low resistivity of the sea water, which is not taken into account by the existing NMR interpretation.

Introduction

The most fundamental questions on groundwater which geophysical techniques can help answer were formulated by Fitterman and Stewart (1986) as follows:

(1) Where is it?
(2) How much of it is there?
(3) What is its quality

[1]Currently with the Institute for Geophysics and Meteorology, University of Cologne, Germany.

0926-9851/94/$07.00
SSDI 0926-9851(93)E0017-4

(4) At what rate can the resource be used without adverse effect?

Among all the geophysical methods available, geoelectric techniques (including both electrical and electromagnetic) are best suited to answer the last two questions. This is due to the very close connection between electrical conductivity measured by geoelectrical methods and groundwater salinity which determines its quality.

As regards the first two questions the feasibility of geoelectric methods is far more questionable. This is because the electrical conductivity of fresh groundwater-bearing aquifers does not differ from that of many dry lithological units (Palacky, 1987). The search for fresh groundwater is, therefore, always indirect. No doubt, even indirect exploration under favorable conditions may lead to the successful solution of the problem. Nevertheless, experience shows that the degree of success in solving the last two of the above-mentioned questions is by far higher than that for fresh groundwater exploration.

The idea of how the efficiency of fresh groundwater exploration may be drastically improved is generally quite clear, i.e. the appropriate geophysical technique must be sensitive to that physical parameter which distinguishes water from any other material in the subsurface. The method which is, in principle, able to do this is called the Nuclear Magnetic Resonance (NMR) method and the appropriate parameter is the resonance frequency of protons (H^+) contained in the water (H_2O) in the presence of a static magnetic field (e.g. the Earth's magnetic field). The strength of the method comes from the fact that nuclei of the same species in different chemical environments (as for example the hydrogen nuclei in water, benzene or cyclohexane) possess different resonance frequencies (Emsley et al., 1967). Therefore, the NMR is at present the only physical method which, in principle, facilitates a direct search not only for groundwater but also for hydrocarbons and some other mineral deposits. Theoretically, the only condition for the applicability of NMR technology is the existence of a non-zero magnetic moment for atomic nuclei of the material in question. The NMR signal is observed at a frequency $f_0=\gamma H_0$, where H_0 is the static magnetic field applied to a sample and γ is the magnetogyric ratio which has some specific value for each type of nucleus. Therefore, the existence of the NMR signal at a given frequency, called the resonance frequency, testified to the presence of the material in the sample containing the specific type of nucleus.

To date the NMR technique is widely used in many applications ranging from chemical analysis to medical tomography. In the case of NMR tomography, the static magnetic field applied to the sample is non-uniform. This means that the NMR signal can be obtained not only from the specific material in question, but also from a certain part of the sample; as a result the spatial distribution of the material within the sample is also recorded. This phenomenon is the basis for existing medical NMR tomography and a similar idea using a non-uniform magnetic field to study the spatial distribution of the target material in the subsurface is realized in geophysical NMR tomography. However, it is appropriate to note that there is a significant difference between geophysical and medical NMR tomography. In both cases some non-uniform excitation of the sample is required to recover its spatial structure; however, whilst in laboratory NMR tomography the static magnetic field is non-uniform, in geophysical applications the latter (Earth's magnetic field) is nearly uniform in the scale of regular exploration targets. Therefore, the non-uniform excitation in geophysical NMR tomography is achieved by applying an alternating magnetic field which operates at the resonance frequency, f_0 (a detailed description is given below in the section on the NMR method).

The first mention of the possibility of using the NMR phenomenon in geophysical explo-

ration can be found in an American patent granted to R.H. Varian in 1962 (Varian, 1962). Since that time up until the late 1970s no attempt was made to apply this idea. In 1978, the first geophysical NMR instrument, called the Hydroscope, was developed and field tested by a group of Russian physicists from the Institute of Chemical Kinetics and Combustion in Novosibirsk (Semenov et al., 1982). After the successful feasibility study, the Hydroscope was applied in numerous hydrogeological surveys throughout the former Soviet Union. Unfortunately, all publications concerning these surveys are available in Russian only. Very few applications of the Hydroscope have been reported outside of Russia (India and Australia). A description of the feasibility study conducted in Australia is available in English (Schirov et al., 1991).

The operating principle of the Hydroscope is based on the excitation of protons in subsurface water in the Earth's magnetic field. The instrument consists of transmitter and receiver units. The transmitter drives an alternating current at the resonance frequency through the wire loop laid on the Earth's surface. The current is abruptly terminated and the NMR signal is then measured using the same wire loop as the receiving antenna. This procedure is repeated from several tens to a few hundred times, during which the NMR signal is recorded and averaged to improve the signal-to-noise ratio. The signal is then interpreted in terms of hydrological parameters as a function of depth using an especially developed inversion program.

The NMR signal depends directly on the amount of water protons. Therefore, in order to estimate the groundwater quality, either the NMR measurements must be integrated with conventional geoelectric measurements or the salinity of the groundwater must be indirectly determined using the NMR itself (Semenov et al., 1989). We propose the former approach, in which the conventional geoelectric method known as the Time Domain Electromagnetic (TDEM) method is applied together with the NMR measurements. The choice of this method was not an accidental one, but was dictated by the following:

(1) The TDEM method has proved its superior accuracy and resolving power in detecting saline groundwater the world over (Fitterman, 1986; Mills et al., 1988; Goldman et al., 1991).

(2) The integration of TDEM and NMR is technically most suitable since both methods can use similar, if not identical, transmitter/receiver arrays.

(3) The TDEM results can be used not only in the combined NMR/TDEM interpretation stage, but also for more accurate interpretation of the NMR data alone. This is because the NMR interpretation algorithm includes calculations of the magnetic field within the Earth. The latter heavily depends on the distribution of electrical conductivity with depth. This information is most accurately obtained from the interpretation of the TDEM data.

The TDEM method

The TDEM method has been elucidated in great detail in numerous publications, including those devoted to groundwater exploration (Fitterman and Stewart, 1986; Goldman et al., 1988). The method is, therefore, described here very briefly, emphasizing those features essential for further discussion.

A typical TDEM array consists of a transmitter loop and a receiver coil. The most common transmitter/receiver configuration, called a central loop array, consists of a squared loop of insulated wire laid on the Earth's surface. The size of the transmitter loop varies between 50×50 m and 500×500 m, depending on the exploration depth required. The rule of thumb is that the size is approximately equal to the depth. The receiver coil is much smaller (usually a multi-turn air coil of 1 m diameter) and is located at the center of the transmitter loop. Another popular transmitter/receiver (T/R)

configuration, known as the one-loop array, uses the same transmitter loop as a receiving antenna. Such an array is identical to that used in the Hydroscope system.

The current driven through the transmitter loop consists of equal periods of time-on and time-off. The TDEM signal is measured during the transmitter "time-off" period only, i.e. in the absence of a primary field. This unique feature of the TDEM method leads to several significant advantages as compared to other geoelectric methods (e.g. the TDEM signal is far less sensitive to errors in the T/R geometry, the receiver coil can be located anywhere or even be combined with the transmitter loop as in the above-mentioned on loop array, etc.).

Due to the skin-effect, the exploration depth in the TDEM method is determined by the time interval after the transmitter current is turned off. In order to make deeper explorations, it is necessary only to record the signal for a longer time (typical times vary in the range of several microseconds for an exploration depth of 5–10 m to tens of milliseconds for exploration depths of a few hundred meters).

As time increases, the current intensity migrates to greater depths. This eliminates the so-called static shift, the problem which causes significant difficulties in the application of other geoelectric methods.

The NMR method

General description

Generally speaking, the nuclear magnetic resonance phenomenon is an extension of optical spectrocopy to the microwave (roughly 10^3 to 10^5 MHz) and the radiofrequency (roughly 10 KHz to 10³ MHz) regions (Emsley et al., 1967). In these regions radiation is absorbed and emitted by the same basic process as at any other wavelength in the electromagnetic spectrum.

The concept of the NMR method is based on the fact that many atomic nuclei, including protons in water, possess a non-zero dipole magnetic moment. The classical model describing the presence of the moment is a spinning charged particle. Although this model is somewhat simplified (for example it provides no explanation for the magnetic moment of a neutral particle such as the neutron, nor does it explain why some nuclei have negative magnetic moments), it is extremely useful for a general understanding of the NMR phenomenon. If a spinning charged particle having a magnetic moment, μ, is placed in a magnetic field of strength, H_0 (Fig. 1a), the magnetic moment will experience a torque tending to align it parallel to the field. As a result, the magnetic moment precesses around the applied field with the precession frequency defined by the Larmor equation (Emsley et al., 1967):

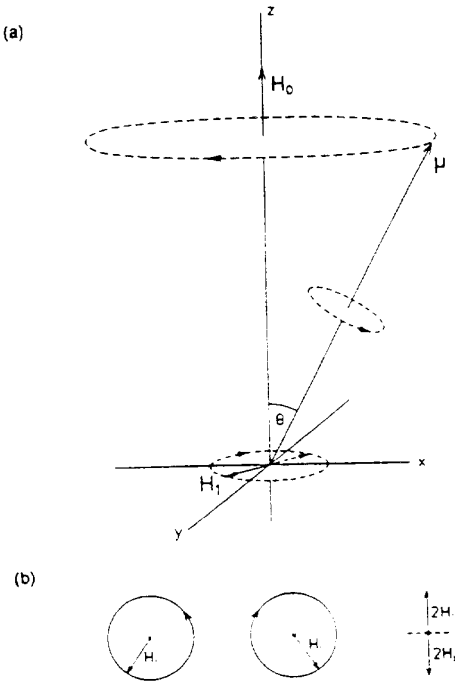

Fig. 1. Vectorial representation of the classical Larmor precession (after Emsley et al., 1967).

$$\nu_0 = \frac{\gamma H_0}{2\pi} \quad (1a)$$

where γ is the magnetogyric ratio defined by:

$$\gamma = \frac{g\beta}{\hbar} \quad (1b)$$

The Landi or spectroscopic splitting factor, g, is a measure of the spin and orbital motion of a particle in relation to its total angular momentum. For a completely free electron, g has a value of 2.0023 while g for a hydrogen nucleus is 5.58490. The Bohr (or nuclear) magneton, β, has numerical values of 9.2712×10^{-21} and 5.0493×10^{-24} erg/gauss for free electrons and protons in water, respectively. $\hbar$ is Planck's constant ($\hbar = 6.625\times10^{-27}$ erg·s). Substituting these values into Eqs. (1a) and (1b) and using SI units, we obtain for the precession frequency of protons in water:

$$f_0(\mathrm{Hz}) = 0.04258 H_0(\mathrm{nT}) \quad (1c)$$

An important feature of this equation is that the precession frequency is independent of the initial angle of inclination of the particle magnetic moment to the field direction.

If a small magnetic field, H_1, is applied at right angles to the main field, H_0, then in order to change the orientation and thus the magnetic energy of the particle, the secondary field, H_1, must rotate in synchronization with the precession of the magnetic moment about H_0 (otherwise the total change in Θ is zero; Fig. 1a). In other words, the rotation of H_1 must be in resonance with the Larmor precession about H_0. A rotating magnetic field of this type is associated with circularly polarized radiation of frequency f_0. The sense of the Larmor precession depends upon the sign of the magnetic moment, for example a positive moment requires a left circularly polarized H_1. For most purposes linear polarization is quite adequate since a linearly oscillating field may be regarded as the superposition of two fields rotating in opposite directions (Fig. 1b). Only the component having the correct sense will synchronize with the precessing magnetic moment; the other component will have no effect. In practice, an alternating current is passed through a coil mounted perpendicular to H_0 so as to produce a magnetic field oscillating along the axis of the coil, say along the x-direction. The voltage applied to the coil at frequency f_0 produces the equivalent of two counter-rotating fields having the vector representation ($H_1 \cos \omega_0 t$, $H_1 \sin \omega_0 t$, 0) and ($H_1 \cos \omega_0 t$, $-H_1 \sin \omega_0 t$, 0), where $\omega_0 = 2\pi f_0$. When ω_0 corresponds to the resonance frequency, the magnetic dipole will absorb energy from the coil, thereby causing the magnetic moment vector to dip towards the x–y-plane (Fig. 1a). When the alternating resonance field is removed, the magnetic moment vector returns to its equilibrium position precessing around the static magnetic field H_0. This complicated precession generates a time varying field which can be measured by a receiver coil. The precession is damped as the magnetic moments return to their equilibrium positions, thus inducing a damped sine signal at the precession or resonance frequency in the receiver coil.

Geophysical application

The NMR method was first successfully applied as a geophysical sounding technique in the late 1970s by a group of Russian physicists from the Institute of Chemical Kinetics and Combustion, USSR Academy of Science, Siberian Branch (Schirov et al., 1991). It was shown by both theoretical and experimental investigations that the dependence of the initial amplitude of the NMR signal on the area of the exciting current impulse (the product of the current and duration of the impulse) is the crucial factor in determining depths and thicknesses of water-bearing aquifers. Following Pusep et al. (1991), let us consider this point in greater detail.

The radio-frequency magnetic field, H_1 is excited by the alternating current $I = I_0 \cos \omega_0 t$, which is driven into a loop of wire laid out on

the Earth's surface. According to the description above, only that component of the alternating magnetic field which is perpendicular to the static field, H_0, will result in the change of the magnetic moment, μ, by means of the so-called nutation of the moment around the static field. The frequency of the nutation is proportional to the intensity of the alternating magnetic field. If the latter is linearly polarized and has an amplitude $2H_1$, then the frequency of nutation if defined by $\omega_1=\gamma H_1$.

Thus the angle Θ between the H_0-axis and the magnetic moment μ changes with time by:

$$\Theta=\omega_1=\gamma H_1 t \tag{2}$$

provided that the equilibrium magnetic moments are parallel to the static magnetic field, H_0. The components of the magnetic moment in the laboratory coordinate system are determined by:

$$\begin{aligned}\mu_x(t)&=\mu_0\sin\Theta\sin\omega_0 t\\ \mu_y(t)&=\mu_0\sin\Theta\cos\omega_0 t\\ \mu_z(t)&=\mu_0\cos\Theta=\mu_0\cos[\gamma H_1(0)t]\end{aligned} \tag{3}$$

where μ_0 is the equilibrium magnetic moment (for $t=0$), which is directed along the z-axis and the linearly polarized exciting field $H_1(t)=H_1(0)\cos\omega_0 t$ is located in the x–z-plane. Thus, under the influence of both magnetic fields, the magnetic moment is involved in a complicated motion which includes the precession with frequency ω_0 and nutation with frequency ω_1.

If the magnetic moment is concentrated in a small volume (i.e. point moment), then the electromotive force (emf) induced in the receiver coil is proportional to the time derivative of μ. Indeed, representing the moment μ by a magnetic dipole such as:

$$\mu=I\cdot S \tag{4}$$

where I is a current and S is a vector perpendicular to the plane of the dipole and has a value equal to the area of the dipole. Then, according to Faraday's law, the emf in the receiver coil is defined by:

$$\text{emf}=-\frac{\partial}{\partial t}\Phi(t)=-\frac{\partial}{\partial t}(L_{12}\cdot I) \tag{5}$$

where L_{12} is the coefficient of mutual inductance of the magnetic dipole and receiver coil.

Using reciprocity, the coefficient can be determined through the magnetic flux induced in the dipole by the current I flowing in the receiver coil:

$$L_{12}=L_{21}=\frac{B\cdot S}{I} \tag{6}$$

where B is the magnetic induction vector created by the receiver coil at the location of the magnetic moment. Since B at any point is proportional to the current in the coil, I, it is reasonable to consider the specific induction vector:

$$\beta=\frac{B}{I} \tag{7}$$

It should be noted that the specific induction vector β depends only on coordinates of the point and its value decreases as the distance between the coil and the point increases.

Substituting Eq. (7) into Eqs. (6) and (5) gives:

$$\text{emf}(t)=-\beta\cdot\frac{\partial\mu}{\partial t} \tag{8}$$

Since the magnetic induction of the receiver coil is essentially non-uniform within the limits of a real water layer, Eq. (8) must be integrated along the volume of the deposit:

$$\text{emf}(t)=-\int_v \beta(r)\frac{\partial}{\partial t}M(r,t)\,dv \tag{9}$$

where $M(r,t)$ is the magnetic moment of the unit volume and $\beta(r)$ is the specific magnetic induction vector of the receiver coil at the point r within the water layer (Fig. 2).

If the nutation is excited by the alternating current:

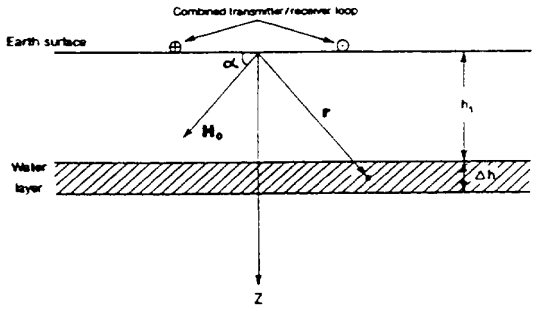

Fig. 2. Model geometry of the NMR survey using the Hydroscope.

$$I(t)=I_0\cos\omega_0 t \tag{10}$$

then using Eqs. (3) and (9), we obtain for the emf measured at the receiver coil:

$$\mathrm{emf}(t)=-\mathrm{emf}^\circ(t)\sin\omega_0 t \tag{11}$$

where:

$$\mathrm{emf}^\circ(t)=\omega_0 M_0\int_v \beta_\perp(r)\sin[\gamma\beta_\perp(r)I_0 t]\,dv \tag{12}$$

where M_0, called nuclear magnetization, is a magnetic moment of the unit volume under equilibrium conditions ($t=0$) and $\beta_\perp(r)$ is a component of the specific induction vector perpendicular to the Earth's magnetic field. It should be noted that Eq. (12) is valid only for those points in which the nutation frequency, ω_1, is much less than the precession frequency, ω_0, (in other words $H_1 \ll H_0$).

In order to increase the signal-to-noise ratio, the exciting current in the transmitter loop is terminated and the NMR signal is recorded during the time-off period only. This procedure is automatically repeated many times (usually from several tens up to a few hundred times) to provide stacking of the recorded signal. The amplitude of this signal (called the free precession or free induction signal) is determined by:

$$\mathrm{emf}^\circ(q)=\omega_0 M_0\int_v \beta_\perp(r)\sin[\gamma\beta_\perp(r)q]\,dv \tag{13}$$

where $q=I_0\tau_p$ and τ_p is the duration of the current impulse.

Parameter q which is equal to the area beneath the envelope of the impulse, is called the area of the impulse or excitation parameter. It plays a crucial role in NMR soundings since it determines the resulting amplitude of the NMR signal. If the alternating magnetic field is practically uniform within the limits of the target, then a well-known sinusoidal relation between the signal and excitation parameter is obtained from Eq. (13):

$$\mathrm{emf}^\circ(q)=\omega_0 M_0 v\beta_\perp\sin(\gamma\beta_\perp q) \tag{14}$$

This relation, which is valid for small samples, is widely used to calculate the signals of free induction in laboratory experiments. If the nutation is excited by an essentially non-uniform alternating field (i.e. in the case of large samples such as water layers in the subsurface), then the evaluation of Eq. (13) can be carried out only numerically.

Figure 3a shows a typical curve $\mathrm{emf}^\circ(q)$ calculated using Eq. (13) for the model shown in Fig. 2. The value of the nuclear magnetization $M_0=1.92\times10^{-7}$ J/(T·m^3) is taken for free water at a temperature of 293 K. The transmitter/receiver antenna is represented by a two-turn circular loop, 25 m in radius. The geomagnetic field inclination, α, is 64°, the resonance frequency, f_0, is 2.5 KHz. The limiting value of the excitation parameter, $q=2000$ A·ms, has been chosen due to reasonable technical limitations ($I_0\leqslant 40$ A) and also because Eq. (13) is valid only if the duration of pulse is less than the spin–spin relaxation time of water protons (i.e. $\tau_p\leqslant 50$ ms).

Figure 3b is a comparison of the calculated and field data for a known water-bearing aquifer in the Balkhash area of Russia. In order to achieve a fairly good fit between synthetic and

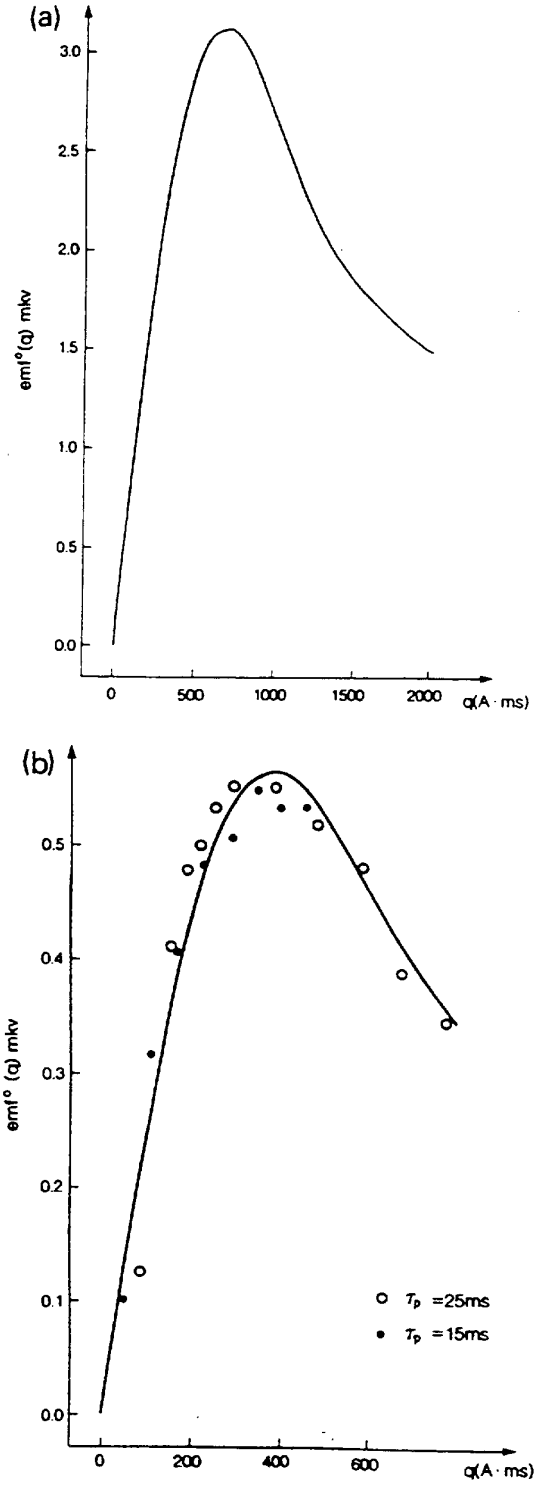

field data, the former had to be multiplied by a factor of 0.18. This factor roughly coincides with the coefficient of porosity of the aquifer. Another parameter which similarly affects the initial amplitude of the NMR signal is the thickness of the water layer. Thus, the main factor in determining the value of the first maximum of emf° (q) is the total amount of water beneath the loop.

As regards the depth to the water layer, this is clearly associated with the position of the maximum along the q-axis. This is illustrated in Fig. 4 which shows the calculated NMR responses for different depths and thicknesses of the water layer. These curves can, in principle, be used for solving an inverse problem (i.e. finding the parameters of the water layer) by means of either manual or automatic curve fitting as carried out in conventional geoelectric methods.

It should be noted that the specific induction vector, $\beta_\perp$, in Eq. (13) has been calculated for the loop of wire located in a free space, i.e. without accounting for the conductivity of the ground. This over-simplification of the real conditions may lead to significant errors in the interpretation of the NMR data (see section Results).

In reality, present equipment does not measure the amplitude emf° (q), but rather the signal of free induction defined for a thin homogeneous water layer by:

$$\mathrm{emf}(t,q)=\mathrm{emf}^\circ(q)\exp(-t/T2)\sin\omega_0 t \qquad (15)$$

This last expression is obtained from the Bloch equations (Abragam, 1961) for $t>\tau_p$. Eq. (15) is used during the interpretation in order to determine the relaxation time, T_2, which is closely

Fig. 3. (a) Synthetic NMR response for $h_1=10$ m and $\Delta h=20$ m. (b) Synthetic NMR response (solid line) for $h_1=5.5$ m and $\Delta h=14.5$ m and appropriate field data (dots and circles) (after Pusep et al., 1991).

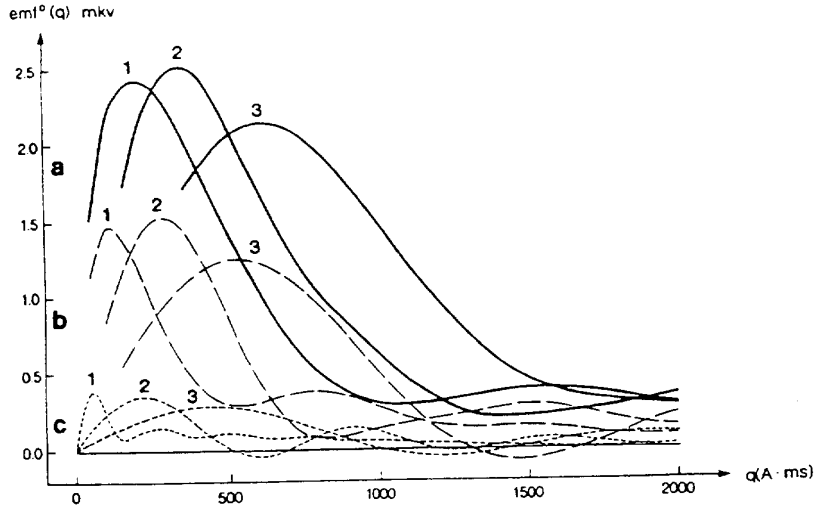

Fig. 4. Synthetic NMR responses for different depths and thicknesses of the water layer (after Pusep et al., 1991). (a) $\Delta h = 10$ m. h_1: 1 = 1 m, 2 = 5 m, 3 = 10 m. (b) $\Delta h = 5$ m. h_1: 1 = 1 m, 2 = 5 m, 3 = 10 m. (c) $\Delta h = 1$ m. h_1: 1 = 1 m, 2 = 5 m, 3 = 10 m.

connected to the pore size of the aquifer (Schirov et al., 1991).

Hydroscope output

A typical Hydroscope output is shown in Fig. 5 (it differs slightly for different software versions). It consists of two main parts: the heading and the histogram. The heading includes the following information:

(1) The diameter of the circular transmitter loop, the date and time of the survey.
(2) Observation site identification.
(3) Altitude of the site.
(4) Resonance frequency and number of stacks.
(5) Inclination of the geomagnetic field in degrees.

The histogram itself is in fact a hydrological cross-section of the sounding site. The whole depth range between 0 and 138 m is divided by 26 horizontally-layered subaquifers for which the NMR responses are calculated for different concentrations of water within each layer.

The inverse problem is solved by a minimization of the misfit between the calculated and measured responses. The resulting histogram consists of the following columns (reading from left to right):

(1) Depths to the top of each layer (m).
(2) Depths to the bottom of each layer (m).
(3) The cumulative amount of free water (m^3) from the surface to the bottom of each layer in a column of 1 m^2 base.
(4) The cumulative transmissivity of a column from the surface to the bottom of each layer (m^2/24H).
(5) The percentage of water within small pores for each layer.
(6) The percentage of water within medium pores for each layer.
(7) The percentage of water within large pores for each layer.
(8) The total percentage of water for each layer.

The right hand picture provides the concentration of water within each layer by printing a *W* for each 2% of the total percentage of water (e.g. a 10% concentration of water is represented by *WWWWW*).

It should be noted that the most reliable re-

"HYDROSCOPE" CENTRE, USSR
SOFTWARE V03.01

LOOP 100 M DATE 18.08.92 TIME 08.30

OBSERVATION SITE: NMR-777 .....

ABS.ALTITUDE .....M

FREQUENCY 1870 HZ STACKING NUMBER 100

EARTH FIELD INCLINATION 45 DEGR

DEPTH FROM M	TO M	VE 3 M	T 2 M/24H	TS	TM	TL	PERCENTAGE OF WATER 0 10 20 30 40 50
							:....:....:....:....:....:
0.00	1.00	0.00	0	0	0	0	0 I I
1.00	2.00	0.00	0	0	0	0	0 I I
2.00	3.00	0.00	0	0	0	0	0 I I
3.00	4.00	0.00	0	0	0	0	0 I I
4.00	5.00	0.00	0	0	0	0	0 I I
5.00	6.00	0.00	0	0	0	0	0 I I
6.00	7.00	0.00	0	0	0	0	0 I I
7.00	8.00	0.03	0	3	0	0	3 IWW I
8.00	9.00	0.05	0	2	0	0	2 IW I
9.00	10.00	0.05	0	0	0	0	0 I I
10.00	12.00	0.09	0	2	0	0	2 IW I
12.00	14.00	0.09	0	0	0	0	0 I I
14.00	16.00	0.09	0	0	0	0	0 I I
16.00	18.00	0.09	0	0	0	0	0 I I
18.00	20.00	0.19	1	5	0	0	5 IWWW I
20.00	22.00	0.19	1	0	0	0	0 I I
22.00	24.00	0.19	1	0	0	0	0 I I
24.00	28.00	0.19	1	1	0	0	1 IW I
28.00	32.00	0.23	1	1	0	0	1 IW I
32.00	36.00	0.27	2	0	1	0	1 I I
36.00	40.00	0.27	2	0	0	0	0 I I
40.00	46.00	0.27	2	0	0	0	0 I I
46.00	54.00	0.27	2	0	0	0	0 I I
54.00	62.00	0.27	2	0	0	0	0 I I
62.00	74.00	0.27	2	0	0	0	0 I I
74.00	138.00	0.27	2	0	0	0	0 I I
							:....:....:....:....:....:
							0 10 20 30 40 50

Fig. 5. An example of the Hydroscope histogram (detailed description in section on Hydroscope output).

covered parameter is the cumulative amount of free water (m^3) from the surface to the bottom of the last layer within a column of 1 m^2 base. This parameter is simply calculated as the area beneath the measured curve emf° (q) and depends on the noise level to a lesser degree. The distribution of water in the cross-section (the amount of water in each layer and the depths and thicknesses of the layers) is a result of inversion which depends heavily on the form of the emf° (q) curve. Obviously a low-signal-to-noise level could be the reason for emf° (q) curve distortion and, consequently, could cause inaccuracies in the inversion results. As previously mentioned, the texture of the aquifer (pore size) is determined from the relaxation time T_2 of the free induction decay signal, which is measured in the field and which, of course, depends on noise level. The transmissivity value is calculated from previously obtained values of water quantities and pore size for each layer and is, therefore, considered the less reliable parameter.

Results

The location map of the integrated NMR–TDEM survey shows (Fig. 6) all measurement stations established. A significant number of NMR measurements was distorted by ambient EM noise of different origins. It should be noted that the number of distorted points would be much higher had the measurements been carried out at all points planned. However, in accordance with the Hydroscope manual, those points located closer than 1 km from the power lines were cancelled. As a result almost the entire Mediterranean coast of Israel, which was originally chosen as the main test site for the survey, was unsuitable owing to the extremely low ambient noise protection of the Hydroscope.

The first three NMR stations were established in the Alumim area, in the southern coastal plain of Israel (Fig. 6). The lithology of this region consists of a loess cover overlying sand, sandstone, gravel with silt and clay alternations of Quaternary age. The thickness of the sediments is more than 100 m, while the groundwater depth is less than 100 m. The aquifer supplies a significant amount of brackish water. The main objective here was to test the NMR instrument only, therefore no TDEM measurements were carried out here. The hydrogeological control of the NMR results was carried out using the borehole data from two nearby observation wells. The first well, Alumim-2, is located very close to NMR points 1 and 2 while the second well, T-6, is some 600 m away from point 3.

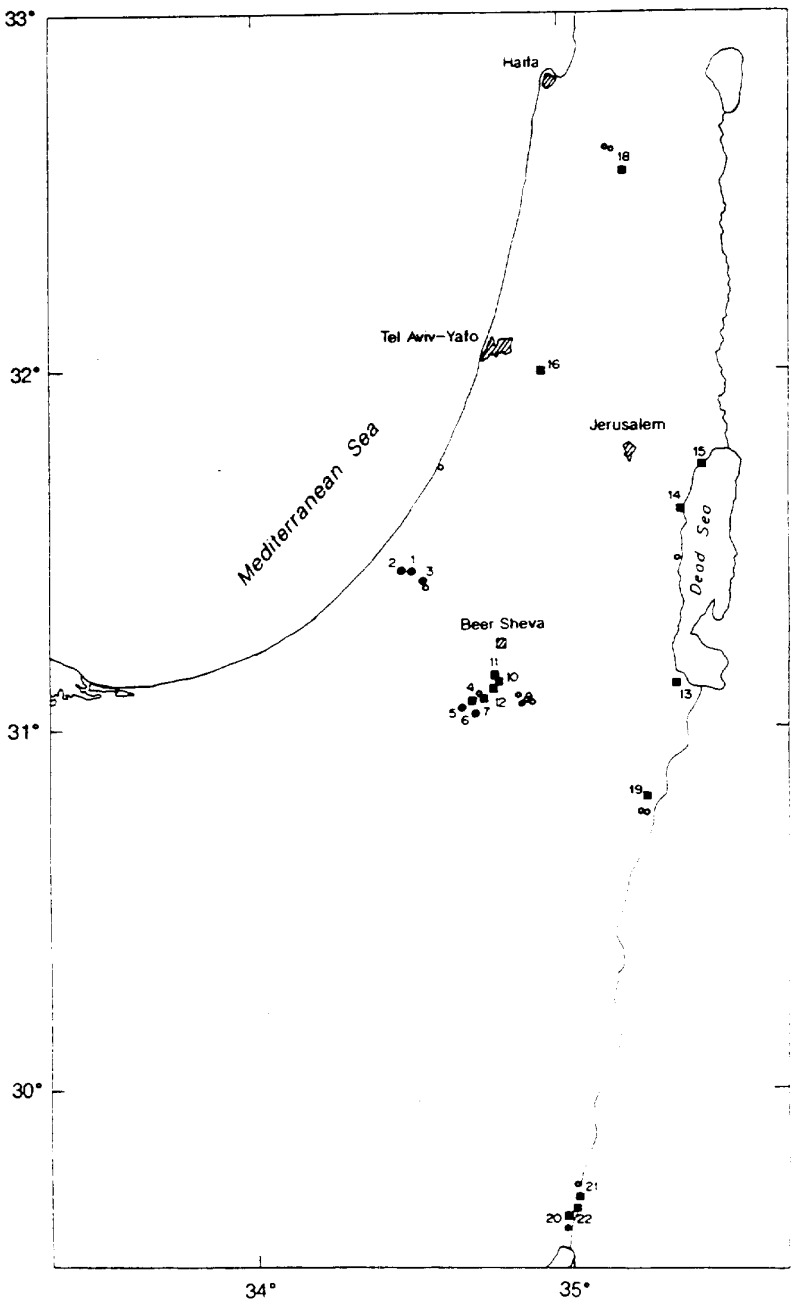

Fig. 6. General location map of the integrated NMR/TDEM survey in Israel (1992) ● = NMR interpreted; ○ = NMR (noisy data); ■ = NMR–TDEM.

A comparison of the NMR results from all three points with the appropriate borehole data shows a fairly good agreement in the depths to the water layer but an essential disagreement in the transmissivity and pore sizes. As an example, let us consider the Hydroscope histogram obtained at station 1 (Fig. 7). The histogram shows a relatively small amount of water in its deeper section (460 l/m^2 in the depth range between 62 to 138 m). The water is located in small pores and the transmissivity is very low (2 m^2/24 h for the lowermost layer). Approximately the same depths were obtained at points 2 and 3, while the transmissivity obtained was greater by about two orders of magnitude. The water at points 2 and 3 is located mainly in large and medium pores respectively. The static water level (SWL) determined in the nearby observation well, Alumim-2, is located at a depth of 73 m. The aquifer is composed of gravels and coarse sands at points 1 and 2 and of calcereous sandstone at point 3. The water salinity is approximately 1400 mgl Cl at points 1 and 2 and about 4000 mgl Cl at point 3. The low signal-to-noise ratio is a probable explanation for the drastic difference in transmissivity at points 1, 2 and 3. It should be noted that in additional measurements at point 1, the same amount of water (460 l/m^2) was found in the large pores and the calculated transmissivity value was much higher (75 m^2/24 h), which fitted the borehole data.

"HYDROSCOPE" CENTRE, USSR
SOFTWARE V03.01

LOOP 100 M DATE 18.08.92 TIME 06.30

OBSERVATION SITE: 1 .....

ABS.ALTITUDE .....M

FREQUENCY 1870 HZ STACKING NUMBER 100

EARTH FIELD INCLINATION 45 DEGR

DEPTH FROM	DEPTH TO	VE 3 M	T 2 M/24H	TS	TH	TL	PERCENTAGE OF WATER 0 10 20 30 40 50
0.00	1.00	0.00	0	0	0	0	0 I I
1.00	2.00	0.00	0	0	0	0	0 I I
2.00	3.00	0.00	0	0	0	0	0 I I
3.00	4.00	0.00	0	0	0	0	0 I I
4.00	5.00	0.00	0	0	0	0	0 I I
5.00	6.00	0.00	0	0	0	0	0 I I
6.00	7.00	0.00	0	0	0	0	0 I I
7.00	8.00	0.00	0	0	0	0	0 I I
8.00	9.00	0.00	0	0	0	0	0 I I
9.00	10.00	0.00	0	0	0	0	0 I I
10.00	12.00	0.00	0	0	0	0	0 I I
12.00	14.00	0.00	0	0	0	0	0 I I
14.00	16.00	0.00	0	0	0	0	0 I I
16.00	18.00	0.00	0	0	0	0	0 I I
18.00	20.00	0.00	0	0	0	0	0 I I
20.00	22.00	0.00	0	0	0	0	0 I I
22.00	24.00	0.00	0	0	0	0	0 I I
24.00	28.00	0.00	0	0	0	0	0 I I
28.00	32.00	0.00	0	0	0	0	0 I I
32.00	36.00	0.00	0	0	0	0	0 I I
36.00	40.00	0.00	0	0	0	0	0 I I
40.00	46.00	0.00	0	0	0	0	0 I I
46.00	54.00	0.00	0	0	0	0	0 I I
54.00	62.00	0.00	0	0	0	0	0 I I
62.00	74.00	0.12	0	1	0	0	1 IW I SWL
74.00	138.00	0.48	2	1	0	0	1 IW I////////

0 10 20 30 40 50

Fig. 7. The Hydroscope histogram from the Alumim area (Station 1, Fig. 6).

NMR stations 4–12 are located in the northern Negev area (Fig. 6). Here the lithology is composed of thin Quaternary sediments of conglomerates, sand and loess covering the Eocene chalk. The aquifer is poor and contains brackish water. Part of the area is used for liquid waste ponds. The objective of the first three measurements (points 4–7) was to test the feasibility of the NMR method in detecting the presence of groundwater at relatively shallow depths in the chalky aquitard and to estimate the water quality by using TDEM data previously acquired at approximately the same locations. Hydrological control is achieved by interpolation of the borehole data from four observation wells as well as by direct observations from the nearby streams and draw wells.

All of these data correlate fairly well at all points. Moreover, the geophysical data sometimes provide information unavailable from wells or direct observation. By way of an example, let us consider the results of the NMR and TDEM measurements at station 7 (Fig. 8). The NMR histogram shows two thick layers containing small amounts of water at depths of 6–14 and 24–46 m (or probably 20–46 m, see Fig. 8), respectively. The small amount of water shown at the shallow depth of 2–3 m is most likely caused by the low signal-to-noise ratio. The TDEM resistivity/depth section correlates quite accurately with the NMR data.

"HYDROSCOPE" CENTRE, USSR
SOFTWARE V03.01

LOOP 100 M DATE 19.08.92 TIME 14.00

OBSERVATION SITE: 7 .....

ABS.ALTITUDE .....M

FREQUENCY 1856 HZ STACKING NUMBER 64

EARTH FIELD INCLINATION 45 DEGR

DEPTH FROM M	TO M	VE 3 M	T 2 M/24H	TS	TM	TL		PERCENTAGE OF WATER 0 10 20 30 40 50
0.00	1.00	0.00	0	0	0	0	0 I	I
1.00	2.00	0.00	0	0	0	0	0 I	I
2.00	3.00	0.01	0	1	0	0	1 IW	I
3.00	4.00	0.01	0	0	0	0	0 I	I
4.00	5.00	0.01	0	0	0	0	0 I	I
5.00	6.00	0.01	0	0	0	0	0 I	I
6.00	7.00	0.02	0	1	0	0	1 IW	I
7.00	8.00	0.03	2	0	0	1	1 IW	I
8.00	9.00	0.04	4	0	0	1	1 IW	I
9.00	10.00	0.05	4	1	0	0	1 IW	I
10.00	12.00	0.07	4	1	0	0	1 IW	I
12.00	14.00	0.09	4	1	0	0	1 IW	I
14.00	16.00	0.09	4	0	0	0	0 I	I
16.00	18.00	0.09	4	0	0	0	0 I	I
18.00	20.00	0.09	4	0	0	0	0 I	I
20.00	22.00	0.11	5	0	1	0	1 IW	I
22.00	24.00	0.11	5	0	0	0	0 I	I
24.00	28.00	0.15	5	1	0	0	1 IW	I
28.00	32.00	0.19	5	1	0	0	1 IW	I
32.00	36.00	0.23	5	1	0	0	1 IW	I
36.00	40.00	0.31	7	1	1	0	2 IW	I
40.00	46.00	0.49	22	0	2	1	3 IWW	I
46.00	54.00	0.49	22	0	0	0	0 I	I
54.00	62.00	0.49	22	0	0	0	0 I	I
62.00	74.00	0.49	22	0	0	0	0 I	I
74.00	138.00	0.49	22	0	0	0	0 I	I

0 10 20 30 40 50

TDEM (Ohm-m)

10

1.5

10

2.5

Fig. 8. Results of the combined NMR/TDEM interpretation, Retamim area, central Negev (Station 7, Fig. 6).

The first drop in resistivity at about 6 m depth (from 10 to 1.5 Ω·m) coincides with the top of the upper water layer detected by NMR and with the water level measured in the nearby draw well. The second drop in the TDEM resistivity profile occurs at a depth of approximately 14 m, which roughly coincides with the lower water layer detected by NMR (Fig. 8).

The discrepancy between the TDEM and NMR results is quite significant (6 m) and can most likely be explained by insufficient accuracy of either (or both) methods. Unfortunately, the well data are not available at this depth, therefore the real depth to the lower subaquifers is unknown. However, taking into account the general coincidence of the NMR and TDEM results (Fig. 8), the existence of two subaquifers as well as the approximate depth to the lower subaquifer are determined with high reliability.

According to the previous TDEM survey, the absolute resistivity values for the water-bearing subaquifers (approximately 1.5 and 2.5 Ω·m respectively) testify to very high salinity of the water (Goldman et al., 1991). However, direct salinity measurements show relatively

low mineralization of the water (2000–4000 mgl Cl) over the whole area under consideration. These results confirm a well known fact that resistivity of the aquifer depends not only on the water salinity, but also on the properties of the aquifer. A similar phenomenon was pointed out in the TDEM survey of the coastal aquifer (Goldman et al., 1991, TDEM station No. 35).

The remainder of the NMR measurements (excluding points 8, 9 and 17 in which the low signal-to-noise ratio did not permit interpretation) were accompanied by simultaneous TDEM soundings.

The next three NMR/TDEM stations (10–12, Fig. 6) in the northern Negev area were established in the Ramat Hovav area several kilometers to the northeast of the previous survey area. All three sounding sites were located in the immediate proximity of a large liquid waste pond. The object was to test the feasibility of the combined NMR/TDEM method in detecting groundwater and evaluating water quality.

In spite of the presence of observation wells nearby the sounding sites, no quantitative comparison of the geophysical and hydrological data was possible owing to the aquitard properties of the aquifer. The latter is represented by hard chalk with a thin separated fracture system. Groundwater is distributed within the fractures which are not continu-

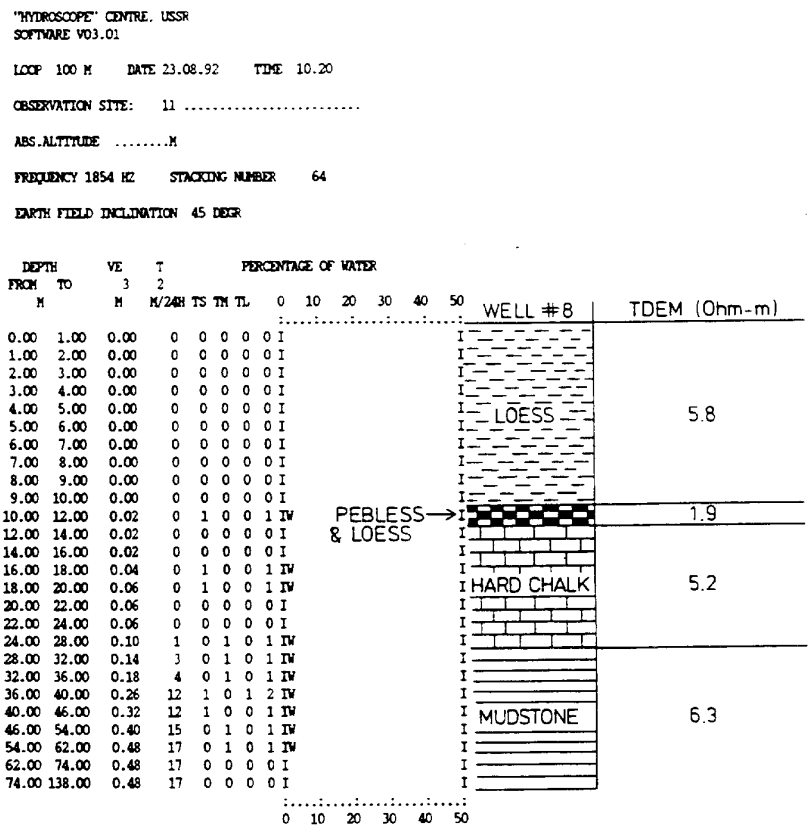

Fig. 9. Comparison of the geophysical (both NMR and TDEM) and well log data, Ramat Hovav, central Negev (Station 11, Fig. 6).

ously connected to each other. Therefore there may be significant differences in the distribution of water throughout the well, in other words the water level measured in the well may essentially differ from that within the undistorted parts of the aquifer.

The NMR histograms at all three points are quite similar. They show a small amount of water ($\sim 50\ l/m^2$ per layer) in the depth range 10–60 m. In the upper part (10–20 m), water layers are intercalated with dry layers. The lower part is represented by a continuous water layer. The pore sizes are variable and the average transmissivity is approximately the same at all three points (~ 15–$20\ m^2/24$ h).

TDEM results show a rather homogeneous distribution of the resistivity with depth. The absolute resistivity values are rather low (about 6 Ω·m) testifying to a possible percolation of the polluted water from the pond to the aquifer. As far as the upper, dry part of the section is concerned, it is represented by low-resistivity loess, which provides approximately the same resistivity as the lower hard chalk aquifer filled with mineralized water. Figure 9 shows an example of both the geophysical (NMR and TDEM) and well log data collected at NMR point 11. Both NMR and TDEM data show the anomaly at a depth of about 12 m. The anomaly is most likely explained by the infiltration of the polluted water from the adjacent Secher strain, the elevation of which coincides approximately with the top of the anomaly (Fig. 9).

The water level in the well coincides fairly well with the water layer obtained by the NMR measurements. Nevertheless, taking into account the aquitard character of the aquifer, this coincidence does not provide a quantitative evaluation of the NMR results.

The next three NMR/TDEM measurement stations are located at the Dead Sea shore (Fig. 6). This narrow strip between the mountain ridge and the Dead Sea consists of alluvial fill comprised of gravels, sand with marl and clay alternations. A number of springs emerge along the sea shore; most of them are brackish with an annual discharge of about $1 \times 10^8\ m^3$. The water table is shallow for the most part, 10–50 m. Although the hydrogeological conditions are similar all along the shore, the points are located so far from each other that it is reasonable to discuss them separately.

Station NMR-13 (Fig. 10)

Two small NMR anomalies at the upper part of the section (6–7 and 9–10 m) are most likely explained by the low signal-to-noise ratio. The low concentration and very thick NMR anomaly in the depth range of 16–46 m is confirmed neither by the borehole data nor by the TDEM results. The water level measured in the nearby well is located at a depth of 40 m. The NMR histogram shows a drastic increase in the amount of water at a depth of 46 m (from 1–2% to 6% of water concentration). The TDEM interpretation also shows a significant drop in the resistivity at a depth of about 40 m. Thus, the combined use of the NMR and TDEM measurements significantly increases the reliability of the results.

It is interesting to note that at about the same depth of 40 m, the lithological change between the upper Quaternary fill gravels and the lower dolomitic Cenomanian aquifers occurs. This suggests an explanation for the appearance of the upper water layer in the NMR histogram. It could be caused by rainwater accumulated in the unsaturated zone since the wet winter of 1991–1992. This water (or, more precisely, moisture) is not detected by the TDEM measurements owing to the low concentration and mineralization. The water in the main aquifer is highly mineralized (4100 mgl Cl) and is, therefore, reliably detected by the TDEM sounding. The only questionable point is the absolute resistivity value of 15 Ω·m obtained from the TDEM interpretation. This resistivity seems somewhat of an overestimation for the above noted water salinity.

There is another drop in TDEM resistivity

"HYDROSCOPE" CENTRE, USSR
SOFTWARE V03.01

LOOP 100 M DATE 24.08.92 TIME 08.25

OBSERVATION SITE: 13 .....

ABS.ALTITUDE .....M

FREQUENCY 1858 HZ STACKING NUMBER 144

EARTH FIELD INCLINATION 45 DEGR

DEPTH FROM M	TO M	VE 3 M/24H	T 2 TS	TM	TL	PERCENTAGE OF WATER 0 10 20 30 40 50	TDEM (Ohm-m)
0.00	1.00	0.00	0	0	0	0 I	
1.00	2.00	0.00	0	0	0	0 I	
2.00	3.00	0.00	0	0	0	0 I	
3.00	4.00	0.00	0	0	0	0 I	
4.00	5.00	0.00	0	0	0	0 I	
5.00	6.00	0.00	0	0	0	0 I	
6.00	7.00	0.02	2	1	0	1 2 IW	
7.00	8.00	0.02	2	0	0	0 0 I	
8.00	9.00	0.02	2	0	0	0 0 I	
9.00	10.00	0.04	2	2	0	0 2 IW	
10.00	12.00	0.04	2	0	0	0 0 I	105
12.00	14.00	0.04	2	0	0	0 0 I	
14.00	16.00	0.04	2	0	0	0 0 I	
16.00	18.00	0.06	6	0	0	1 1 IW	
18.00	20.00	0.08	10	0	0	1 1 IW	
20.00	22.00	0.10	14	0	0	1 1 IW	
22.00	24.00	0.12	18	0	0	1 1 IW	
24.00	28.00	0.16	26	0	0	1 1 IW	
28.00	32.00	0.20	26	1	0	0 1 IW	
32.00	36.00	0.28	28	1	1	0 2 IW	
36.00	40.00	0.36	29	1	1	0 2 IW	
40.00	46.00	0.48	29	2	0	0 2 IW	
46.00	54.00	0.96	96	1	1	4 6 IWW	15
54.00	62.00	1.28	160	0	0	4 4 IW	
62.00	74.00	1.76	256	0	0	4 4 IW	5.2
74.00	138.00	1.76	256	0	0	0 0 I	

0 10 20 30 40 50

Fig. 10. The Hydroscope histogram and TDEM resistivity/depth section, coastal area of the Dead Sea (Stations 13, Fig 6).

which coincides with the bottom of the water layer in the NMR histogram. This phenomenon is consistently observed at all points along the Dead Sea shore. The phenomenon may be explained by the intrusion of seawater into the aquifer at this depth. This intrusion causes a severe drop in the TDEM resistivity on one hand and prevents the NMR data from being correctly interpreted due to the imperfection of the forward algorithm used on the other. The forward algorithm used in the Hydroscope interpretation does not take into account the conductivity of the ground. Again, the absolute resistivity value for the seawater-bearing aquifer (5.2 Ω·m) seems essentially overestimated, but it is consistent with the above-mentioned resistivity of the brackish water. Most likely this anomalous behavior is caused by the properties of the aquifer.

According to the Hydroscope histogram, the water in the upper aquifer lies in the small and large pores and in the large pores only in the lower aquifer. This correlates quite well with the lithological log, which shows gravels with

clay intercalations for the upper and fractured dolomite for the lower aquifers.

Station NMR-14 (Fig. 11)

The upper water layer from the Hydroscope histogram (10–12 m) does not fit both the borehole and TDEM data and is most likely caused by low signal-to-noise ratio. The lower water layer (12–62 m) fits the resistivity section obtained by the TDEM interpretation fairly well. The top of the layer approximately coincides with the drop in resistivity from about 60 Ω·m to 12 Ω·m. The latter value is typical for freshwater-bearing aquifers. The water salinity measured at approximately the same depth in the nearby observation well (T-4) was only 200 mgl Cl.

The bottom of the water layer from the NMR histogram is characterized by a sharp increase in the amount of water and coincides fairly well with the lower drop in the TDEM resistivity from 12 to 1.3 Ω·m. The depth to this anomaly (~60 m) coincides with the calculated depth

"HYDROSCOPE" CENTRE, USSR
SOFTWARE V03.01

LOOP 100 M DATE 24.08.92 TIME 13.45

OBSERVATION SITE: 14 .....

ABS.ALTITUDE .....M

FREQUENCY 1876 HZ STACKING NUMBER 100

EARTH FIELD INCLINATION 45 DEGR

DEPTH FROM M	TO M	VE 3 M	T 2 M/24H	TS	TM	TL	PERCENTAGE OF WATER 0 10 20 30 40 50	TDEM (Ohm-m)
0.00	1.00	0.00	0	0	0	0	0 I	
1.00	2.00	0.00	0	0	0	0	0 I	
2.00	3.00	0.00	0	0	0	0	0 I	4.2
3.00	4.00	0.00	0	0	0	0	0 I	
4.00	5.00	0.00	0	0	0	0	0 I	
5.00	6.00	0.00	0	0	0	0	0 I	
6.00	7.00	0.00	0	0	0	0	0 I	
7.00	8.00	0.00	0	0	0	0	0 I	
8.00	9.00	0.00	0	0	0	0	0 I	
9.00	10.00	0.00	0	0	0	0	0 I	
10.00	12.00	0.08	4	3	0	1	4 IWW	56
12.00	14.00	0.08	4	0	0	0	0 I	
14.00	16.00	0.08	4	0	0	0	0 I	
16.00	18.00	0.08	4	0	0	0	0 I	
18.00	20.00	0.08	4	0	0	0	0 I	
20.00	22.00	0.08	4	0	0	0	0 I	
22.00	24.00	0.08	4	0	0	0	0 I	
24.00	28.00	0.28	14	3	1	1	5 IWWW	
28.00	32.00	0.40	38	0	0	3	3 IWW	
32.00	36.00	0.52	62	0	0	3	3 IWW	12.5
36.00	40.00	0.64	86	0	0	3	3 IWW	
40.00	46.00	0.82	122	0	0	3	3 IWW	
46.00	54.00	1.06	170	0	0	3	3 IWW	
54.00	62.00	2.74	452	0	4	17	21 IWWWWWWWWW	
62.00	74.00	2.74	452	0	0	0	0 I	1.3
74.00	138.00	2.74	452	0	0	0	0 I	

0 10 20 30 40 50

Fig. 11. The Hydroscope histogram and TDEM resistivity/depth section, coastal area of the Dead Sea (Stations 14, Fig 6).

to the fresh/sea water interface (the observation well does not penetrate the interface). Thus the explanation for the NMR anomaly is the same as in the previous case, namely extremely high conductivity of the seawater causes an erroneous result from the NMR interpretation software.

It is interesting to note that, according to the Hydroscope histogram, the water in the upper interval (24–28 m) is found mainly in the small pores, while in the lower interval (28–54 m), the water is located in the large pores. This fits fairly well with the lithology log from the T-4 well, according to which the aquifer is represented on the whole by gravels but also includes a thin clay layer in the depth range 25–30 m.

Station NMR-15 (Fig. 12)

The NMR histogram shows two main aquifers in the depth ranges 10–16 and 24–54 m, respectively. In addition, a small amount of water is shown in the upper 2 m which is probably caused by a low signal-to-noise ratio.

The TDEM resistivity section generally fits the NMR histogram although the latter demonstrates somewhat better resolution. Unfortunately, there are no boreholes in close proximity to the sounding site. Nevertheless, taking into account the experience gathered from the previous two points, located in a similar hydrogeological setup, the following hydrogeological interpretation of the combined NMR/TDEM results seems reasonable:

The aquifer is represented by gravels intercalated by impermeable clays which divide the aquifer into at least two subaquifers in the depth range under consideration. The water in the upper subaquifer (10–16 m) is brackish with a total salinity of approximately 5000 mg Cl, which is the groundwater at the brackish springs located a few meters higher than the Dead Sea level (−407 m). An aquiclude layer is located in the depth interval from 16–24 m which separates the upper and lower subaquifers. The water in the lower subaquifer is far less mineralized than that in the upper subaquifer which contains a large quantity of water, most of it in large pores with high transmissivity values. The freshwater subaquifer is about 20 m thick. At a depth of 46 m, the freshwater is replaced by a seawater intrusion. The latter information is probably the most accurate and reliable, since both geophysical (NMR and TDEM) and hydrological calculations (Geban-Hertzberg formula) lead to very similar results.

As in both the previous cases, seawater intrusion manifests itself in the Hydroscope histogram by a significant increase in the water concentration followed by the absence of water at a greater depth (screening effect).

The next NMR/TDEM station (No. 16, Fig. 13) is the only one which provided a reasonable signal-to-noise ratio in the densely populated, industrialized region of Israel (Fig. 6). The station is located at the edge of the coastal plain aquifer, overlying the main mountain aquifer, a carbonatic karstic feature of Cenomanian age. The aquifer serves as a water supply and there are many pumping wells in this region. The aquifer contains a large quantity of groundwater and has high transmissivity values. The groundwater depth usually coincides with the root of the aquifer, at about 40–50 m. There are some boreholes about 1 km from the site. The general hydrogeological knowledge of the area is quite comprehensive and this facilitates a good qualitative and even semi-quantitative control (by interpolation between numerous observation wells in the area) of the geophysical data. The NMR histogram shows two aquifers. The upper consists of a relatively small amount of water (the concentration varies between 1–3%) in small pores and the lower consists of a large amount of water (7–12%) distributed within large pores. The transmissivity of the aquifers is also essentially different, namely the lower aquifer has a much greater transmissivity (by almost two orders of magnitude) than the upper.

"HYDROSCOPE" CENTRE, USSR
SOFTWARE V03.01

LOOP 100 M DATE 24.08.92 TIME 17.00

OBSERVATION SITE: 15 .....

ABS.ALTITUDE .....M

FREQUENCY 1876 HZ STACKING NUMBER 100

EARTH FIELD INCLINATION 45 DEGR

DEPTH FROM M	TO M	VE 3 M	T 2 M/24H	TS	TM	TL		PERCENTAGE OF WATER 0 10 20 30 40 50	TDEM (Ohm-m)
0.00	1.00	0.01	0	1	0	0	1 IW	I	
1.00	2.00	0.02	0	1	0	0	1 IW	I	
2.00	3.00	0.02	0	0	0	0	0 I	I	
3.00	4.00	0.02	0	0	0	0	0 I	I	
4.00	5.00	0.02	0	0	0	0	0 I	I	7.6
5.00	6.00	0.02	0	0	0	0	0 I	I	
6.00	7.00	0.02	0	0	0	0	0 I	I	
7.00	8.00	0.02	0	0	0	0	0 I	I	
8.00	9.00	0.02	0	0	0	0	0 I	I	
9.00	10.00	0.02	0	0	0	0	0 I	I	
10.00	12.00	0.04	4	0	0	1	1 IW	I	
12.00	14.00	0.16	8	5	0	1	6 IWWW	I	3.4
14.00	16.00	0.22	17	1	0	2	3 IWW	I	
16.00	18.00	0.22	17	0	0	0	0 I	I	
18.00	20.00	0.22	17	0	0	0	0 I	I	
20.00	22.00	0.22	17	0	0	0	0 I	I	
22.00	24.00	0.22	17	0	0	0	0 I	I	
24.00	28.00	0.34	41	0	0	3	3 IWW	I	12
28.00	32.00	0.50	58	1	1	2	4 IWW	I	
32.00	36.00	0.62	75	0	1	2	3 IWW	I	
36.00	40.00	0.74	92	0	1	2	3 IWW	I	
40.00	46.00	0.92	128	0	0	3	3 IWW	I	
46.00	54.00	1.56	256	0	0	8	8 IWWWW	I	
54.00	62.00	1.56	256	0	0	0	0 I	I	1.7
62.00	74.00	1.56	256	0	0	0	0 I	I	
74.00	138.00	1.56	256	0	0	0	0 I	I	
								0 10 20 30 40 50	

Fig. 12. The Hydroscope histogram and TDEM resistivity/depth section, coastal area of the Dead Sea (Stations 15, Fig 6).

According to the general hydrogeological knowledge of the region, groundwater exists in two lithologically different aquifers. The upper, at a depth of 10–40 m, is represented by finely porous chalks and sandstones of Quaternary to Senonian age, while the lower is the regional karstic dolomite aquifer of Cenomanian age, which is highly fractured and usually supplies large quantities of water. Thus, the NMR data at this specific point provide reliable information not only about the location and amount of groundwater, but also about the properties of the aquifer (such as pore size and transmissivity).

The TDEM resistivity section correlates fairly well with the NMR data as regards the thickness and depth to the lower aquifer. In the absence of borehole data, this information permits quantitative evaluation of the NMR results. In addition, the absolute resistivity value of the low-resistivity unit suggests that the lower aquifer is filled with fresh or only slightly mineralized water, which corresponds with the real groundwater salinity of about 300 mgl Cl.

"HYDROSCOPE" CENTRE, USSR
SOFTWARE V03.01

LOOP 100 M DATE 26.08.92 TIME 07.15

OBSERVATION SITE: 16 .....

ABS.ALTITUDE .....M

FREQUENCY 1879 HZ STACKING NUMBER 121

EARTH FIELD INCLINATION 45 DEGR

DEPTH FROM M	TO M	VE 3 M	T 2 M/24H	TS	TM	TL		PERCENTAGE OF WATER 0 10 20 30 40 50	TDEM (Ohm-m)
0.00	1.00	0.00	0	0	0	0	0	I	
1.00	2.00	0.00	0	0	0	0	0	I	2.4
2.00	3.00	0.00	0	0	0	0	0	I	
3.00	4.00	0.00	0	0	0	0	0	I	
4.00	5.00	0.00	0	0	0	0	0	I	
5.00	6.00	0.00	0	0	0	0	0	I	
6.00	7.00	0.00	0	0	0	0	0	I	
7.00	8.00	0.01	0	1	0	0	1	IW	
8.00	9.00	0.01	0	0	0	0	0	I	
9.00	10.00	0.01	0	0	0	0	0	I	
10.00	12.00	0.07	2	0	3	0	3	IWW	
12.00	14.00	0.11	3	0	2	0	2	IW	240
14.00	16.00	0.11	3	0	0	0	0	I	
16.00	18.00	0.17	3	3	0	0	3	IWW	
18.00	20.00	0.21	3	2	0	0	2	IW	
20.00	22.00	0.25	4	2	0	0	2	IW	
22.00	24.00	0.27	8	0	0	1	1	IW	
24.00	28.00	0.31	8	1	0	0	1	IW	
28.00	32.00	0.39	8	2	0	0	2	IW	
32.00	36.00	0.51	9	3	0	0	3	IWW	
36.00	40.00	0.63	9	3	0	0	3	IWW	
40.00	46.00	0.63	9	0	0	0	0	I	
46.00	54.00	1.59	78	7	1	4	12	IWWWWW	8.5
54.00	62.00	2.15	190	0	0	7	7	IWWW	
62.00	74.00	2.99	358	0	0	7	7	IWWW	
74.00	138.00	2.99	358	0	0	0	0	I	148

0 10 20 30 40 50

Fig. 13. Results of the NMR/TDEM interpretation in central Israel, near the city of Lod (Station 16, Fig. 6).

As far as the upper subaquifer is concerned, it is not reflected in the TDEM resistivity section. A very thin conductive layer at the earth's surface which exists only in the TDEM resistivity section, is explained by the location of the TDEM station. The TDEM transmitter loop was located in the permanently irrigated agricultural field several tens of meters away from the NMR station.

The next NMR–TDEM site was located in the Yizre'el Valley of northern Israel, which is a closed sedimentary basin with only one outlet. Since the Neogene, a thick sequence of sediments, mostly clays, has been accumulated. Among these clays, usually at the basin frings, thin gravel horizons have been deposited. These shallow horizons are poor aquifers used for water supply and to solve drainage problems. The two first NMR stations were noisy; however, NMR measurements were carried out at the second station in spite of the relatively high signal-to-noise ratio, in single measurements up to 1:15. These measurements did not detect any water presence, although a nearby

pumping well (150 m from the site) provides some fresh water (10 m^3/h) from a gravel lens at a depth of 4.5 m. This unsuccessful result demonstrated once again the low level of Hydroscope ambient noise protection.

At the third station (No. 18, Fig. 6), the noise level was very low and successful NMR and TDEM soundings were taken. The Hydroscope histogram shows the existence of five thin, permeable horizons in the depth range 2–32 m containing small amounts of water, a total of 110 l/m^2 (Fig. 14). Unfortunately, only a general hydrogeological description of the region can be made based on data from a small number of shallow boreholes (up to 10 m) located in the region. The shallow part of the cross-section is represented by clay sediments with thin permeable horizons which contain small amounts of fresh water (400 mgl Cl). The latter is proved by the TDEM results which show the presence of two layers, the first to a depth of 3.5 m with a resistivity of 2.6 $\Omega \cdot m$, evidently the result of irrigation, and the second with a resistivity of 14 $\Omega \cdot m$ which is typical for a freshwater-bearing aquifer.

The next station (No. 19, Fig. 6) is located

"HYDROSCOPE" CENTRE, USSR
SOFTWARE V03.01

LOOP 100 M DATE 27.08.92 TIME 09.30

OBSERVATION SITE: 18 .....

ABS.ALTITUDE .....M

FREQUENCY 1891 HZ STACKING NUMBER 149

EARTH FIELD INCLINATION 45 DEGR

DEPTH FROM M	DEPTH TO M	VE 3 M	T 2 M/24H	TS	TM	TL	PERCENTAGE OF WATER 0 10 20 30 40 50	TDEM (Ohm-m)
0.00	1.00	0.00	0	0	0	0	0 I	
1.00	2.00	0.00	0	0	0	0	0 I	2.6
2.00	3.00	0.01	0	1	0	0	1 IW	
3.00	4.00	0.01	0	0	0	0	0 I	
4.00	5.00	0.03	0	1	1	0	2 IW	
5.00	6.00	0.03	0	0	0	0	0 I	
6.00	7.00	0.03	0	0	0	0	0 I	
7.00	8.00	0.03	0	0	0	0	0 I	
8.00	9.00	0.03	0	0	0	0	0 I	14
9.00	10.00	0.05	1	0	2	0	2 IW	
10.00	12.00	0.05	1	0	0	0	0 I	
12.00	14.00	0.05	1	0	0	0	0 I	
14.00	16.00	0.07	1	1	0	0	1 IW	
16.00	18.00	0.07	1	0	0	0	0 I	
18.00	20.00	0.07	1	0	0	0	0 I	
20.00	22.00	0.07	1	0	0	0	0 I	
22.00	24.00	0.07	1	0	0	0	0 I	
24.00	28.00	0.07	1	0	0	0	0 I	
28.00	32.00	0.11	1	1	0	0	1 IW	
32.00	36.00	0.11	1	0	0	0	0 I	
36.00	40.00	0.11	1	0	0	0	0 I	
40.00	46.00	0.11	1	0	0	0	0 I	
46.00	54.00	0.11	1	0	0	0	0 I	
54.00	62.00	0.11	1	0	0	0	0 I	
62.00	74.00	0.11	1	0	0	0	0 I	
74.00	138.00	0.11	1	0	0	0	0 I	

0 10 20 30 40 50

Fig. 14. The Hydroscope histogram and TDEM resistivity/depth section, Yizre'el Valley (Station 18, Fig. 6).

in the Arava desert in southern Israel. The lithology of the region consists of clastic deposits of gravel, sand, silt and clay, several hundred meters thick. The groundwater is usually confined, sometimes artesian, and mostly brackish. While in the northern Arava the borehole depths are less than 100 m and the watertable is close to the surface, in the southern Arava the aquifer is deeper and the NMR method does not have a sufficient investigation depth within its present limitations.

The sounding site is some 300 m east of the abandoned Hazeva-14 well. Both NMR and TDEM measurements show a very shallow anomaly (0–2 m) which is obviously caused by irrigation (Fig. 15). At a depth of 10–12 m a small amount of water was detected by both methods, which fits the gravel lens in the borehole. The first valuable aquifer is shown by the Hydroscope histogram at a depth of 20–22 m. This approximately fits both the resistivity drop in the TDEM results and the lithology of the sand and gravels in the well log. The absolute resistivity value of 9.5 Ω·m suggests that the water is fresh. This also fits the groundwater salinity of 400 mgl Cl obtained in the well. Both the NMR and TDEM interpretations testify to the presence of water within the depth interval of 28–54 m. This contradicts the lithological log from the well, which shows an aquiclude clay layer in the depth range 29–41 m and clayey sand at 41–47 m. Further disagreement between the geophysical and well log data occurs at a greater depth below 54 m. Both NMR and TDEM show the absence of water at this depth, while the lithological log shows a sandy aquifer. The consistent coincidence of the NMR and TDEM results suggests that this disagreement between the geophysical and lithological data could be caused by lateral lithological changes within 300 m of the site from the well location. It should be noted that the well was abandoned owing to poor discharge.

The last three interpreted NMR stations are located in the southernmost part of Israel, several kilometers north of the Eilat Bay. Both NMR and TDEM results are similar at all three points. The NMR histograms show a number of thin water interlayers distributed within the depth range 5–50 m approximately. The water is located mainly in small pores and the transmissivity of all layers is extremely low. The TDEM resistivity sections show a primarily low resistivity ($< 10\ \Omega$·m) which is caused by both groundwater salinity and low-resistivity lithology (clays). Similarly in the above points, 10–12, the hydrogeological interpretation of the TDEM results is thus rather complicated.

Let us consider as an example, the correlation between the geophysical results (both NMR and TDEM) at observation site 20 (Fig. 6) and the hydrogeological data from the nearby observation well Eilat-106. Figure 16 shows all three sets of data in the form of the appropriate depth sections. The NMR histogram shows the existence of water within thin isolated layers in the depth range 0–10 m. This generally fits the thickness of the upper sandy subaquifer, although the distribution of water within the layer as shown by the Hydroscope histogram does not seem very reliable. It is appropriate to note here that, in many cases where NMR histograms show a small amount of water within isolated layers, this is caused by a low signal-to-noise ratio rather than by the existence of water in the appropriate depth. This is especially true in the case of shallow depths, since according to the principles of NMR tomography previously described, the NMR signal decreases with depth to the water layer.

The absence of water in the depth range 10–36 m in the Hydroscope histogram coincides well with the lithological log from the Eilat-106 observation well. The latter shows an impermeable clay layer in the depth range 9–37 m. The most impressive correlation between the NMR and borehole data is demonstrated by the excellent coincidence between the location of the thin water layer at the depth range between 36–40 m in the Hydroscope histogram with the lower sandy subaquifer shown

"HYDROSCOPE" CENTRE, USSR
SOFTWARE V03.01

LOOP 100 M DATE 30.08.92 TIME 10.30

OBSERVATION SITE: 19 .....

ABS.ALTITUDE .....M

FREQUENCY 1853 HZ STACKING NUMBER 64

EARTH FIELD INCLINATION 45 DEGR

DEPTH FROM M	TO M	VE 3 M	T 2 M/24H	TS	TM	TL	PERCENTAGE OF WATER 0 10 20 30 40 50	TDEM (Ohm-m)
0.00	1.00	0.02	2	1	0	1	2 IW	3.9
1.00	2.00	0.03	2	0	1	0	1 IW	
2.00	3.00	0.03	2	0	0	0	0 I	
3.00	4.00	0.03	2	0	0	0	0 I	
4.00	5.00	0.03	2	0	0	0	0 I	
5.00	6.00	0.03	2	0	0	0	0 I	73
6.00	7.00	0.03	2	0	0	0	0 I	
7.00	8.00	0.03	2	0	0	0	0 I	
8.00	9.00	0.03	2	0	0	0	0 I	
9.00	10.00	0.03	2	0	0	0	0 I	
10.00	12.00	0.05	6	0	0	1	1 IW	
12.00	14.00	0.05	6	0	0	0	0 I	23
14.00	16.00	0.05	6	0	0	0	0 I	
16.00	18.00	0.05	6	0	0	0	0 I	
18.00	20.00	0.05	6	0	0	0	0 I	
20.00	22.00	0.21	18	0	6	2	8 IWWW	
22.00	24.00	0.21	18	0	0	0	0 I	
24.00	28.00	0.21	18	0	0	0	0 I	9.5
28.00	32.00	0.29	34	0	0	2	2 IW	
32.00	36.00	0.37	50	0	0	2	2 IW	
36.00	40.00	0.45	66	0	0	2	2 IW	
40.00	46.00	0.69	79	3	0	1	4 IWW	
46.00	54.00	0.85	97	0	1	1	2 IW	
54.00	62.00	0.85	97	0	0	0	0 I	50
62.00	74.00	0.85	97	0	0	0	0 I	
74.00	138.00	0.85	97	0	0	0	0 I	

0 10 20 30 40 50

Fig. 15. The Hydroscope histogram and TDEM resistivity/depth section, Hazeva, Arava desert (Station 19, Fig. 6).

in the well log between 37–40 m. This coincidence shows that, under favorable conditions (a relatively high concentration of water and sufficient signal-to-noise ratio) the NMR tomography possesses exceptionally high resolving powers as compared to all conventional geophysical methods. It should be noted that at a depth of 82–88 m there is a groundwater horizon in sand and gravels and a screen pipe for pumping has been installed. The Hydroscope did not detect this horizon, probably because of the poor amount of water and its deep location.

The TDEM resistivity cross-section generally fits the lithological log: low-resistivity value intervals (9–49 m and 90–115 m) corresponding to clay sediments and high-resistivity intervals corresponding to gravel and sand layers. All the NMR stations in the southern Arava detected only poor, separated groundwater horizons which, unfortunately, fits the drill findings.

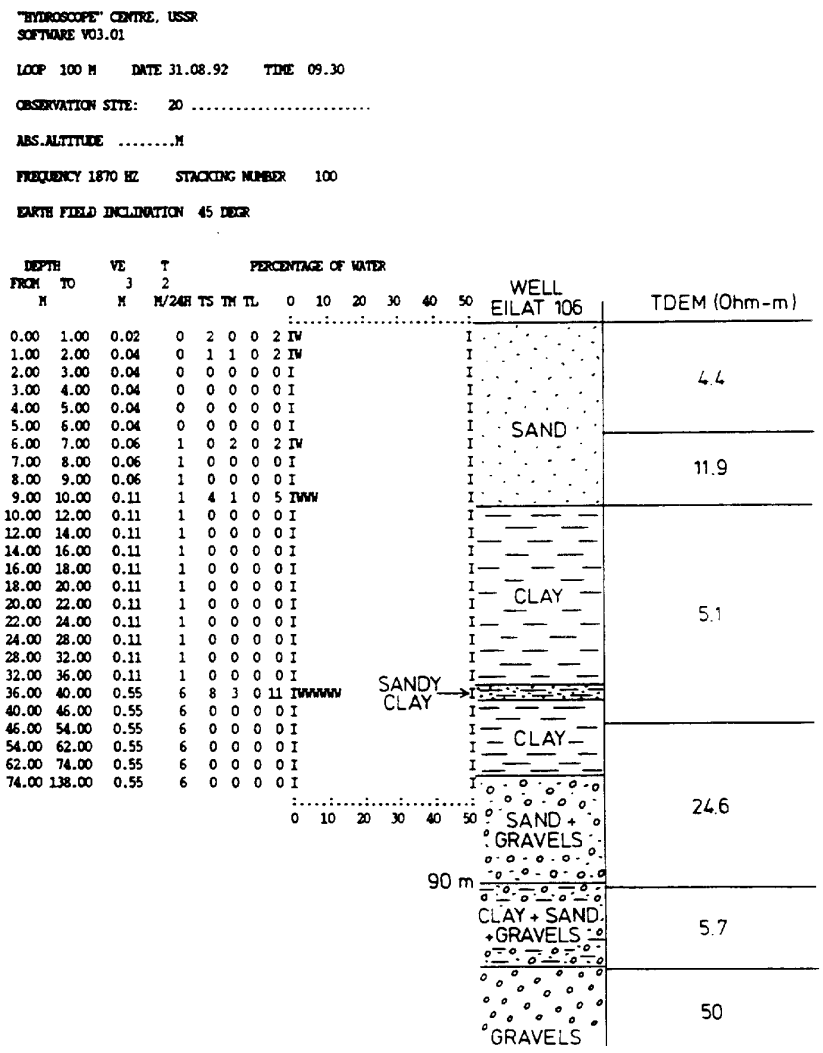

Fig. 16. Comparison of the geophysical (NMR/TDEM) and hydrogeological data, Eilat area (Station 20, Fig. 6).

Conclusions

The integration of NMR/TDEM data has proved highly effective in detecting the presence and amount of groundwater and in evaluating its salinity. In the majority of cases where NMR shows water and TDEM shows decreasing resistivity at approximately the same depth, the presence of water is confirmed by borehole data. Individual interpretations, however, did not in many cases fit the hydrogeological data available. This is particularly true as regards the TDEM interpretation. In most cases, the false anomalies obtained by the TDEM were caused by low-resistivity lithology. The reliability of NMR interpretation in detecting groundwater is much higher; nevertheless, some false anomalies, probably caused by a low signal-to-noise ratio, can be noted.

Since the causes of misinterpretation are

different for both methods, one may expect that integration will lead to more reliable results. This has been proved by the results of the feasibility study. A comparison of the individual NMR and TDEM interpretations shows that the NMR response has a higher resolving power than the TDEM in detecting different subaquifers. In turn, the TDEM method proved its higher accuracy in determining mineralized groundwater. Although in most cases the NMR also showed the presence of highly mineralized water, the water concentration was drastically over-estimated while the thickness of the saline water layer was significantly underestimated.

Thus, highly mineralized groundwater can act as a screen for the NMR method or, more precisely, for the existing NMR interpretation. This problem can apparently be solved in future versions of NMR interpretation software by using the results of the TDEM interpretation. These results, in the form of interpreted geoelectric parameters, can be used for accurate calculations of the radio frequency magnetic field at an arbitrary point within the earth. It should be noted that the current software calculates the field for an oversimplified model of the subsurface (a homogeneous insulating space).

In addition to the above-mentioned interpretation problem, the NMR method in general and the Hydroscope instrument in particular, suffer from severe hardware limitations. These are low ambient noise protection and very limited penetration depth (approximately 70 m in the feasibility study under consideration). It should be noted that both these problems are caused by the objective limitations of the NMR method, namely a much lower signal level than that used in conventional geoelectric methods and by limited skin depth (determined by a given value of the resonance frequency).

The results of this first integrated NMR/TDEM feasibility study lead us to recommend the method as the most efficient and reliable geophysical tool for groundwater detection and evaluation of its amount and quality. As regards more delicate hydrological characteristics of the aquifer, such as transmissivity and pore size, these are less reliably determined.

In addition to groundwater exploration, the NMR method has great potential in environmental studies since it is the only physical method which can directly determine not only the presence of contaminated water, but also the type of certain contaminates composed of H^+ nuclei (e.g. hydrocarbons). The application of the NMR method in environmental studies seems particularly feasible, considering its limitations such as exploration depth as mentioned above.

Acknowledgements

The authors wish to thank all participants in the field experiments: Ya'akov Lipshitz and Leonid Lanzman of the Institute of Desert Research, Avri Livne of Polgei Ha-Main and Yuri Sventsky of the Institute of Chemical Kinetics and Combustion, Russia. Our thanks also to those who helped in organizing this project: Anatoly Burshtein and Shimon Vega of the Weitzmann Institute, Rehovot, Yair Rotstein, Avi Levi, Meir Marzan and Shaul Dagmi of the Institute for Petroleum Research and Geophysics, Holon. Special thanks to Debbie Artzi for improving the style of the manuscript.

This project was carried out under the auspices of the Ministry of Science and Technology, the Hydrological Service of Israel and the Weitzmann Institute of Science.

References

Abragam, A., 1961. The Principles of Nuclear Magnetism. Oxford Univ. Press, New York, NY, 599 pp.

Emsley, J.W., Feeney, J. and Sutcliffe, L.H., 1967. High Resolution Nuclear Magnetic Resonance Spectroscopy. Pergamon, Oxford, 663 pp.

Fitterman, D.V., 1986. Transient electromagnetic soundings in the Michigan Basin for groundwater evaluation. Proc. Nat. Water Well Assoc. Conf. Surface and

Borehole Geophysical Methods, Dublin, OH, pp. 334–353.

Fitterman, D.V. and Stewart, M.T., 1986. Transient electromagnetic soundings for groundwater. Geophysics, 51: 995–1006.

Goldman, M., Arad, A., Kafri, U., Gilad, D. and Melloul, A., 1988. Detection of freshwater/seawater interface by the Time Domain Electromagnetic (TDEM) method in Israel. In: W. de Breuck and L. Walschot (Editors), Proc. 10th SWIM, Ghent. Natuurwet. Tijdschr., pp. 329–344.

Goldman, M., Gilad, D., Ronen, A. and Melloul, A., 1991. Mapping of seawater intrusion in to the coastal aquifer of Israel by the Time Domain Electromagnetic Method. Geoexploration, 28: 153–174.

Mills, T., Hoekstra, P., Blohm, M. and Evans, L., 1988. Time Domain Electromagnetic Soundings for mapping seawater intrusion in Monterey County, California. Ground Water, 26: 771–782.

Palacky, G.J., 1987. Resistivity characteristics of geologic targets. In: Mr. Nabighian (Editor), Electromagnetic Methods in Applied Geophysics Theory. SEG, Tulsa, OK, pp. 53–129.

Pusep, A.Y., Bashurova, V.S., Shokhirev, N.V. and Burshtein, A.I., 1991. Software development for the NMR tomography of subsurface water bearing horizons. USSR Acad. Sci., Novosibirsk, 89 pp. (in Russian).

Schirov, M., Legchenko, A. and Creer, G., 1991. A new direct non-invasive groundwater detection technology for Australia. Explor. Geophys., 22: 333–338.

Semenov, A.G., Pusep, A.Y. and Schirov, M.D., 1982. Hydroscope—an installation for prospecting without drilling. USSR Acad. Sci., Novosibirsk, 26 pp. (in Russian).

Semenov, A.G., Schirov, M.D., Legchenko, A.V., Burshtein, A.I. and Pusep, A.Y., 1989. Device for measuring parameters of an underground mineral deposit. GB Patent 2198540.

Varian, N.H., 1962. Ground Liquid Prospecting Method and Apparatus. US Patent 3.019.383.

Geophysical Prospecting, 1994, 42, 855–862

The potential of a noise-reducing antenna for surface NMR groundwater surveys in the earth's magnetic field[1]

D.V. Trushkin,[2] O.A. Shushakov[2, 3] and A.V. Legchenko[3]

Abstract

A method of non-invasive NMR in the earth's field has been developed and is now used for groundwater surveys to depths of investigation of 100 m or more.

A circular wire loop of diameter 100 m, laid out on the ground, is employed to excite and receive the NMR signal in the earth's field. However, in areas with high electromagnetic noise, the NMR measurements may be inaccurate.

To overcome this problem, a noise-reducing figure-of-eight-shaped antenna, consisting of two touching coils each of diameter 50 m, has been utilized.

Using this antenna, the NMR signal has been calculated for different depths of water-saturated layers with various inclinations of the geomagnetic field. The model calculations and experimental data have been compared and found to be mutually consistent. The two-coil antenna is shown to be suitable for studies at depths of up to 30–40 m, which is of practical importance for engineering geology.

Introduction

Varian (1962) proposed applying the effect of nuclear magnetic resonance (NMR) in the earth's field to non-invasive underground fluid prospecting. Semenov *et al.* (1988, 1989) showed the dependence of an NMR signal amplitude on the excition pulse intensity, and proposed using it for determining the distribution with depth of the amount of underground water. In addition, the phase of the NMR signal was thought to give an estimate of water salinity. Semenov *et al.* (1988, 1989) have developed an apparatus for making non-invasive measurements of an NMR signal in the earth's field. This has been named 'hydroscope' and it is the basis for a novel geophysical non-invasive technique used for subterranean water prospecting (Semenov, 1987).

The current Hydroscope equipment uses a circular wire loop of diameter 100 m situated on the ground to excite and receive the NMR signal. Rectangular pulses of

---

[1] Received May 1993, revision accepted May 1994.

[2] Novosibirsk State University, 2 Pirogova Street, Novosibirsk, 630090, Russia.

[3] Russian Academy of Sciences, Institute of Chemical Kinetics and Combustion, 3 Institutskaya Street, Novosibirsk 630090, Russia.

harmonically oscillating current are passed through the wire at the resonance frequency ω equal to that of proton resonance in the geomagnetic field. The excitation pulse is followed by an e.m.f. induction signal due to the Larmor precession of the water protons in the earth's magnetic field.

The relationship between relaxation time and soil type has been discussed by Semenov (1987) and Schirov, Legchenko, and Creer, (1991) and the effects of variations in the earth's field H_0 have been discussed by Trushkin, Shushakov and Legchenko (1993).

This non-invasive NMR survey technique is sensitive to atmospheric and industrial electromagnetic noise (particularly lightning discharges and magnetic storms, the noise created by power transmission lines and automobile generators).

In this paper an antenna, proposed and tested by Semenov (*) is described and investigated. It consists of two touching coils with currents flowing in opposite directions. The antenna is shaped as figure-of-eight (Fig. 1).

The noise-reducing property of the two-coil antenna utilizes the fact that when recording an NMR signal the external electromagnetic noise induces an e.m.f. in each coil. The e.m.f.s compensate each other because the coils are switched in opposite directions, whereas the NMR signals, induced by underground water, are recorded, to a first approximation, by each coil separately and are then summed.

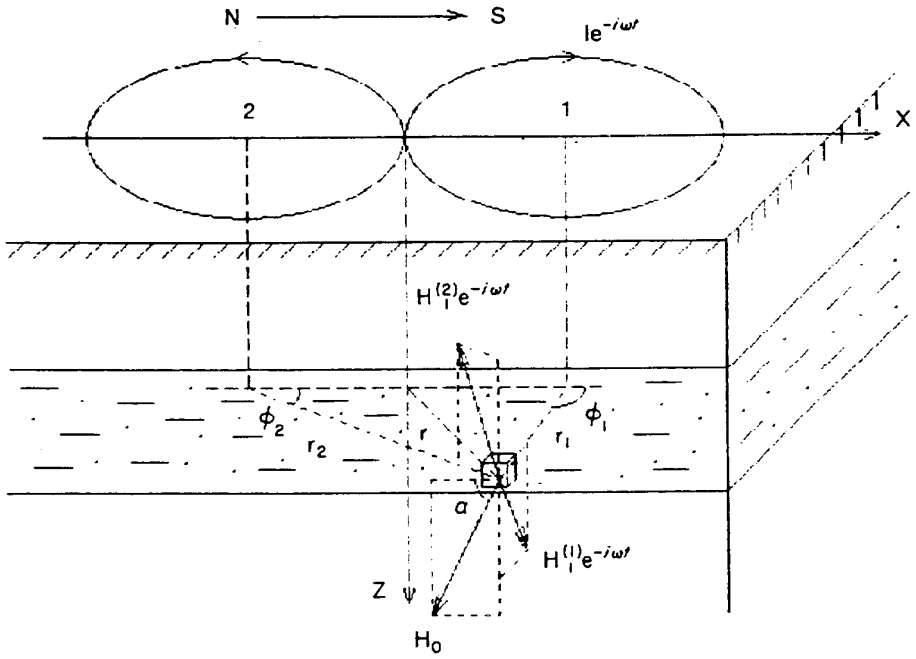

Figure 1. Vector diagram of the magnetic fields of the earth and the two-coil loop when the line, joining the coil centres is oriented from north to south.

Our aim is to study the potential advantages of the two-coil antenna, relative to the conventional loop antenna for non-invasive NMR in the earth's magnetic field, in particular, by numerical computation of the underground water NMR signals. The dependence of NMR signals on the depth of a water-saturated layer has been studied. The model calculations were compared with experimental data.

Calculation of the magnetic field for a two-coil loop

The magnetic field of a circular loop exhibits an axial symmetry about the straight line passing through the centre of the loop perpendicular to its plane. In cylindrical coordinates, the origin coincides with the centre of the loop and the z-axis coincides with the axial axis. Only two components of the magnetic field strength differ from zero, the radial (H_r) and vertical (H_z) components.

The magnetic field of the two-coil antenna has no axial symmetry. The earth's magnetic field displays a different inclination, depending on latitude, since the antenna orientation relative to the geomagnetic field must be taken into account.

The position of the antenna is considered in two directions: from north to south and from west to east.

The NMR signal is dependent on the component of the oscillating magnetic field perpendicular to the constant magnetic field (Abragam 1961), which in this case is the geomagnetic field. The component of the oscillating magnetic field of the two-coil antenna $H_{1\perp}$, perpendicular to the vector H_0 of the earth's magnetic field with an arbitrary inclination α at the given point of space r, can be expressed in terms of the Cartesian components of the oscillating magnetic field vector of the two-coil antenna H_1 as follows (see Fig. 1):

$$|H_1\perp(r)| = \{H_{1y}^2(r) + (H_{1x}(r)\sin(\alpha) + H_{1z}(r)\cos(\alpha))^2\}^{1/2}. \quad (1)$$

Under the action of a pulse of duration t_p, the equilibrium macroscopic nuclear magnetization M_0 at point r, initially oriented in the direction of the earth's magnetic field, has a vector rotation angle Θ obeying the following expression (Abragam 1961):

$$\Theta(r) = 0.5\gamma_H |H_{1\perp}(r)| t_p,$$

where γ_H is the gyromagnetic ratio of a proton.

Consider now the orientation of the line connecting the coil centres in the north to south direction. At point $r = (r, \phi, z)$ the Cartesian components of the total vector H_1, the oscillating magnetic field of the two-coil antenna, are of the form (see Fig. 1):

$$H_{1x}(r) = H_r[r_1, z]\cos(\phi_1) - H_r[r_2, z]\cos(\phi_2), \quad (3)$$

$$H_{1y}(r) = H_r[r_1, z]\sin(\phi_1) - H_r[r_2, z]\sin(\phi_2), \quad (4)$$

$$H_{1z}(r) = H_z[r_1, z] - H_z[r_2, z], \quad (5)$$

where $H_r[r_j, z]$ and $H_z[r_j, z]$ ($j = 1, 2$) are the radial and vertical components respectively of the magnetic field of the jth coil of the two-coil antenna at the point (r_j, z).

When the antenna is located so that the straight line, connecting the coil centres is oriented from west to east, $|H_{1\perp}|$ can be calculated by the same method.

The e.m.f. induced in the loop by the magnetic field of the water nuclei, is determined by integrating over the volume of the underground water-saturated layer (Semenov *et al.*, 1988):, i.e.

$$e_0(q) = (\omega/I) \int_V M_\perp(r) H_{1\perp}(r)\, dV(r), \tag{6}$$

where $q = It_p$ is the excition current pulse intensity,

$$M_\perp(r) = M_0(r) \sin \theta(r) \tag{7}$$

is the H_0-perpendicular macroscopic nuclear magnetization and $e_0(q)$ is the NMR signal measured.

Experimental site

The underground water NMR signal was measured using the geophysical NMR system 'Hydroscope' (Semenov, 1987), developed in the Institute of Chemical Kinetics and Combustion in the Siberian Branch of the Russian Academy of Sciences.

Experiments were carried out in Russia near the town of Yurga in the Kemerovo region (at borehole site #810). Figure 2 depicts the lithological log of borehole #810, used for the experiments.

The electrical resistivity at the measurement site was controlled by measuring the efficient loop self-impedance upon excitation. The resistivity was not less than 50 Ωm. According to our investigations, this magnitude of medium resistivity has practically no effect on the NMR signal and no corrections need be considered.

Results and discussion

Figure 3 depicts the dependences of the NMR signal amplitude on excitation pulse intensity (Semenov *et al.* 1988) for horizontal water-saturated layers of thickness 10 m and 100%, water content located at different depths (10–20 m, 30–40 m, 50–60 m), and geomagnetic field inclinations of 45° and 90°.

As can be seen in Fig. 3 the difference between the NMR signals for the two-coil antenna and the circular-loop antenna is less for small depths. When the geomagnetic field inclination is 45°, the NMR signal for the two-coil antenna is calculated for two orientations of the antenna relative to the earth's field. It can be seen (Fig. 3) that the influence of the antenna orientation on the NMR signal is negligible.

At depths of up to 40 m, the NMR signal, recorded by the two-coil antenna, differs by no more than 3 times from that recorded by the circular-loop antenna.

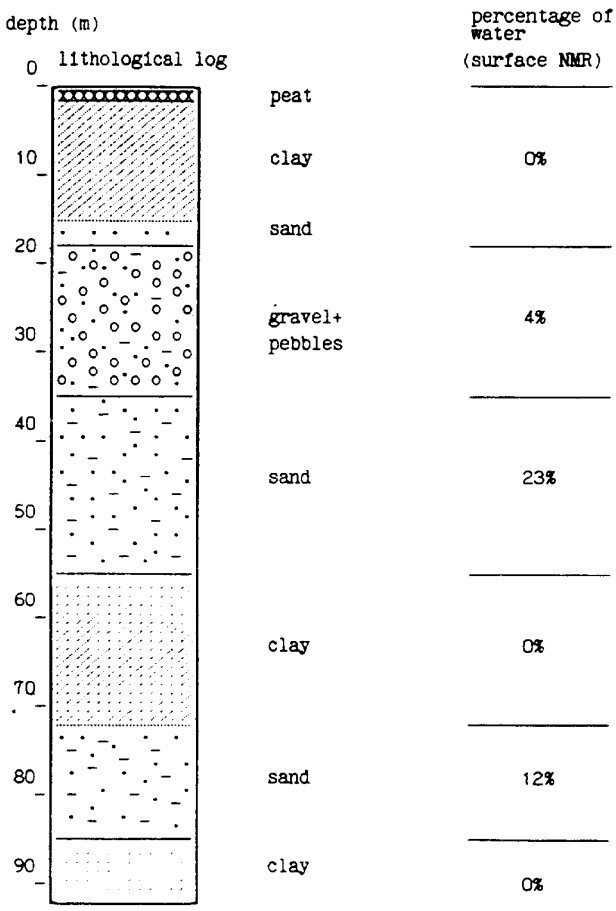

Figure 2. The lithological log of borehole #810 site.

Thus, the two-coil antenna can be used in engineering geology for investigating depths of up to 30 m.

The two-coil antenna is antisymmetric about the plane through the point of contact, perpendicular to the line joining the coil centres. The electromagnetic noise observed is frequently symmetric about a plane, e.g. electromagnetic fields created either by power transmission lines or by point sources. When the antenna is oriented so that this plane passes through the point of coil contact perpendicular to the line joining the coil centres, the noise received is much lower. Thus, the two-coil antenna can be used to decrease the effect of both homogeneous noise across the antenna and that which is symmetric about the plane perpendicular to the line joining the coil centre. Our preliminary experimental evaluation near

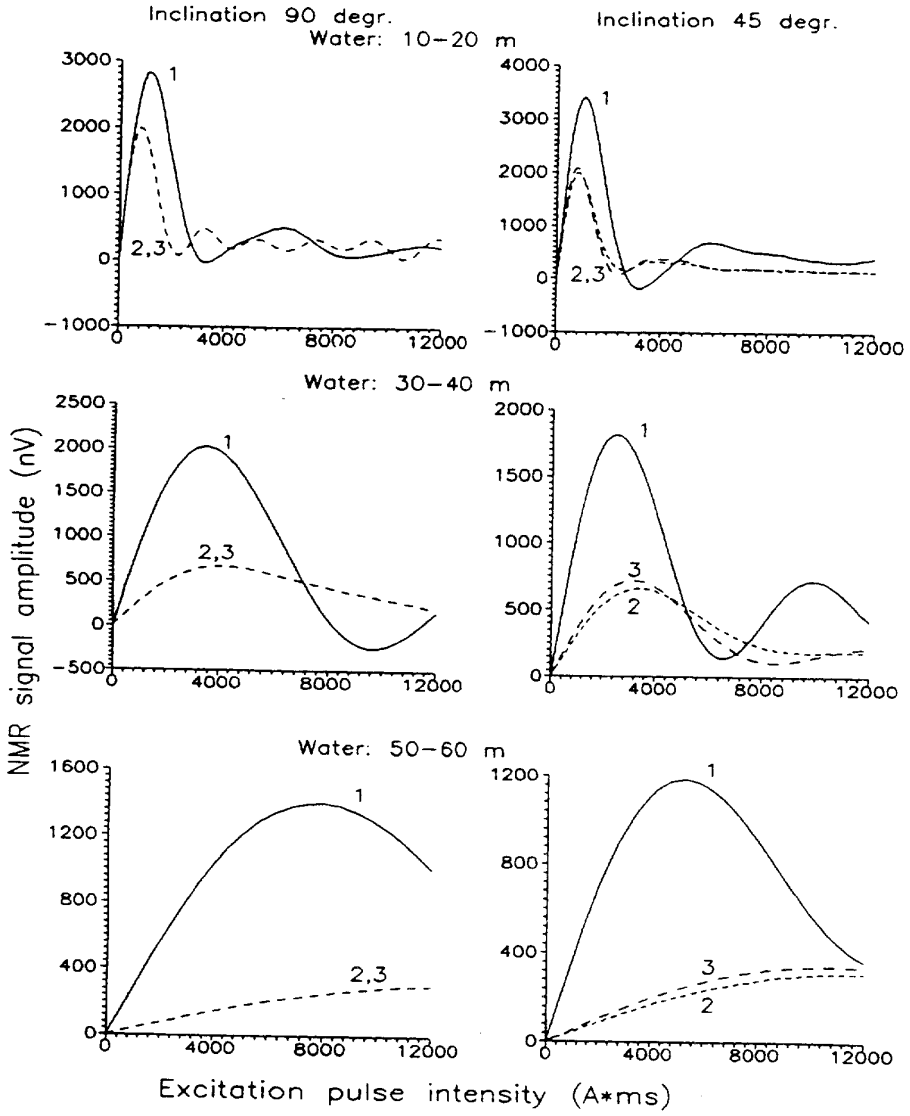

Figure 3. The dependence of the NMR signal amplitude on the excitation pulse intensity for various depths of a water-saturated layer and geomagnetic field inclinations for (1) a circular loop, and (2) a two-coil loop oriented from north to south, and (3) a two-coil loop oriented from east to west.

power transmission lines shows a significant increase (more than 10 times) of the NMR signal-to-noise ratio as the result of using the two-coil antenna.

Calculations were performed for the same parameters of a water-saturated layer. Experiments were carried out at the same location for both a circular-loop antenna of radius 50 m and a two-coil antenna, each coil having a radius of 25 m with the orientation of the line joining the coil centres being (a) from north to south and (b) from east to west.

Figure 4 gives the results of the comparison between experimental and calculated data. Based on the data obtained from a borehole, the calculations were performed for the following three water-saturated layers:

(1) from 35 to 55 m with 23% water content;
(2) from 72 to 85 m with 12% water content;
(3) from 18 to 35 m with 4% water content.

The medium resistivity effect was neglected. The geomagnetic field inclination was assumed to be 75°.

According to Fig. 4, the results obtained from the calculations are in the fair reasonable agreement with the experimental data. Note that at these depths, the two-coil antenna yields, satisfactory NMR signals recorded in field conditions.

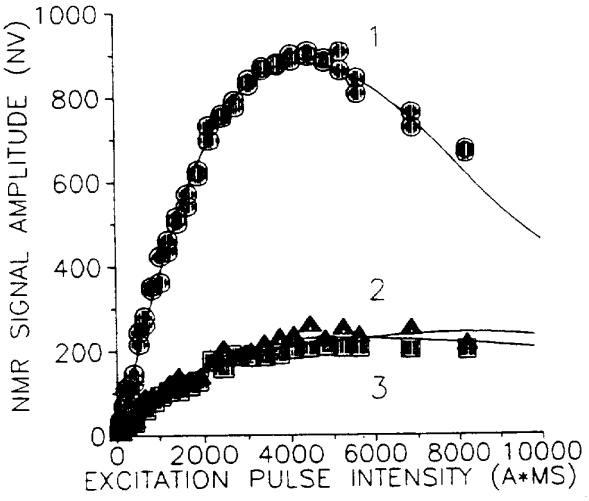

Figure 4. Comparison of experimental and calculation data for the dependence of the NMR signal amplitude on the excitation pulse intensity for borehole #810. Circles denote the experimental data for a circular loop, triangles denote those for the two-coil antenna oriented from north to south, and squares denote those for the two-coil antenna oriented from west to east. The numbers denoting the calculation curves correspond to those in Fig. 3.

Conclusions

The dependence of the NMR signal amplitude recorded by a two-coil antenna, consisting of two touching coils, on the depth of a water-saturated layer has been studied for various inclinations of the geomagnetic field and different antenna orientations. The results of the calculations on the groundwater NMR signal obtained using the two-coil antenna (as the source of the oscillating magnetic field and as the receiver of a free precession signal) are in reasonable agreement with the experimental results.

The NMR signal of the two-coil antenna is less than that of the circular-loop antenna of the same wire length at the same location. Nevertheless the two-coil antenna can be used to investigate water-saturated layers at depths of about 30 – 40 m, which is of practical importance for engineering geology.

The two-coil antenna orientation relative to the earth's magnetic field direction is shown to have a minor effect on the measurement results in the absence of noise. Therefore it is possible to reduce the noise by choosing the proper antenna orientation without it being necessary to correct for the earth's magnetic field direction.

Acknowledgements

The authors are grateful to O.K. Smolsky for his assistance in experiments and fruitful discussion, and also to P. Valla for helpful discussions of this paper.

References

Abragam A. 1961. *The Principles of Nuclear Magnetism*. Oxford University Press.

Semenov A.G. 1987. NMR Hydroscope for water prospecting. *Proceedings of a seminar on Geotomography*, pp. 66–67. Indian Geophysical Union.

Semenov A.G., Burshtein A.I., Pusep A. Yu. and Schirov M.D. 1988. *A device for measurement of underground mineral parameters* (in Russian). USSR Patent 1079063.

Semenov A.G., Schirov M.D., Legchenko A.V., Burshtein A.I. and Pusep A. Yu. 1989. *A device for measuring the parameters of an underground mineral deposit*. GB Patent 2198540.

Schirov M.D., Legchenko A.V. and Creer J.G. 1991. New direct non-invasive groundwater detection technology for Australia. *Exploration geophysics* 22, 333–338.

Trushkin D.V., Shushakov O.A. and Legchenko A.V. 1993. Modulation effects in non-drilling NMR in the earth's field. *Applied Magnetic Resonance* 5, 399–406.

Exploration Geophysics (1991) 22, 333–338

A New Direct Non-invasive Groundwater Detection Technology for Australia

M. Schirov and A. Legchenko
Institute of Chemical Kinetics and Combustion
630090 Novosibirsk USSR

G. Creer
BHP Melbourne Research Laboratories
Mulgrave, Victoria, Australia 3170

Abstract

Recently, novel geophysical technology has been developed which is capable of determining groundwater content at various depths without drilling wells. The instrument is the Hydroscope and relies on the principles of Nuclear Magnetic Resonance (NMR) tomography. Using the Hydroscope, it is now possible to undertake a regional hydrogeological survey to map the distribution of groundwater reserves both in plan and in depth with high efficiency, thus ensuring a reliable choice of the most productive areas for water supply bores. Some results of Hydroscope tests on sedimentary, water-containing rocks in South-Eastern Australia, undertaken during February and March 1990, together with several theoretical and experimental results obtained previously by the developers of the NMR water prospecting technology, are presented.

Introduction

The Hydroscope employs the selective properties of NMR (Abragam, 1961) combined with innovative techniques of signal excitation, detection and processing. The application of NMR to prospecting for underground fluids is not new (Varian, 1962) but to the best of the author's knowledge, there was no successful technical or commercial realization of the technique.

The feasibility of applying NMR to prospecting for groundwater was first demonstrated in 1978 during the field tests conducted with a prototype installation developed in the Institute of Chemical Kinetics and Combustion, Novosibirsk, (Semenov *et al.*, 1982; Semenov 1987; Semenov *et al.*, 1988). Following these trials, between 1980 and 1982 a pilot version of the Hydroscope was developed, capable not only of groundwater detection, but also the measurement of occurrence depth, thickness and free water content of aquifers. Development of the technique is continuing and latest versions of the Hydroscope can, in addition, measure the total salt content in groundwater (Semenov *et al.*, 1989).

Operational Principles

Many atomic nuclei, including $_1H^1$, possess a non-zero dipole magnetic moment. When an external field is applied to these nuclei, the energy degeneracy is removed and resonant absorption of electromagnetic radiation can occur. The resonance frequency varies with applied magnetic field and is different for different nuclei. For protons in water:

$$f_0 = 0.04258\ H_0 \qquad (1)$$

where f_0 (Hz) is the resonance frequency and H_0 (nT) the static magnetic field. The classical model of NMR is of a spinning top, where the axis of rotation (nuclear magnetic moment vector) is moved away from its equilibrium position on application of electromagnetic radiation of the resonant frequency. When the alternating resonance field is removed, the magnetic moment precesses around the static magnetic field generating a time varying field which can be detected in a pick-up coil. The precession is damped as the magnetic moments return to their equilibrium positions thus inducing a damped sine wave at the precession or resonance frequency in the detection coil.

In operation, the Hydroscope control unit drives a pulse train at the proton resonance frequency into a loop of wire on the surface of the earth. The static field is provided by the geomagnetic field of the earth. Following the excitation pulses, the loop is connected to a detection system where the NMR response of the water molecules is recorded. For the case of a thin, homogeneous aquifer, the free induction decay signal has the form

$$E = E_0 \exp(-t / T_2^*) \sin(2\pi f_0 t) \qquad (2)$$

where T_2^* is the spin-spin relaxation time of water protons, E_0 is a function of the number of precessing water molecules and instrument parameters and t is the time since removal of the excitation field.

Measurement of the above signal will detect the presence or absence of groundwater. To achieve a quantitative distribution as a function of depth, it was proposed (Semenov *et al.*, 1988) to record the signal amplitude E_0 as a function of excitation parameter $q = I\,t_p$, where I is the amplitude of the exciting current and t_p is the duration of the pulse train. Figure 1 shows the results of early experiments which proved that it was possible to extract aquifer parameters from the curve of E_0 vs q. The solid line in the figure was calculated from the integral (Semenov *et al.*, 1988):

$$E_0(q) \propto \int dv\ \eta(z) \sin(\tfrac{1}{2}\,\gamma\, q\, \beta_1(r)) \qquad (3)$$

where γ is the proton gyromagnetic ratio, $\beta_1(r)$ is the component of loop magnetic induction vector at right angles

to the static field at unit loop current at a point r(x,y,z) and η(z) is the water distribution as a function of depth z for the assumed horizontally layered structure.

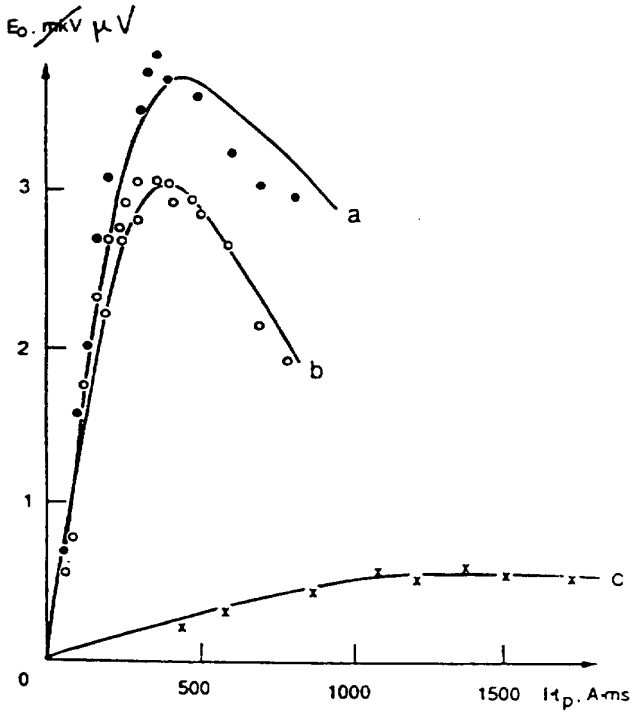

FIGURE 1
Comparison of experimental and theoretical $E_0(q)$ for various aquifers. Curve a — 25.5 m aquifer at 5.5 m depth, water content 12%; curve b — 14.5 m aquifer at 5.5 m depth, water content 18%; curve c — 4 m aquifer at 24 m depth, water content 17%. After Semenov *et al.*, 1988.

For a thin isolated layer of large lateral extent, $E_0(q)$ has an oscillatory decay (Curve a, Figure 2) with a pronounced first maximum which varies directly with the water volume in the aquifer. As the depth to the aquifer increases, the maximum moves to higher values of q. In practice the maximum available q is limited by the performance of the pulse train generator and it is not possible to measure the complete dependence of $E_0(q)$ for the deeper layers. Provided the first maximum of the curve is recorded (Curve b, Figure 2), the aquifer parameters can be satisfactorily estimated from equation (2). Where only the initial part of the curve is recorded (Curve c, Figure 2), aquifer parameters can only be estimated. The depth resolution of the technique decreases with depth due to this variation of the curve $E_0(q)$ vs q with aquifer depth coupled with practical power limitations.

For several aquifers at various depths the resulting $E_0(q)$ is obtained by summing the contributions from the elementary layers i:

$$E_0(q) = \sum_i E_{0i}(q) \qquad (4)$$

Experimental curves of $E_0(q)$ obtained at various sites in the USSR (Figure 3) demonstrate that the shape of the curve depends on both the aquifer depth and water content.

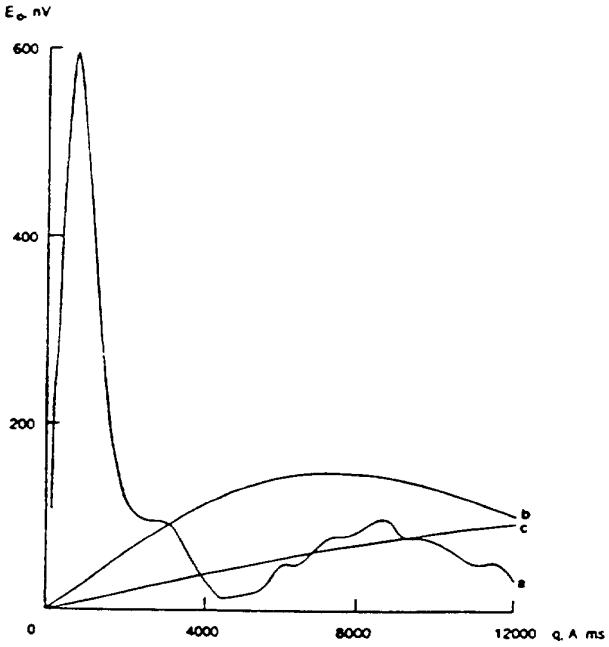

FIGURE 2
Behaviour of $E_0(q)$ as a function of aquifer depth up to q_{max} =12,000 A ms. a — shallow aquifer, b — mid depth aquifer, c — aquifer at depth equal to loop diameter.

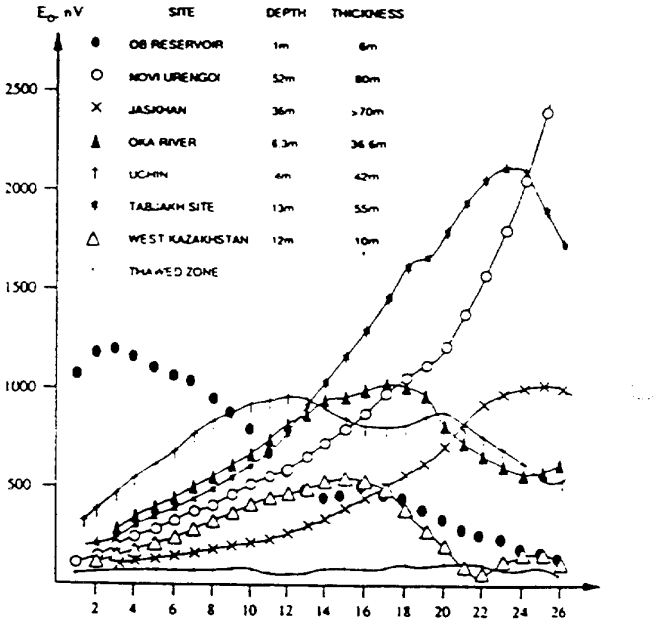

FIGURE 3
Experimental curves obtained in various hydrogeological conditions in the USSR showing variation in response due to various hydrogeological conditions.

The NMR signal, equation (1), decays with the time constant T_2^* only when the water containing pores of the strata are homogeneous, whereas in nature, the distribution of pore sizes gives an NMR signal which is a sum of exponentials over the range of pore sizes. As the Hydroscope receiving circuit has a recovery time of 30-40 ms, signals with a

relaxation time of less than about 15 ms are not recorded. Water bound to the surface of the pores has short relaxation times and thus only free or gravitational water which has longer relaxation times is detected by the unit. A curve of $T_2^*(q)$ is recorded, which, in a homogeneous magnetic field, is a function of the pore sizes, both within the beds and between the beds at various depths. Numerous field tests have led to approximate correlations between relaxation time and strata descriptions, as shown in Table 1.

TABLE 1.
Approximate correlations between observed relaxation time and type of water containing strata.

Relaxation time (ms)	Water containing strata
< 30	sandy clays
30 - 60	clayey sands, very fine sands
60 - 120	fine sands
120 - 180	medium sands
180 - 300	coarse and gravelly sands
300 - 600	gravel deposits
600 - 1500	surface water bodies

The interpretation software utilized in the technology is based on a mathematical model which includes some assumptions in order that the measurement of the subsurface free water by the Hydroscope is independent of additional geological or geophysical information. Mathematical modelling has shown the accuracy of the detection of free water strata boundaries to be plus or minus one level provided that the actual subsurface system and the mathematical model are sufficiently similar and the signal is at least twenty times the noise level. The equipment used in the Australian trials consisted of the control unit, a wire loop and four 12 V car batteries. The wire loop was laid out in a circle, typically 100 m in diameter, preferably from a reel fixed to a vehicle, and connected to the control unit. The measurement process, which consists of alternating transmission and acquisition cycles, was under the control of inbuilt software. Measurement times were between 40 and 150 minutes, dependent on noise environment and the volume of underground free water. An external computer was used to generate the depth distribution of free water concentration from the NMR signals.

Results

The output of the Hydroscope is a histogram and tabulated values of free water content as a function of depth. In a typical output, Figure 4, the left hand column, headed V (CUB.M.) shows the cumulative amount of free water, detected in a column of base area one square meter to the selected depth which is given in the adjacent column. The histogram of percentage water also gives a numerical value for the free water content of each modelled layer. For the Australian trials,

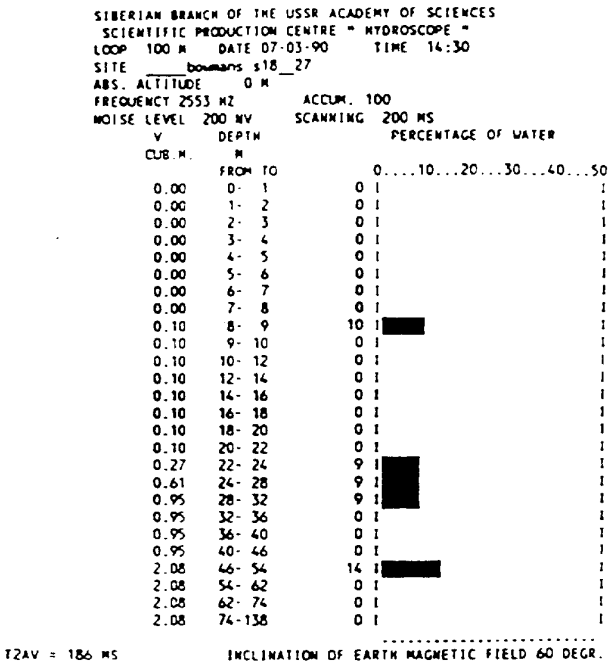

FIGURE 4
Hydroscope log, Bowmans, South Australia.

the altitude of each test site was not measured. The measured value of the average relaxation time, T_2^*, from which an average pore size can be inferred, is also given.

A survey over the frozen Ob reservoir, the objective of which was to confirm the accuracy of the Hydroscope with respect to depth indication and water content, was performed. The results, Figure 5, show satisfactory agreement in both aspects.

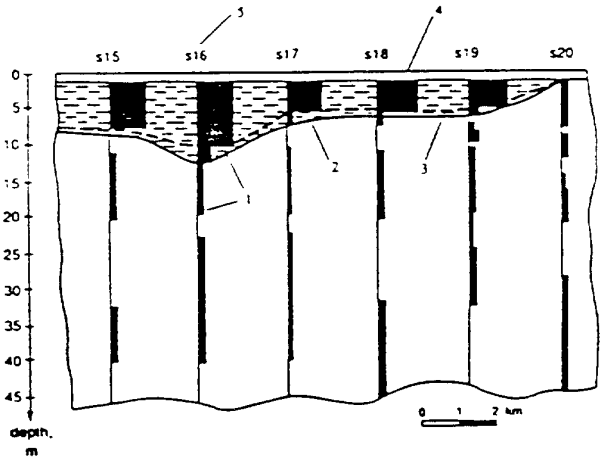

FIGURE 5
Hydroscope profile mapping of the Ob reservoir, USSR, 1986, showing good agreement between the Hydroscope logs and the control data.
1 — Histogram of water content vs depth.
2 — River bed profile from depth measurement.
3 — Hydroscope river bed profile.
4 — Ice, 1 to 1.2 m thickness.
5 — Measurement site number.

In Kazakhstan, an arid area of 100 km² was surveyed with one Hydroscope in three weeks. As a result of this survey, a narrow productive freshwater zone was detected, Figure 6. In addition to the most prospective drilling sites, hydrogeological parameters, including water conductivity, were predicted. Subsequent drilling and water production over the past four years have fully substantiated the Hydroscope results.

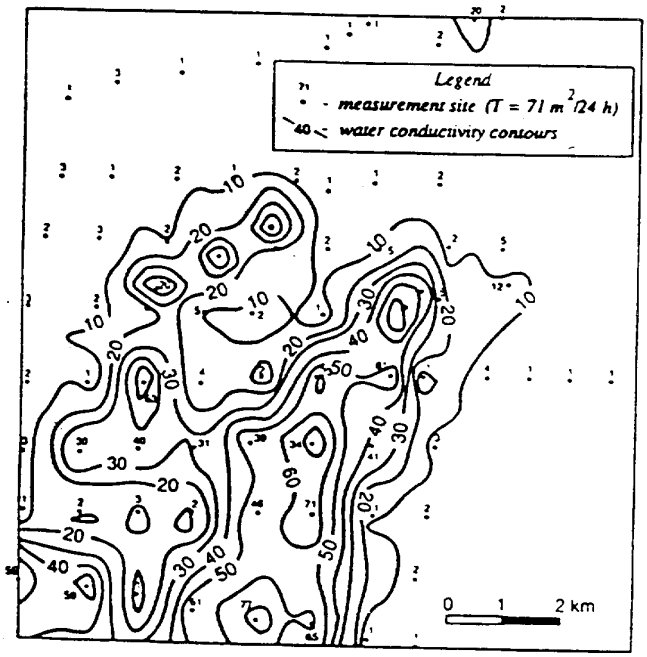

FIGURE 6
Results of a water exploration project, West Kazakhstan, USSR, 1985. Water conductivity in a prospective aquifer inferred from an Hydroscope survey of a 100 km² area.

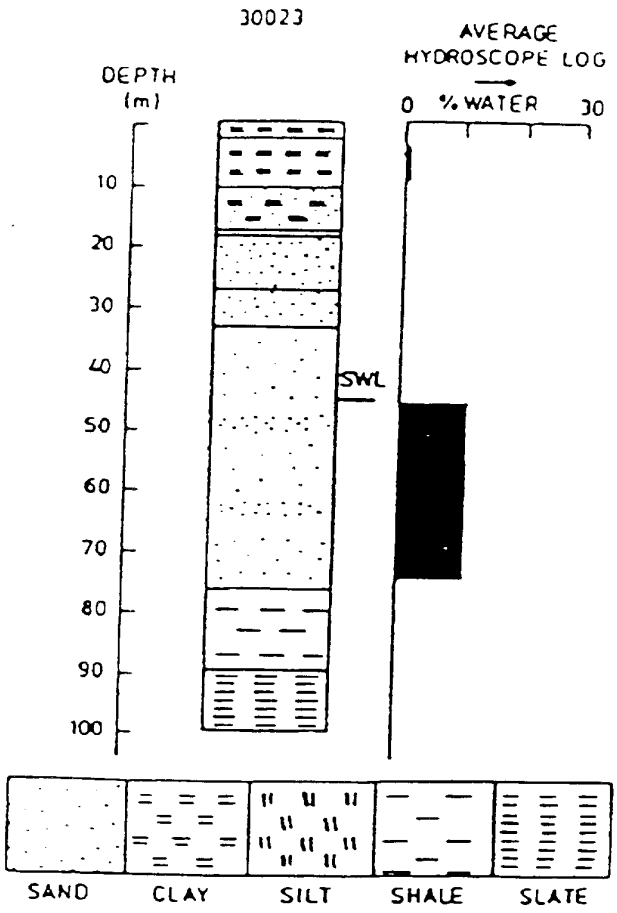

FIGURE 7
Hydroscope and strata logs, Matakana, NSW, showing good correlation between the two techniques.

These two examples show the major application of Hydroscope technology, ie the direct, non-invasive quantitative mapping of groundwater distribution along a traverse or over a grid of points. From this data, maps of both water concentration and permeability distributions can be generated.

During the trials in Australia, neither profile measurement nor regional mapping was performed. However, the possibility of these types of measurement is evident as the applicability of the technology to aquifer detection at individual points was demonstrated. For example, Figure 7 shows the arithmetic average of duplicate logs recorded at Matakana, some 95 km north-west of West Wyalong, NSW. Also shown in Figure 7 is the strata log from the adjacent borehole and the measured SWL which show good correlation with the Hydroscope log.

The Hydroscope log taken at Bowmans, 90 km north of Adelaide, SA, is shown as Figure 4. The aquifers detected with Hydroscope are in accordance with the structures found in neighbouring bores although the aquifer detected at 22-32 m probably consists of two discrete aquifers, not resolved by the Hydroscope.

In contrast with the two above tests in sedimentary basins, a trial at Carpenter Rocks, some 38 km west of Mt. Gambier, SA, was run to demonstrate that the Hydroscope would function in a karstic sandstone-limestone environment, Figure 8. The SWL in two bores measured and interpolated to 10 m at the test site, is in rough agreement with the depth to the major aquifer detected by the Hydroscope of 7 m.

In the course of the Australian trials, a total of 41 measurements were undertaken, including 17 duplicate runs at 15 field trial sites located in Victoria, New South Wales and South Australia. The main limitation of the application of the Hydroscope technology is industrial noise generated, for example, by overhead power lines. For this reason, the positions of some trial sites were re-located.

In the cases where there was no free water below 74 m, duplicate measurements showed that the uncertainty of the measurement of free water volume to a depth of 62 m, was less than 15% of the volume of free water measured. The accuracy with which the aquifer boundaries were detected depended generally on the noise environment and the coincidence of the physical system with the mathematical model. For this reason, the aquifer boundaries could be detected less reliably. Over the range of soil conductivities

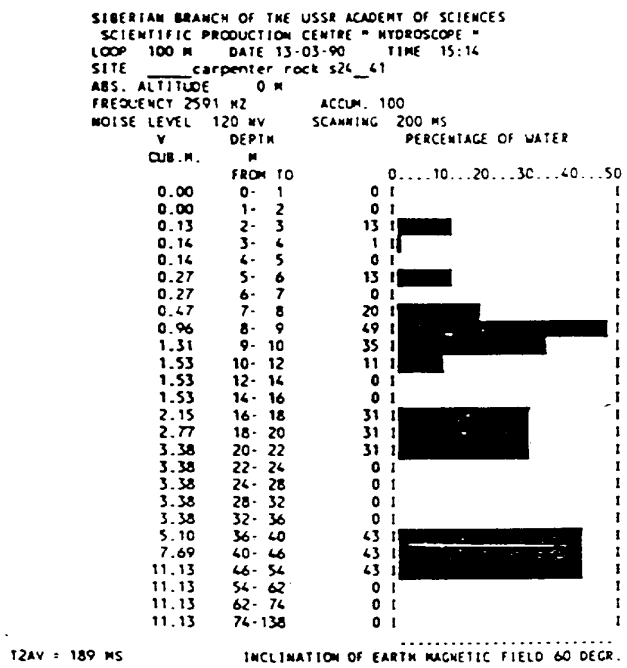

FIGURE 8
Hydroscope log generated in a karstic environment, Carpenter Rocks, SA.

encountered, the conductivity of underground layers was not a limiting factor, but increased the errors of the measurements in some cases.

Conclusions

The application of the selective properties of nuclear magnetic resonance to the non-invasive detection of subsurface water has been demonstrated. By operating the Hydroscope in a regional mapping or traverse mode, aquifer depth and water content maps can be generated. Although the complete results of the first Australian trials of the Hydroscope have not been detailed here, the examples given indicate that the Hydroscope technology is applicable to Australian conditions. At all measurement sites, the Hydroscope was used to reliably measure the volume of underground free water, and, less precisely, the depth and porosity of the free water containing strata.

Acknowledgements

The authors wish to acknowledge the pioneering work of, and stimulating discussions with, Prof. A. G. Semenov. The assistance of J. Odins, Department of Water Resources, NSW, and D. Armstrong, Geological Survey of South Australia, in the organization of the tests reported here is gratefully acknowledged.

References

Abragam, A., (1961). 'The principles of Nuclear Magnetism'. Oxford University Press, New York, 424–479.

Semenov, A. G., (1987). 'NMR Hydroscope for water prospecting'. *Proc. Seminar on Geotomography*, 66–67, Indian Geophysical Union, Hyderabad.

Semenov, A. G., Burshtein, A. I., Pusep, A. Ju., and Schirov, M. D., (1988). (in Russian) 'A device for measurement of underground mineral parameters'. USSR Patent 1079063.

Semenov, A. G., Pusep, A. Ju., and Schirov, M. D., (1982). (in Russian) 'Hydroscope — an installation for prospecting without drilling'. *USSR Academy of Sciences*, Novosibirsk, USSR.

Semenov, A. G., Schirov, M. D., Legchenko, A. V., Burshtein, A. I., and Pusep, A. Ju., (1989). 'Device for measuring parameters of an underground mineral deposit'. GB patent 2198540.

Varian, R. H., (1962). 'Ground Liquid Prospecting Method and Apparatus'. US Patent 3,019,383.

BRGM
Service Reprographie
Impression et façonnage

Spies, B.R., 1989. Depth of investigation in electromagnetic sounding methods. Geophysics 54, 872–888.
Turberg, P., Muller, I., Flury, F., 1994. Hydrogeological investigations of porous environments by radiomagnetotelluric-resistivity. J. Appl. Geophys. 31, 133–143.
Zacher, G., Tezkan, B., Neubauer, F.M., Hordt, A., Muller, I., 1996. Radiomagnetotellurics: a powerful tool for waste-site exploration. Eur. J. Environ. Eng. Geophys. 1, 139–159.

ELSEVIER

Journal of Applied Geophysics 39 (1998) 77–83

JOURNAL OF APPLIED GEOPHYSICS

Processing of surface proton magnetic resonance signals using non-linear fitting

Anatoly Legchenko [a,*], Pierre Valla [b]

[a] *BRGM, Direction de la Recherche, BP 6009, 45060 Orléans Cedex, France*
[b] *IRIS Instruments, BP 6007, 45060 Orléans Cedex, France*

Received 28 May 1997; accepted 20 February 1998

Abstract

When performing proton magnetic resonance (PMR) soundings, the observed signal is the relaxation electromagnetic field from subsurface water molecules which have been energised by an electromagnetic pulse at the Larmor frequency. Using currently available instruments, this signal is detected through a synchronous detection analyser. The four basic unknowns then to be recovered from a given time record are the amplitude, the decay time constant and the phase of the relaxation decay, the frequency shift between the energising frequency, and the true Larmor frequency at the site. This is best performed using a global non-linear least square parameter fitting scheme in order to reduce possible bias from noise.

Keywords: magnetic resonance; signal processing; Larmor frequency; decay time

1. Introduction

The proton magnetic resonance sounding method is a geophysical method (Semenov et al., 1988) which aims at determining hydrogeological parameters—such as water content and mean pore size—from magnetic resonance measurements (Semenov, 1987; Lieblich et al., 1994; Gev et al., 1996; Legchenko et al., 1996). A loop laid on the ground is used both as a transmitting antenna and as a receiving one (Fig. 1).

A pulse of an oscillating current with a quite high intensity (up to a few hundred amperes) is generated in the loop to create an electromagnetic field for energising the spin of water molecule protons: the oscillating frequency of the pulse must be equal or close to the Larmor frequency for these protons in the local Earth static magnetic field. Once the energising field is terminated, the protons induce a relaxation electromagnetic field at the Larmor frequency. This relaxation field generates an electromotive force in the loop which is measured by the PMR instrument. However, due to the weakness of the measured signal (from 10–1000 nV), a well-designed signal processing scheme must be

* Corresponding author.

PII S0926-9851(98)00011-1

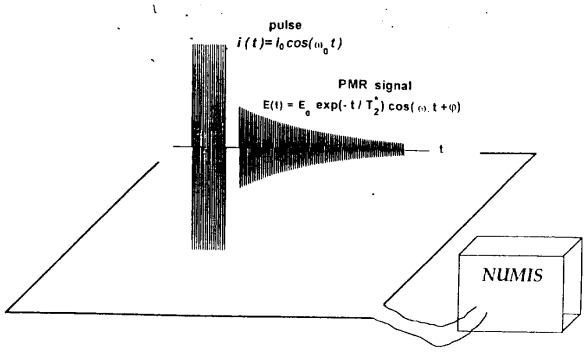

Fig. 1. Sketch of the PMR sounding layout.

used to determine the relevant parameters as accurately as possible.

2. The output from the synchronous detection analyser

The PMR signal (time record) is expected to be an oscillating decay (Legchenko, 1996) with a possible non-zero phase relative to the energising pulse:

$$E(t) = E_0 \cdot \cos(2\pi \cdot f \cdot t + \varphi) \cdot \exp[-t/T_2^*] + N(t)$$

where E_0 is the initial signal amplitude, T_2^* the decay time constant, φ the phase of the relaxation signal, $N(t)$ is the noise (both natural magnetotelluric- and man-made), and where the Larmor frequency f may differ slightly from the energising frequency f_0:

$f = f_0 + \delta f$.

The best known technique for measuring such a signal amidst strong noise is the synchronous detection (Fig. 2), whereby the signal is first multiplied by a pure harmonic wave at the known frequency f_0 and then low-pass filtered (Farrar and Becker, 1971).

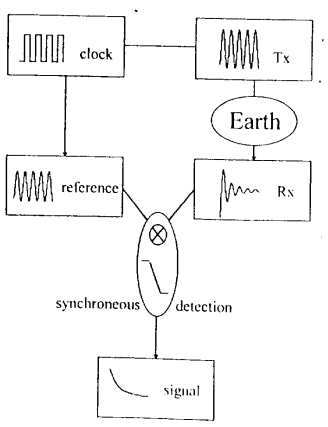

Fig. 2. Diagram of the synchronous detection for a magnetic resonance signal.

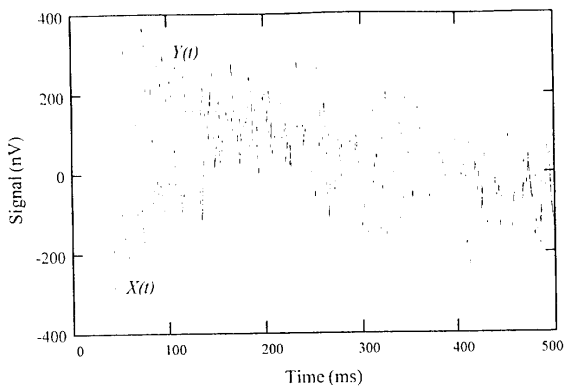

Fig. 3. Example of the signals (in phase and out of phase) recorded through the synchronous detection analyser.

In this way, two derived signals are obtained, one in phase and one out of phase:

$$X(t) = E_0 \cdot \cos(2\pi \cdot \delta f + \varphi) \cdot \exp[-t/T_2^*] + N_X(t)$$

$$Y(t) = E_0 \cdot \sin(2\pi \cdot \delta f + \varphi) \cdot \exp[-t/T_2^*] + N_Y(t)$$

where $N_X(t)$ and $N_Y(t)$ are the output noises through the synchronous detection analyser.

This technique offers two main advantages (Max, 1981):

- first it acts as a pass-band filter (for a base frequency of a few kilohertz it filters out all but the very high harmonic multiples of the power line 50 or 60 Hz noise);
- second, it allows a much slower rate of analogue to digital conversion.

An example of such signals is given in Fig. 3, as obtained in the field with the NUMIS system from IRIS-Instruments; some quite significant noise can be observed. A typical noise record is given in Fig. 4 together with its Fourier transform amplitude. It should be noted that the spacing between two spikes in the Fourier transform of the noise is 100 Hz which corresponds to the spacing between two contiguous odd harmonics of the 50-Hz power line frequency. Since the reference frequency for this recording was 2004.8 Hz, the first spike seen at 46.3 Hz corresponds to 2004.8 + 46.3 = 2051.0 Hz, that is the 41st harmonic of the power line frequency.

The aim of the post-detection signal processing is to estimate the four parameters E_0, T_2^*, φ and δf.

3. A simple but biased estimator

A simple and apparently obvious estimator scheme to obtain E_0 and T_2^* is to work with the logarithm of the combined amplitude of the time records:

$$L(t) = \log(|X(t) + i \cdot Y(t)|) = \log\left(\sqrt{X(t)^2 + Y(t)^2}\right) = \log(E_0) - \frac{t}{T_2^*} + N_t(t)$$

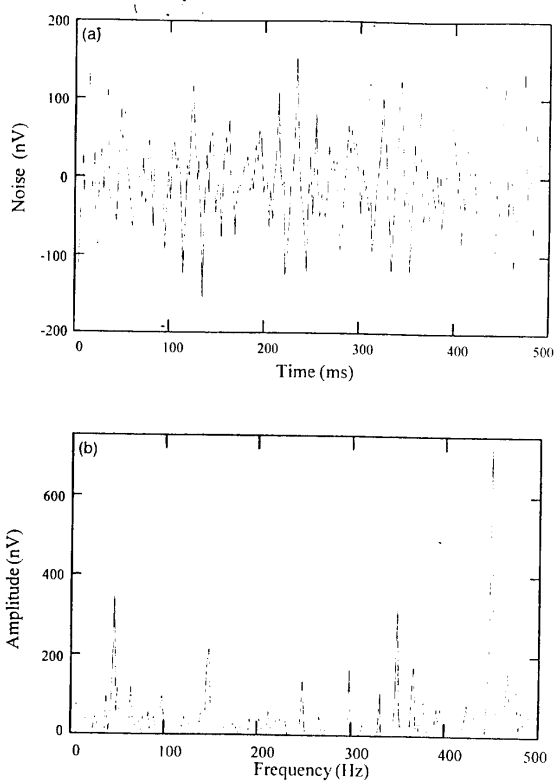

Fig. 4. Example of a noise record (top) and its Fourier analysis (bottom) as seen at the output of the synchronous detection analysis.

and to perform a linear regression fit (Fig. 5). Because of the nature of the amplitude computation, the noises $N_x(t)$ and $N_y(t)$ induce a noise $N_t(t)$ which shifts upwards the average value of $L(t)$ for small signal amplitude. Hence, the effect of noise is to bias $L(t)$ towards higher values, especially at late time when the signal amplitude become close or even lower than the noise amplitude: this leads to an overestimation of T_2^*, and to an underestimation of E_0.

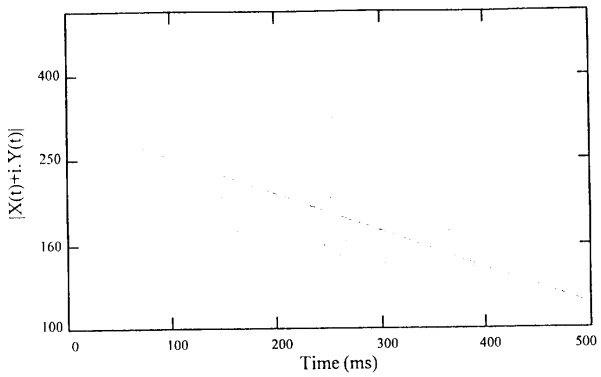

Fig. 5. Linear regression fitting of the amplitude (log scale) of the signal to get the amplitude (intercept) and the decay time constant (inverse of slope).

Similarly, if one performs a linear regression on the argument of the complex signal (Fig. 6):

$$A(t) = \arg(X(t) + i \cdot Y(t)) = 2\pi \cdot \delta f \cdot t + \varphi + N_A(t)$$

both δf and φ will be underestimated in absolute values because the effect of noise on low signal is to generate a random phase whose mean value will tend to zero (for phase values taken between $-\pi$ and $+\pi$).

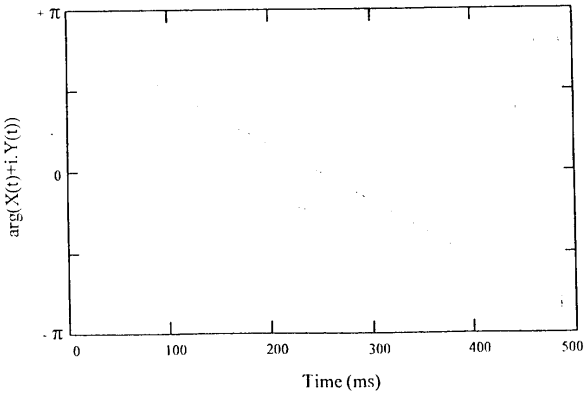

Fig. 6. Linear regression fitting of the argument of the signal to get the phase (intercept) and the frequency shift (slope).

4. The least square curve fitting estimator

In order to avoid such bias, a curve fitting non-linear regression scheme based on least square minimisation must be used:

$$\text{Minimize}\left[\sum_k \left(X(t_k) - X_c(t_k)\right)^2 + \sum_k \left(Y(t_k) - Y_c(t_k)\right)^2\right]$$

where:

$$X_c(t) = E_0 \cdot \cos(2\pi \cdot \delta f \cdot t + \varphi) \cdot \exp[-t/T_2^*]$$

$$Y_c(t) = E_0 \cdot \sin(2\pi \cdot \delta f \cdot t + \varphi) \cdot \exp[-t/T_2^*].$$

The starting guess might be derived from the above presented schemes, however biased they are. A comparison of the results obtained with the biased (linear regression) and unbiased (non-linear least square fit) estimators is presented in Fig. 7 and Table 1. Visual inspection clearly points out that the 'expected' fit is that obtained with the unbiased estimator; this is also confirmed by the residual mean square error listed in Table 1.

Table 1
Comparison of the estimated value of the four parameters (amplitude, decay time, phase and frequency shift) using the biased and unbiased estimators

	Linear regression	Non-linear least square fit
E_0	310 nV	350 nV
T_2^*	502 ms	425 ms
φ	152°	157°
δf	−1.7 Hz	−1.8 Hz
rms	55 nV	53 nV

5. A synthetic example

In order to verify the above results, the same computations have been performed on a synthetic example obtained by adding the recorded noise shown above to a theoretical signal. The results are listed in Table 2. They corroborate the observations made from the field example.

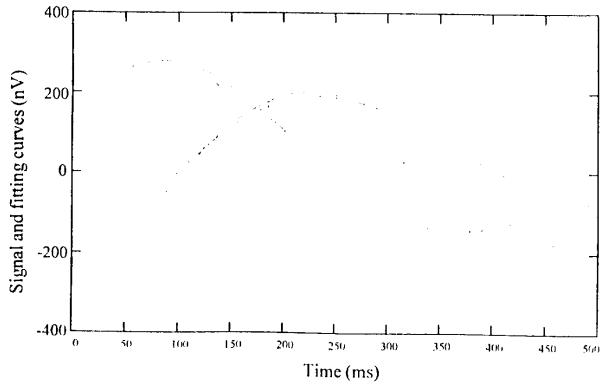

Fig. 7. Comparison of the recorded signals (same as Fig. 3) with the linear regression fit (dash line) and the non-linear least square fit (solid line).

Table 2
Comparison of the estimated value of the four parameters for a synthetic example using the biased and unbiased estimators

	True value	Linear regression	Non-linear least square fit
E_0	350 nV	307 nV	348 nV
T_2^*	400 ms	489 ms	399 ms
φ	160°	157°	159°
δf	−1.5 Hz	−1.47 Hz	−1.49 Hz
rms		54 nV	53 nV

6. Conclusion

The discussion of the parameter estimation from PMR sounding time records and the example shown illustrate the need for a careful choice of the proper estimators to avoid bias. The correct choice is the one based on non-linear least squares curve fitting from the raw time records obtained as the outputs of the synchronous detection analyser.

Acknowledgements

The above described curve fitting scheme was originally put forward by the late Professor A.G. Semenov to whom the first author is respectfully indebted.

References

Farrar, T.C., Becker, E.D., 1971. Pulse and Fourier transform NMR, Academic Press, New York.

Gev, I., Goldman, M., Rabinovich, B., Rabinovich, M., Issar, A., 1996. Detection of the level in fractured phreatic aquifers using nuclear magnetic resonance (NMR) geophysical measurements. J. Appl. Geophys. 34, 277–282.

Legchenko, A.V., 1996. A practical accuracy of the surface NMR measurements. Extended Abstr. EAGE 58th Conf. Tech. Exhibition, Vol. 1, paper M025, 3–7 June 1996, Amsterdam.

Legchenko, A., Beauce, A., Guillen, A., Valla, P., Bernard, J., 1996. Capability of the NMR applied to aquifers investigation from the surface. Proc. EEGS 2nd Meeting, 2–5 September 1996, Nantes, France, pp. 70–73.

Lieblich, D.A., Legchenko, A., Haeni, F.P., Portselan, A., 1994. Surface nuclear magnetic resonance experiments to detect subsurface water at Haddam Meadows (CT). Proceedings of the Symposium on the Application of Geophysics to Engineering and Environmental Problems, Vol. 2, Boston, MA, USA, pp. 717–736.

Max, J., 1981. Méthodes et Techniques de Traitement du Signal et Applications aux Mesures Physiques, tome II, troisième édition, Masson.

Semenov, A.G., 1987. NMR hydroscope for water prospecting. Proceedings of the Seminar on Geotomography, Indian Geophysical Union, Hyderabad, pp. 66–67.

Semenov, A.G., Burshtein, A.I., Pusep, A.Y., Shirov, M.D., 1988. A device for measurement of underground mineral parameters, USSR Patent 1079063, in Russian.

TECNICAS DE
INVESTIGACION
HIDROGEOLOGICA,
S.A.

EL SISTEMA DE BÚSQUEDA, RECONOCIMIENTO, Y VALORACIÓN DE AGUAS SUBTERRÁNEAS

HIDROSCOPE

ANÁLISIS FÍSICO

TECNICAS DE INVESTIGACION HIDROGEOLOGICA S.A.

Muchos nucléidos poseen un momento magnético dipolar no-cero

Emisión de un pulso de corriente alterna con desarrollo cuadrado. La frecuencia de la corriente portadora es igual a la frecuencia Larmor (ω_0)=λH_0, en el campo geomagnético

Para los protones f_0=0,04258 H_0

La componente h(r,ρ(r) del campo magnético transmitido causa la magnetización nuclear de los protones

Desplazamiento en el campo geomagnético, del eje de giro (vector momento magnético nuclear M0(r)) desde la posición de equilibrio a un ángulo $\gamma=(1/2)\lambda h(r,\rho(r))q$ (1)

El vector M_0 rota en el campo geomagnético con frecuencia Larmor creando oscilación del campo magnético

Dado que λ es el radio giromagnético para los protones, la aparición de otra señal RMN es imposible

La señal RMN es función de la profundidad:

$E_0(q)= \int k(q,\rho(z),\alpha,z)n(z)dz$ (2)

$K(q,\rho(z),\alpha,z)=\omega_0 M_0 \int h(r,\rho(z),\alpha)sen(\gamma)dxdy$

E_0 es la amplitud inicial

α es la inclinación del campo geomagnético

$0 \sim n(z) \leq I$ es la concentración de agua

Asumiendo que el campo geomagnético es homogéneo y la estratificación horizontal, la señal RMN se puede representar como:

$e(t,q)=\int A(z,q)\ sen(\omega_0 t+\phi_0(z,\rho(z)))dz$ (3)

$A(z,q)=K(q,\rho,\alpha,z)n(z)\ exp(-t/T_2\ (z)$

$\phi_0(z,\rho(z),T_2(z)$ tiempo de relajación transversal (spin-spin)

La amplitud inicial de la señal RMN corresponde a la localización del volumen de agua. El decaimiento de la señal corresponde al tamaño del poro de la zona no-saturada

Inversión de las ecuaciones (2) y (3)determinan la concentración de agua (n(z)); el tiempo de decaimiento $T_2(z)$ la resistividad del terreno y ρ(z) como función de profundidad

PRINCIPIO OPERACIONAL

Muchos nucléidos, incluyendo $_1H^1$, poseen un momento dipolar magnético no-cero. Cuando se aplica un campo a estos núcleos atómicos la energía degenerada se elimina y acontecen absorciones resonantes de radiación electromagnética.

La frecuencia de resonancia varia con el campo magnético aplicado y es diferente para cada nucléido, el valor para los protones en el agua es:

$$f_0 = 0,04258\ H_0 \qquad (1)$$

donde f_0(Hz) es la frecuencia de resonancia y H_0(nT) el campo magnético estático.

El modelo clásico de resonancia magnética nuclear (RMN) es de espín top, donde el eje de rotación (vector momento magnético nuclear) se mueve hacía adelante desde su punto de equilibrio cuando se aplica una radiación electromagnética en frecuencia de resonancia.

Cuando el campo alterno de resonancia se elimina, el momento magnético precede sobre el campo magnético estático generando al tiempo una variación de campo que puede ser detectada mediante una bobina. La precesión se amortigua así como el momento magnético retorna al punto de equilibrio, esto induce una amortiguación de onda senoidal en la precesión de la frecuencia de resonancia en la bobina de detección.

En operación el Sistema HIDROSCOPE conduce un tren de impulsos en la frecuencia de resonancia a través de un cable dispuesto como un lazo y depositado en la superficie del terreno. El campo estático es el geomagnético de la Tierra. Una vez emitidos los impulsos de excitación el lazo se conecta al sistema de detección, registrándose la respuesta RMN de las moléculas de agua.

En el caso de un acuífero homogéneo y delgado, la señal de decaimiento de inducción libre tiene la forma:

$$E = E_0 \exp(-t/T_2^*) \operatorname{sen}(2\pi f_0 t) \qquad (2)$$

en donde:

T_2^* es el tiempo de relajación espín-espín de los protones del agua, E_0 es función del número de precesión de las moléculas de agua y de los parámetros de instrumentación y t es el tiempo transcurrido desde la supresión del campo de excitación

Medida de la señal antes indicada detecta la presencia o ausencia de agua subterránea. Para obtener una distribución cuantitativa en función de la profundidad, se registra la amplitud de la señal E_0 como una función del parámetro de excitación $q=It_p$, siendo I la amplitud de la corriente de excitación y t_p la duración del tren de impulso.

La figura nº1 muestra los resultados de los primeros experimentos que confirman que se pueden obtener los parámetros del acuífero de la curva E_0 en función de q. La línea continua de la figura se calculó mediante la integral (Semenova 1988):

$$E_0(q) \propto \int dv\ ^n(z)\ \mathrm{sen}\left(\tfrac{1}{2}\ \gamma\ q\ \beta_1(r)\right) \qquad (3)$$

siendo:

γ el radio giromagnético del protón,
$\beta_1(r)$ es el componente del vector de inducción magnética del lazo, ángulos positivos a derecha, para el campo estático en el punto $r(x,y,z)$,
$^n(z)$ es la distribución del agua como función de la profundidad z para la estructura horizontal de la lámina.

Para una lámina aislada delgada con una gran extensión lateral, $E_0(q)$ tiene un decaimiento oscilatorio (curva a, Fig 2) con un primer máximo pronunciado el cual varia directamente con el volumen de agua en el acuífero. Como la profundidad del acuífero aumenta, el máximo se mueve a altos valores de q. En la práctica el máximo disponible q está limitado por el comportamiento del generador del tren de impulsos y no es posible medir la relación completa de $E_0(q)$ para acuíferos profundos.

Obtenido el primer máximo de la curva (Curva b, figura 2), los parámetros del acuífero pueden ser estimados satisfactoriamente a partir de la ecuación (2). Donde únicamente la parte primera de la curva se registra (Curva C, figura 2) los parámetros del acuífero pueden únicamente ser estimados.

La resolución de la técnica decrece con la profundidad debido a la variación de la curva $E_0(q)$ versus q, con acuíferos profundos y la limitación práctica de energía.

Para diferentes acuíferos a diferentes profundidades el resultado $E_0(q)$ se obtiene como la sumatoria de las contribuciones de las láminas elementales:

$$E_0(q) = \sum_i E_{0i} \qquad (4)$$

Curvas experimentales de $E_0(q)$ obtenidas en diferentes emplazamientos de la antigua Unión Soviética (Figura 3) demuestra que el perfil de la curva depende simultáneamente de la profundidad del acuífero y del contenido de agua.

En la ecuación (1), la señal RMN decae con la constante de tiempo T_2 únicamente cuando los poros que contienen agua en los estratos son homogéneos, en la naturaleza la distribución del tamaño del poro suministra una señal RMN como suma exponencial sobre-escala de los tamaños del poro.

El circuito receptor de HIDROSCOPE posee un tiempo de registro de 30-40 ms, por lo que señales con un tiempo de relajación iguales o menores a 15 ms no se registran. El agua confinada en la superficie de los poros tiene tiempos de relajación menores por lo que únicamente puede ser detectado el agua libre o gravitacional que posee tiempos de relajación más largos.

Para registrar una curva $T_2^*(q)$, la cual en un campo magnético homogéneo es función del tamaño del poro sobre el lecho y entre lechos y las diferentes profundidades, se han realizado múltiples pruebas en campo, ajustando la correlación entre los tiempos de relajación y una descripción de los estratos, encontrándose la siguiente correlación.

CORRELACIÓN APROXIMADA ENTRE LOS TIEMPOS DE RELAJACIÓN OBSERVADOS Y EL TIPO DE ESTRATO PORTADOR DE AGUA

TIEMPO DE RELAJACIÓN (MS)	ESTRATO PORTADOR DE AGUA
<30	Arcillas arenosas
30-60	Arenas arcillosas, arenas muy finas
60-120	Arenas finas
120-180	Arenas grano medio
180-300	Arenas gruesas y gravas
300-600	Depósitos de grava
600-1500	Superficie del agua

El software de interpretación de datos utilizado en la tecnología está basado en un modelo matemático el cual incluye determinadas asunciones en orden a que la medida de la superficie de agua libre sea independiente de la información geofísica y geológica adicional.

El modelo matemático ha demostrado su seguridad en la detección de los estratos portadores de agua siempre que la señal sea al menos veinte veces superior al nivel de ruido eléctrico.

Como resumen de la interpretación de datos partiendo de la señal RMN se obtiene la siguiente información de cada acuífero:

* La concentración de agua $E_0(q)$ permite determinar profundidad, espesor y volumen del agua. Ausencia de señal ($E_0 = 0$ para cualquier valor de q garantiza la ausencia de agua subterránea.

* El tiempo de relajación (T_2^* (q)) corresponde al tamaño promedio del poro de las rocas de agua saturada, existiendo una relación empírica entre el tipo de roca y el tiempo de decaimiento, de tal forma varía entre 700-800 ms para el agua libre en un lago y menos de 30 ms en arcilla.

El equipo utilizado consiste normalmente en una unidad de control, un cable eléctrico que hace las veces de antena y cuatro baterías de automoción de 12 V. El cable eléctrico se extiende sobre el terreno formando un círculo de 180 a 100 metros de diámetro y se conecta a la unidad de control.

El proceso de medida consiste en transmisiones y recepciones en ciclos alternativos bajo control del software. Las mediciones pueden durar entre 40 y 180 minutos, dependiendo del nivel de ruido medioambiental y del volumen de agua subterránea. Se utiliza un ordenador externo para generar la distribución en profundidad de la concentración de agua.

RESULTADOS OBTENIDOS

La salida suministrada por el equipo HIDROSCOPE es un histograma y valoración tabulada del contenido del agua libre en función de la profundidad (ver anexo), en donde:

La columna izquierda muestra el volumen en metros cúbicos de agua libre acumulada detectada por una columna de un metro cuadrado de base para la profundidad que se determina en la columna adyacente.

El histograma refleja el porcentaje de agua, suministrando valores numéricos del contenido de agua libre para cada lámina modelizada. Asimismo se da información sobre el tiempo de relajación promedio, T_2^*, y la dimensión promedio de los poros, así como la altitud sobre el nivel del mar.

FIGURA 1

COMPARACIÓN DE E0(q) ENTRE EXPERIENCIA Y TEORÍA PARA DIFERENTES ACUÍFEROS

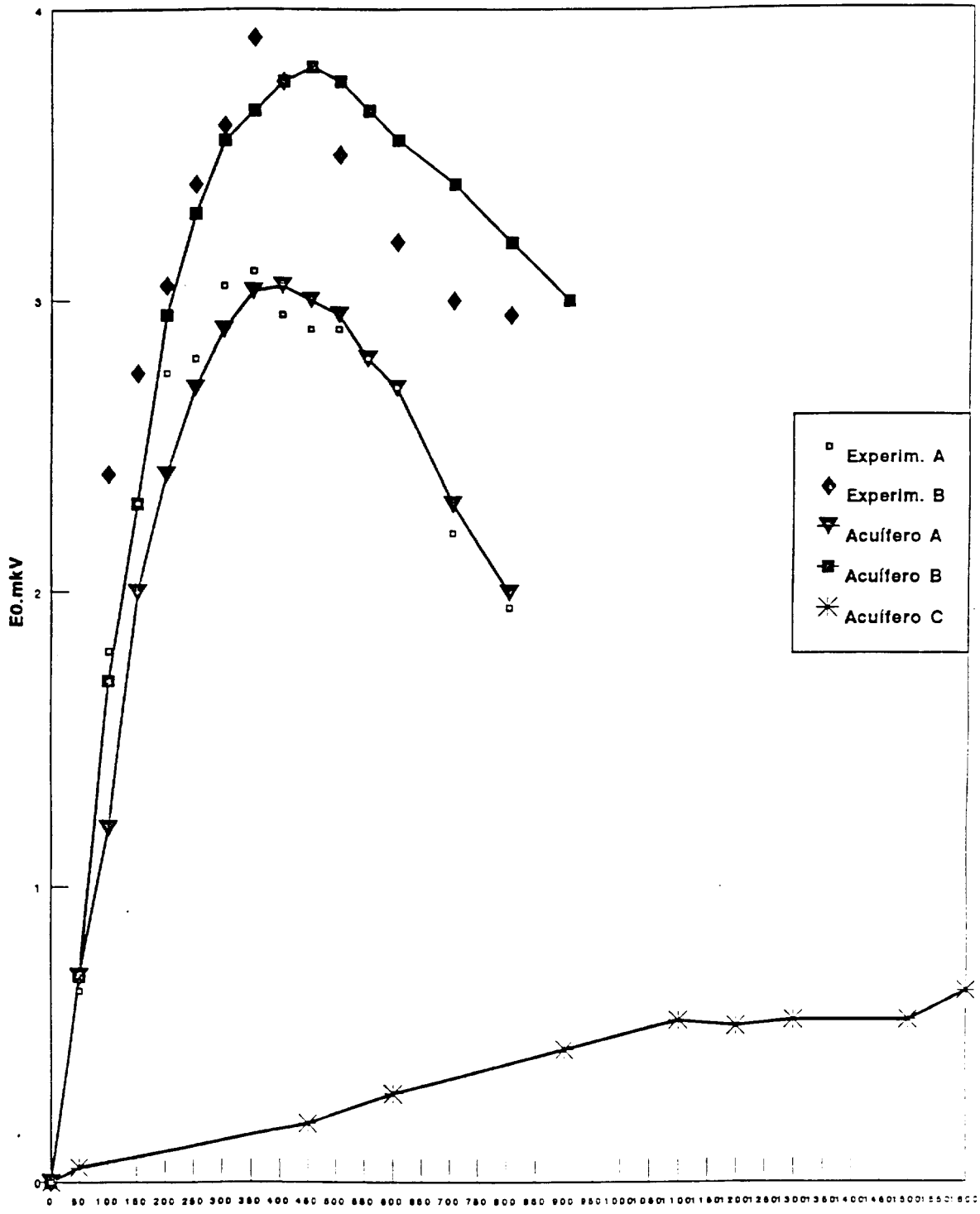

A) Acuífero 25,5 m a 5,5 m profundidad, 12% contenido agua
B) Acuífero 14,5 m a 5,5 m profundidad, 18% contenido agua
c) Acuífero 4,0 m a 24 m profundidad, 17% contenido agua

TECNICAS DE
INVESTIGACION
HIDROGEOLOGICA
S.A.

FIGURA 2

COMPORTAMIENTO DE E0(q) EN FUNCIÓN DE LA PROFUNDIDAD DEL ACUÍFERO

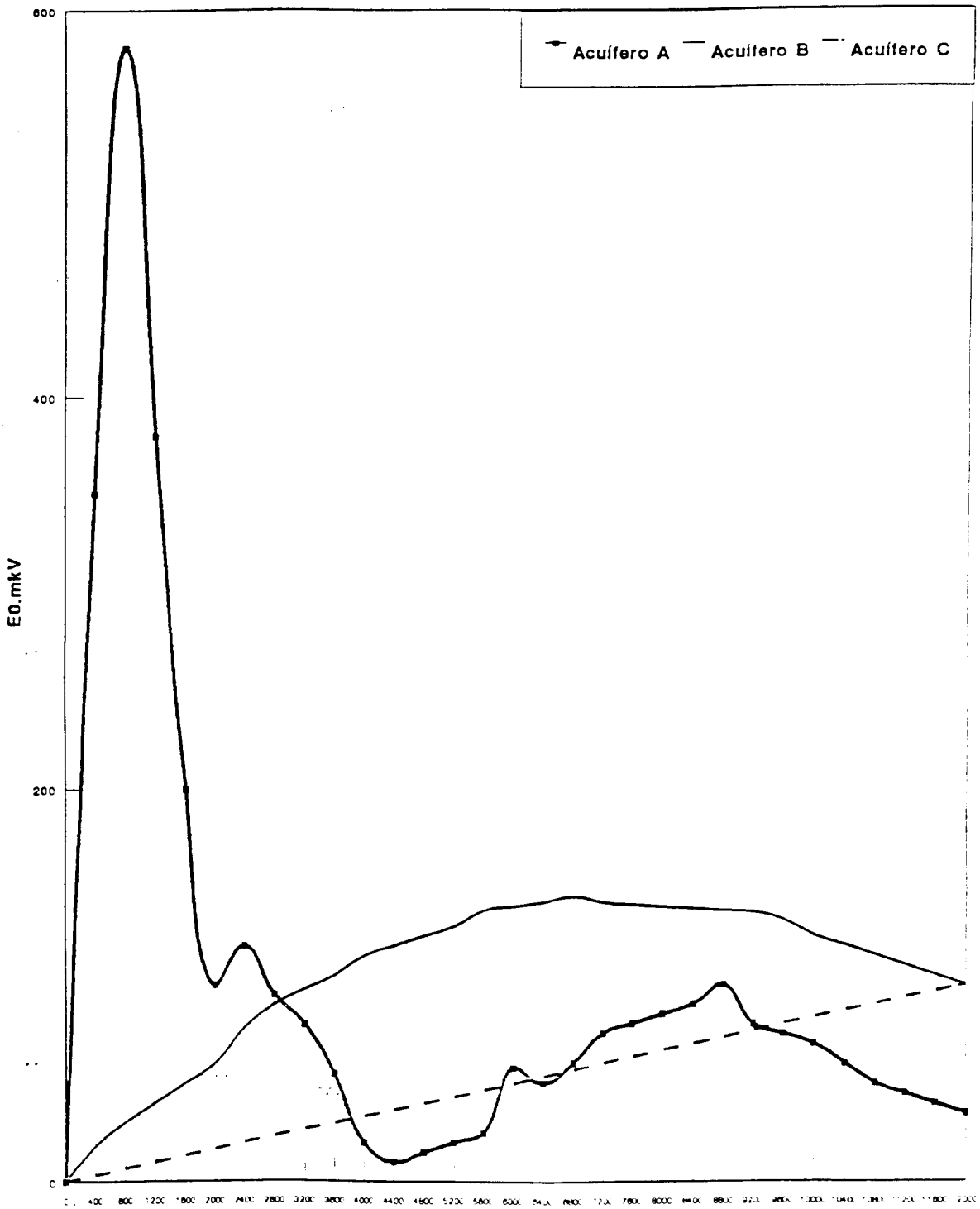

A) Acuífero superficial
B) Acuífero de media profundidad
c) Acuífero de profundidad igual al diámetro de lazo

TECNICAS DE
INVESTIGACION
HIDROGEOLOGICA,
S.A.

EL SISTEMA DE BÚSQUEDA, RECONOCIMIENTO, Y VALORACIÓN DE AGUAS SUBTERRÁNEAS

HIDROSCOPE

SOPORTE MATEMÁTICO

CAMPOS MAGNÉTICOS CONSTANTES
MOMENTO DIPOLAR

Considerando el campo producido por un sistema de cargas a grandes distancias comparadas con las dimensiones del sistema, e introduciendo un sistema de coordenadas cuyo origen sea un punto cualquiera interior al sistema de cargas. Los vectores de posición de las diferentes cargas se denominan $\mathbf{r}_a$. El potencial del campo producido por todas las cargas en el punto determinado por el vector posición $\mathbf{R}_0$ es:

$$\phi = \sum_a e_a / |\mathbf{R}_0 - \mathbf{r}_a|$$

en donde: $\mathbf{R}_0 - \mathbf{r}_a$ son los vectores de origen en las cargas e_a

Para valores grandes de $R_0 > r_a$, la anterior ecuación se desarrolla en serie de potencia de $\mathbf{r}_a/R_0$ mediante:

$$f(\mathbf{R}_0 - \mathbf{r}) = f(\mathbf{R}_0) - \mathbf{r}.\text{grad } f(\mathbf{R}_0)$$

(el operador grad se refiere a la derivación respecto de las componentes del vector $\mathbf{R}_0$)

Salvo términos superior al primero,

$$\phi = 1/R_0 \sum e_a - \sum e_a \mathbf{r}_a.\text{grad } 1/R_0$$

La suma $\mathbf{d} = \sum e_a \mathbf{r}_a$ se llama **momento dipolar**
Importa observar que si la suma de todas las cargas, $\sum e_a$, es cero, el momento dipolar no depende de la elección del origen de coordenadas, ya que los vectores $\mathbf{r}_a$ y $\mathbf{r}_a'$ de una misma carga, en dos sistemas de coordenadas diferentes están relacionados entre sí por:

$$\mathbf{r}_a' = \mathbf{r}_a + \mathbf{a}$$

donde $\mathbf{a}$ es un vector constante. Por lo tanto si $\sum e_a = 0$, el momento dipolar es el mismo en ambos sistemas:

$$\mathbf{d}' = \sum e_a \mathbf{r}_a' = \sum e_a \mathbf{r}_a + \mathbf{a} \sum e_a = \mathbf{d}.$$

Si representamos por $e_a^+, \mathbf{r}_a^+$ y $e_a^-, \mathbf{r}_a^-$ las cargas positivas y negativas del sistema y sus correspondientes vectores posición, podemos escribir el momento dipolar en la forma:

$$\mathbf{d} = \sum e_a^+ \mathbf{r}_a^+ - \sum e_a^- \mathbf{r}_a^- + \mathbf{R}_a^+ \sum e_a^+ - \mathbf{R}^- \sum e_a^-$$

donde,

$$\mathbf{R}^+ = \sum e_a^+ \mathbf{r}_a^+ / \sum e_a^+ \;,\; \mathbf{R}^- = \sum e_a^- \mathbf{r}_a^- / \sum e_a^-$$

son los "centros de cargas" para las cargas positivas y negativas Si $\Sigma e_a^+ = \Sigma e_a^- = e$, se tendrá;

$$\mathbf{d}=e\mathbf{R}_{+-}$$

donde $\mathbf{R}_{+-}=\mathbf{R}^+ - \mathbf{R}^-$ es el vector de origen en el centro de las cargas negativas y extremo en el centro de cargas positivas. En particular, si solo existen dos cargas, $\mathbf{R}_{+-}$ es vector que las une

Si la carga total del sistema es nula, el potencial de campo creado por el sistema a grandes distancias es:

$$\phi=-\mathbf{d}.\nabla 1/R_0 = \mathbf{d}.\mathbf{R}_0 /R^3_0.$$

La intensidad de campo es:

$$\mathbf{E}=-\nabla \mathbf{d}.\mathbf{R}_0 /R^3_0 = -1/R^3_0 \nabla(\mathbf{d}.\mathbf{R}_0)-(\mathbf{d}.\mathbf{R}_0)\nabla 1 /R^3_0$$

o, finalmente

$$\mathbf{E}=3(\mathbf{n}.\mathbf{d})\mathbf{n}-\mathbf{d} /R^3_0$$

donde **n** es el vector unitario correspondiente a R_0, también se puede expresar como:

$$\mathbf{E}=(\mathbf{d}.\nabla)\nabla 1/R_0$$

Así pues, el potencial del campo producido por un sistema de cargas cuya carga total es igual a cero, a grandes distancias es inversamente proporcional al cuadrado de la distancia, y su intensidad es inversamente proporcional al cubo de la misma.

Este campo presenta simetría axil respecto de la dirección del vector **d**. En el plano que pase por él (y en cuya dirección se toma el eje Z), las componentes del vector **E** son:

$$E_z=d(2 \cos\theta-1/R^3_0) , \quad E_x=d(3 \operatorname{sen}\theta \cos\theta/R^3_0) .$$

Las componentes radial y tangencial en este plano son:

$$E_R=d(2 \cos\theta/R^3_0) , \quad E_\theta=-d(\operatorname{sen}\theta /R^3_0) .$$

MOMENTOS MULTIPOLARES

En el desarrollo del potencial en potencias de $1/R_0$,

$$\phi=\phi^{(0)}+\phi^{(1)}+\phi^{(2)}+\ldots,$$

el término ϕ es proporcional a $1/R_0^{n+1}$. El primer término $\phi^{(0)}$ está determinado por la suma de todas las cargas; el segundo $\phi^{(1)}$ está determinado por **el momento dipolar del sistema** denominándose **potencia dipolar del sistema.**

El tercer término en el desarrollo $\phi^{(2)}$, es igual a

$$\phi^{(2)} = \tfrac{1}{2}\Sigma\ e x_\alpha\ x_\beta\ \partial^2/\partial X_\alpha\ \partial X_\beta\ \ (1/R_0)$$

donde la suma se extiende a todas las cargas; prescindiendo del índice que fija el número de carga; x_α son las componentes del vector **r**, y X_α las del vector $\mathbf{R_0}$

Esta parte del potencial se suele llamar **potencial cuadripolar.** Si la suma de las cargas y el momento dipolar del sistema son ambos iguales a cero, el desarrollo comienza con el término $\phi^{(2)}$

En la expresión anterior aparecen seis cantidades $\Sigma\ e x_\alpha\ x_\beta$, el campo depende de cinco cantidades independiente, este resultado se sigue del hecho que la función $1/R_0$ satisface la ecuación de Laplace,

$$\Delta(1/R_0) = (\partial^2/\partial X_\beta^2)(1/R_0) = 0$$

Esta igualdad se puede escribir en la forma:

$$\delta\partial^2/\partial X_\alpha\ \partial X_\beta\ (1/R_0) = 0$$

Por consiguiente $\phi^{(2)}$ es igual a

$$\phi^{(2)} = \tfrac{1}{2}\Sigma\ e(x_\alpha\ x_\beta - \tfrac{1}{3}r^2\ \delta_{\alpha\beta})(\partial^2/\partial X_\alpha\ \partial X_\beta)\ \ (1/R_0)$$

el tensor

$$D_{\alpha\beta} = \Sigma\ e\ (3\ x_\alpha x_\beta - r^2\delta_{\alpha\beta})$$

se llama **momento cuadripolar del sistema**. Resultando evidente que de la definición de $D_{\alpha\beta}$ la suma de los elementos diagonales es iguala cero, $D_{\alpha\beta} = 0$.

Mediante el tensor podemos escribir

$$\phi^{(2)} = D_{\alpha\beta}/6\ (\partial^2/\partial X_\alpha \partial X_\beta)\ \ (1/R_0)$$

o bien derivando

$$(\partial^2/\partial X_\alpha \partial X_\beta)\ \ (1/R_0) = 3X_\alpha X_\beta/R_{05} - \delta_{\alpha\beta}/R_0^3$$

y teniendo en cuenta que $\delta_{\alpha\beta}D_{\alpha\beta} = D\alpha\alpha = 0$,

$$\phi^{(2)} = D_{\alpha\beta}\ n_\alpha n_\beta/2R_0^3$$

Si el sistema de cargas es simétrico respecto de un cierto eje (eje z), este eje es uno de los ejes principales del tensor $D_{\alpha\beta}$ los tres valores principales están ligados entre sí por relación:

$$D_{xx} = D_{yy} = -\tfrac{1}{2}D_{zz}$$

Siendo D_{zz} el **momento cuadripolar**

$$\phi^{(2)}=D/4R_0^3\left(3\cos^2\theta-1\right)=D/2R_0^3\left(P_2(\cos\theta)\right)$$

donde θ es el ángulo formado por $\mathbf{R_0}$ y el eje z y P_2 es un polinomio de Legendre

El término l-ésimo del desarrollo se define por un tensor denominado **tensor momento 2^l-polar** de orden l, simétrico respecto de todos sus índices, y cuya contracción respecto de un par cualquiera de ellos es nula, consta de 2l+1 componentes independientes. Partiendo de la fórmula de los armónicos esféricos

$$1/|\mathbf{R_0}-\mathbf{r}|=1/\sqrt{R_0^2+r^2-2rR_0\cos\chi}=\sum_{l=0}^{\infty}\left(r^l/R_0^{(l+1)}\right)P_l(\cos\chi)$$

en la que χ es el ángulo formado por $\mathbf{R_0}$ y $\mathbf{r}$. Introduciendo las coordenadas esféricas θ, Φ y θ, ϕ de los vectores $\mathbf{R_0}$ y $\mathbf{r}$ respectivamente y aplicando el teorema de adición de armónicos esféricos

$$P_l(\cos\chi)=\sum_{m=1}^{l}\left((l-|m|)!/(l-|m|)!\right)P_l^{|m|}(\cos\theta)P_l^{|m|}\cos(\theta)e^{-im(\phi-\phi)}$$

donde P_{lm} son los polinomios Legendre asociados. El desarrollo toma entonces la forma

$$1/|\mathbf{R_0}-\mathbf{r}|=\sum_{l=0}^{\infty}\sum_{m=-l}^{l}\left(r^l/R_0^{(l+1)}\right)(l-|m|)!/(l-|m|)!P_l^{|m|}(\cos\theta)P_l^{|m|}\cos(\theta)e^{-im(\phi-\phi)}$$

Aplicando este desarrollo al término de la suma de potencial de campo, se obtiene el término l-ésimo del desarrollo de potencial

$$\phi^{(l)}=1/R_0^{(l+1)}\sum\sqrt{\left((l-|m|)!/(l-|m|)!\right)}\,P_l^{|m|}(\cos\theta)\,e^{-im\Phi}D_m^{(l)}$$

donde

$$D_m^{(l)}=\sum e_a r_a^l\sqrt{\left((l-|m|)!/(l-|m|)!\right)}\,P_l^{|m|}(\cos\theta_a)\,e^{-im\phi a}$$

CAMPO MAGNÉTICO CONSTANTE

El campo magnético producido por cargas que efectúan un movimiento finito, las partículas se encuentran en todo tiempo dentro de una región finita del espacio y los impulsos acotados, tiene un carácter estacionario y es interesante considerar el valor medio, respecto del tiempo, del campo magnético **H** creado por las cargas; este campo será ahora función sólo de las coordenadas y no del tiempo, esto es será constante.

Las ecuaciones que determinan el valor medio del campo magnético **H**, derivan del promedio temporal de las ecuaciones de Maxwell

$$\text{div}\,\mathbf{H}=0;\ \text{rot}\,\mathbf{H}=(1/c)(\partial\mathbf{E}/\partial t)+(4\pi/c)\mathbf{j}$$

La primera de ellas da simplemente

$$\text{div } \mathbf{H}=0$$

En la segunda ecuación, el valor medio de la derivada $\partial\mathbf{E}/\partial t=0$, por consiguiente esta ecuación pasa a ser

$$\text{rot } \mathbf{H}=(4\pi/c)\mathbf{j}$$

Estas dos ecuaciones determinan el campo constante **H**. El valor medio del potencial vector de acuerdo con rot **A**=**H** y sustituyendo en la anterior ecuación

$$\text{grad div } \mathbf{A} - \Delta\mathbf{A} = (4\pi/c)\mathbf{j}$$

El potencial vector no está definido unívocamente, por lo que podemos imponerle una condición suplementaria arbitraria, eligiendo **A** de forma que div **A**=0, la ecuación que define el potencial vector en un campo magnético constante toma la forma

$$\Delta\mathbf{A} = -(4\pi/c)\mathbf{j}$$

Esta ecuación es completamente análoga a la ecuación de Poisson para el potencial escalar de un campo eléctrico constante , salvo que en vez de la densidad de carga ρ tenemos aquí la densidad de corriente **j**/c, por lo que por analogía

$$\mathbf{A}=1/c \int \mathbf{j}/R \, dV$$

donde R es la distancia del punto de observación al elemento de volumen dV. Se puede pasar a una suma sobre las cargas, que son puntuales

$$\mathbf{A}=1/c \; \Sigma \; \overline{e_a \; \mathbf{v}_a}/R_a$$

Conocido **A** la intensidad de campo magnético viene dada por

$$\mathbf{H}=\text{rot } \mathbf{A}= \text{rot } 1/c \int (\mathbf{j}/R) \, dV$$

El operador rot se refiere a las coordenadas del punto de observación. Permutando el operador rotacional con el signo de integración y tratando **j** como constante de derivación y aplicando

$$\text{rot } f= f \text{ rot } \mathbf{a} + \text{grad } f \times \mathbf{a}$$

donde f y **a** son un escalar y un vector arbitrarios, al producto **j**.1/R, se encuentra:

$$\text{rot } \mathbf{j}/R= \text{grad } 1/R \times \mathbf{j} = \mathbf{j} \times \mathbf{R} /r^3$$

y en consecuencia

$$\mathbf{H}=1/c \int (\mathbf{j} \times \mathbf{R} /r^3) \, dV$$

el vector **R** tiene por origen dV, por extremo el punto observación

MOMENTOS MAGNÉTICOS

Considerando el campo magnético medio producido por un sistema de cargas en movimiento estacionario, a grandes distancias del sistema, e introduciendo un sistema de coordenadas cuyo origen coincida con un punto cualquiera interior al sistema de cargas, y representando por $\mathbf{r}_a$ y el vector con origen de carga e_a y el vector posición del punto en que se calcula el campo por $\mathbf{R}_0$. La diferencia $\mathbf{R}_0-\mathbf{r}_a$ es el vector con origen en la carga e_a y extremo en el punto de observación. Se tiene para el potencial vector

$$\mathbf{A}= 1/c\ \Sigma\ \overline{e_a\ \mathbf{v}_a}\ /\ |\mathbf{R}_0-\mathbf{r}_a|$$

Desarrollando esta expresión en potencias de $\mathbf{r}_a$

$$\mathbf{A}= 1/cR_0\ \Sigma\ \mathbf{ev}- 1/c\ \Sigma\ \overline{\mathbf{ev}\ \{\mathbf{r}.\nabla(1/R_0)\}}$$

en el primer término se puede hacer

$$\Sigma\ \mathbf{ev}= d/dt\ \Sigma\ \mathbf{er}$$

Dado que el valor medio de $\Sigma\mathbf{er}=0$ ya que varía en intervalo finito

$$\mathbf{A}=-1/c\ \Sigma\ \overline{\mathbf{ev}\{\mathbf{r}.\nabla(1/R_0)\}}= 1/cR_0^3\ \Sigma\ \overline{\mathbf{ev}(\mathbf{r}.\mathbf{R}_0)}$$

Observando que $\mathbf{v}= \cdot\mathbf{r}$ y dado que $\mathbf{R}_0$ es un vector constante

$$\Sigma\ e(\mathbf{R}_0.\mathbf{r})\mathbf{v}=\tfrac{1}{2}(d/dt)\Sigma\ \mathbf{er}(\mathbf{R}_0.\mathbf{r})+\tfrac{1}{2}\Sigma\ e[\mathbf{v}(\mathbf{R}_0.\mathbf{r})-\mathbf{r}(\mathbf{v}.\mathbf{R}_0)]$$

Sustituyendo esta expresión en la de **A**, el valor medio del primer término (que contiene la derivada respecto del tiempo) es también cero y se obtiene

$$\mathbf{A}=1/(2cR_0^3)\ \Sigma\ \overline{e[\mathbf{v}(\mathbf{R}_0.\mathbf{r})-\mathbf{r}(\mathbf{v}.\mathbf{R}_0)]}$$

Introduciendo el vector llamado **momento magnético del sistema**

$$\mathfrak{S}= 1/2c\ \Sigma\ \mathbf{er}\times\mathbf{v}$$

$$\mathbf{A}= \mathfrak{S}\times\mathbf{R}_0/R_0^3=\nabla(1/R_0)\times\mathfrak{S}$$

La intensidad del campo magnético viene determinada por la fórmula; $\mathrm{rot}(\mathbf{a}\times\mathbf{b})=(\mathbf{b}.\nabla)\mathbf{a}-(\mathbf{a}.\nabla)\mathbf{b}+\mathbf{a}\ \mathrm{div}\ \mathbf{b}-\mathbf{b}\ \mathrm{div}\ \mathbf{a}$

$$\mathbf{H}= \mathrm{rot}\ \mathbf{A}= \mathrm{rot}\ (\mathfrak{S}\times\mathbf{R}_0/R_0^3)= \mathfrak{S}\ \mathrm{div}\ \mathbf{R}_0/R_0^3\ -(\mathfrak{S}.\nabla)\mathbf{R}_0/R_0^3$$

$$\mathrm{div}\ (\mathbf{R}_0/R_0^3)=\mathbf{R}_0.\mathrm{grad}\ (1/R_0^3)+(1/R_0^3)\ \mathrm{div}\ \mathbf{R}_0=0$$

$$(\mathfrak{S}.\nabla)(\mathbf{R}_0/R_0^3)=(1/R_0^3)(\mathfrak{S}.\nabla)\mathbf{R}_0+(\mathfrak{S}.\nabla)\mathbf{R}_0(1/R_0^3)=\mathfrak{S}/R_0^3-3\mathbf{R}_0(\mathfrak{S}.\mathbf{R}_0)/R_0^5$$

De esta manera

$$H=[3n(\mathfrak{I}.n)-\mathfrak{I}]/R_0^3$$

El campo magnético se expresa en función del momento magnético por la misma fórmula que el campo eléctrico se expresa en función del momento dipolar

Si para todas las cargas del sistema es la misma la razón de la carga a la masa, podemos escribir

$$\mathfrak{I}=\tfrac{1}{2}.\Sigma \mathbf{er}\times\mathbf{v} = e/2mc\ \Sigma\ m\mathbf{r}\times\mathbf{v}$$

Si las velocidades de todas las cargas $v \ll c$, el impulso se puede sustituir por mv y se obtiene

$$\mathfrak{I}= e/2mc\ \Sigma\ \mathbf{r}\times\mathbf{p} = (e/2mc)\ \mathbf{M}$$

donde $\mathbf{M} = \Sigma\ \mathbf{r}\times\mathbf{p}$ es el **momento cinético mecánico del sistema**

LA FRECUENCIA DE LARMOR

El punto de vista clásico de la teoría de campos nos confirma que el vector **M** (y con él el momento magnético **m**) gira con velocidad angular $-\Omega$ en torno de la dirección del campo, mientras que su módulo y el ángulo que forman con esta dirección se conservan constantes, denominándose a este movimiento **PRECESIÓN DE LARMOR**

Si consideramos un sistemas de cargas en un campo magnético exterior uniforme y constante, el valor medio temporal de la fuerza que actúa sobre el sistema

$$\mathbf{F}= \Sigma\ e/c\ \mathbf{v}\times\mathbf{H} = d/dt\ \Sigma e/c\ \mathbf{r}\times\mathbf{H}$$

se anula, como el valor medio respecto del tiempo de la derivada temporal de cualquier función del tiempo varía en un intervalo finito. El valor medio del momento de las fuerzas

$$\mathbf{k} = \Sigma\ e/c\ (\mathbf{r}\times(\mathbf{v}\times\mathbf{H}))$$

es en cambio diferente de cero. Se puede expresar en función del momento magnético del sistema sin más que desarrollar el doble producto vectorial

$$\mathbf{k} = \Sigma\ e/c\left[\mathbf{v}(\mathbf{r}.\mathbf{H})-\mathbf{H}(\mathbf{v}.\mathbf{r})\right] = \Sigma\ e/c\ \left[\mathbf{v}(\mathbf{r}.\mathbf{H})-\tfrac{1}{2}\mathbf{H}\ d/dt\ \mathbf{r}^2\right] .$$

El valor medio del segundo término es cero, de forma que

$$\mathbf{k} = \Sigma\ e/c\ \mathbf{v}(r\times\mathbf{H})=1/2c\ \Sigma\ e\ \left[\mathbf{v}(\mathbf{r}.\mathbf{H})-\mathbf{r}(\mathbf{v}.\mathbf{H})\right]$$

finalmente

$$\mathbf{k}= \mathfrak{I} \times \mathbf{H} \qquad (1)$$

siendo $m=1/2c\ \Sigma\ \mathbf{er} \times \mathbf{v}$ vector momento magnético del sistema

La función de Lagrange de un sistema de cargas en un campo magnético exterior y constante contiene (comparado con la función de Lagrange de un sistema aislado) el término adicional:

$$L_H = \sum e/c\ \mathbf{A}.\mathbf{v} = \sum e/2c\ \mathbf{H}\times\mathbf{r}.\mathbf{v} = \sum e/2c\ \mathbf{r}\times\mathbf{v}.\mathbf{H}$$

(se ha utilizado la expresión $\mathbf{A} = \frac{1}{2}\ \mathbf{H}\times\mathbf{r}$ que expresa el potencial vector de un campo magnético uniforme en función de la intensidad de campo). Introduciendo el momento magnético del sistema se tiene

$$L_H = \mathfrak{M}.\mathbf{H}. \qquad (2)$$

Si consideramos un sistema de cargas que efectúan un movimiento finito (con velocidades $v \ll c$) en el campo eléctrico central producido por una carga fija, que gira con movimiento uniforme en torno de un eje que pasa por la partícula fija, la velocidad $\mathbf{v}$ de la partícula en este sistema está ligada con la velocidad del sistema primitivo por la relación:

$$\mathbf{v}' = \mathbf{v} + \Omega \times \mathbf{r}$$

donde $\mathbf{r}$ es el vector posición de la partícula y Ω es la velocidad angular del sistema de coordenadas en rotación. En el sistema fijo, la función de Lagrange del sistema de cargas es:

$$L = \sum mv^{-2}/2 - U$$

donde U es la energía potencial de las cargas en el campo exterior más la energía de sus interacciones mutuas. La magnitud U es función de las distancias de las cargas a la partícula fija y de las distancias que las separan dos a dos; cuando se pasa al sistema de coordenadas en rotación, esta expresión permanece evidentemente inalterada. Por lo tanto, en el nuevo sistema la función de Lagrange será:

$$L = \sum m/2(\mathbf{v}+\Omega \times \mathbf{r})^2 - U$$

Suponiendo que para todas las cargas es la misma la razón de la carga a la masa, e/m, y haciendo

$$\Omega = e/2mc\ \mathbf{H}$$

En estas condiciones, para H suficientemente pequeño la función de Lagrange se convierte en:

$$L = \sum mv^2/2 + \frac{1}{2} \sum e\mathbf{H}\times\mathbf{r}.\mathbf{v} - U$$

Confirma esta función con la describía el movimiento de las cargas considerando sistemas de coordenadas del laboratorio en presencia de un campo magnético constante (ver 2)

Se obtiene el resultado de que, en el sentido no relativista, el comportamiento de un sistema de cargas que tiene el mismo valor de e/m que efectúan un movimiento finito en un campo magnético eléctrico con simetría central y en un campo magnético uniforme débil **H**, es equivalente al comportamiento de este mismo sistema de cargas, en el mismo campo eléctrico, respecto de un sistema de coordenadas que giran uniformemente con la velocidad angular.

Esto es precisamente lo que afirma el llamado **TEOREMA DE LARMOR**, y la velocidad angular $\Omega = eH/2mc$ se llama **FRECUENCIA DE LARMOR**

Analizado desde otro punto de vista, si el campo magnético es suficientemente débil, la frecuencia de Larmor será pequeña respecto a las frecuencias del movimiento finito del sistema dado de cargas. Podemos entonces considerar los valores medios en intervalos de tiempos pequeños comparados con el período $2\Pi/\Omega$ de las magnitudes ligadas al sistema. Estos valores varían lentamente con el tiempo (con frecuencia Ω)

Considerando el cambio de momento mecánico medio **M** del sistema, que de acuerdo con una conocida ecuación mecánica, la derivada de **M** es igual al momento **k** de las fuerzas que actúan sobre el sistema

Por consiguiente y valiéndonos de (1):

$$d\mathbf{M}/dt = \mathbf{k} = \mathfrak{M} \times \mathbf{H}$$

si la razón e/m es la misma para todas las partículas del sistema, los momentos mecánicos y magnéticos son proporcionales entre sí y se encuentran, teniendo en cuenta que:

$$\Omega = e/2mc\ \mathbf{H}$$

y

$$m = e/2mc \int \mathbf{r}\times\mathbf{p} = e/2mc\ \mathbf{M}$$

donde $\mathbf{M} = \int \mathbf{r}\times\mathbf{p}$ es el momento cinético mecánico del sistema, la razón del momento magnético al momento cinético mecánico es constante y es igual a e/2mc.

$$d\mathbf{M}/dt = -\Omega \times \mathbf{M}$$

Esta ecuación indica que el vector **M** (y con él el momento magnético $\mathfrak{M}$) gira con velocidad angular $-\Omega$ en torno de la dirección del campo, mientras que su módulo y el ángulo que forma con esta dirección se conservan contantes, este movimiento se llama **PRECESIÓN DE LARMOR.**

SPIN

Establezcamos una partícula compuesta, un núcleo atómico, que efectúa un cierto movimiento en su conjunto. La energía interna del núcleo posee un valor determinado. Si embargo, con esto el estado interno del núcleo no queda aún determinado por completo; así, el **momento cinético "interno" del núcleo L** (momento de las partículas en su movimiento dentro del núcleo), puede estar todavía orientado de diferentes maneras en el espacio. El número de posibles orientaciones distintas de este momento cinético, es igual a 2L+1.

De esta manera, debemos considerar junto a sus coordenadas, una variable discreta: la proyección de su momento cinético interno sobre una dirección cualquiera en el espacio.

Cuando la partícula es elemental no tenemos a priori ningún elemento que permita suponer que dicha variable no existe, admitimos en mecánica cuántica que hay que atribuir a una partícula elemental cierto momento cinético propio no ligado a su movimiento en el espacio. Esta propiedad de las partículas elementales es típicamente cuántica (desaparece cuando $\hbar \to 0$) y no admite, por propia esencia, una interpretación clásica.

En particular, carecía de sentido el representar el momento cinético propio de una partícula elemental como resultado de su rotación en torno de su eje.
El momento cinético propio de una partícula se llama spin, y el momento cinético ligado al movimiento de la partícula en el espacio se denomina momento cinético orbital, ambos se miden en unidades $\hbar$ y se representa por **s**.

Las tres coordenadas no constituyen un sistema completo de magnitudes para una partícula, dadas las cuales queda totalmente determinado el estado de la misma, para que esto ocurra debe darse la dirección del vector spin. Por ello, también, la función de onda de una partícula debe ser función de cuatro variables. Los valores que toma la proyección del spin sobre la dirección elegida del espacio toma un número limitado de valores discretos.

De esta manera la función de onda de una partícula que tiene spin no-nulo, es en realidad el conjunto formado por un cierto número de funciones de las coordenadas distintas, funciones que difieren por su **índice spin**

El operador que en mecánica cuántica corresponde al spin de una partícula es tal que al aplicarlo a una función de onda actúa sobre la "variable de spin" . Los operadores $\hat{S}_x, \hat{S}_y, \hat{S}_z$ satisfacen las mismas condiciones de conmutación que los operadores del momento cinético orbital.

El operador del momento cinético coincide en esencia con el operador de una rotación infinitesimal.

$$\{\hat{s}_y,\hat{s}_z\}=i\hat{s}_x \quad \{\hat{s}_z,\hat{s}_x\}=i\hat{s}_y \quad \{\hat{s}_x,\hat{s}_y\}=i\hat{s}_z$$

De las ecuaciones que sigue el momento cinético podemos determinar los valores del módulo y las componentes del spin:

$$\psi_{M+1} = \text{constante} \times \hat{s}_{+\psi M} \quad \psi_{M-1} = \text{constante} \times \hat{s}_{-\psi M}$$

Si en la primera de estas igualdades se hace M=ŝ, y dado que por definición no existen estados con M>S, debe tenerse idénticamente

$$\hat{s}_{+\psi s} = 0$$

Aplicando esta igualdad al operador $\hat{s}_-$ y teniendo en cuenta que

$$\hat{s}^2=\hat{s}_+\hat{s}_-+\hat{s}_z^2-\hat{s}_z$$

$$=\hat{s}_-\hat{s}_++\hat{s}_z^2+\hat{s}_z$$

se obtiene

$$\hat{s}_-\hat{s}_{+\psi s} = \left(\hat{s}_2-\hat{s}_z^2-\hat{s}_z\right)\psi s = 0$$

pero dado que las ψ_M son las funciones propias comunes a los operadores S^2 y $\hat{s}_z$ se obtiene

$$\hat{s}^2\psi_s=S^2\psi s, \quad \hat{s}_z^2\psi_s=S^2\psi s, \quad \hat{s}_z^2\psi_s=S\psi s$$

que conduce a la ecuación que determina los valores propios del cuadrado del spin

$$S^2=S(S+1)$$

De los anterior se infiere que los valores propios de la componente-z del spin forman una sucesión de números que difieren en una unidad. La sucesión de valores está limitada por valores que son iguales en valor absoluto y de signos opuestos ±s. La diferencia 2s entre los valores máximo y mínimo de s_z debe ser un número entero o cero, tomando los valores 0, ½, 1, 3/2,.... donde s puede ser un número entero o semi-entero (incluido el valor nulo).

Prueba la experiencia que la mayoría de las partículas elementales, electrones, positones, protones, neutrones, mesones-μ, y todos los hiperones (Λ, Σ, Θ), poseen spin ½. Existen partículas elementales , los mesones Π y los mesones K, que poseen spin 0.

El momento cinético total de una partícula es la suma de su momento cinético orbital l y del spin s. Los valores propios del momento cinético total

$$\mathbf{j} = \mathbf{l} + \mathbf{s}$$

se determina según la regla del modelo vectorial que se aplica a la suma de los momentos cinéticos orbitales de dos partículas distintas. Así para valores dados l y s, el momento cinético total puede tomar los valores l+s, l+s-1,..., |l-s|.

El operador del momento cinético total **J** de un sistema de partículas es igual a la suma de los operadores de los momentos cinéticos **j** de cada una de ellas, de modo que sus valores vienen de nuevo determinados por las reglas del modelo vectorial. El momento cinético **J** se puede representar en la forma:

$$\mathbf{J} = \mathbf{L} + \mathbf{S},\ \mathbf{L}=\Sigma\mathbf{l}_a,\ \mathbf{S}=\Sigma\mathbf{s}_a$$

S es el spin total, y L momento cinético orbital total

Si el spin del sistema es semientero (o entero), lo mismo valdrá también para el momento cinético total, ya que el momento cinético orbital es siempre entero. Si el sistema está constituido por un número par de partículas idénticas, su spin total será siempre entero, y por consiguiente, también será entero el momento cinético total.

IHGSA

TECNICAS DE
INVESTIGACIÓN
HIDROGEOLÓGICA,
S.A.

SISTEMA DE BÚSQUEDA, RECONOCIMIENTO Y VALORACIÓN DE LOS RECURSOS Y RESERVAS DE LAS AGUAS SUBTERRÁNEAS.

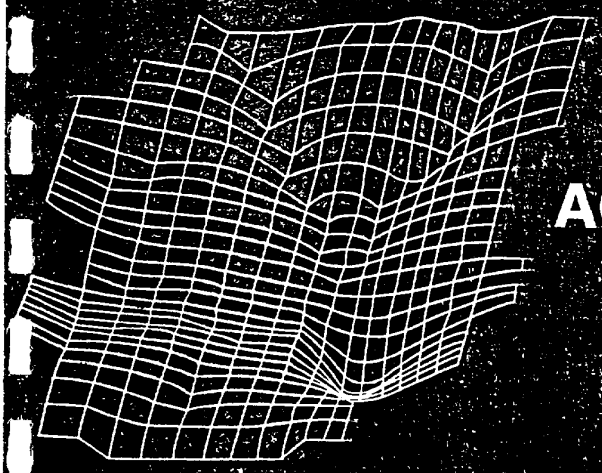

ESQUEMA DE FUNCIONAMIENTO DEL SISTEMA HIDROSCOPE

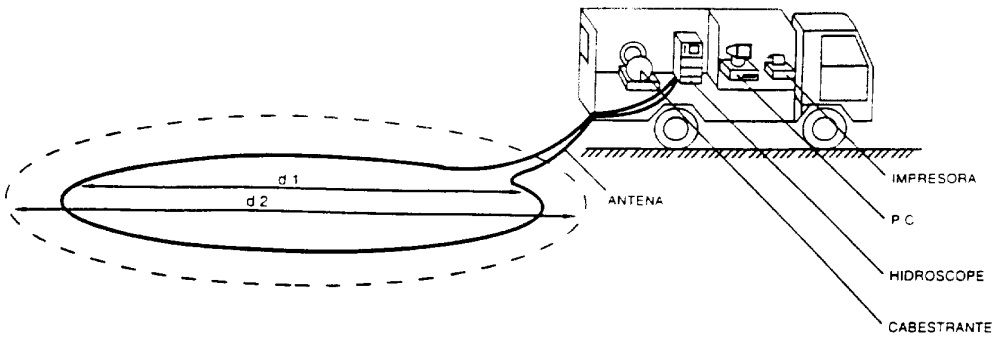

COLUMNA GEOLOGICA E HIDROGEOLOGICA

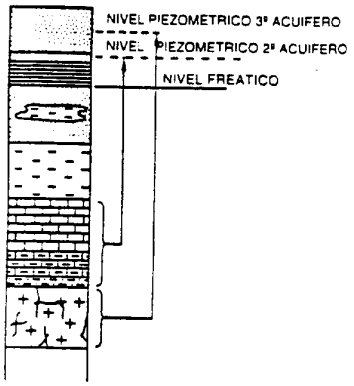

HISTOGRAMA

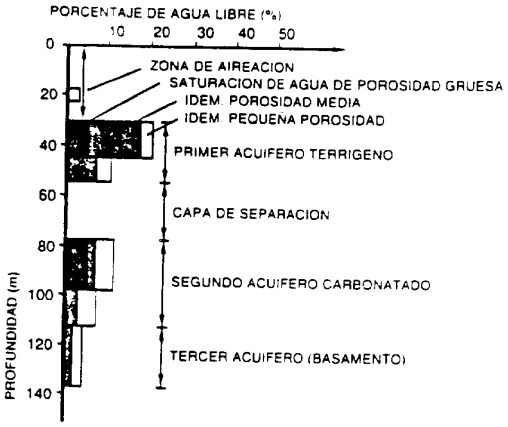

CURVA DE RELAJACIÓN DE LA SEÑAL R.M.N. DEL PROTON

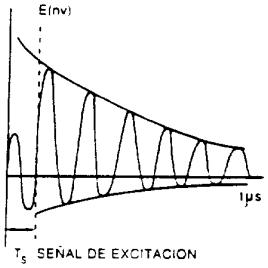

HIDROSCOPE es un instrumento hidrogeológico de campo que visualiza el agua subterránea en las capas portadoras por **lo que no son necesarios los trabajos de perforacion del terreno,** de esta manera y sin necesidad de muestras físicas del agua se cuantifica y determina la distribucion de los recursos hídricos subterráneos.

HIDROSCOPE es un tomógrafo basado en una señal de Resonancia Magnética Nuclear de los protones del agua libre en el punto de observación.
El sistema es autónomo con una masa total de unos 600 kg, ocupando una superficie de 5 m^2, permitiendo su traslado en un vehiculo todo-terreno.

DISTRIBUCIÓN DEL AGUA LIBRE EN LA ZONA

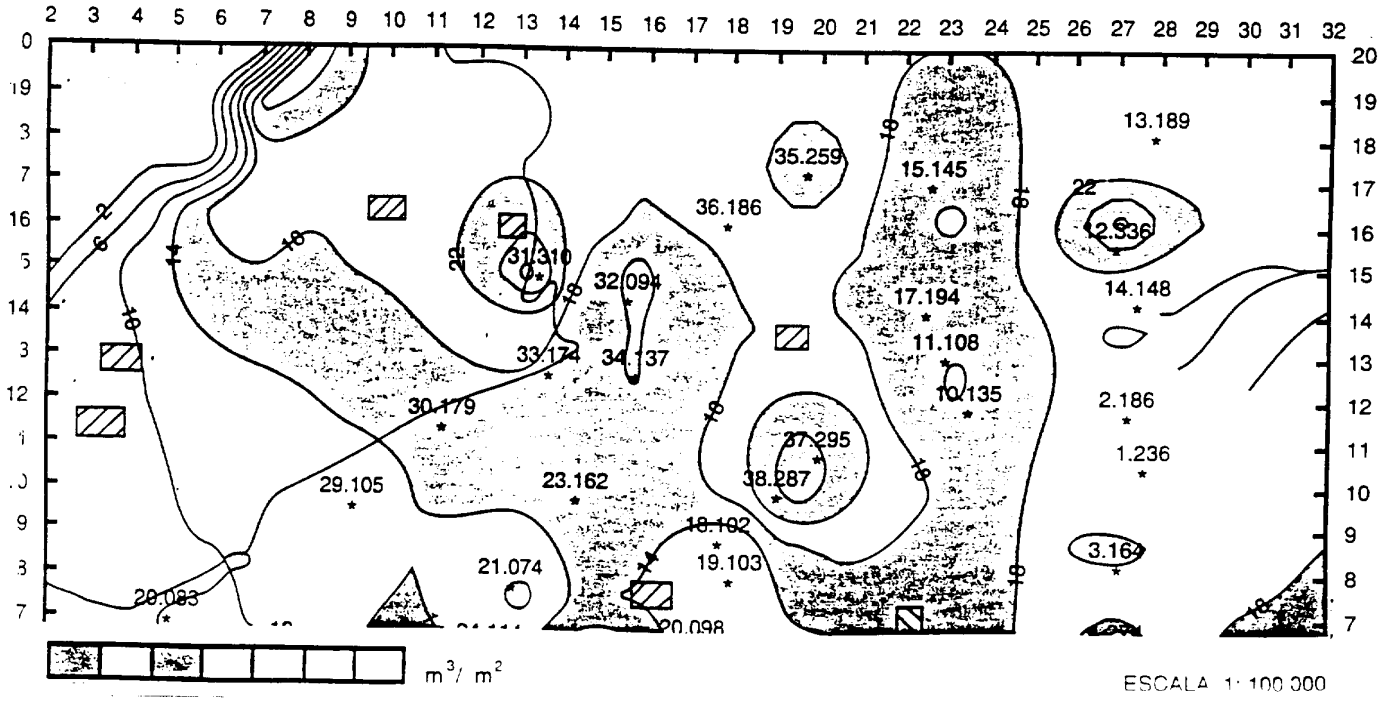

ESCALA 1: 100.000

COMO RESPUESTA A LA DEMANDA DE MEJORAR, AMPLIAR Y GARA
DISPONIBILIDADES DE LOS RECURSOS HIDRICOS, TIGHSA ASESORA

- Cartografía directa de las formaciones hidrogeológicas mejoranda
  indispensable preconocimiento de los trabajos hidrológicos posteriore
- Estudios para la agricultura, la industria y otros fines civiles como los almacenamientos
  combatir la contaminación de las aguas subterráneas, protección y renabilitación de los re
- Proyectos de perforación, alumbramiento y aforo para estructuras de captación y sistemas de
- Modelos computarizados de los recursos de agua y sistemas de suministro de agua
- Cartografía con fines ecológicos, hidrogeológicos y geológicos para la gestión del abastecimiento
- Desarrollo de programas software para cálculo de los recursos, interfase agua fresca-salinizada y

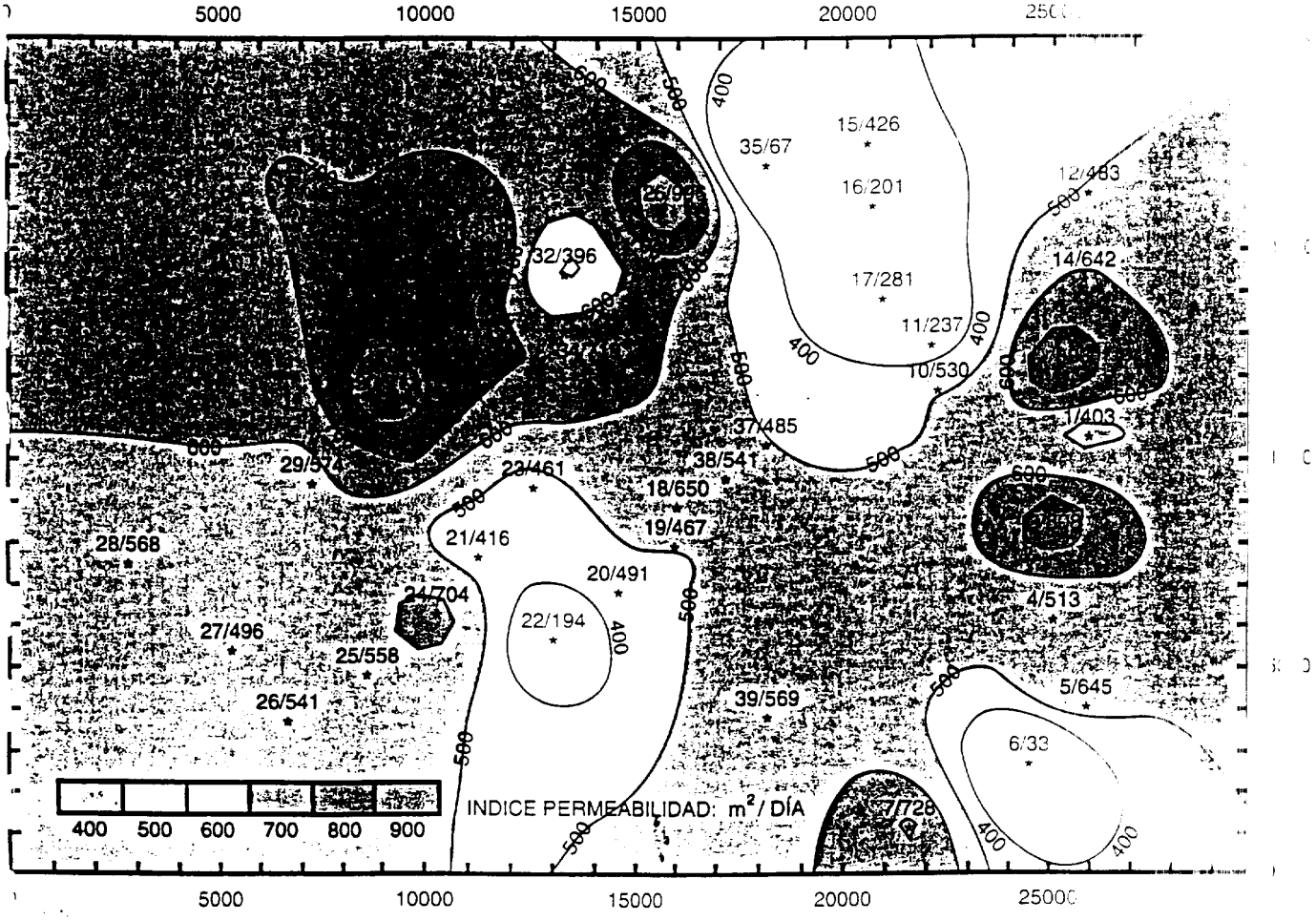

Especificaciones de funcionamiento:

• Profundidad de localización y descripción de las capas acuíferas:	120 m.
• Profundidad para investigación general:	185 m.
• Discriminación de capas acuíferas en alzado:	0,5-1.00 m
• Rendimiento:	100 - 400 km² por mes
• Duración del trabajo de campo:	1 a 6 meses.
• Requisitos de operadores:	2-3 especialistas

- Campo aplicación: Aguas subterraneas en estratos de aguas congeladas

PERFIL DE SATURACION DEL AGUA

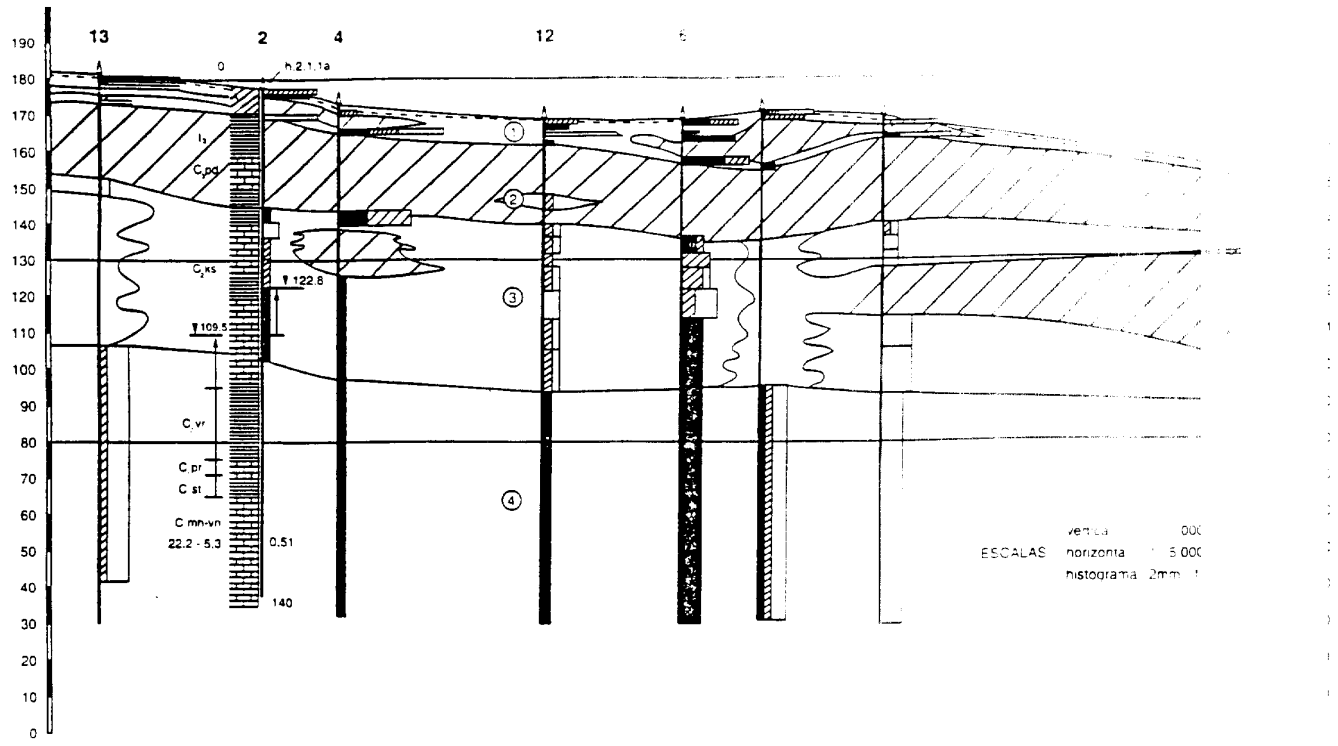

CARTOGRAFÍA -

El estudio de las condiciones geológicas e hidrológicas en la zona, suministra la siguiente información:

- Distribución del agua libre.
- Características hidrogeológicas de los acuíferos.
- Espesor y estructura en sección vertical.
- Evaluación de los valores y regularidades de cambio de los parámetros hidrogeológicos más importantes en los horizontes portadores de agua.
- Determinación y cuantificación de las áreas con mayor riqueza acuífera.

El soporte corresponde a los siguientes mapas y diagramas.

- Plano general del área de investigación.
- Contenido de agua en el total de la profundidad estudiada.
- Contenido de agua discriminado por acuífero.
- Perfil transversal de saturación de agua.
- Espesor de las láminas separadoras y potencia de los acuíferos.
- Planos de porosidad común discriminado por acuífero.
- Permeabilidad del agua discriminado por acuífero.
- Plano específico de predicción de fuentes de agua.
- Parámetros hidrológicos de las aéreas de mayor capacidad acuífera y de los acuíferos colindantes.

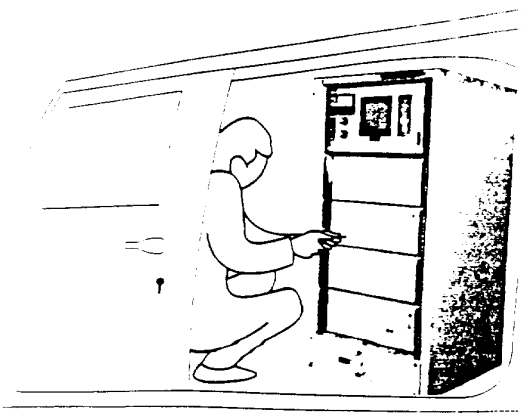

ÁREAS DE LOCALIZACIÓN ESTRUCTURAS DE TOMA

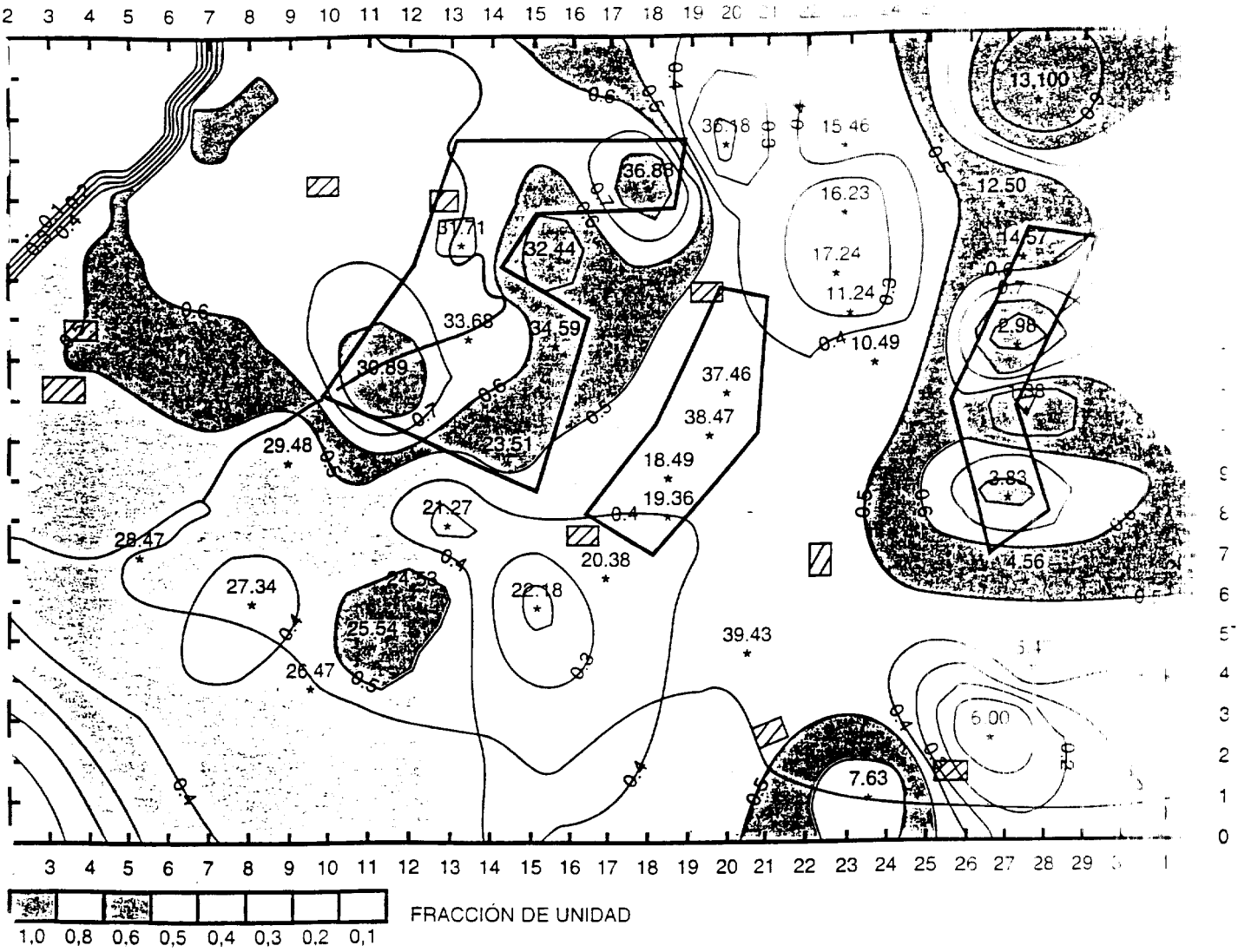

PROSPECCIÓN

Se evaluan las condiciones generales por la interacción de las aguas subterráneas y las aguas superficiales, determinando:

- Principales recursos para la formación de reservas.
- Cuantificación de los recursos y suministro de agua.
- Cálculo de las condiciones de suministro.
- Cálculo mediante modelo de la calidad del agua.
- Cálculo para la explotación de las reservas del agua subterránea.
- Determinación de los ratios de perspectivas de explotación en función de los valores de volúmenes y caudales.
- Parámetros principales para el proyecto de captación de agua.

El estudio incluye descripciones geológicas e hidrológica, trabajos geofisicos mediante HIDROSCOPE a fin de realizar las reco mendaciones oportunas para los trabajos de perforación y para la estructura de captación de agua, Análisis de los problemas investigados y sus posibles soluciones, resultados principales y propuestas de localización para subsecuentes investigaciones hidro-geológicas.

SERVICIOS PRESTADOS

CARTOGRAFÍA E INVESTIGACIÓN HIDROGEOLÓGIA DE LAS FORMACIONES DE AGUA SUBTERRÁNEA.

DETERMINACIÓN DE LOS EMPLAZAMIENTOS PARA LOS ALUMBRAMIENTOS DE AGUA.

PROYECTOS DE SUMINISTRO DE AGUA Y DRENAJES.

INVESTIGACIÓN ECOLÓGICA E HIDROGEOLÓGICA.

MODELACIÓN DE CONDICIONES HIDROGEOLÓGICAS.

DESARROLLO DE SOFTWARE PARA CÁLCULOS DE RECURSOS DE AGUA, INTERFASE SALINIZACIÓN, PREVISIÓN DE CONTAMINACIÓN.

ESTUDIO DE LAS CONDICIONES HIDROGEOLÓGICAS TERRITORIALES CON PROPÓSITOS HIDROLÓGICOS, GEOLÓGICOS, ECOLÓGICOS,...

General Asensio Cabanillas, 15 • 28003 Madrid

ANEXO IV

PMR SOUNDING WITH NUMIS EQUIPMENT

OPERATING PROCEDURE

Version 1.1
February 1998

TABLE OF CONTENTS

PMR SOUNDING WITH NUMIS EQUIPMENT

1. SELECTION OF THE EXCITATION FREQUENCY
2. SELECTION OF THE LOOP SHAPE
3. ESTIMATION OF THE AMPLITUDE OF THE EXPECTED PMR SIGNAL
4. SELECTION OF PARAMETERS FOR DATA ACQUISITION
5. CONTROL OF THE QUALITY OF THE MEASUREMENT
6. OVERVIEW OF THE MEASURING PROCESS
7. SELECTION OF PARAMETERS FOR THE INTERPRETATION
8. LIST OF PROGRAMS SUPPLIED WITH NUMIS SYSTEM

PMR SOUNDING WITH NUMIS EQUIPMENT

OPERATING PROCEDURE

NUMIS system is a PMR equipment fully controlled by a PC computer which makes its operation as automatic as possible.

However, a few tricks have to be known for optimizing the quality of the data and for interpreting the results.

The present document, which gathers various types of information regarding PMR soundings with NUMIS system is a complement of the operating manual and is the base of the training course of the equipment.

MEASUREMENT OF THE EARTH'S MAGNETIC FIELD

- Proton magnetometer: B (nT)
- Larmor excitation frequency: F (Hz) = 0.0426 B(nT)
- Required accuracy on frequency: 1 Hz (20 nT)
- No PMR signal means: (no water) or (wrong frequency)
- Possible difficulty with volcanic rocks

VALIDATION OF FREQUENCY

- Initial value of excitation pulse frequency: F
- Trial sounding: five pulse moments q_1 to q_5

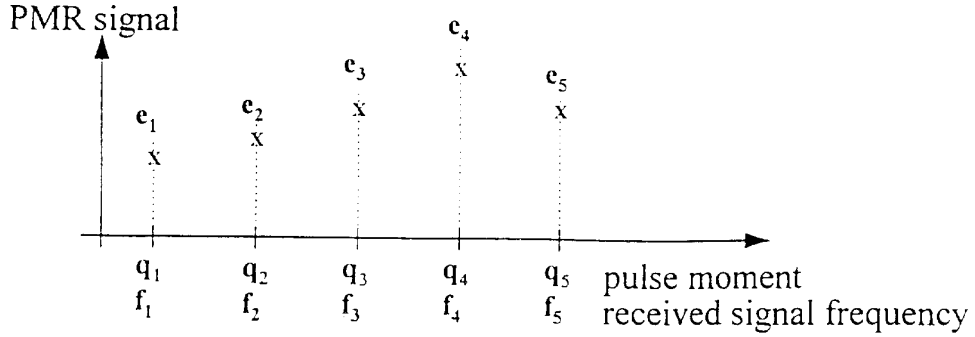

- New value of excitation pulse frequency: F'

  $F' = f_4$ $\quad [e_4 = \max(e_i)]$

  If $|F - f_4| > 1$ Hz $\quad$ F' : new trial sounding

  If $|F - f_4| < 1$ Hz $\quad$ F' : full sounding

1. SELECTION OF THE EXCITATION FREQUENCY

1.1. MEASUREMENT OF THE EARTH'S MAGNETIC FIELD

The PMR theory states that the precession frequency of the H protons depends on the amplitude of the Earth's static magnetic field. The amplitude of the Earth's field varies between 30000 (Equator) to 60000 nT (Pole), which makes excitation frequency varying between 1300 and 2600 Hz [F(Hz) = 0.0426B(nT)]. The horizontal gradient is of the order of 4 nT / N-S km at 45° latitude. It is important to precisely determine the amplitude of the magnetic field for being sure that the protons will be excited at their proper precession frequency. A wrong determination of this amplitude would lead to no PMR signal and to the conclusion that there is no water, while in fact the H protons would not be properly excited.

[GSM-19 GEM overhouser]

A standard proton magnetometer can be used for such Earth's field measurement. The operator must make measurements on various places where the loop has been laid. In case there are some lateral variations of the field; one must take an average of the obtained values. The accuracy required for a good excitation is of the order of ten nanoteslas (a variation of the order of 20 nT in the amplitude of the field corresponds to a variation of 1 Hz in the excitation frequency).

It has to be noted that the Earth's field usually features depth variations of the order of 2 nT / 100m inducing variations in frequency of 0.1 Hz / 100 m. In case of such a standard vertical gradient, there will be no incidence on the measurements. However, in case the gradient is stronger, there can be some significant discrepancies between the value of the Earth's field on the surface and that at depth where the H protons have to be excited. In such a case, some scanning procedure will have to be carried out with NUMIS to confirm the proper excitation frequency (see following paragraph).

In case of difficulty in getting good quality data, it can be advisable to check that the Earth's field amplitude did not change significantly between the beginning and the end of the PMR sounding, which could explain the difficulty in exciting the protons properly.

In case of volcanic rocks background, the Earth's field can be highly variable which makes the application of PMR more difficult. However, it is worthwhile trying to apply the method, even in such environment, as in more than half percents of these cases it is possible to obtain at least qualitative information on the presence of water at depth.

1.2. VALIDATION OF THE FREQUENCY

The value of the Earth's field amplitude has to be introduced in the PC computer so that NUMIS can transmit pulses of current at the corresponding excitation frequency. Once a set of pulses has been transmitted and that the resulting PMR signal has been recorded, NUMIS carries out a frequency analysis of the received signal and determines the base frequency included in this signal. If the difference between the excitation pulse frequency and the received signal frequency is less than 1 Hz, the measurements should be continued without changing the excitation frequency.

NON FAVOURABLE ENVIRONMENT FOR PMR

- URBAN AREAS (high and variable noise)
- SMALL AMOUNT OF WATER (in urban area)
- DEEP AQUIFERS (depth > 100m)
- CLAY STUDY (Time constant < 30 ms)
- VOLCANIC ROCKS (non unique frequency)

If this difference is greater than 1 Hz, it is recommended to take the received signal frequency as the new value for the excitation pulse frequency. If necessary, this adjustment has to be renewed until reaching a stable frequency value for being sure that the H protons are properly excited.

Before starting the full PMR sounding, the excitation pulse frequency should be validated with various values of the pulse moments. If, during this investigation, it appears that the received signal frequency slightly varies with the value of the pulse moment (Earth's field gradient effect), the value of frequency which should be validated for the PMR sounding is that giving the highest amplitude of the received signal, among the whole set of pulse moments investigated.

At this stage, it should be noted that, if there is no or very little water on the site surveyed, it will be hard to validate a frequency, as the amplitudes of all the received signals will remain low for all the pulse moments. In that case, one should look carefully at the amplitudes of the signals having a frequency close (at plus or minus a few hertz) to the frequency determined from the measurement of the Earth's field on the surface.

In case no signal can be detected and if there is no volcanic rock around, the conclusion should be that there is indeed no water in the area investigated.

STANDARD LOOP SHAPE

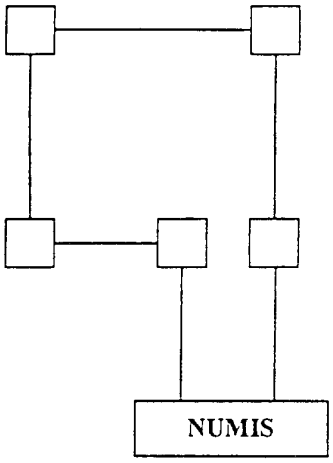

75 m side square loop

- Noise: N
- Signal: S
- N < 1500 nV => shape OK
- Maximum investigation depth: 100 m

FIGURE OF EIGHT LOOP SHAPE

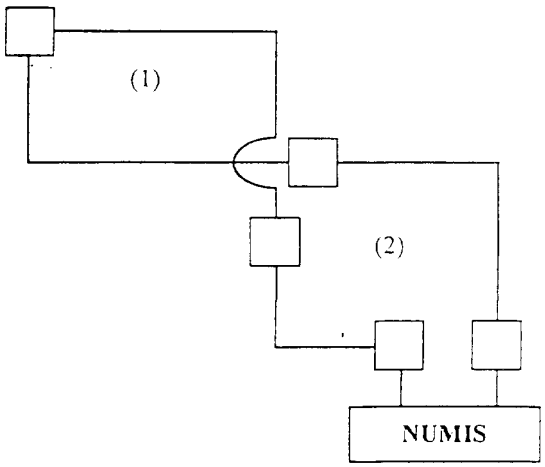

37.5 m side figure eight square loop

- Noise: $N = n_1 - n_2 \approx \varepsilon$
- Signal: $S = s_1 - (-s_2) \approx 2s$
- Shape optimization until $\varepsilon < 10\%$ initial noise
- Maximum investigation depth: 50 m

2. SELECTION OF THE LOOP SHAPE

2.1. STANDARD SHAPE

The NUMIS system is supplied with a 300 m length cable in four reels of 75 m each. The basic loop configuration which is recommended in the square shape with 75 m side. The size of the loop influences the depth of investigation which is of the order of 80 to 100 m with a 75 m square configuration.

2.2. FIGURE OF EIGHT SHAPE

If the ambient noise measured by NUMIS is greater than typically 1500 nV, the PMR measurement can be very difficult except if there is a lot of water.

In such a noisy condition, the operator can select a figure-of-eight loop configuration which consists in two adjacent small squares of 37.5 m side each.

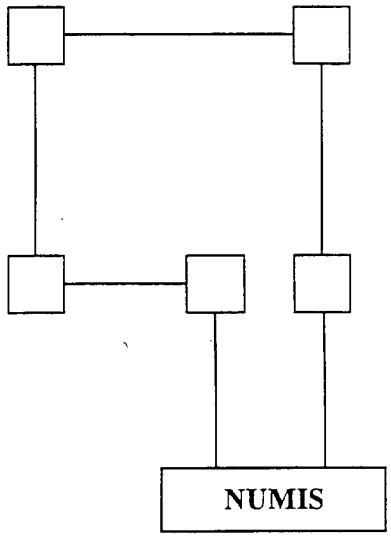

75 m side square loop

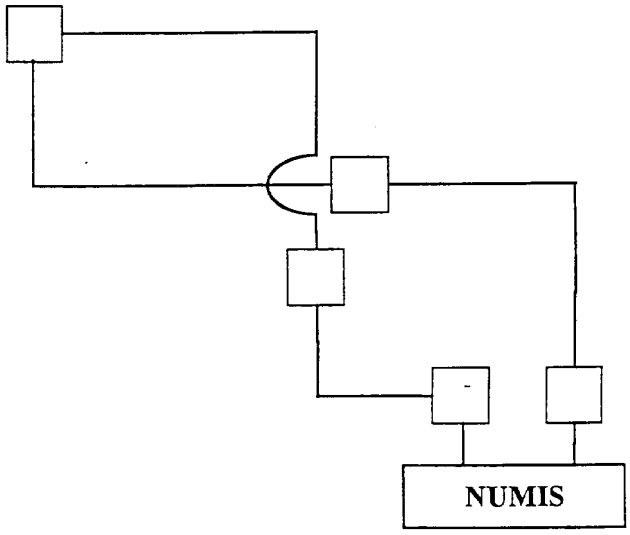

37.5 m side figure eight square loop

The aim of this figure-of-eight configuration is to drastically reduce the noise level, thanks to the fact that the noise will be almost similar on the two small squares (NUMIS will only measure the difference of noise between these two squares), while the PMR signals of both squares will be added (NUMIS will measure the difference of two PMR signals obtained with opposite excitation magnetic moments).

ORIENTATION OF THE FIGURE OF EIGHT LOOP

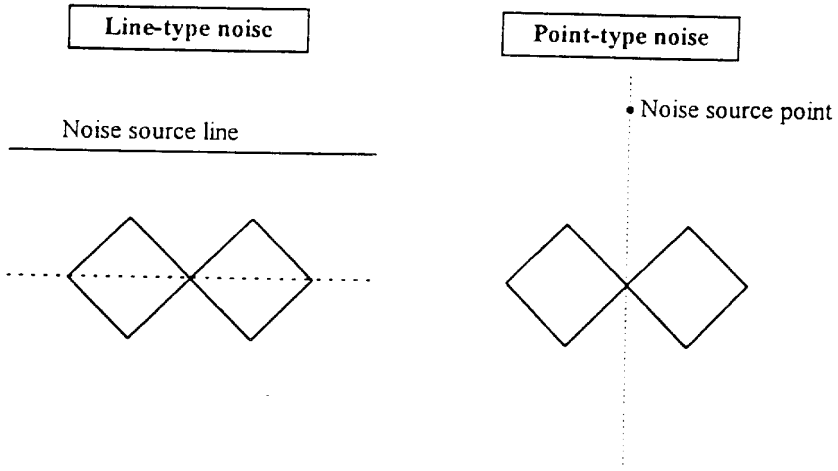

NOISE CHARACTERISTICS

- Change with time and with place
- Natural noise : MT signals
- Cultural noise : 50 or 60 Hz, and Harmonics (2n+1, 2n)

  Trains, Industries, Telecommunications

It is usually possible to reduce the noise by a factor of 10 compared to the 75 m side square loop. If, after having set up the figure-of-eight loop, the noise is stronger than the expected new value, it is recommended to slightly move the central wires of the figure-of-eight loop so as to increase the surface of one of the small squares (and consequently to reduce the surface of the other one). By successive moves, it is possible to minimize the resulting noise and generally to reach this 10 times improvement.

The drawback of this figure of eight configuration is that the depth of investigation is limited to about 40 m instead of 80 m for the large square. It also has to be noted that the volume investigated will not be the same in the two configurations, due to the different structures of the excitation fields in both cases.

When the noise is expected to mainly come from one electric power line, it is recommended to set up the figure-of-eight loop parallel to this line so that both small squares receive the same magnetic field from the power line.

If the noise is expected to mainly come from one localized point (immerged pump, ...), it is recommended to set up the figure of eight loop symmetrically with respect to this point.

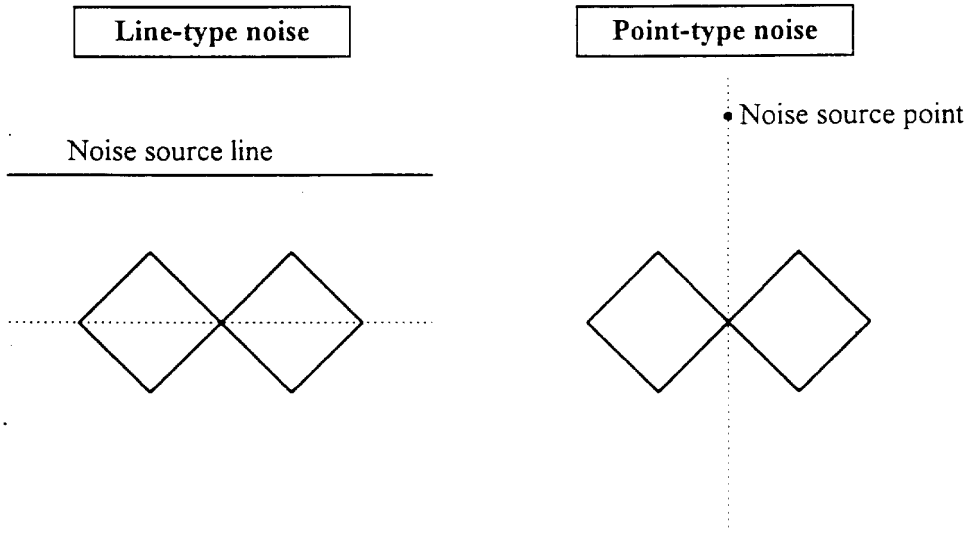

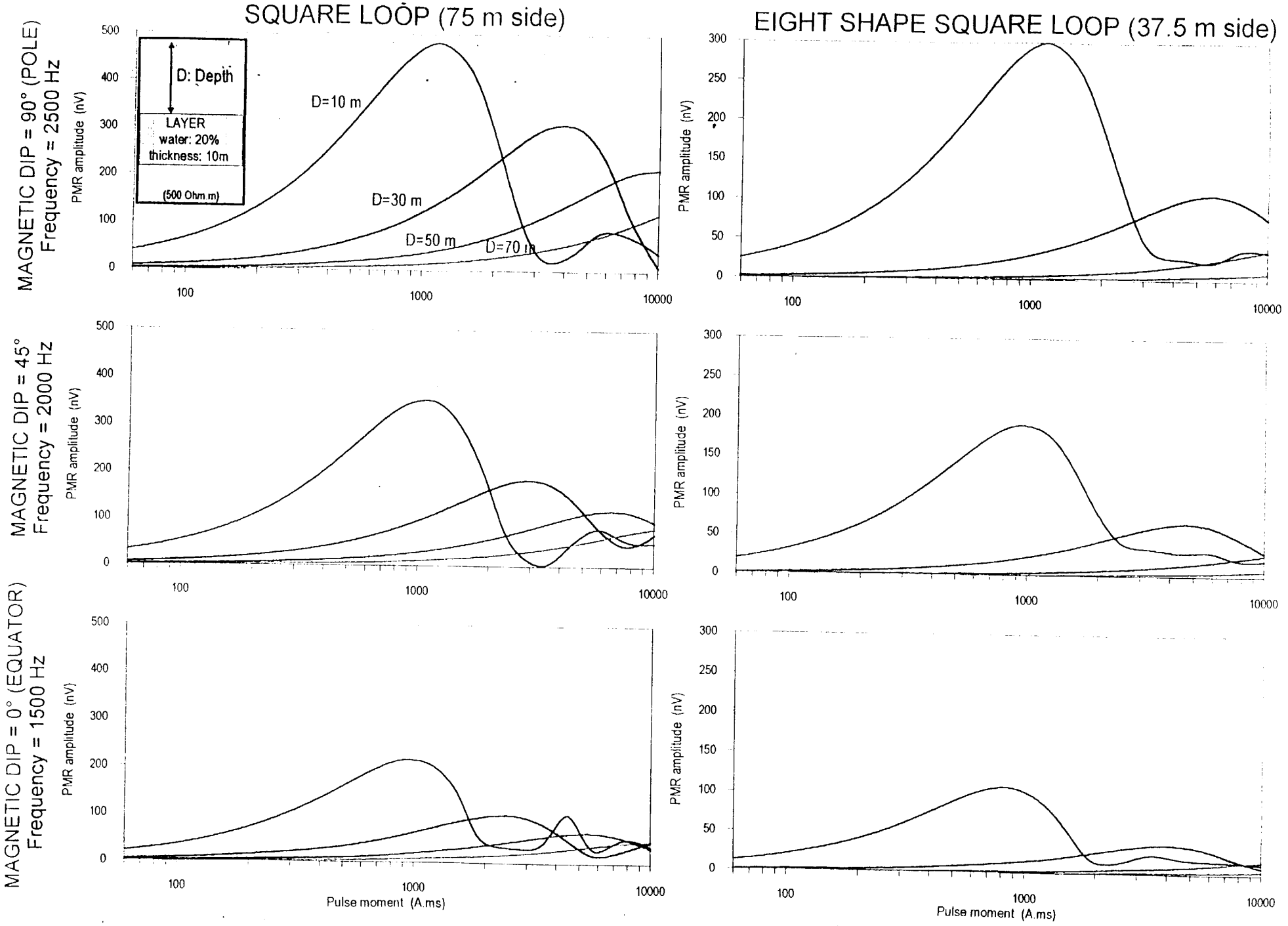
SQUARE LOOP (75 m side)
EIGHT SHAPE SQUARE LOOP (37.5 m side)
MAGNETIC DIP = 90° (POLE)
Frequency = 2500 Hz
MAGNETIC DIP = 45°
Frequency = 2000 Hz
MAGNETIC DIP = 0° (EQUATOR)
Frequency = 1500 Hz
PMR amplitude (nV)
D: Depth
LAYER
water: 20%
thickness: 10m
(500 Ohm.m)
D=10 m
D=30 m
D=50 m
D=70 m
100
1000
10000
Pulse moment (A.ms)

3. ESTIMATION OF THE AMPLITUDE OF THE EXPECTED PMR SIGNAL

3.1. PMR SIGNAL AMPLITUDE AND NOISE LEVEL

When some geological data are available in the prospected area (such as an idea of the depth and the thickness of the aquifer layer, and its porosity) it is useful to have a rough estimation of the amplitude of the PMR signal it is reasonable to expect from NUMIS measurements.

This amplitude may be compared to the ambient noise level which will be given by NUMIS at the beginning of the measuring process. The number of stacks necessary to detect and measure the PMR signal can then be estimated from these two values (see § 3.3)

It is also important to know for which pulse moment values the PMR signal will give its highest amplitudes for each loop shape. The knowledge of these values permits to decide wether the standard square shape (75 m side) is necessary or if the figure of eight square shape (37.5 m side) may be sufficient in terms of depth of investigation.

It is also useful to know which pulse moment gives the highest PMR amplitude for using this pulse moment as the trial pulse moment when the noise has a high level compared to the signal, so as to confirm the value of the frequency to use for the whole PMR sounding.

3.2. PMR MASTER CURVES

The here attached figure gives the PMR response of a 10 m thick water layer (with 20 % water), for various depths, for three Earth's field inclination (Equador, 45°, Pole) and for both loop shapes (Square and Eight shape square).

As the PMR signal is a linear function of the water content, the previous curves can be used to determine the response of other water contents than the one used for computing them (20 %). For instance for a water content of the layer of 10 % the previous curves have to be reduced in amplitude by a ratio of two.

It has to be noted that when the ground is conductive the depth of investigation can be reduced up to 30 % and that the amplitude of the PMR response can be attenuated of the order of 30 % too.

RANGE OF MEASUREMENT

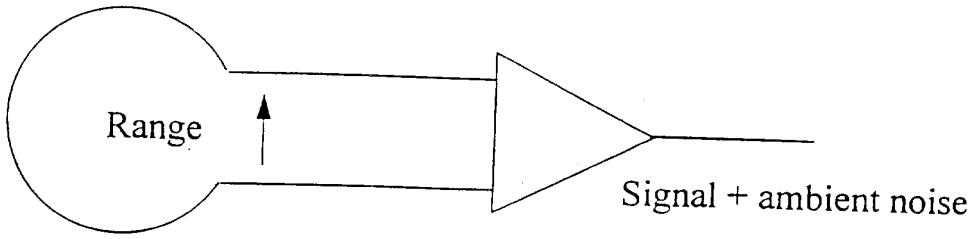

- **Range Max = 60 000 nV**
- **Range Min = 500 nV**
- **Select range = 4 x ambient noise**
- **Default range value = 30 000 nV**

INTERVAL OF RECORDING PULSE DURATION

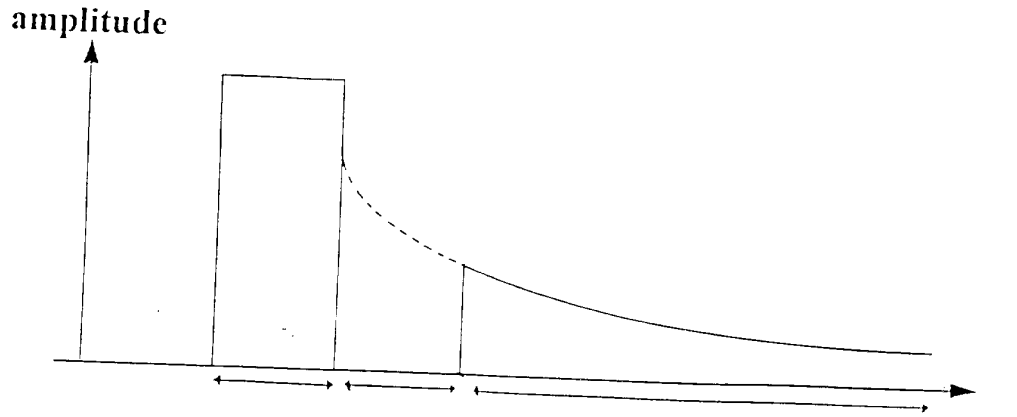

PULSE DURATION	DELAY TIME	INTERVAL OF RECORDING
40 ms	35 ms	250 ms : default
Default	Fixed	500 ms, 1000 ms: others

4. SELECTION OF PARAMETERS FOR THE ACQUISITION

Beside the frequency of the excitation pulse (see §1.2), a few parameters have to be selected by the operator before starting the measurements.

4.1. THE RANGE OF MEASUREMENT (nV)

This represents the highest value which will be measurable by NUMIS without overload effect. It can be set between 60 000 nV and 500 nV. Usually, the noise measured after the analog filtering ("ambient noise") is higher than the PMR signal itself detected after analog and digital filtering. It is recommended to take a range value of four times the ambient noise. The reason of this coefficient is that the ambient noise value given by NUMIS is an averaged value and that spikes noise values may be higher than averaged noise values. In case no information is available on the noise of the site, the value of 30 000 nV can be taken for first test, and modified afterwards. Each time this value is modified the full measuring process is re initialized.

However, during the measurement, it is possible to change the graphic scale of the amplitude curve (decay PMR signal versus time) without stopping the measurement. This graphic scale may be set from the range of measurement down to 100 nV by factor of 2 steps.

4.2. THE INTERVAL OF RECORDING (ms)

This parameter has to be set in relation with the expected time constant of the PMR signal. Usually, 250 ms can be taken as standard, while 500 ms can be taken when long time constant are expected such as in karzt aquifers. The interval of recording influences the duration of the recording and, to save acquisition time, the operator has to select this parameter in relation with what is really needed.

4.3. THE PULSE DURATION (ms)

The pulse duration has to be set up at 40 ms for a standard PMR measurements with T_2^* determination.

4.4. THE NUMBER OF PULSE MOMENTS

The standard value of pulse moments for a complete PMR sounding is 16. The values of these moments are automatically selected by the program between 30 A.ms and 9000 A.ms. Before starting the full sounding, it is advisable to carry out a preliminary sounding with, for instance, just 5 pulse moments, so as to confirm that the pulse frequency selected is the proper H atom excitation frequency (see §1.2).

NUMBER OF PULSE MOMENTS AND STACKS

- Number of pulse moments : . 5 for trial sounding
  . 16 for full sounding
- Number of stacks:

AMBIENT NOISE	SIGNAL AMPLITUDE		
	30 nV	100 nV	300 nV
200 nV	64	32	16
500 nV	128	64	32
1 000 nV	256	128	64

SIGNAL/NOISE RATIO ~ (STACK NUMBER)$^{1/2}$

4.5. THE NUMBER OF STACKINGS

This number depends on the signal-to-noise ratio. It has to be selected as a compromise between the quality of the measurement and the total duration of the sounding. There is no absolute rule, but the following table gives an estimation of what can be used as the number of stacks for a first sounding in an unknown area.

AMBIENT NOISE	SIGNAL AMPLITUDE		
	30 nV	100 nV	300 nV
200 nV	64	32	16
500 nV	128	64	32
1 000 nV	256	128	64

Recommended number of stacks for an unknown area

If during the acquisition some noise spikes occur with an amplitude greater than the "range of measurement" set by the operator, there will be an overload, but this stack will be considered as a "bad stack" and will not be taken into account in the average. If 32 stacks have been asked per pulse moment, the program will wait for 32 "good stacks" before moving to the next pulse moment value.

At any time during the stacking process, the operator can ask for a PAUSE for freezing the data being acquired. This procedure has to be used for instance when a car is approaching the loop, which causes a strong EM noise. Once the operator decides to resume the measuring process measurement, the acquisition process continues smoothly without any loss of previously acquired data.

CONTROL OF THE QUALITY OF THE MEASUREMENT

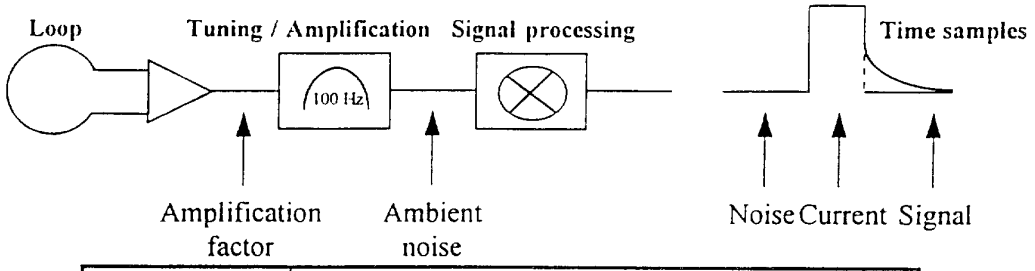

Synchronous detection	Noise	Current	Signal
Amplitude and phase			
Stacking	Stacked noise		Stacked signal

THE STACKED SIGNAL AND NOISE

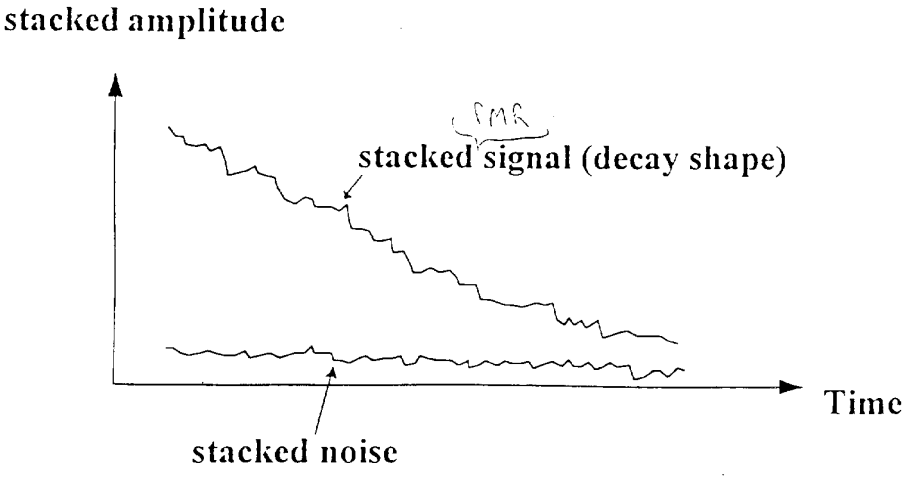

Theoretical shapes of the envelopes of the stacked PMR signal and of the stacked noise versus time.

5. CONTROL OF THE QUALITY OF THE MEASUREMENT

A few parameters are available to check that the measurements are going on properly:

5.1. THE AMPLIFICATION FACTOR

This parameter given by NUMIS before starting the pulse transmission permits to confirm that the loop is well connected. The amplification factor is linked to the inductance of the loop and should be in any case greater than 5000. It depends on the loop shape and dimensions, on the wire diameter and on the resistivity of the ground. The amplification factor is of the order of 30000 for a 75 m side square loop over a 100 Ωm medium.

5.2. THE AMBIENT NOISE (nV)

The ambient noise is the average value of the total signal coming out from the loop (noise + PMR signal) and filtered by the analogue part of NUMIS, measured at the level of the ADC converter. It corresponds to a frequency band which is of the order of 10 to 20 Hz depending on factors such as loop inductance, tuning etc, ... This parameter is a good indication for confirming that the square shape loop is convenient or if it is recommended to use a figure-of-eight square shape loop. It also permits to have an idea of the number of stacks which will be necessary for measuring the PMR sounding (see §3.5).

5.3. THE STACKED SIGNAL (nV) AND THE STACKED NOISE (nV)

While the ambient noise is measured in the frequency width of the analog part of NUMIS, the stacked noise is measured after digital processing and is also really comparable with the stacked signal. The stacked noise is measured just before the current excitation pulse, the stacked signal being measured just after this pulse. The fact that the stacked signal amplitude becomes greater than the stacked noise amplitude during stacking and shows a decay shape is, of course, an indication of the detection of a PMR signal and of the presence of water.

The curves plotted on the screen of the PC are the envelops of the instantaneous readings, that is without the frequency carrier wave.

The noise may come from industrial or natural sources (MT signals). One important source of natural source is the power lines which carry 50 Hz or 60 Hz currents. The harmonies of these frequencies due to the non perfect shapes of the currents and to transient effects can be observed in the frequency range of the PMR signals : the odd harmonics (such as 2000, 2100 Hz etc for 50 Hz and 2040, 2160 Hz for 60 Hz) are stronger than even harmonics (such as 1950, 2150 Hz for 50 Hz and 1980, 2100 Hz for 60 Hz).

THE STACKED PHASE

- Excitation pulse frequency = F
- Received signal frequency = f
- $\Delta F = F - f$
- After synchronous detection:

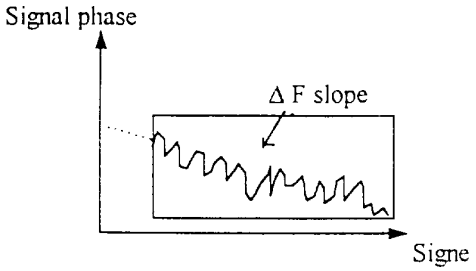

Linear type curve

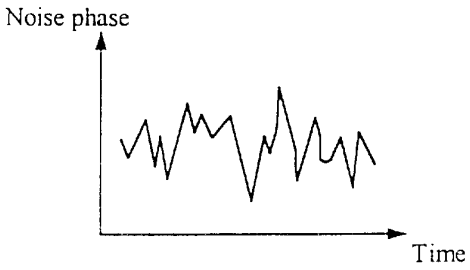

Random type curve

5.4. *THE STACKED PHASE (DEGREES)*

The phase measured by NUMIS is the phase between the excitation current and the relaxation signal. It is measured for each individual time sample during the record interval. The phase is measured for both the signal (after the pulse) and the noise (before the pulse). As the noise has no reason to have a phase relation with the excitation current, the stacked noise phase should be a random function of time, while the stacked signal phase should be a linear function of time, slightly altered by noise.

In case the frequency of the relaxation signal is exactly the same as the excitation current, the stacked signal phase should be constant with time (horizontal straight line).

If there is some discrepancies between these two frequencies, the stacked signal phase should be a linear function of time (increasing or decreasing, according to advance or delay difference).

The observations on the screen of the linear property of the stacked signal phase with time during the acquisition, while the stacked noise phase remains random, is a good criteria of quality of signal.

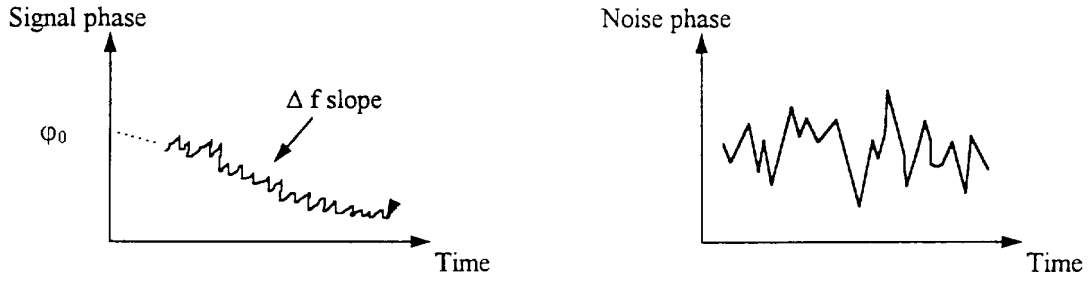

GENERATION OF THE CURRENT

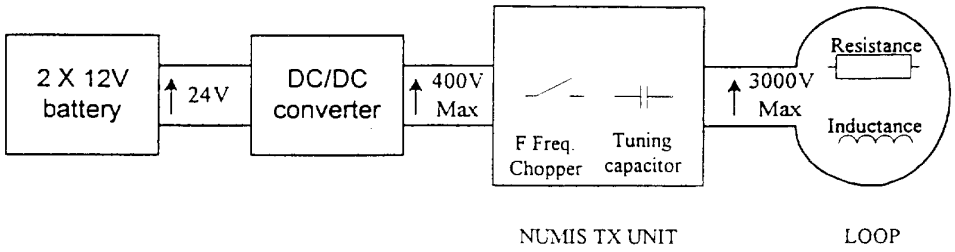

Capacitor + inductance + resistance = Resonant circuit

MAXIMUM PULSE MOMENT VERSUS CONDUCTIVITY AND LATITUDE

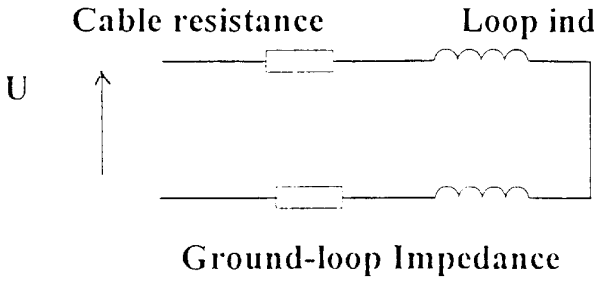

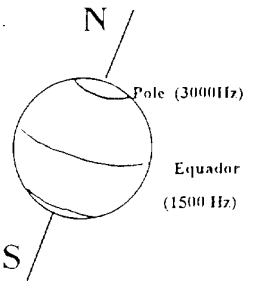

GROUND	Maximum Pulse Moment (75 m side square loop)		
	Moderate latitude (2 kHz)	Equator	Poles
Resistive	9 000 - 10 000 Ams	+ 20 %	- 20 %
Conductive	7 000 - 8 000 Ams		

6. OVERVIEW OF THE MEASURING PROCESS

6.1. GENERATION OF THE CURRENT

The transmitting antenna of the NUMIS system consists in a 300 m cable loop laid on the surface of the ground. This loop has a resistance of 0.2 Ω and an inductance of the order of 0.6 mH which depends on the precise loop geometry and on the resistivity of the ground.

To increase the current available for a given voltage, a tuning is carried out by placing capacitors in series in the loop. For each value of the excitation frequency which depends on the amplitude of the Earth's magnetic field, there is a value of the capacitance which leads to the loop resonance. This tuning which is carried out manually by the operator with screws located in the back of the system, is designed by steps of the order of 70 Hz at a 2 kHz frequency.

The overvoltage coefficient obtained with such a tuning is of the order of 8, and permits to reach currents of 300A for a maximum output voltage of 3000 V. The voltage of the excitation pulse is controlled through the value of the DC/DC converter output voltage which ranges from a few volts to a maximum of ±400V.

6.2. RELATION BETWEEN PULSE MOMENT, CONDUCTIVITY AND LATITUDE

When the ground is very resistive in the first ten meters under the loop, the mutual coupling between the ground and the loop is very low, and the total impedance of the loop (cable resistance + loop inductance + ground loop impedance) is minimum. In such a case the maximum pulse moment can be as high as 9 000 to 10 000 Ams for the 75 m side square loop (2kHz frequency). When the ground under the loop is conductive, the mutual coupling between the ground and the loop is high and the total impedance of the loop is large. In a 20 Ωm resistivity , the maximum pulse moment can be no greater than 7 000 to 8 000 Ams for the 75 m side square loop.

Near the Equator, the Earth's Magnetic field has its lowest amplitude (typically 30 000 nT), the Proton Precession Frequency is low (typically 1 500 Hz) and the total impedance lower than at moderate latitudes. The maximum pulse moment can be as high as 12 000 Ams. In opposite, the maximum pulse moment near the Poles can be no greater than 5 000 Ams.

MEASUREMENT OF THE SIGNAL

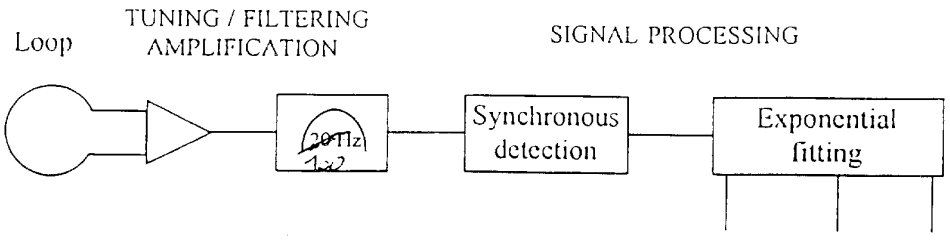

Total maximum gain: 10^6 (filtering + amplification)

Filtering = Tuning on frequency F selected by the operator

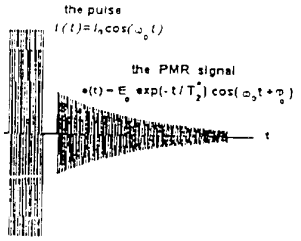

CYCLE OF MEASUREMENT OF A PMR SOUNDING

- **ONE AUTOMATIC PMR SOUNDING (1 HOUR 1/2) WITH 250 ms PULSE DURATION INCLUDES:**
  - **16 pulse moments from 200 to 8000 A.ms**
  - **32 stacks each pulse moment**

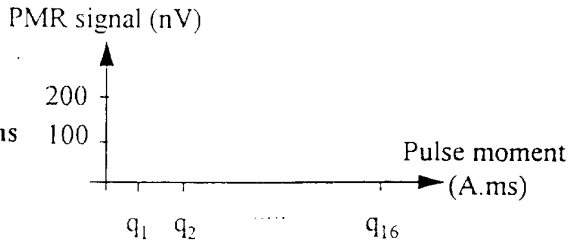

- ONE STACK (10 SECONDS) INCLUDES:
  - Charge of capacitors
  - Noise measurement
  - Current measurement
  - Signal measurement
  - Data transmission to PC computer

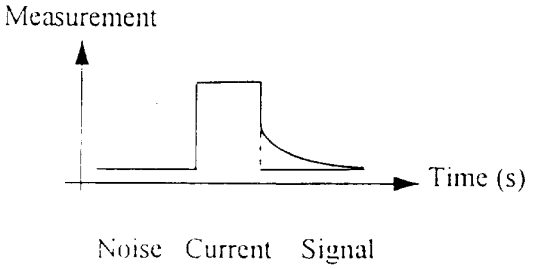

6.3. *MEASUREMENT OF THE SIGNAL*

The same loop is used for transmitting the excitation current and for measuring the relaxation signal. After the current is switched off, a relay (which can be heard) connects the loop to the receiver part of NUMIS. A calibration procedure is carried out, followed by an automatic tuning with a bandwidth of the order of 100 Hz. This tuning consists in connecting capacitors so as to make the frequency introduced by the operator the central frequency of the analogue filter of the receiver. Then, the received signal is amplified with a gain which is related to the maximum signal amplitude introduced by the operator into the PC (see § 3.1). The ambient noise amplitude is determined at this stage of circuits.

A fixed delay time of 35 ms is used after each pulse for discharging the loop and to permit to electronic circuits to switch from the Tx position (3 000 V max) to Rx position (down to 10 nV).

A stacking is carried out for the noise (before the pulse), the current (during the pulse) and the signal (after the pulse). Then, a synchronous detection is performed for measuring the signal and the noise, the current being used as the phase reference.

Finally, a fitting algorithm is used for determining the intercept and the time constant of the exponential which best represents the PMR decay signal. Signal levels as low as a few tens nanovolts can be measured thanks to the sensitivity and low noise of the analog circuits of NUMIS and to the dedicated signal processing applied on data time series.

6.4. *CYCLE OF MEASUREMENT OF A PMR SOUNDING*

A PMR sounding starts by the lowest pulse moments (shallow investigation) and finishes by the highest ones (deeper investigation).

Each pulse moment is stacked the number of times indicated by the operator during the setup stage.

A cycle of measurement for one stack includes the following steps: charge of capacitors, noise measurement, current pulse generation, delay time for switching from Tx to Rx position, signal measurement, data transmission from NUMIS CPU board to the PC computer. One stack with a pulse duration of 250 ms takes an average of 8 seconds time, which represents a total time of 1 hour and a quarter for a sounding including 32 stacks of 16 pulse moments.

At the end of the full cycle, the capacitors are discharged for preventing any further misoperation, which produces a jerky sound during about 20 seconds.

FORWARD PROBLEM

$$E = E_0 \exp(-t / T_2^*) \sin(2\pi f_0 t + \varphi_0) \qquad f_0 = H_0 \ \gamma / 2\pi$$

$$E_0 = \int_v 2\pi f_0 H_\perp(r) M_0 f(r) \sin\left(\frac{g}{2} H_\perp(r) q\right) dv$$

- The PMR signal is NON LINEAR with respect to the current (q = It). Doubling the current does not double the signal but increases the depth of investigation.
- But the PMR signal is LINEAR with respect to the water content f(r).

PMR MATRIX

- After 1D discretization, [E(q)] = [M(z,q)] [f(z)]
- M(z,q) is a n x m matrix, with:
  - n: number of layers at depth (100)
  - m: number of pulse moment values (100)
- Each (i,j) element is the contribution:
  - of the i th layer
  - to the total PMR signal
  - for the j th pulse moment
- For inversion: $[f(z)] = [M(z,q)]^{-1} [E(q)]$

  For a 16 pulse moment sounding, the inversion will be carried out on a 16 x 16 matrix, after interpolation in q and integration in z of the elements of the initial 100x100 matrix.

7. SELECTION OF PARAMETERS FOR THE INTERPRETATION

7.1. PARAMETERS FOR THE MATRIX

Before inverting data, it is necessary to compute a matrix which takes into account various local parameters related to the surveying area:

- Antenna shape and size.
- Frequency (a rough estimation is sufficient, such as 2 000 or 2 500 Hz etc ...)
- Inclination of the Earth's magnetic field (a rough estimation is sufficient too, such as 50 or 60 ° etc...).
  The maximum depth of investigation required. This parameter which depends on the loop size and on the depth of the geological target influences the resolution in depth, and also the computation time.
- The resistivity of the ground ; the model can be homogeneous or stratified. The resistivity of the ground influences the depth of investigation since the excitation field is attenuated at depth when the ground is conductive. Errors of the order of 30% in depth can be introduced if the resistivity is not properly estimated. The phase value given by NUMIS can help to know whether the ground is conductive or not ; however, no quantitative estimate is yet available.

The computation of the matrix takes of the order of one day time, but one matrix can be used for the interpretation of several PMR soundings as the local parameters do not usually change significantly in a given local survey area.

The matrix consists in a n x m array where:

- n is the number of layers (n = 100). The thicknesses of the layers depend on the maximum depth of investigation required ; they are pseudo logarithmicly spaced.
- m is the number of pulse moments (m = 100). The values of the pulse moments depend on the depths and thicknesses of the layers and are selected in relation with the amplitude of their responses with respect to the layers.

Each (i.j) element of the matrix represents the contribution of the i th layer to the response of the j th pulse moment value to the total PMR signal measured.

The matrix is computed with 100 x 100 elements for a high accuracy. During the inversion itself, an interpolation will be carried out for fitting the proper number of pulse moments used during the sounding.

PARAMETERS FOR INVERSION

Signal length : for suiting to time constant of the signal

- Time constant for filtering: 5 to 40 ms

  For smoothing raw data in case of noise
- TIKHONOV INVERSION :

  Minimization of $[E] - [M][f] + \alpha[\delta[f]/\delta z]^2$

  The regularization coefficient α permits to stabilize the solution in case of noise :

α	Regularization	Type of solution authorized
0	None	Many thin aquifer layers
100 000	Strong	Basically, one aquifer layer, with smooth depth-dependant variations

INVERSE PROBLEM

- (Water content) = $(Matrix)^{-1}$ x (PMR signal)
- The adjustment of the model to the data is carried out on time samples series (Inversion time: about 10 seconds)

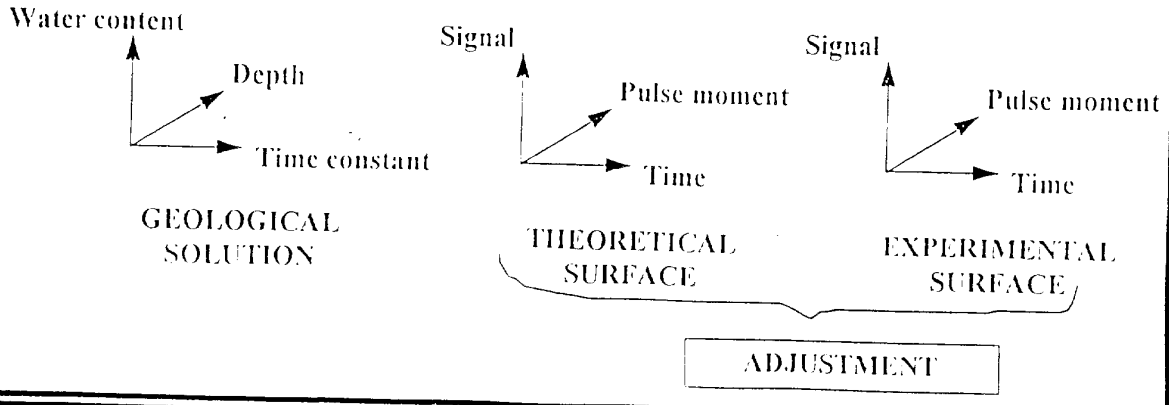

7.2. *PARAMETERS FOR THE INVERSION*

Once the matrix of the base model has been computed, the solution (water content and time constant versus depth) corresponding to a set of experimental sounding data is quick to obtain by inverting a linear system, since the PMR theory states that there is a linear relation between the measured PMR signals measured on the surface of the ground and the water contents of the layers at depth. The inversion takes in the order of 10 seconds.

A few parameters are asked to the operator before the inversion starts:

- The signal length: the inversion can be made with the total interval of recording selected during the acquisition, but can also be made with a smaller length.

  The time constant for filtering (5 to 40 ms): raw data can be post processed to recompute signal amplitude and time constant. Depending on noise level during the acquisition, it can be useful to filter the raw data for a smoother water content versus depth solution.

- The regularization coefficient: when inverting noisy data, the algorithm can be unstable and can determine a very unsmooth solution. For this reason, a regularization is available, which consists in minimizing the water content contrast between two adjacent layers (that is to say smoothing the solution) when the data are noisy.

This regularization can be made in two modes:

- Automatically: in that case the program sets the coefficient by itself through an estimation of the noise in the data.
- Manually: in that case the operator has to give a value for this regularization coefficient which has to be a positive number. A zero value means that there is no regularization ; a value of 5 000 is proposed as the standard value of this manual option.

The filtering time constant and the regularization coefficient are parameters which can modify significantly the final solution from low spatial frequency solutions (smooth vertical contrasts) to high spatial solution (large vertical contrasts). In particular, the solutions can change from one aquifer layer to two or more aquifer layers depending on the values of these coefficients. Modifying these coefficients may help estimating the equivalence rules in PMR in relation with the noise level of the experimental data.

As for all other geophysical methods, it is not possible to decide which one of all equivalent solutions is more true unless other geophysical or geological data is available.

REMARKS ON PMR METHOD

- Directly measures the presence of water at depth.
- UNIQUE method for groundwater exploration.
  All other methods are undirect methods.
- PMR as well as all other geophysical methods presents several hydrogeological solutions for one set of data due to EQUIVALENCE RULES.

GPH METHOD	DIRECT	INDIRECT	EQUIVALENCE 1 Exp. Data Set =
PMR	Water content		several
OTHERS		Physical parameter	1 D solutions

INTERPRETATION OF THE TIME CONSTANT

- TIME CONSTANT ⇔ PORE SIZE ⇔ PERMEABILITY

Decay time	Water containing strata
< 30	sandy clays
30 - 60	clayey sands, very fine sands
60 - 120	fine sands
120 - 180	medium sands
180 - 300	coarse and gravelly sands
300 - 600	gravel deposits
600 - 1000	surface water bodies

- NUMIS delay time : 35 ms
- Noise time constant : often 1 000 ms

7.3. *INTERPRETATION OF THE TIME CONSTANT*

For each measurement corresponding to a given pulse moment, the time constant of the decay is computed and displayed (in ms).
During the inversion, a time constant is computed for each layer at depth and is displayed together with the water content of the layer.
The time constant is linked to the mean pore size of the layer, and hence, to the permeability of this layer. The following table gives the decay time (time constant) values for various types of water bearing layers :

Decay time (ms)	Water containing strata
< 30	sandy clays
30 - 60	clayey sands, very fine sands
60 - 120	fine sands
120 - 180	medium sands
180 - 300	coarse and gravelly sands
300 - 600	gravel deposits
600 - 1000	surface water bodies

Layers featuring low decay times will be poorly productive in terms of water resources as their sediments have small pore sizes, while those featuring long time constants will provide interesting water yields.

It has to be noted that NUMIS system has a delay time of 35 ms after the pulse current has been switched off. This means that short decay times layers (typically less than 40 ms), will not provide a detectable PMR signal.

During the exponential fitting procedure, the decay time is limited to a maximum value of 1 000 ms which corresponds to the decay time of free water such as river or lake. In case of a strong noise (when the amplitude of the PMR signal is of the same order as that of the noise), no decay can be observed, and the resulting decay time is often 1000 ms. Of course, when no decay can be observed on the curve acquired, the time constant determined by the fitting algorithm has no hydrogeological meaning. Interpreting the decay time requires to have a PMR signal with a significant amplitude compared to the noise.

USER'S PROGRAMS

PROGRAM NAME	PLATFORM	FUNCTION	FILE CREATED
NUMIS ACQUISITION	Windows 95	Data acquisition	• #: raw data • inp: synthesis
NUMIS INVERSION	Windows 95	Data inversion	• inr: synthesis • out: results
NMR97_4C	DOS	Matrix computation	NMR_MC.DAT

EXPERIMENTAL DATA FILES

◆ RAW STACKED DATA

"File .1" Time series for q_1 moment

"File .2" Time series for q_2 moment

. . .

. . .

. . .

"File .16" Time series for q_{16} moment

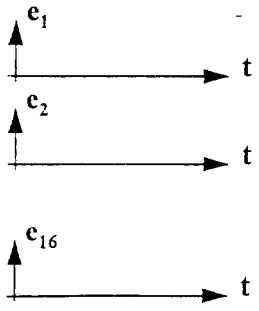

◆ SYNTHETIC DATA "File .inp" Sounding curve

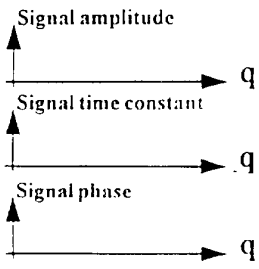

8. LIST OF PROGRAMS SUPPLIED WITH NUMIS SYSTEM

8.1. USER'S PROGRAMS

The following programs are the user's programs for the day-to-day operation of the system.

PROGRAM NAME	PLATFORM	FUNCTION	FILE CREATED
NUMIS ACQUISITION	Windows 95	Data acquisition	• #: raw data • inp: synthesis
NUMIS INVERSION	Windows 95	Data inversion	• inr: synthesis • out: results
NMR97_4C	DOS	Matrix computation	NMR_MC.DAT

Remarks:

A) NUMIS ACQUISITION software controls the whole operation of the NUMIS system during the measurement. For a 16 pulse moment sounding which the operator would have called "TEST" during the setup phase of the measurement, the following files will be created at the end of the acquisition:

* Sixteen "TEST.#" files, with # ranging from 1 to 16, where all the information including the time series (raw data) will be included, one pulse moment value per file.
* One "TEST.inp" file, including the synthetic data of the sounding: signal amplitude, signal time constant as a function of the pulse moment values.

* These various files are automatically stored on the hard disk of the PC computer. After each day of measurement, it is recommended to copy these files on mobile disks. One 1.4 Mo disk can store two PMR sounding data with 16 moments of 250 ms record interval each.

B) NUMIS INVERSION software reprocesses the raw data with the filtering time constant given by the operator. Consequently, this software has to use the "TEST.#" raw data files created by NUMIS ACQUISITION software. At the end of the inversion, NUMIS INVERSION software creates two types of files:

* One "TEST.inr" file, which has the same structure as the "TEST.inp" file, but contains the synthetic information after reprocessing (filtering) of the raw data.
* One "TEST.out" file, which contains the information related to the inversion of the data: water content and time constant of each layer at depth, synthetic experimental data.

HARDWARE CONTROL PROGRAMS

PROGRAM NAME	PLATFORM	FUNCTION	FILE CREATED
CAPFORM	Windows 95	Capacitor formation	None
NUM_TEST	DOS	Hardware test	NUM_TEST.dat
NUM_REMD	DOS	Hardware test (complement)	NUM_REMD.dat

C) NMR97_4C software computes the matrix which is necessary for inverting the raw data. At the end of the computation, the coefficients of the matrix are stored in a file called NMR_MC.dat. It is recommended to rename this file to make its characteristics more explicit (see operating manual of the software).

8.2. HARDWARE CONTROL PROGRAMS

The following programs are technical programs which have to be used only in special cases.

PROGRAM NAME	PLATFORM	FUNCTION	FILE CREATED
CAPFORM	Windows 95	Capacitor formation	None
NUM_TEST	DOS	Hardware test	NUM_TEST.dat
NUM_REMD	DOS	Hardware test (complement)	NUM_REMD.dat

Remarks:

A) CAPFORM program (7 hours operation) has to be used to reformat the energy capacitors when the system has not been used for more than one month.

B) NUM_TEST program (10 minutes operation) has to be used when the NUMIS system is supposed to have some hardware trouble. The NUMIS has to be connected to the small test loop supplied with the system. The program creates a file NUM_TEST.dat which can be read by any text editor and contains the results of various technical tests. The OK sign at the end of each line confirms that the test is successful.

C) NUM_REMD program (20 to 30 minutes operation) is a complement of NUM_TEST program and contains a more detailed file NUM_REMD.dat, which has to be send back to IRIS INSTRUMENTS Sales Service Department for further diagnosis.

DESCRIPTION OF NUMIS RAW DATA FILES (1 file per pulse moment)

A1 - clock frequency (Hz)
A2 - phase shift of the generator (degr)
A3 - phase shift of the amplifier (degr)
A4 - antenna type :
1 - c. r=50m, 2 - c. r=75m, 3 - 8 r=2x25m, 4 - 8 r=2x37m, 5 - c. r=2x25m.
A5 - average noise evaluation (nV)
A6 - Udc/dc
A7 - coefficient of amplification
A8 - antenna impedance for generation of the pulse (ohm)
A9 - number of lines in the file for data

line with data 'B' is a content of the vector conf[11]
B1 - number of readings of the noise (recording time=B1*(4/cfreq) ms)
B2 - pause between recording of the noise and the pulse (pause duration=B2*(0.25/cfreq) ms)
B3 - duration of the pulse (pulse duration=B3*(4/cfreq) ms)
B4 - pause between the pulse and recording of the signal (pause duration=B2*(0.25/cfreq) ms)
B5 - number of readings of the signal (recording time=B5*(4/cfreq) ms)
B6 - pause (pause duration=B6*(0.25/cfreq) ms)
B7 - duration of the second pulse (pulse duration=B7*(4/cfreq) ms)
B8 - pause (pause duration=B8*(0.25/cfreq) ms)
B9 - number of readings of the signal (recording time=B9*(4/cfreq) ms)
B10 - pause (pause duration=B10*(0.25/cfreq) ms)
B11 - number of readings of the signal (recording time=B11*(4/cfreq) ms)

readings of the noise, the pulse and the signal
C1 - recording time (ms)
C2 - noise X (nV)
C3 - noise Y (nV)
C4 - pulse X current=(300.*0.9375)*(C4/8192) (A)
C5 - pulse Y current=(300.*0.9375)*(C5/8192) (A)
C6 - signal 1 X (nV)
C7 - signal 1 Y (nV)
C8 - second pulse X current=(300.*0.9375)*(C8/8192) (A)
C9 - second pulse Y current=(300.*0.9375)*(C9/8192) (A)
C10 - signal 2 X (nV)
C11 - signal 2 Y (nV)
C12 - signal 3 X (nV)
C13 - signal 3 Y (nV)

Example of real file with added comments (marked by *)

* A 1	A2	A3	A4	A5	A6	A7	A8	A9
2005.20	17	-30	1	1244	40	38829.7	10.466	522

* B1	B2	B3	B4	B5	B6	B7	B8	B9	B10	B11
521	80	20	240	521	0	0	240	0	0	0

* C1	C2	C3	C4	C5	C6	C7	C8	C9	C10	C11	C12	C13
0.00	-390	-707	515	-115	-350	174	0	0	0	0	0	0
1.99	-307	-316	1202	219	-156	197	0	0	0	0	0	0
3.99	-250	-72	1517	374	62	322	0	0	0	0	0	0
5.98	92	-40	1731	517	-42	136	0	0	0	0	0	0
7.98	46	196	1847	559	220	-130	0	0	0	0	0	0
9.97	-165	521	1890	603	338	-92	0	0	0	0	0	0
11.97	-245	38	1915	617	154	28	0	0	0	0	0	0
13.96	-76	-232	1905	619	-3	55	0	0	0	0	0	0
15.96	-169	-388	1889	621	-70	7	0	0	0	0	0	0
17.95	-183	-484	1863	615	-410	-74	0	0	0	0	0	0
19.95	276	-730	1830	606	-378	-114	0	0	0	0	0	0
21.94	281	-412	1800	596	-212	-8	0	0	0	0	0	0

DESCRIPTION OF NUMIS SYNTHETIC FILES (.inp or .inr files)

Example of real file with added comments (marked by *)

*	type of antenna		number of measurements				
	1			16			
*	q(A-ms)	E(nV)	T2(ms)	noise(nV)	Udc/dc(V)	signal freq(Hz)	phase(degr)
	0	0	0	0	0	0.00	0
	318	118	1000	1390	8	1998.50	11
	390	99	1000	1223	9	1998.50	91
	576	77	238	1455	12	2003.30	63
	709	80	363	1312	14	1994.00	49
	1006	82	525	780	18	2007.80	206
	1253	83	211	798	22	1998.50	31
	1569	60	674	1057	27	2000.40	130
	1933	49	1000	1167	33	2002.00	161
	2369	29	1000	1244	40	1992.00	-23
	2899	24	1000	998	49	2012.00	-11
	3608	77	1000	1655	61	2011.00	-46
	4337	78	1000	1375	74	2001.50	224
	5215	36	1000	1852	91	1991.80	51
	6210	37	1000	1536	112	2015.90	-66
	7360	66	99	1141	137	1998.00	74
	8673	34	339	3681	167	1999.90	279

Attention : for the current format number of lines begins from 0 and hence there is (16+1) lines

DESCRIPTION OF NUMIS INVERSION RESULT FILES (.out files)

* A	B	C	D	E	F	G		H	I	J
0.0	1.0	0.5	0.6207	155.1	0.7519	9.628234e-01	247	19	21	
1.0	2.0	1.5	0.6221	155.5	0.7532	9.674874e-01	347	34	25	
2.0	3.0	2.5	0.6257	155.9	0.7571	9.753243e-01	446	20	28	
3.0	4.0	3.5	0.6307	156.3	0.7629	9.857576e-01	605	36	31	
4.0	5.0	4.5	0.6363	158.2	0.7679	1.006266e+00	801	29	31	
5.0	6.0	5.5	0.6447	160.3	0.7761	1.033354e+00	1047	49	29	
6.0	7.5	6.8	0.6546	163.3	0.7854	6.977207e-01	1385	36	24	
7.5	10.0	8.8	0.6660	165.5	0.7971	4.377271e-01	1715	36	20	
10.0	13.4	11.7	0.6678	169.0	0.7963	3.357872e-01	2162	11	16	
13.4	17.9	15.7	0.6468	175.5	0.7664	2.531255e-01	2748	10	14	
17.9	23.9	20.9	0.5874	191.2	0.6863	1.877394e-01	3383	7	14	
23.9	31.9	27.9	0.4831	225.8	0.5512	1.366221e-01	4147	4	15	
31.9	42.5	37.2	0.3521	298.6	0.3891	9.871703e-02	5045	10	13	
42.5	56.7	49.6	0.2185	608.6	0.2295	9.355697e-02	6050	5	11	
56.7	75.7	66.2	0.1342	1000.0	0.1383	7.075936e-02	7277	3	10	
75.7	100.0	87.8	0.1100	1000.0	0.1133	4.524903e-02	8678	4	11	

A - depth of model layer from (m)
B - depth of model layer to (m)
C - depth of centre of model layer (m)
D - the water content without extrapolation (%)
E - the decay time (ms)
F - the water content after extrapolation (%)
G - not used by now
H - pulse parameters of measuring (A-ms)
I - measured signal (nV)
J - reconstructed theoretical signal (nV)

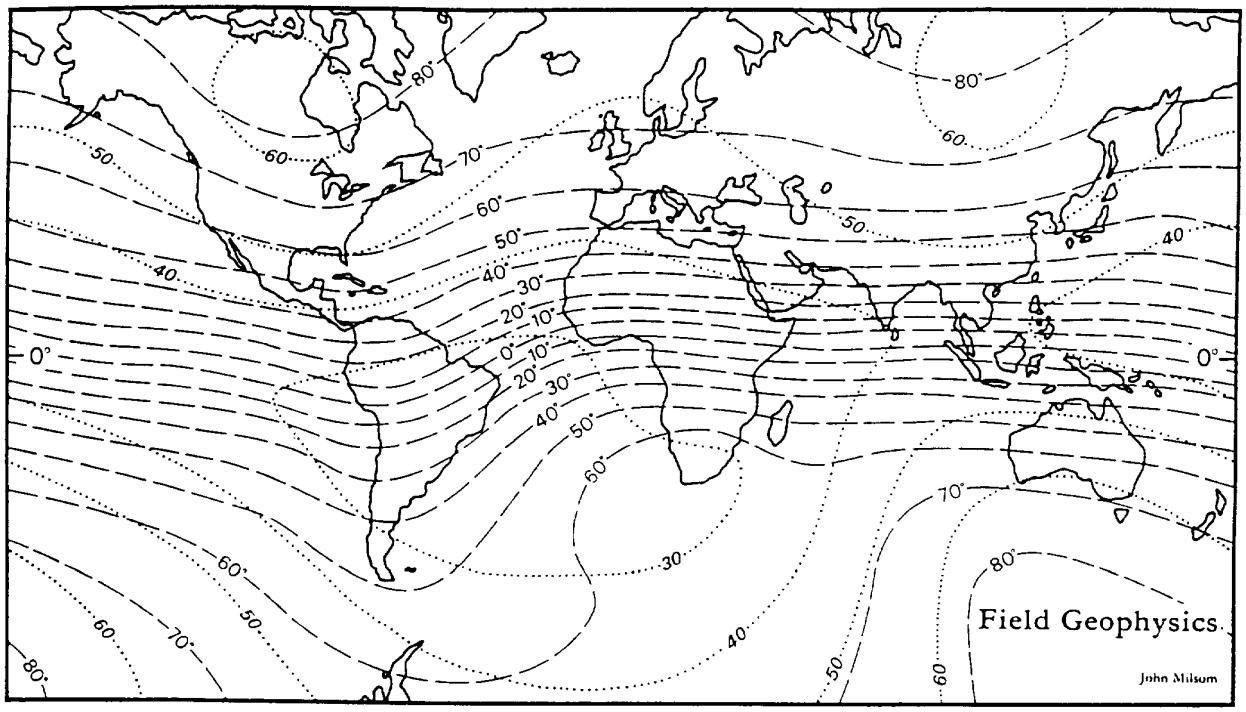

EARTH'S MAGNETIC FIELD MAP

30 Amplitude values (in thousands of nT)

70° Dip values (in degrees)

ANEXO V

NUMIS

Surface PMR system for water prospecting

Operating Manual

December 1997

IRIS INSTRUMENTS
1, avenue Buffon
B.P. 6007 - 45060 Orléans cedex 2, France
Téléphone : + 33 (0)2 38 63 81 00
Télécopieur : + 33 (0)2 38 63 81 82
E-mail : irisins@ibm.net
BRGM & OYO Joint Venture

S.A. au capital de 7 878.000 F - RCS PARIS B 380 202 390
SIRET 380 202 390 00015 - Code Activité 332 B

CONTENTS

FIGURES

1. Introduction

NUMIS Proton Magnetic Resonance (PMR) instrument allows non invasive measurements of a PMR signal from subsurface water-saturated layers. Direct measurement of the signal from water molecules guarantees a high reliability of water detection. Interpretation of experimental data reveals location of aquifers, their depth and water content. Mean size of water-saturated rocks pores can also be estimated. Knowledge of the water content and of the decay time is useful for an estimation of the yield of a borehole before drilling. The PMR method can be used not only for water-supply purpose but also for water-saturation monitoring in civil engineering.

For field measurements, the working set should be loaded into a car. The total unpacked equipment weights about 300 kg. Usual time required for one measurement is two hours including field set up, but largely depends on signal-to-noise ratio.

2. NUMIS PMR system

2.1. Basic principles of the PMR method

Time diagram of measuring is presented in Figure 1. Through the antenna is passing a pulse of alternating current:

$$i(t) = I_0 \cos(\omega_0 t), \qquad 0 \le t \le \tau. \qquad (1)$$

Duration and amplitude of the pulse are τ and I_0 respectively. Frequency of the current is equal to Larmor frequency for protons in the geomagnetic field:

$$\omega_0 = \gamma H_0. \qquad (2)$$

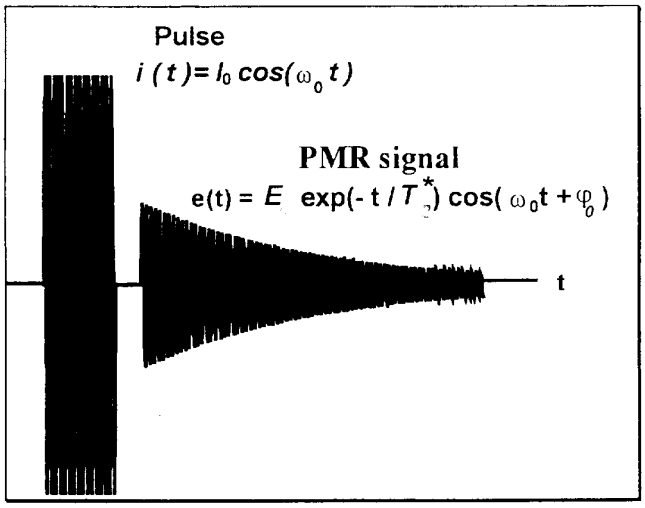

Fig. 1 : Time diagram of measuring.

The signal

$$e(t) = E_0(q)\ \sin(\omega_0 t + \varphi_0)\ \exp(-t / T_2^*), \quad (3)$$

is to be measured after an instrumental delay so called the 'dead time'. The frequency of the signal is equal to Larmor frequency ω_0. The amplitude E_0, the decay time T_2^* and the phase φ_0 contain useful information about depth, thickness and water content of water-saturated layers.

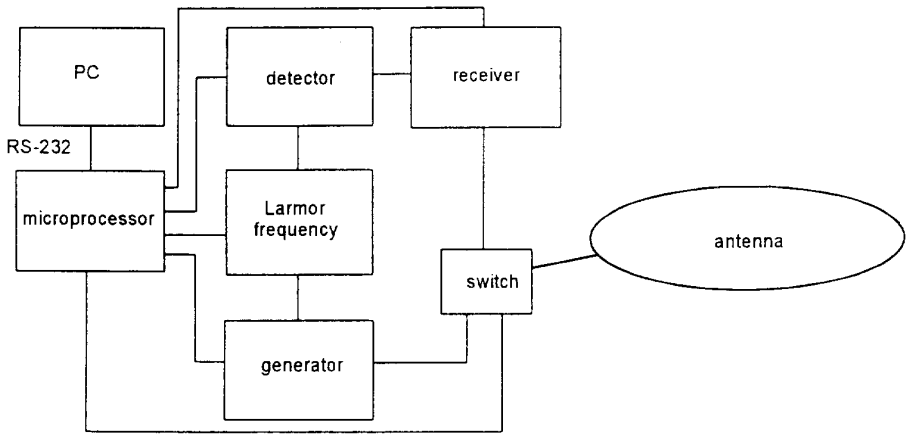

Fig. 2 : Scheme of the system.

The NUMIS system consists of (Figure 2):
- An oscillating-current generator
- A receiver
- A PMR signal detector
- An antenna
- A microprocessor

The antenna is used for both transmission of the oscillating magnetic field and reception of the PMR signal. The microprocessor switches the antenna from generator to receiver mode by an electronic switch. It also controls the generation of the reference frequency equal to the Larmor frequency. An envelope of the signal from the phase-sensitive detector is recorded by the microprocessor in digital form. A portable PC is used for data processing. The PC is connected to the microprocessor by a standard RS-232 serial link.

2.2. Working set

The working set consists of:

- GENERATOR (800x600x600 mm, weight 70 kg).
- DC/DC CONVERTER (550x600x420 mm, weight 40 kg).
- Cables of connection:
  - control DC/DC (1)
  - power supply of generator (1)
  - serial link RS 232 (1)
  - power supply of PC (1)
  - Tx/Rx loop connection (1)
  - connection box for antenna wire (5)
- Wire loop (four reels with 75 m of cable on each, weight of one reel is 35 kg).
- Lab test antenna unit. (1)
- Two car batteries (more than 60 Ah each) with a 24V total voltage.
- Personal laptop computer (IBM PC compatible).
- Proton magnetometer.

2.3. General specifications of the hardware

DC/DC CONVERTER is a power supply unit for the pulse generator.

- Input voltage: 24(±4)V, 20A
- Output voltage: 380V, 1A
- Capacity: 0.1F

GENERATOR sends the alternative current pulse into the antenna.

- Max. output current: 200A typical (300A at lowest frequencies)
- Frequency: 1200-3000Hz
- Max. output voltage: 2500V
- Duration of the pulse: 10 - 80 ms (standard)

RECEIVER amplifies the signal:

- Scale: 500 - 30000 nV
- Noise level: 10 (nV / $\sqrt{\text{Hz}}$)
- 'Dead time': 35 ms

Temperature range: (without taking into account the PC):

- Operating : -30 to +50C°
- Storage: -40 to +60C°

Tx/Rx LOOP is an antenna for pulse transmission and signal reception. Performance of the instrument depends on shape and size of the antenna. Here are the standard types of antenna:

Circular, D=100 m, one turn (314 m of cable, R=0.2 Ohm, L=0.6 mH).
Circular, D=150 m, one turn (471 m of cable, R=0.3 Ohm, L=0.9 mH).
Circular, D=50 m, two turns (314 m of cable, R=0.2 Ohm, L=0.6 mH).
Circular, D=75 m, two turns (471 m of cable, R=0.3 Ohm, L=0.9 mH).

Square, side=75 m, one turn (300 m of cable, R=0.2 Ohm, L=0.6 mH).
Square, side=120 m, one turn (480 m of cable, R=0.3 Ohm, L=0.9 mH).
Square, side=37.5 m, two turns (300 m of cable, R=0.2 Ohm, L=0.6 mH).
Square, side=60 m, two turns (480 m of cable, R=0.3 Ohm, L=0.9 mH).

Eight-shape, D=50 m (314 m of cable, R=0.2 Ohm, L=0.6 mH).
Eight-shape, D=75 m (471 m of cable, R=0.3 Ohm, L=0.9 mH).
Eight-shape square, side=37.5 m (300 m of cable, R=0.2 Ohm, L=0.6 mH).
Eight-shape square, side=60 m (480 m of cable, R=0.3 Ohm, L=0.6 mH).

The depth of investigation depends of the shape and size of the loop (60-100 m for the 75 m square configuration) and of the rocks electrical conductivity.

The eight-shape configurations allows to reduce considerably the noise level, thanks to the fact that this one will be almost similar on the two small squares, while the PMR signals of both squares will be added (NUMIS will measure the difference of two PMR signals obtained with opposite excitation magnetic moments).
The drawback of these configurations is that the depth of investigation will be divided by two.

Successive moves of the wires can help to minimize the resulting noise.

3. Preparation to work

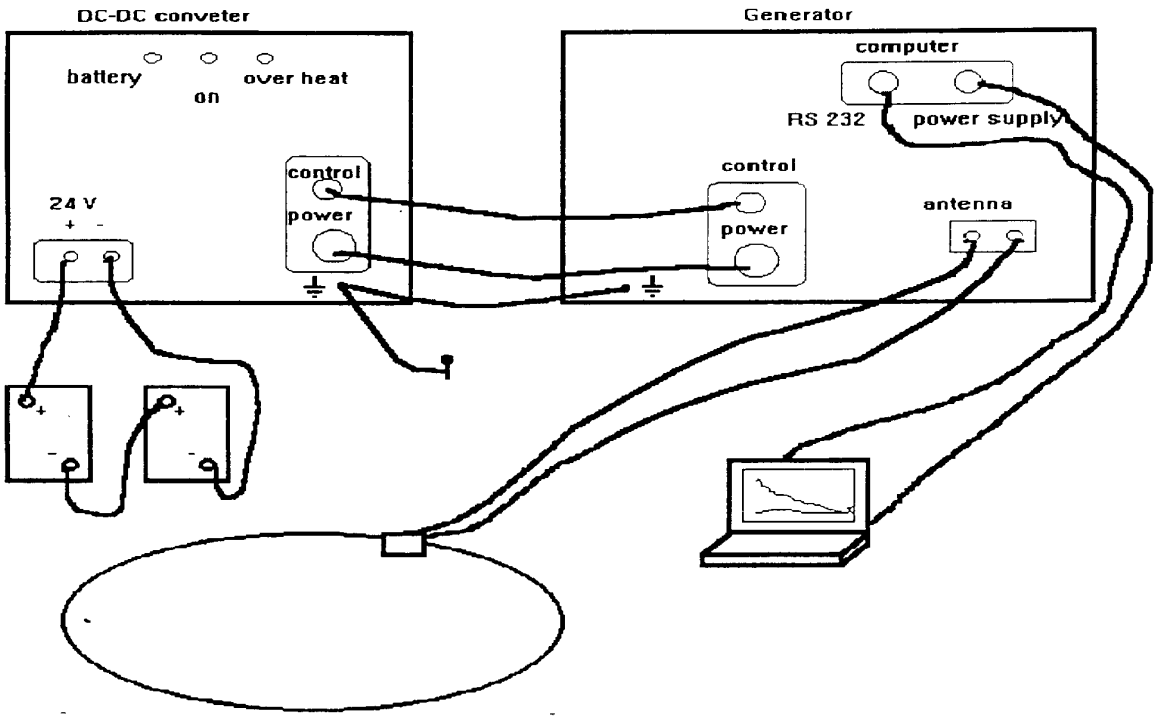

Fig. 3 : Scheme of interconnections.

All parts of the instrument have to be connected as shown above:

- The first connection to realize is grounding. In order to avoid any electromagnetic compatibility problems, the two mechanical assemblies must be connected together and then grounded. In case NUMIS is installed in a vehicle, you must connect NUMIS to the car and then ground the car. Then, you can connect the different cables in the following order:
- Power cord DC/DC side, then, generator side
- Control cable
- Computer RS232
- Computer power supply
- Car batteries

Notes:

- To achieve perfect connection of power cord, you have to be sure to have a good alignment axis of the right angled plug before screwing it. Then, you must push onto the plug while screwing it completely. This way will prevent poor resistance connection due to misalignment and uncomplete tightening.

- The NUMIS system hasn't been designed to charge the computer that will be connected thanks to the RS232 computer link. It only allows keeping it in charge. **SO THE PC HAS TO BE CHARGED BEFORE CONNECTING IT TO THE "POWER SUPPLY" PLUG OF THE GENERATOR.**

3.1. Antenna

An insulated copper wire of 25 mm^2 cross section is used as an antenna. The wire have to be laid out on the surface of the ground with the required shape (standard antennas are presented in page 6). In order to test equipment in a laboratory, instead of the wire loop, an electrical equivalent of antenna can be used (this test has to be carried out in a low noise level place: less than 1 µV typically). The cables going to the "antenna" plugs of the generator have to be intertwined to avoid any induction of the transmitter on the receiving loop.

3.2. Pulse generator

Depending on working frequency, the generator capacitors must be connected according to Figure 5 for 0.6 mH antenna (300 m length loop) and according to Figure 6 for 0.9 mH antenna (larger loop). So you need to have an idea of the local magnetic earth field (so of the transmitter frequency) before configurate the capacitors.

To increase the current available for a given voltage, a tuning is carried out by placing capacitors in series in the loop. For each value of the excitation frequency, there is a value of the capacitance that leads to the loop resonance. This tuning which is carried out manually by the operator with screws located in the back of the system, is designed by steps of the order of 70 Hz at a 2 kHz frequency.

The overvoltage coefficient obtained with such a tuning is of the order of 8, and permits to reach currents of 300 A for a maximum output voltage of 3000 V. The voltage of the excitation pulse is controlled through the value of the DC/DC converter output voltage which ranges from a few volts to a maximum of ±400V.

A metallic bolt will connect the corresponding capacitor whereas a plastic one will disconnect it. To get access to the capacitors you should take off the back panel of the instrument. Position of the bolts is depicted in Figure 5.

Safety rule

Dangerous voltages are generated into this unit. **It is strongly recommended that generator's discharging procedure has been executed before opening instrument's back face.** Nevertheless do not forget the important following rule:

"Touch only one bolt at a time and nothing else !!!"

Frequency(Hz)	C2 (mkF)	Number Of bolts	C1 (mkF)	Number of bolts
3000-2750	12	0	12	0
2750-2500	12	0	18	1
2500-2250	18	1	18	1
2250-2150	18	1	24	2
2150-1980	24	2	24	2
1980-1880	24	2	30	3
1880-1780	30	3	30	3
1780-1700	30	3	36	4
1700-1640	36	4	36	4
1640-1570	36	4	42	5
1570-1510	42	5	42	5
1510-1460	42	5	48	6
1460-1410	48	6	48	6
1410-1380	48	6	54	7
1380-1350	54	7	54	7
1350-1310	54	7	60	8
1310-1280	60	8	60	8

Fig. 4 : Setting of generator capacitors for 0.6 mH antenna.

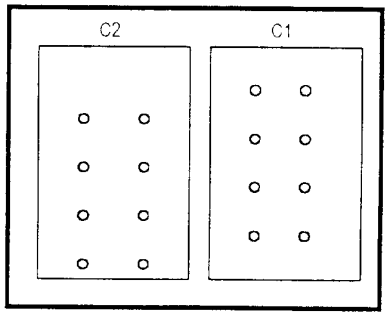

Fig. 5 : Position of bolts for the setting of generator capacitors.

Frequency(Hz)	C2 (mkF)	Number Of bolts	C1 (mkF)	Number of bolts
2500-2300	12	0	12	0
2300-2100	12	0	18	1
2100-1900	18	1	18	1
1900-1750	18	1	24	2
1750-1650	24	2	24	2
1650-1550	24	2	30	3
1550-1450	30	3	30	3
1450-1375	30	3	36	4
1375-1300	36	4	36	4
1300-1250	36	4	42	5
1250-1220	42	5	42	5
1220-1190	42	5	48	6
1190-1160	48	6	48	6
1160-1130	48	6	54	7
1130-1100	54	7	54	7
1100-1070	54	7	60	8
1070-1040	60	8	60	8

Fig. 6 : Setting of generator capacitors for 0.9 mH antenna.

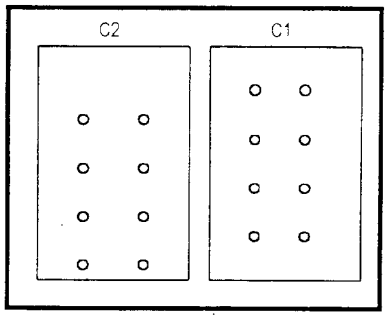

Fig. 5 : Position of bolts for the setting of generator capacitors.

3.3. DC/DC converter

If the DC/DC converter has not been used for more than one month its capacitors must be prepared to work thanks to a special procedure so called 'formation'. For 'formation', the whole instrument's cables should be connected as shown above (Figure 3). The program ***Capform.exe*** (see § 5.3.) will automatically perform this 'formation'.

After 7 hours, once the 'formation' program has been completed, you'll have to **discharge the capacitors**. To do that, disconnect the cables in the following order:

- Power supply of DC/DC (car battery)
- Cable 'control' of DC/DC
- Cable 'generator power supply' from the front panel of DC/DC

And wait 3 minutes.

Then, capacitors are discharged and the DC/DC converter is now ready to operate.

→ The green "battery" LED will light about ten seconds after connecting the batteries to the DC/DC converter. During this time, the DC/DC converter is not operational.
→ The red LED "On" will flash each time the unit will charge the internal capacitors.
→ The red LED "OVERHEAT" lights when the internal temperature exceeds the nominal value. In that case, the output power will be reduced, leading to longer charging time between two pulses. This situation can last a few minutes without damages (necessary for example to complete the sounding), but if the time to finish the acquisition is too long, it would be advisable to realize a pause in order to lower the temperature and switch off the red LED.

WARNING !

1) For discharging capacitors of DC/DC you must follow the above procedure.
2) If the cable 'power supply of generator' is disconnected from the front panel of generator, the capacitors will not be discharged.

4. Measurement procedure

4.1. Safety rules

This equipment has been designed to deliver very high voltages. These ones are dangerous for human body, so only duly trained persons should be authorized to operate.

1) The maximum output pulse voltage is 3000V. Do not touch the Tx/Rx loop terminals or any connecting point of the antenna during the operating. Do not work with opened instrument.

2) Do not change the antenna during the acquisition. If you wish to modify it (for example a circular antenna was used and afterwards you want to use an eight-shape antenna), you must reset the device.

3) Do not work without formation of capacitors of DC/DC converter if it was not used for more than one month (see § 3.3./5.3.).

4) In any case, DC/DC output voltage should never be allowed to exceed 380V.
If such a case happens, use the discharging procedure presented in 3.3 in order to discharge the capacitors of the DC/DC converter.

4.2. Hardware set up

Measuring procedure :
- Connect all the cables. The PC should be used with fully charged internal battery.
- Put down the antenna. The antenna consists of four pieces of wire. The wire should be put down in selected form of antenna (circular, square, eight-shape) and connected using connection boxes as shown in Figure 7 (the circular antenna with D=100 m is depicted as an example):

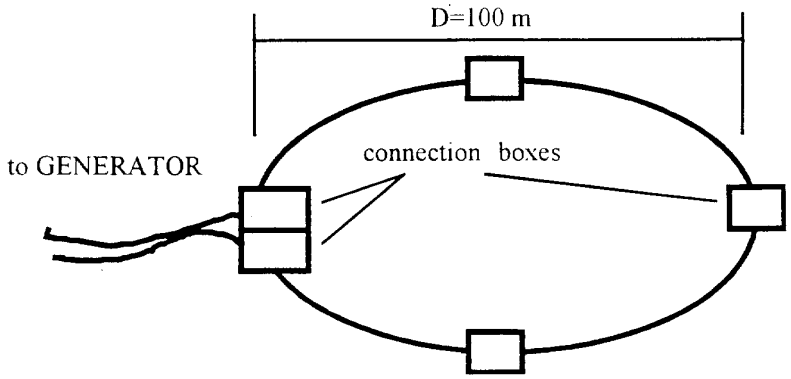

Fig. 7 : Circular antenna connections - D=100 m.

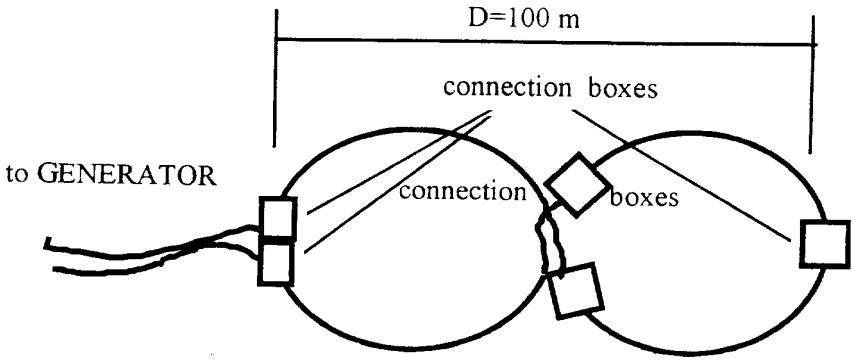

Fig. 8 : Eight shape antenna connections - D=100 m.

Note: The connection boxes between the pieces of wire have to be cleaned and dry (mud can disturb the system operating). It's also advised to screw them strongly to the wires.

- Connect capacitors of the generator according selected antenna and working frequency (see § 4.2.).
- Start the acquisition program (see § 5.1.).

4.3. Signal measurement

The same loop is used for transmitting the excitation current and for measuring the relaxation signal. After the current is switched off, a relay (which can be heard) connects the loop to the receiver part of NUMIS. A new tuning (this time automatic) is carried out with a bandwidth of the order of 20 Hz. Then, the received signal is amplified with a gain, which is related to the maximum signal amplitude introduced by the operator into the PC. The ambient noise amplitude is determined at this stage of circuits.

A stacking is carried out for the noise (before the pulse), the current (during the pulse) and the signal (after the pulse). Initial time samples are averaged before being plotted on the PC screen. Then, a synchronous detection is performed for measuring the signal and the noise, the current being used as the phase reference.

Finally, a fitting algorithm is used for determining the intercept and the time constant of the exponential, which best represents the PMR decay signal. Signal levels as low as a few 10 nV can be measured thanks to the sensitivity and low noise of the analog circuits of NUMIS and to the dedicated signal processing applied on data time series.

4.4. Measurement cycle

A PMR sounding starts by the lowest pulse moments (shallow investigation) and finishes by the highest ones (deeper investigation).

A cycle of measurement for one stack includes the following steps: charge of capacitors, noise measurement, current pulse generation, delay time for switching from Tx to Rx position, signal measurement, data transmission from NUMIS CPU board to the PC computer. One stack takes an average of 8 seconds time, which represents a total time of 1 hour and a quarter for a sounding including 32 stacks of 16 pulse moments.

At the end of the full cycle, the capacitors are discharged for preventing any further misoperation, which produces a jerky sound during about 20 seconds.

5. Software package

The NUMIS system is supplied in a setup diskette. Run just the "setup.exe" file to create the whole associated files that will de decompressed automatically: six softwares are included:

User's:
- Numis: acquisition
- NumisInversion : interpretation – Nmr97_4c : matrix computation
- Capform: initialisation

Maintenance:
- Num_test: diagnostic
- Numremd: diagnostic complement

The setup file will create also a text file (Readme) in which a trick to improve the NUMIS performances is described.

Numis, *NumisInversion* and *Capform* are Windows 95 based versions whereas the other programs are DOS versions. *Nmr97_4c* is located in the "Matrix" directory. *Num_test* and *Numremd* are located in the "Dos" directory. These programs are described in the "NUMIS - Maintenance manual".

5.1. *Numis.exe program*

5.1.1. Presentation

Numis.exe is a program for data acquisition control, filtering and calculation of amplitude, decay time, phase and frequency of the PMR signal. The program runs on a Windows 95 platform.

The main functions in acquisition mode are the following ones:
- Files creation for data storage
- Noise measurement
- Larmor frequency control
- Pulse generator control
- Amplification control
- Stacking procedure management
- Real time filtering and data processing
- Calculation of amplitude, decay time, phase and frequency of the PMR signal

Once the ***Numis.exe*** program has been run, the original menu bar will appear:

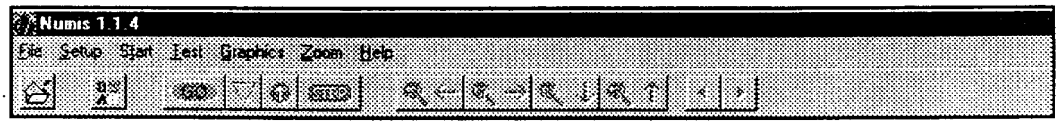

The data acquisition can be started by pressing the GO button or selecting the "Start|Go" option or pressing the "F2" key.

Then the following **Main setup** dialog box will appear:

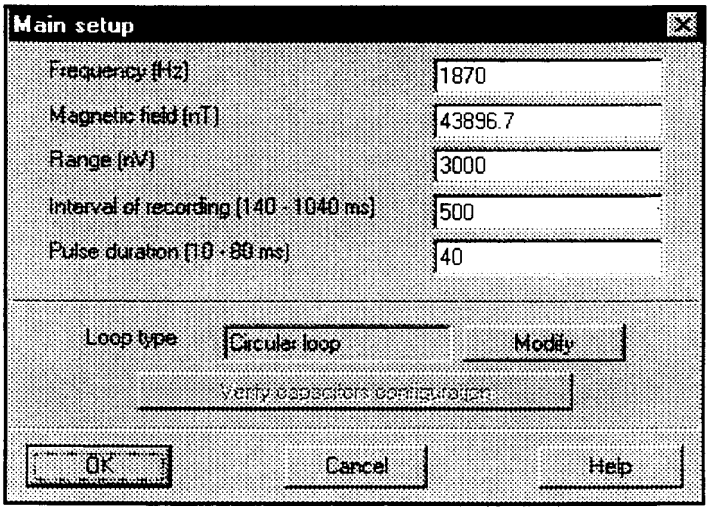

- First, the **Larmor frequency** or the **amplitude of the local magnetic field** has to be given. If the frequency is typed in, then the corresponding magnetic field will be displayed instantaneously, and vice-versa, thanks to the formula:
$f(Hz) = 0.0426 * B(nT)$.

It's important to know precisely this amplitude for being sure that the protons will be excited at their proper precession frequency. An accuracy of about 10 nT is required for a good excitation (in case of lateral variations of the field, one should take an average of the obtained values).

When the magnetic field is measured at the surface by a proton magnetometer, the proper value for PMR measurements often needs to be adjusted later once the received signal frequency is displayed: the discrepancy between the pulse frequency and the signal frequency should not be larger than 1 Hz.

- Then the **amplitude range of the receiver** must be defined. It should be about four times larger than the typical noise value and two times larger than the expected signal. If the noise and signal are unknown, the range value should be set to 30000 nV and modified later according to the observed noise and signal. The reason of this coefficient is that the ambient noise value given by NUMIS is an averaged value and that spikes noise values may be higher than averaged noise values.

- The **interval of recording** should be defined according to the expected decay time of the signal. It also depends on the auto correlation of the noise. It is quite typical to select a recording interval of 250 ms. The maximum value is 1000 ms which has to be used when a thorough analysis of the decay curves is wanted.

- The **pulse duration** should be taken equal to 40 ms for standard use of the equipment.

- At last, the **loop type** has to be specified according to the specific shape of the loop laid on the ground (thanks to the « Modify » button).

5.1.2. Acquisition setup

Once the « OK » button has been pressed, the communication with the Numis instrument microprocessor is started through the RS232 serial link. Error messages are displayed if a bad communication port is selected or the Numis instrument is not connected. In that case, please check all the connections and the communication port configuration; then try again. If everything is right, the **Acquisition setup** dialog box will appear after the system has displayed the main window with the max supply voltage and the pulse frequency that will be used for the measurement.

If the tuning is not possible, check the whole connections of the loop, i.e. tighten strongly and clean the contacts. If the problem persists, this may come from hard conditions (important industrial noise) of the site. Use the NUM_TEST program to validate the correct operating of the instrument (see "Maintenance Manual").

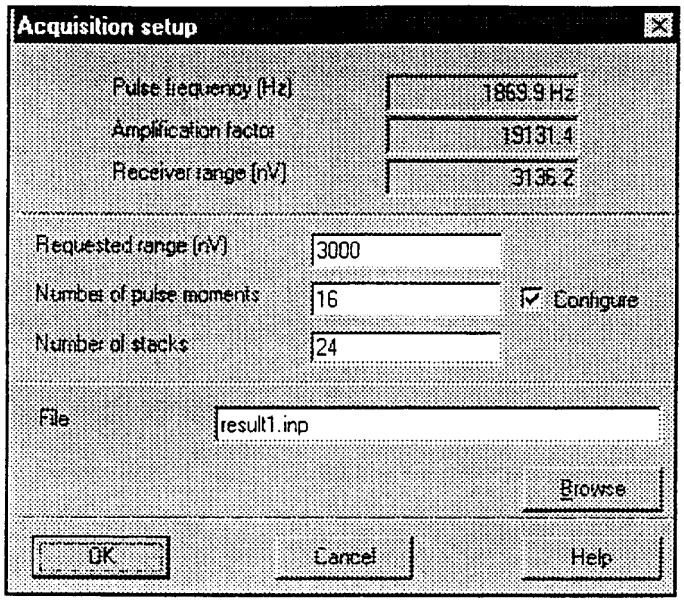

The first three lines display:
- The **effective pulse frequency** which will be used (if the difference with the value previously introduced is greater than 1 Hz, it's recommended to take the received signal frequency as the new value for the excitation pulse frequency).

- The **observed amplification factor** : this parameter given by NUMIS before starting the pulse transmission permits to confirm that the loop is well connected. It is linked to the inductance of the loop and should be in any case greater than 5000. It depends on the loop shape and dimensions, on the wire diameter and on the resistivity of the ground. The amplification factor is of the order of 30000 for a 75 m side square loop over a 100 Ohm.m medium.

- The **effective receiver range** selected by the instrument. If the amplification factor is less than 5000, see "Maintenance Manual".

The next three lines are used to enter:
- A modified **requested range** (if the noise level value is judged inadapted to the receiver range specified before)

- The **number of pulse moments to be used** (typically 16 to 24). The values of pulse moments (range : [300 – 9000] A.ms) are automatically selected by the program.

- The **number of stacks to do for each of these pulse moments**: this number depends on the signal-to-noise ratio. It has to be selected as a compromise between the quality of the measurement and the total duration of the sounding. There is no absolute rule, but the following table gives an estimation of this parameter for a first sounding in an unknown area:

AMBIENT NOISE AMPLITUDE (nV)	SIGNAL AMPLITUDE (nV)		
	30	100	300
200	64	32	16
500	128	64	32
1 000	256	128	64

Fig. 9 : Recommended number of stacks for an unknown area

If during the acquisition some noise spikes occur with amplitude greater than the "range of measurement" set by the operator, there will be an overload, but this stack will be considered as a "bad stack" and will not be taken into account in the average. If, for instance, 32 stacks have been asked, per pulse moment, the program will wait for 32 "good stacks" before moving to the next pulse moment value.

- Optionally the pulse moments might be modified later: to allow that, enable the *Configure* check-box in the previous dialogue box.

Finally, the file name for storing field data has to be given. The « Browse » button may be used to select easily the path name. **Don't forget to introduce the extension "inp" to this file**.

If the file already exists, a message box will warn you and let you select whether you want to overwrite the existing data, append new data at the end of the file or select another filename:

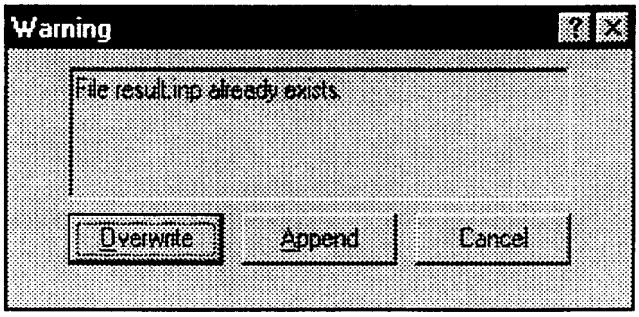

Then, the program will display automatically in real time the ambient noise, measured in nV, in the following window (next page):

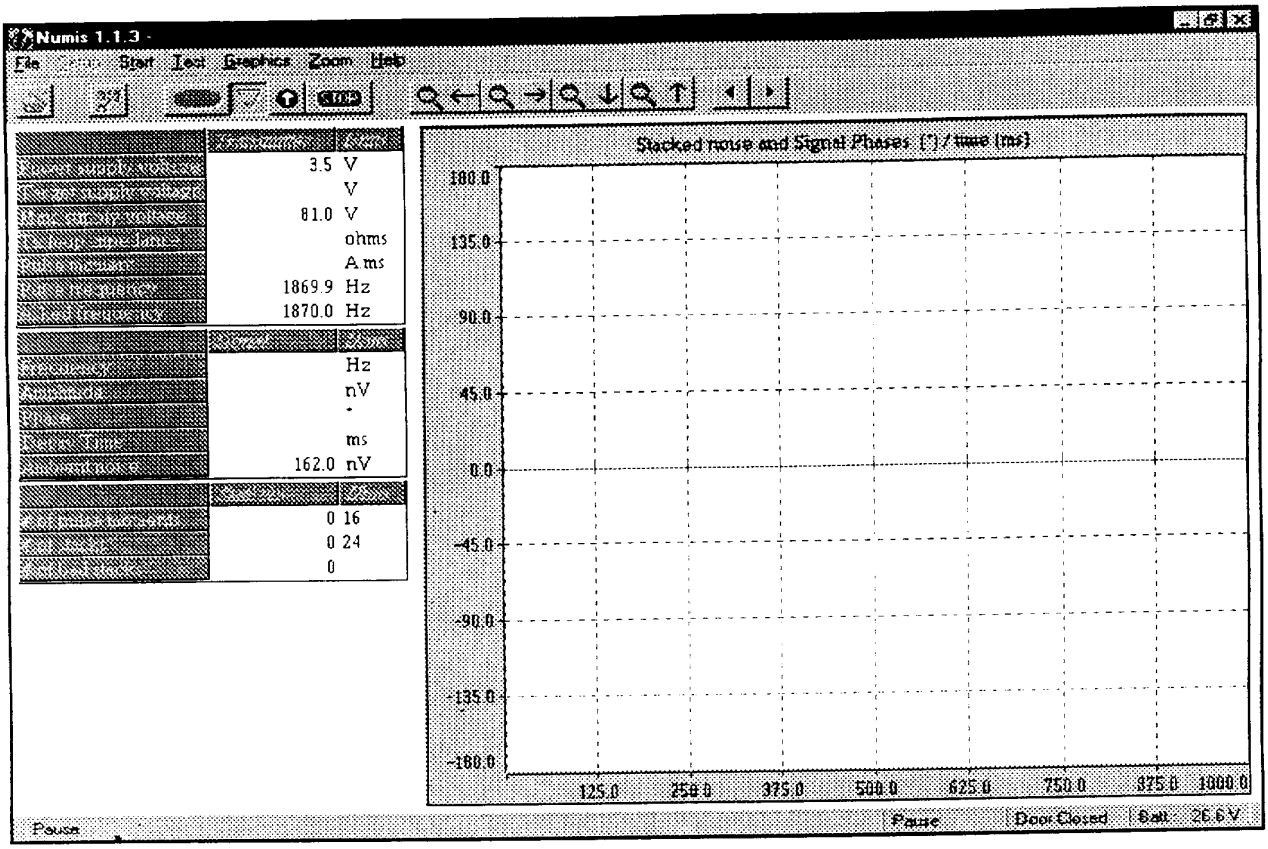

The ambient noise is the average value of the total signal coming out from the loop (noise + PMR signal) and filtered by the analog part of NUMIS, measured at the level of the ADC converter. It corresponds to a frequency band which is of the order of 10 to 20 Hz depending on factors such as loop inductance, tuning, etc... This parameter is a good indication for confirming that the square shape loop is convenient or if it is recommended to use a eight-square shape loop. It also permits to have an idea of the number of stacks which will be necessary for measuring the PMR sounding (see §5.1.2.).

Then run the acquisition whenever you want.

5.1.3. Acquisition

At this stage, the standard acquisition window (control panels and graphical plots) will be displayed and the acquisition program will be set in pause mode. To proceed with the measurements, press the ▶ button or select the "Start|Run" option, or press simultaneously the Ctrl and R keys.
The acquisition sequences will start, beginning with loop impedance measurement (with an 80V DC supply voltage) and followed by the **Pulses configuration** dialogue box (only if you clicked on the *Configure* check-box).

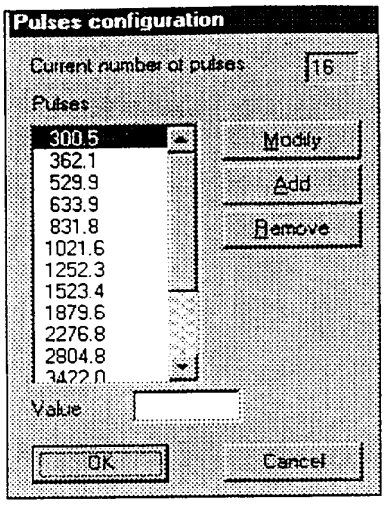

In the previous dialogue box, each Q value can be modified, added or removed. Then, the whole acquisition sequences will start with the lowest one.

During the measurement, it is possible to scan through the various graphical plots available: use « and » buttons, the "Graphics" menu or the left and right keys.

You'll have then access to the following graphic plots:

- Signal decay time versus pulse moment
- Signal phase versus pulse moment
- Signal amplitude versus pulse moment
- Ambient noise versus pulse moment
- Signal frequency versus pulse moment
- Power supply voltage versus pulse moment
- Stacked noise and signal phases versus time
- Stacked noise and signal amplitudes versus time
- Simultaneously : Stacked noise and signal phases versus time
  Stacked noise and signal amplitudes versus time

In all these plots, the signal curves are plotted in black color while the noise curves are plotted in red color.

During the acquisition, the graphics giving results relative to time evolve after each stack. These are the "**Stacked noise and signal**" phases and amplitudes graphics. They allow seeing the noise effect (which decreases with the time (due to the stacking)).

The other ones are created point per point, after having completed the whole stacks for each pulse moment.

It is possible to change the horizontal and vertical scales of the current plot through the "Zoom" menu or the following buttons:

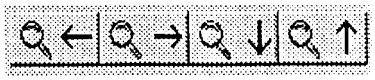

Examples of graphical result:

☞ Stacked noise and signal amplitudes versus time:
The following window shows the results of the stacked signal amplitude (the decreasing curve) and the stacked noise (the other one).
For a given pulse moment, these curves evolve in real time after each stack. The following plot shows the results after 22 stacks for the second pulse moment (313A.ms). The signal values given are those relative to the previous pulse moment (the first one (305.5 A.ms) in that case):

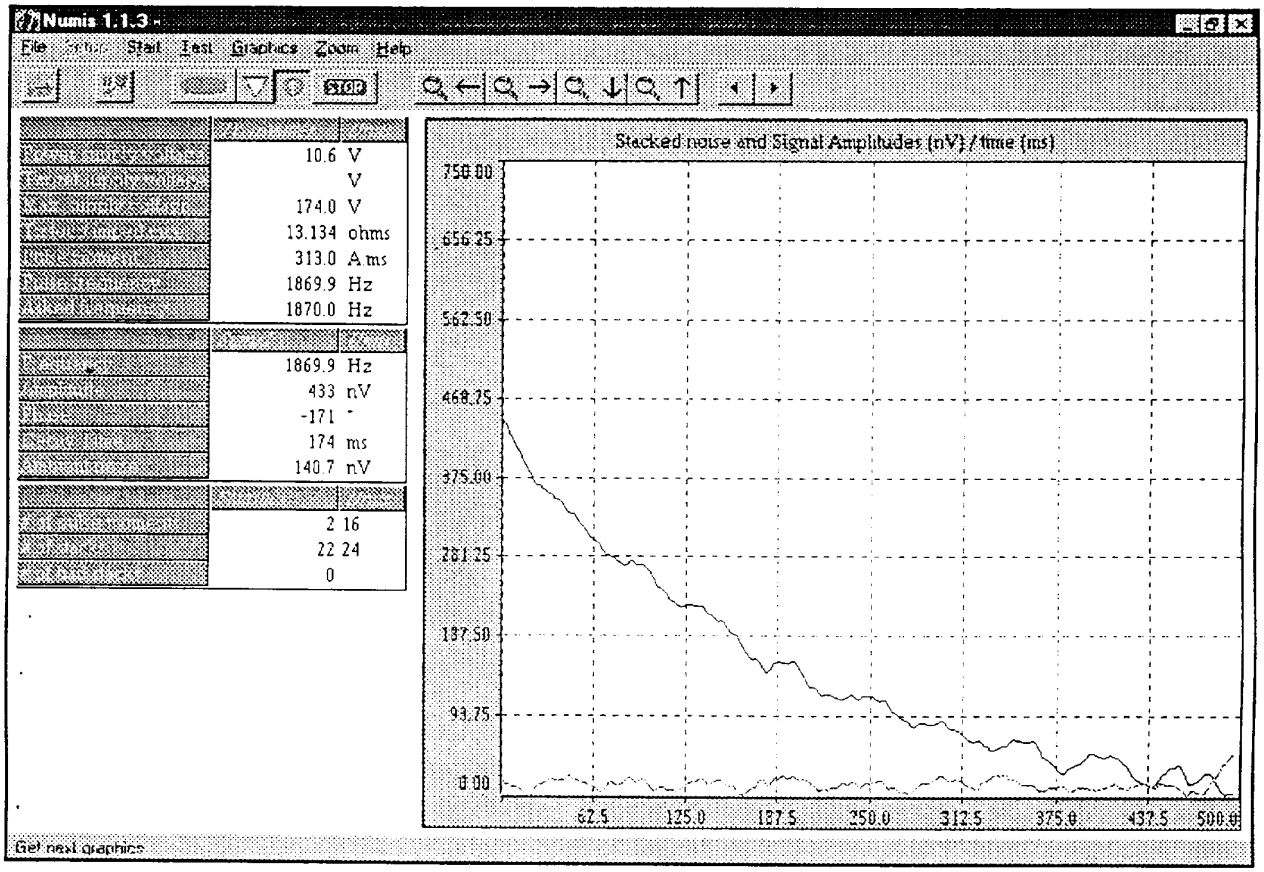

If needed, the ▽ button or the "Start|Pause" option can be used to momentarily interrupt the measurements. Then use the ◐ button or the "Start|Run" to resume.

It is also possible to abort the current acquisition by pressing the STOP button, selecting the "Start|Stop" or pressing the "F3" key. In this case, the data for the on going pulse moment will not be saved, but the previous ones will be kept in the data file (if not overwritten later).

The "Stop" then "Go" options must be used to change any parameter of the **Main setup** or of the **Acquisition setup** dialogue boxes, such as the working frequency, the stack number, etc...

5.1.4. Stacking effect

→ **Amplitude**:
While the ambient noise is measured in the frequency width of the analog part of NUMIS, the stacked noise is measured after digital processing and is also comparable with the stacked signal. The stacked noise is measured just before the current excitation pulse, the stacked signal being measured just after this pulse. The fact that the stacked signal amplitude becomes greater than the stacked noise amplitude during stacking and shows a decay shape is, of course, an indication of the detection of a PMR signal and of the presence of water.

The curves plotted on the screen of the PC are the envelops of the instantaneous readings, that is without the frequency carrier wave.

→ **Phase**:
The phase measured by NUMIS is the one between the excitation current and the relaxation signal. It is measured for each individual time sampler during the record interval. The phase is measured for both the signal (after the pulse) and the noise (before the pulse). As the noise has no reason to have a phase relation with the excitation current, the stacked noise phase should be a random function of time, while the stacked signal phase should be a linear function of time, slightly altered by noise.

• In case the frequency of the relaxation signal is exactly the same as the excitation current, the stacked signal phase should be constant with time (horizontal straight line).

• If there is some discrepancies between these two frequencies, the stacked signal phase should be a linear function of time (increasing or decreasing, according to advance or delay difference).

The observations on the screen of the linear property of the stacked signal phase with time during the acquisition, while the stacked noise phase remains random, is a good criteria of quality of signal.

5.1.5. File storage

For each set of measurement two kinds of files are stored.

- The first one will have a ".inp" extension. This file is unique and can easily be read using any standard text editor ; the format of such a file is described hereafter:

Antenna type		N				
q (A.ms)	e (nV)	T2 (ms)	noise (nV)	power (V)	freq (Hz)	phase (°)
0	0	0	0	0	0	0
*	*	*	*	*	*	*
.....						
.....						
*	*	*	*	*	*	*

Where

N: number of measurement.
Line '0' is reserved for test measurement with particular value of DC/DC voltage entered by operator
q: pulse moment (A.ms)
e: signal amplitude (nV)
T2: decay time (ms)
noise: noise average value (nV)
power: $U_{DC/DC}$ (V)
freq: measured frequency of the signal (Hz)
phase: signal phase (°)

- The second one presents as many files as the number of moments you requested ; each of them will have a ".#" extension (# being 1 or 2 or...). These files contain raw data transmitted by receiver unit before calculations so they are only interpretable by the software, nevertheless they can also be read using any text editor. In case you stopped the measurement sequence before all moments have been executed the files relative to the preceding moments will be stored.

Please note also that clicking on "File|Open..." in the main menu will allow to read back the data previously acquired. To visualize the whole results, use the ◂ and ▸ buttons.

5.2. *NumisInversion.exe program*

The aim of this interpretation program is to transform a set of experimental sounding data (signal amplitude versus pulse moment) into a 1-D hydrogeological section (water content and type of aquifer versus depth).

5.2.1. Type of inversion: smoothness 1-D solution

The 1-D inversion Windows software provided with the NUMIS system determines fully automatically a solution to a set of experimental PMR data. There are as many layers (investigation depths) as pulse moment values, typically 16 with a 100m diameter loop.

Because the sensitivity of the measured data to the water-content distribution is such that there is a better depth resolution for shallow layers than for deeper layers, the thicknesses of the layers are automatically increased with depth.

The inversion algorithm minimizes a cost function, which is the sum of two terms:
- The first one is the residual mean square error between the experimental data and the theoretical curve.
- The second term is the mean square deviation between water content parameters of two successive layers.

The first term creates a best-fit constraint, while the second one creates a smoothness constraint.

In this smoothest inversion program, there is no adjustment on depths (as layer depths are pre-set) but an adjustment on water contents.

5.2.2. Required computer configurations

This program runs on a Pentium PC computer under Windows 95. It needs a minimum of 8M RAM (12M RAM is preferred) and 10M bytes on the hard disk.

5.2.3. Setup menu

Once you Run the *NumisInversion.exe* program, the following menu bar will appear:

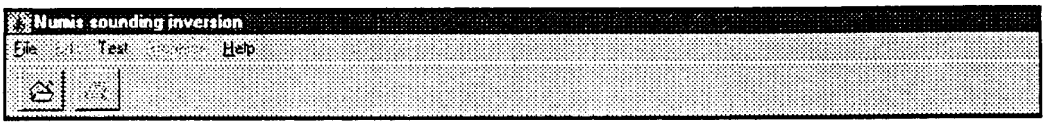

To set up the inversion parameters, select the "File|Run Inversion..." option or press the corresponding push button (the first one):

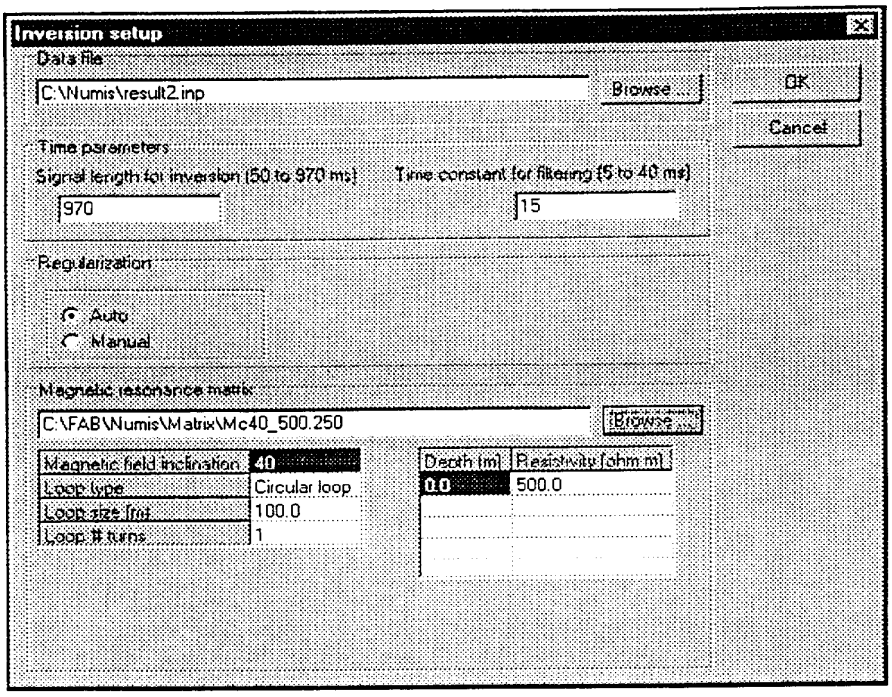

In the previous dialogue box, you'll have then to introduce several parameters:

- The **name of the data file** which includes the NUMIS experimental data to invert (".inp" file).

- The **timing parameters** (the authorized ranged being fixed relative to the acquisition parameters you chose before (see § 5.1.1.):

The signal length: if small time constants are expected in the signal waveform, use a short signal length such as 200ms ; if longer time constants are expected, use a long signal length such as 700ms.

The time constant for filtering: raw data can be post processed to recompute signal amplitude and time constant. It can be useful to filter them for a smoother water content versus depth solution : if the experimental signal curves have a small noise, use a short filtering constant such as 10ms and if the curves are noisy and the signal is long, use a long filtering constant such as 40ms.

- The type of the **regularization**: when inverting noisy data, the algorithm can be unstable and can determine a very unsmooth solution. For this reason, a regularization is available, which consists in minimizing the water content contrast between two adjacent layers (that is to say smoothing the solution). That can be made in two modes:

• Automatically: in that case, the program sets the parameter of regularization by itself through an estimation of the noise in the data.

• Manually: in that case the operator has to give a value for this regularization coefficient which has to be a positive number. A zero value means that there is no regularization ; a value of 5 000 is proposed as the standard one.

The filtering time constant and the regularization coefficient are parameters that can modify significantly the final solution from low spatial frequency solutions (smooth vertical contrasts) to high spatial solution (large vertical contrasts). In particular, the solutions may change from one aquifer layer to two or more aquifer layers depending on the values of these coefficients. Modifying these coefficients may help estimating the equivalence rules in PMR in relation with the noise level of the experimental data.

- The type of **matrix** to be used for the inversion. This depends on the type of loop, which has been used to carry out the measurements (see § 4.2.) ; the « Browse » key permits to select the matrix file among the existing ones:

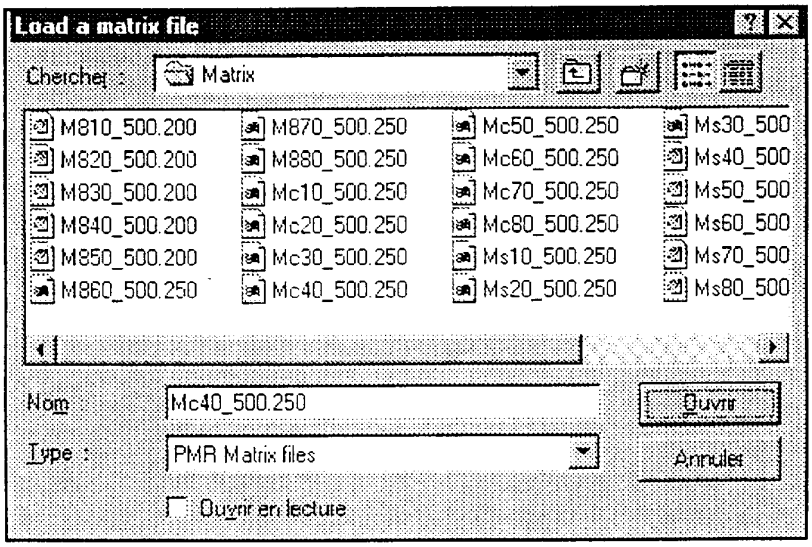

A few pre-set matrix files are provided. For instance Mc40_500.250:

M means Matrix.

c means circular loop shape (s means square loop shape - 8 means circular eight shape - h means squared eight shape).

40 means 40 ° of inclination of the Earth's magnetic field.

500 means 500 Ohm.m for the resistivity of the homogeneous half space.

250 means 2500Hz (the other choice would be 200 (for 2000 Hz)). Select the value closest to the proper precession frequency value of the measurement.

For these matrices the loop size is relative to the loop shape:
- 100m diameter for circular
- 50m diameter for circular eight
- 78.5m side for square
- 39.25m side for eight square

If the required matrix is not available, it should be computed first using the ***Nmr97_4c.exe*** DOS program.

5.2.4. Inversion computation

Press the « Ok » of the **Inversion setup** dialogue box push button to start the inversion.
Inversion in progress is then displayed on the bottom right of the screen.
An inversion takes about 10 s
Note that, to do this inversion, you need to have sufficiently of data.

5.2.5. Result display

Once the matrix of the local base model has been computed, the solution (water content and time constant versus depth) corresponding to a set of experimental sounding data will be simply obtained by inverting a linear system, since the PMR theory states that there is a linear relation between the measured PMR signals measured on the surface of the ground and the water contents of the layers at depth.

At the end of the inversion, the histogram giving the water content and the decay time versus depth is so displayed for the various pre-set layers which depends on the type and on the dimension of the loop:

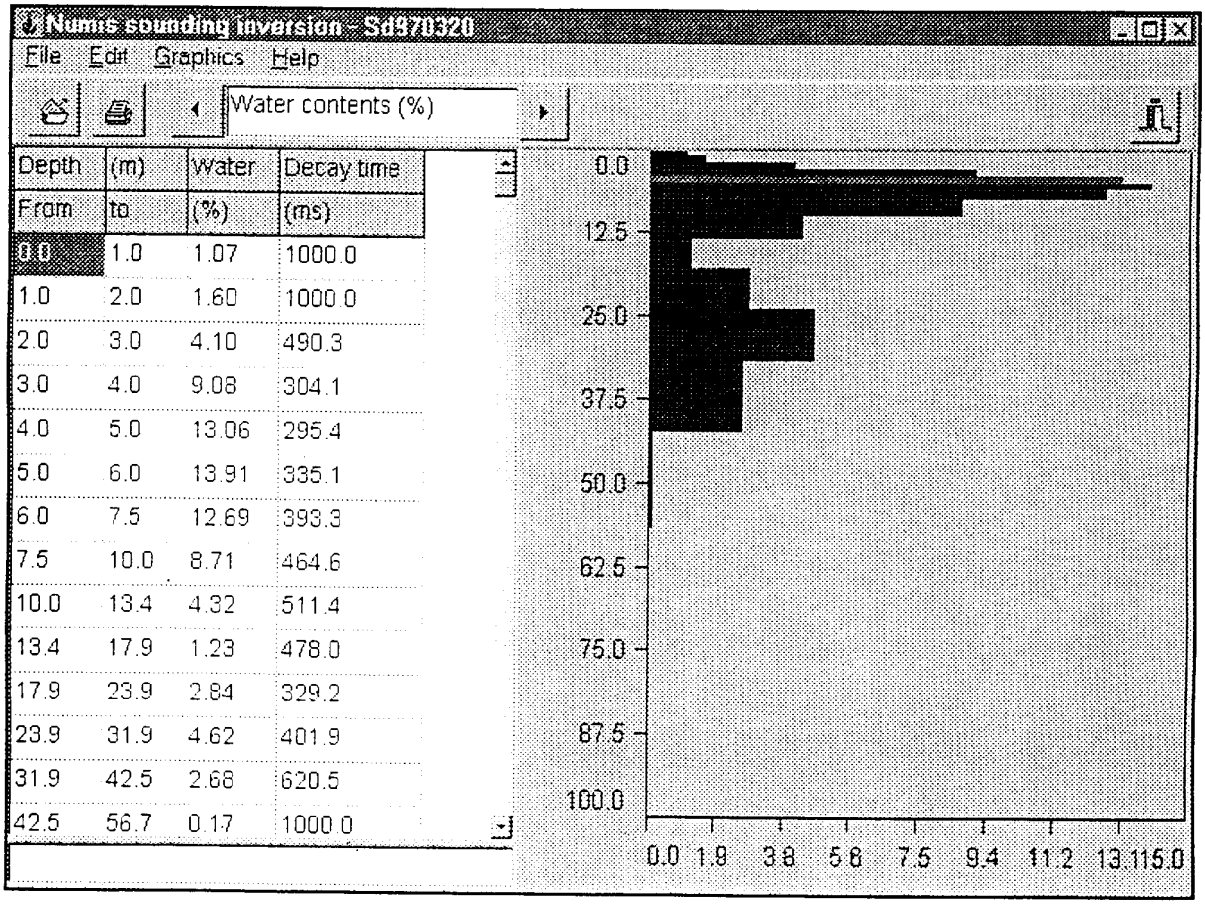

A table summarizes the numerical values, including the time constant values of the PMR relaxation for the various layers. On the histogram, the darker the colour, the longer the time constant and the larger the mean pore size of the layer.

Two arrow push buttons on the tool bar or the "Graphics" function permit to move to the next or to the previous displays:

- The first one shows the experimental sounding data: Signal initial amplitude versus pulse moment:

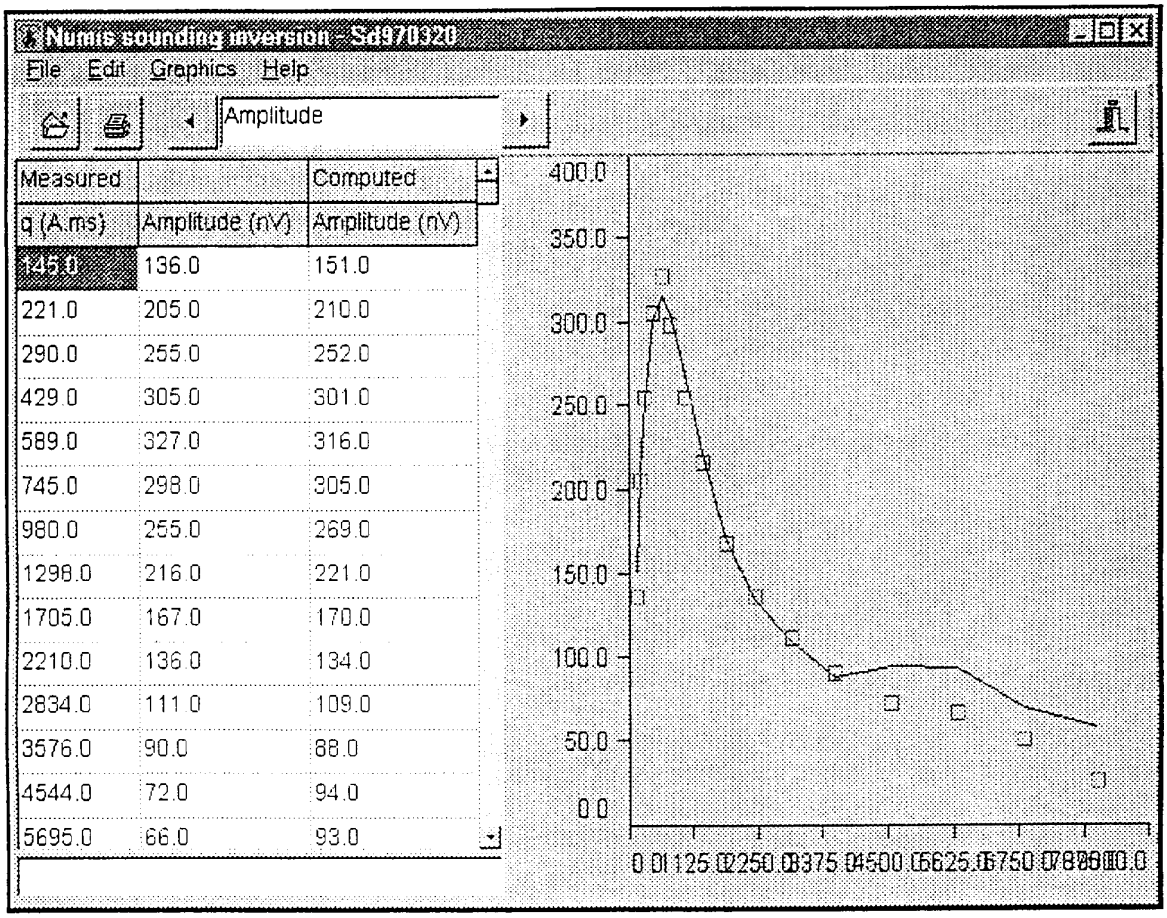

- The second one shows the experimental decay curve:
Graph of the signal amplitude versus time for the pulse moment giving the highest amplitude value:

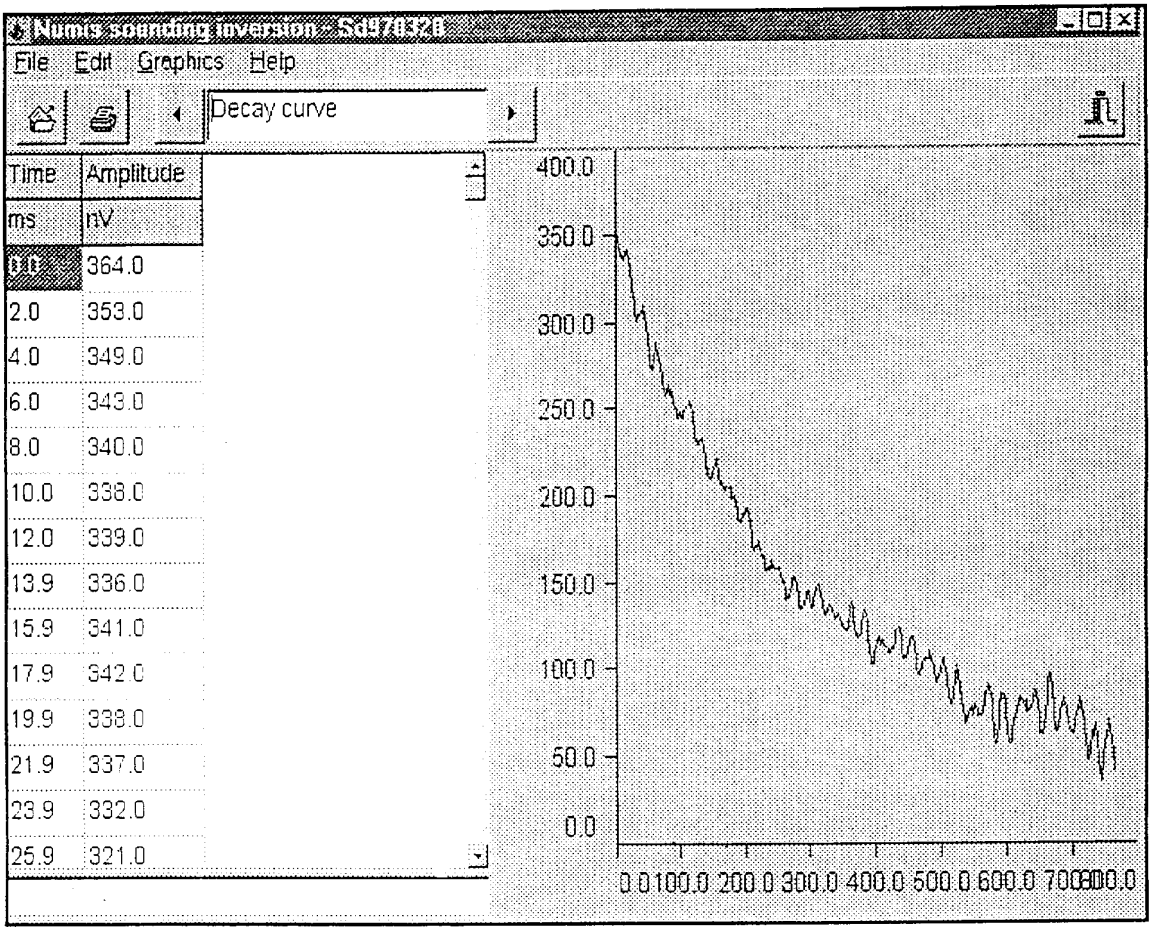

Use the "Edit" function to copy the interpretation results file in the clipboard for export to a word processor or in Metafiles for Windows 3.1, 3.11 or 95.

Files created after this inversion process are ".inr" and ".out" files.
- The ".inr" files have the same structure than the ".inp" ones (see § 5.1.5.).

- The ".out" files have the following structure:

A	B	C	D	E	F	G	H	I	J
*	*	*	*	*	*	*	*	*	*
.	.	.	.	.	.	.	.	.	.
.	.	.	.	.	.	.	.	.	.
*	*	*	*	*	*	*	*	*	*

Where

A: depth of model layer from (m)
B: depth of model layer to (m)
C: depth of center of model layer (m)

D: water content without extrapolation (intermediate parameter) (%)
E: decay time (ms)
F: water content after extrapolation at zero time and after correction for precise frequency values (%)
G: not used by now
H: pulse parameters of measuring (A.ms)
I: measured signal (nV)
J: reconstructed theoretical signal (nV)

Use the « Printer » push button to print the current screen display on paper.

Use the "File|Run inversion..." option or the related push button to run a new inversion.

5.2.6. Matrix computation - *Nmr97_4c.exe* program

For computing the matrix required for the inversion algorithm and corresponding to specific field conditions, the ***Nmr97_4c.exe*** DOS program is to be run.

Once the program is started the following parameters are asked for:
- Loop type: enter the number corresponding to the desired antenna (1: circular - 2: square - 3: eight - 4: squared eight).

- Antenna size: enter the diameter or the side length (meter).

- Number of turns: enter the number of wire turns used in the lay out of the antenna.

- Frequency: enter the value of the precession frequency (Hertz).

- Maximum depth of the matrix: for matrix computation, enter the maximum depth to be taken into account (meter) ; usually that is taken equal between once and twice the antenna size.

- Geomagnetic field inclination: enter the inclination (degrees) of the magnetic field (90° at either pole).

- Maximum value of q: enter the maximum value of the moment parameter (A.ms) for which data are available or might be available (usually 10000 A.ms for the following shapes: Circular (100-150 m diameter) – Square (80 m^2) – Eight shape (50 m diameter per circle) and 7000 A.ms for squared eight shape (40 m^2 per square)).

- Number of conductive layers: enter the number of layers of the 1-D geological section to be taken into account for the matrix computation ; an homogeneous earth corresponds to one layer ; the maximum number of layers is six ; note that the lower half-space is taken as infinitely resistive when there are two layers or more.

- Resistivity of the ith layer: enter the resistivity (Ohm.m) of that layer (the resistivity of the ground influences the depth of investigation since the excitation field is attenuated at depth when the ground is conductive).

- Bottom of the ith layer: enter the depth (meter) to the floor of that layer.

Please note that all floating numbers should be typed in with a decimal point.

The output matrix file is named "nmr_mc.dat" and should be renamed and relocated for future use.
The computation for a homogeneous earth takes a few hours, while for a stratified earth it takes about one daytime, but one matrix can be used for the interpretation of several PMR soundings as the local parameters do not usually change significantly in a given local survey area.

The matrix consists in a n x m array where:

- n is the number of layers (n = 100). The thicknesses of the layers depend on the maximum depth of investigation required ; they are pseudo logarithmically spaced.
- m is the number of pulse moments (m = 100). The values of the pulse moments depend on the depths and thicknesses of the layers and are selected in relation with the amplitude of their responses with respect to the time.

5.3. Capform.exe program

This program has to be used if the DC/DC converter has not been used for more than one month. Its capacitors have to be prepared to work thanks to a special procedure so called 'formation'. For 'formation', the entire instrument's cables should be connected as shown above (Figure 3). A complete 'formation' cycle will be conducted in 7 hours. Voltage and timing during formation are listed in the following figure:

Voltage (V)	Time (h)
100	1
200	2
375	4

Fig. 10 : Timing of formation of capacitors of the DC/DC converter.

5.4. Sum up of the characteristics of the programs

The following programs are the user's ones for the day-to-day operation of the system.

PROGRAM NAME	PLATFORM	FUNCTION	CREATED FILES
NUMIS	Windows 95	Data acquisition	.#: raw data .inp: synthesis
NUMISINVERSION	Windows 95	Data inversion	.inr: synthesis .out: results
NMR97_4C	DOS	Matrix computation	nmr_mc.dat

The following programs are technical ones that have to be used only in special cases:

PROGRAM NAME	PLATFORM	FUNCTION	CREATED FILES
CAPFORM	Windows 95	Capacitor formation	None
NUM_TEST	DOS	Hardware test	Num_test.dat
NUMREMD	DOS	Hardware test (complement)	Numremd.dat